THERMOLUMINESCENCE STUDIES OF SOME TERRESTRIAL AND EXTRATERRESTRIAL MATERIALS

by

KASSIM ABDUL REDHA KHAZAL
M. Sc. (Sussex)

A thesis submitted for the degree of
Doctor of Philosophy

Department of Physics
University of Birmingham

July, 1977

SYNOPSIS

Following a short description of the thermoluminescence kinetics and the experimental techniques and procedures used during the course of this project, the thesis reports on thermoluminescence studies of materials of terrestrial and extraterrestrial origin. The terrestrial materials studied include geological samples such as natural Brazilian quartz and Oklo materials (Gabon, Africa). The extraterrestrial materials are lunar soil samples collected from inside and outside the shadows of certain Apollo 17 boulders.

The experiments described in this thesis are:

1. The study of the changes in the TL sensitivity and sensitisation in crystalline quartz induced by varying doses of protons and gamma-rays. The changes are interpreted as being caused by damage to the Al/alkali recombination centre.
2. The study of a strong dependence of the TL sensitivity and sensitisation upon the temperature at which the quartz sample is irradiated. The temperature effect results in a variation of a factor of ~ 5 in the TL glow intensity over the temperature of irradiation range from $293^{\circ}K$ down to $113^{\circ}K$ with an X-ray dose of 5krad and a factor of $\sim 10^3$ over the temperature range from $293^{\circ}K$ down to $178^{\circ}K$ with a gamma-dose of 600krad. An explanation of the temperature effect is presented and its implication on TL-dating is discussed.
3. The study of natural and artifically induced TL of some Oklo samples as a function of distance from the edge of a reaction zone to compare the TL characteristics of the samples from inside and outside the reaction zone and to assess the degree of radiation damage suffered

by the core samples as a result of the occurrence of the nuclear reaction. The age of the Oklo natural nuclear reactor is calculated, by the fission-track analysis method, to be 1.73×10^9 yr.

4. Attempts to calculate the shade temperature of certain Apollo 17 boulders, and duration yield $256^{\circ}K$ and 6.5×10^4 yr respectively, based on a dose rate of 10rad yr^{-1} in the shade.

TO MY PARENTS

ACKNOWLEDGEMENTS

It is a pleasure to acknowledge the help given during the course of this work.

I should like to thank Dr. S.A. Durrani for his supervision and guidance during the course of this work. I should like to express my deep gratitude to Professor J.H. Fremlin for his continued interest, guidance and constant encouragement throughout this project.

The lunar materials were provided by NASA with the kind help of Dr. Durrani. Thanks are also due to Dr. R. Naudet for providing the Oklo samples.

I should like to thank Dr. S.W.S. McKeever, Dr. S.R. Malik, Mr. A. Ali, Dr. G.F. Alfrey, Mr. R. Reily, Mr. P.J. Groom, Dr. F.S.W. Hwang and M. Balcazar for their helpful discussions, interest and co-operation in some parts of this work.

I also wish to thank Mr. J. Filkin, Mr. J. Harling for their help on technical matters. Special thanks go to Mr. K. Stammers for his technical assistance and for many useful discussion during the course of this work, and also to Mr. E.E. Cartwright and Mr. F.R. Stewart (cyclotron operators) for their assistance.

I should like also to thank Dr. P. Fowles and Dr. L.G. Earwaker for making available the facilities of the Birmingham Radiation Centre and also for the help given in using them.

I wish to thank Dr. G.L. Hendry (Department of Geology) and Dr. J.I. Langford (Department of Physics) for helpful discussions and advice on geological aspects of the work.

I would like to thank the University of Basrah, Iraq, for offering me

the scholarship, and the Calouste Gulbenkian Foundation for its financial support.

I should like to thank my family for their patience during my long absence from home.

Finally, my thanks go to Mrs. P.M. Courtney for her careful typing of this thesis.

CONTENTS

CHAPTER I

GENERAL INTRODUCTION

1.1 The thermoluminescence phenomenon.

When a phosphor, previously subjected to ionizing radiations (such as beta-particles, alpha-particles, gamma-rays, etc.), is heated the energy stored in the phosphor as a result of the irradiation process is liberated in the form of visible light in addition to the normal thermal radiation. Re-heating the phosphor immediately after the first heating gives rise only to the normal thermal emission. The additional visible light emitted during the first heating is called thermoluminescence (TL).

The thermoluminescence phenomenon probably was first observed in the seventeenth century by Sir Robert Boyle when he reported that a diamond, when heated by the warmth of his hands, emitted light which, although very faint, could be noticed by the naked eye in the dark.

The plot of light output intensity emitted by a sample versus the sample temperature is called a glow curve. The method of obtaining a glow curve was first reported by Urbach (1930) and then developed by Randall and Wilkins (1945) due to their researches in the field of TL. The method includes in general two steps: (i) the excitation of the sample at low initial temperature using ionizing radiations, and (ii) the recording of the light output by warming the sample, generally from the temperature at which the sample was excited, at a heating rate which is made as uniform as possible. The glow curve is a characteristic feature of the luminescent solid itself and a detailed analysis of the glow curve can reveal much information concerning the radiation and thermal history of the sample (see Chapters V and VI), apart from providing information vital from a solid-state point of

view (see Chapters III and IV). Figures 1.1a and 1.1b show typical glow curves for Brazilian natural quartz and for a lunar sample respectively.

An explanation of the TL phenomenon can be presented with the aid of the familiar energy band model (see Figure 1.2) which was proposed by Riehl and Schön (1939). The existence of lattice defects and trace impurities in the luminescent solid will give rise to a number of discrete localised energy levels in the forbidden band between the valence and conduction bands. These localised energy levels are called 'traps'. These energy levels, depending on the nature of the impurity, can act as traps for either electrons or holes. Ionizing radiation creates free hole and electron pairs within the luminescent solid. The holes may be captured at centres which are electronegative with respect to the lattice and are known as hole traps. This may be represented energetically by the free hole losing energy and making a transition to a localised energy level within the forbidden band gap. Also, as a result of the collisions which occur in the conduction band, the electrons will lose their energy and make transition either into one of the localised levels, electropositive with respect to the lattice, known as electron traps, or will return to a hole centre which leads to recombination and the emission of light. The latter process is called fluorescence. The emission of light through this process usually occurs at a mean time, t, after excitation, t being the lifetime of the excited state and of the order of 10^{-8} sec (Curie, 1963). If an electron is fallen in an electron trap of energy depth E(eV) below the conduction band, then it will stay in the trap until it acquires this amount of energy, by some means, before it can be freed. When the luminescent phosphor is heated, say during the reading out of the TL, then the trapped electrons will acquire a sufficient thermal energy to enable them

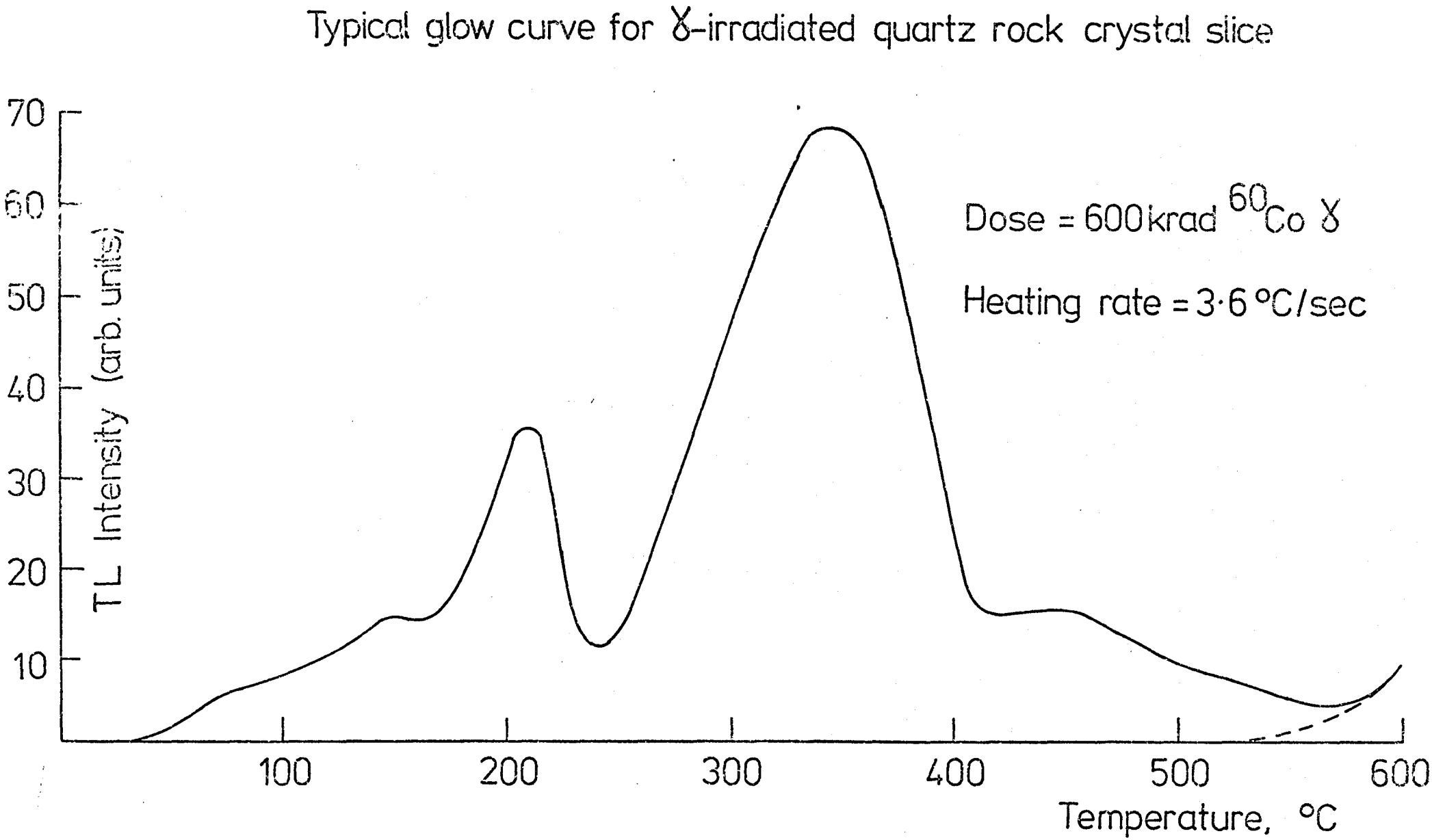
Typical glow curve for γ-irradiated quartz rock crystal slice
70
60
50
40
30
20
10
TL Intensity (arb. units)
Dose = 600krad ^{60}Co γ
Heating rate = 3·6 °C/sec
100
200
300
400
500
600
Temperature, °C

Fig 1·1 (a)

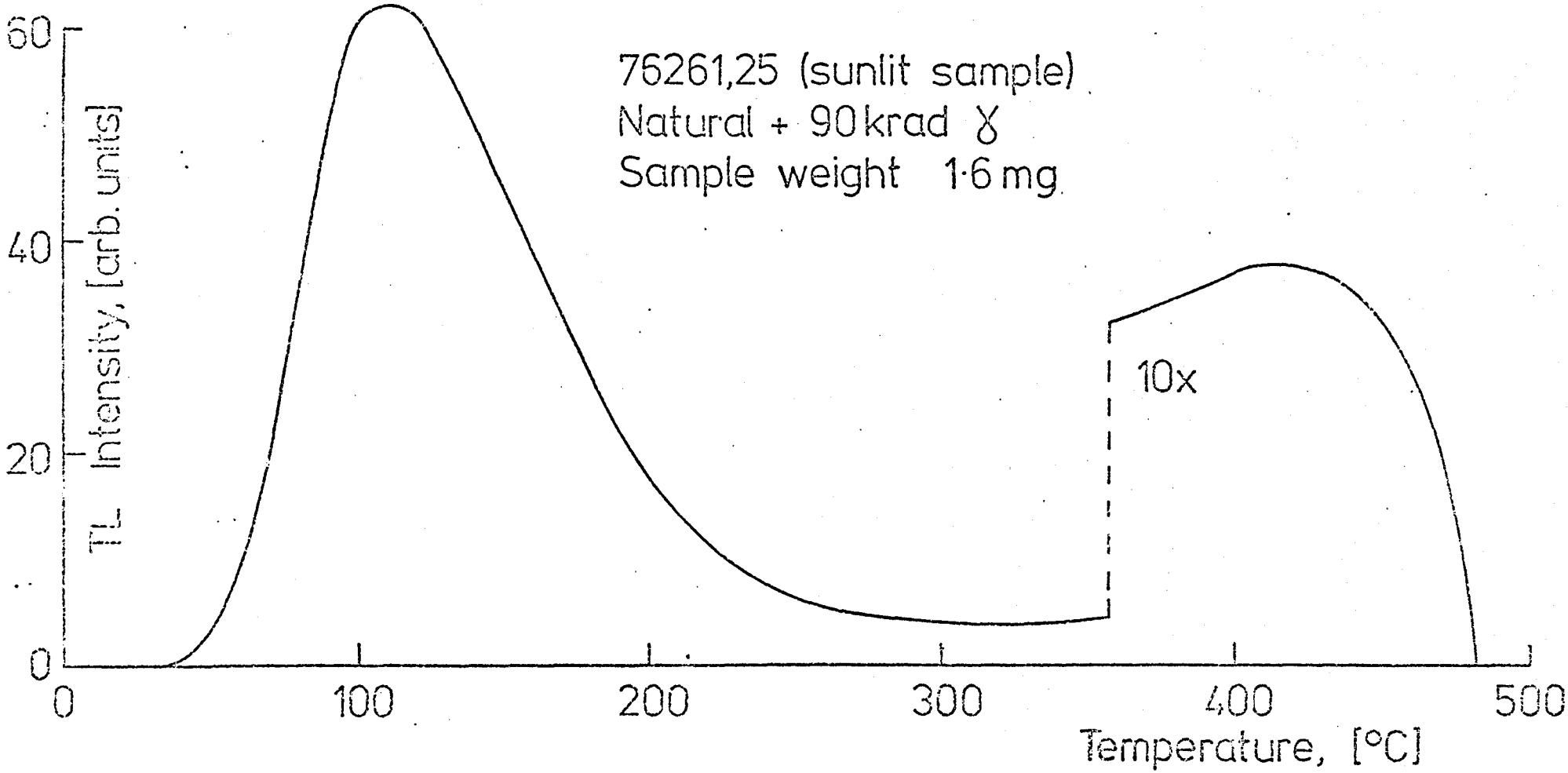
76261,25 (sunlit sample)
Natural + 90 krad γ
Sample weight 1·6 mg
10x
TL Intensity, [arb. units]
60
40
20
0
0
100
200
300
400
500
Temperature, [°C]

Fig 1·1(b)

Schematic Representation of TL Phenomenon

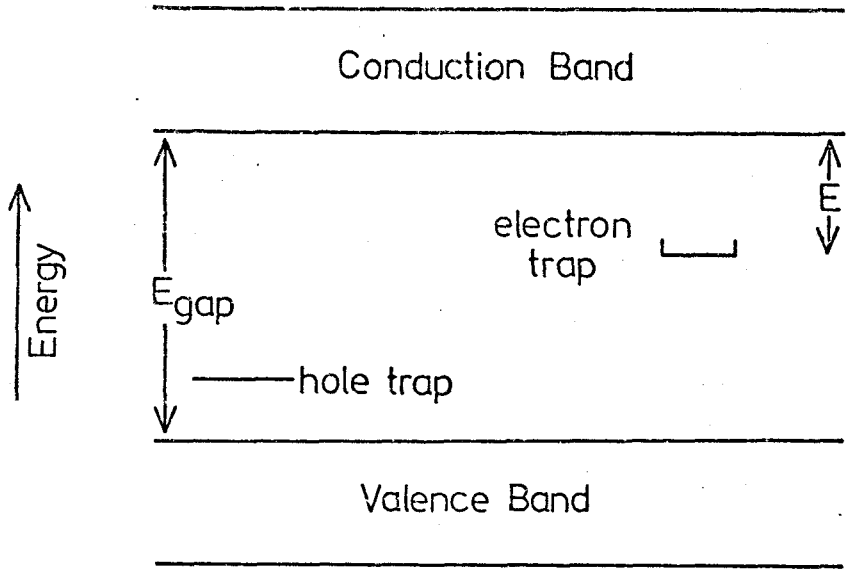

(a) Energy-band model diagram of a thermoluminescent crystal

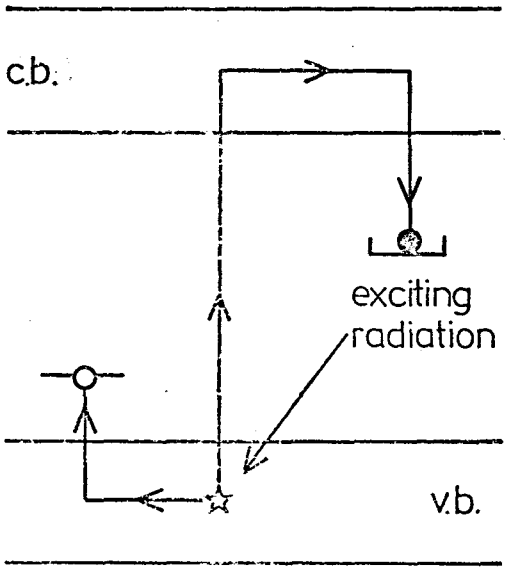

(b) Irradiation

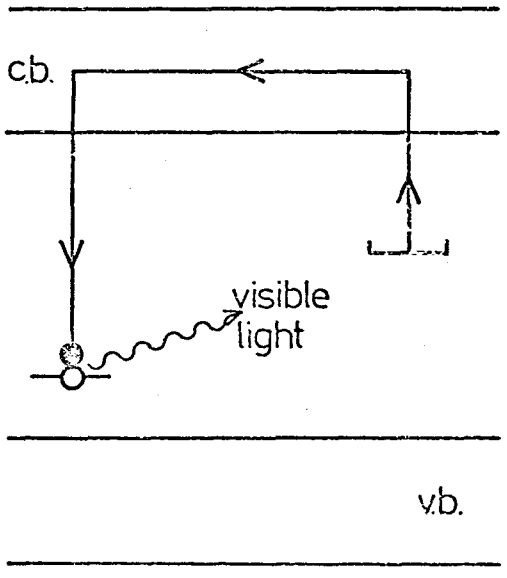

(c) Heating

Fig 1·2

to escape from the traps and migrate through the phosphor until they are either retrapped or they recombine with the holes. The recombination of the electron and the hole on one of the recombination centres will give rise to the emitting of a phonon or perhaps photon depending upon the recombination centre itself. The emitted photons produce the observed TL, and the centre which is capable of emitting photons is called the luminescence centre. In reality only a small fraction of the created electrons and holes are involved with the emission of light and the production of TL. The rest of the created electrons either recombined immediately with their parent atoms or were involved in non-radiative recombination with the trapped holes, the result of which is the emission of phonons instead of photons.

The first mathematical analysis of thermoluminescence glow curves was made by Randall and Wilkins (1945) and later by Garlick and Gibson (1948) who took into account the effect of re-trapping upon the kinetics, a factor which was neglected in the analysis made by Randall and Wilkins (1945). These models will be discussed in detail in the next section.

1.2 The basic theoretical models for TL.

In spite of the many applications of TL in various fields such as archaeological and geological dating, dosimetry and the study of thermal and radiation history of meteorites and lunar samples (Cameron et al, 1968; McDougall, 1968), the theoretical aspects of the subject still lag behind advances in TL application and the fundamental theory of TL is still far from complete. The absence of such theory leads workers in this field to deal with some of the theoretical aspects, making use of available experimental results to test the proposed models. Examples of this are the mathematical models proposed by Cameron and Zimmerman (1965) to explain the supralinearity (i.e. the

increase in the amount of TL induced per unit dose of beta or gamma with the dose received by the sample) observed in lithium fluoride (TLD-100).

In this section the theoretical interpretations of the TL phenomenon which have been proposed by the pioneer researchers in the field, Randall and Wilkins (1945) and also by Garlick and Gibson (1948), will be reviewed. Although based on simplified models, these two theories have had success with some materials and provided some insight into the processes involved in most others.

1.2.1 Randall-Wilkins theory.

According to the first-order kinetics theory of Randall and Wilkins, all liberated electrons (or holes) must recombine with trapped holes (or electrons). This theory neglects the retrapping of electrons at the same trap after they have been able to escape. The recombination which takes place at a certain centre may or may not give rise to the emission of light, depending upon the nature of the centre itself.

Consider electrons trapped at an energy depth E below the conduction band; then at a temperature T (^{o}K) the probability, p, that an electron will be released from the trap up to the conduction band is given by:

$$p = s\exp(-E/kT) \qquad (1)$$

where k is the Boltzmann constant and s is the attempt-to-escape frequency factor. The values of the s factor are of the order of 10^{8} to 10^{13} sec^{-1}. The frequency factor, s, does not appear to vary with temperature (Curie, 1963), but for a given phosphor it can be different for traps of different E values. It was concluded by Williams and Eyring (1947) that the factor s is the product of two factors: first, thermal vibration frequency 10^{12} - 10^{13} sec^{-1}) of the electron trapped in a potential well of depth E, and the second

factor is the quantum mechanical 'transmission coefficient' for the electron transition from the trap to the conduction band.

If n is the number of trapped electrons per unit volume, the rate of release of electrons from the traps at temperature T is given by:

$$\frac{dn}{dt} = -np \tag{2}$$

$$= -ns \exp(-E/kT) \tag{3}$$

or

$$\frac{dn}{n} = -s \exp\left(\frac{-E}{kT}\right) dt \tag{4}$$

If a linear heating rate β was used during heating up the phosphor:

$$dT = \beta\, dt \tag{5}$$

Then:

$$\int_{no}^{n} \frac{dn}{n} = -\int_{T_o}^{T} \frac{s}{\beta} \exp\left(-\frac{E}{kT}\right) dT \tag{6}$$

which gives rise to:

$$n = n_o \exp\left(-\int_{o}^{T} \frac{s}{\beta} \exp\left(-\frac{E}{kT}\right) dT\right) \tag{7}$$

where n_o is the initial number of trapped electrons before the heating is started, and the initial temperature (T_o) was taken here as $0\,(^{o}K)$.

The intensity, I(T), of the glow curve is proportional to the rate of supply of electrons to radiative centres, namely:

$$I(T) = -\frac{dn}{dt} \tag{8}$$

Therefore:

$$I(T) = n_o s \exp\left(-\frac{E}{kT}\right) \exp\left(-\int_{o}^{T} \frac{s}{\beta} \exp\left(-\frac{E}{kT}\right) dT\right) \tag{9}$$

From equation 9 the maximum of light intensity can be obtained by differentiating I(T) with respect to temperature T and setting the result equal to zero, i.e. $\frac{dI}{dT} = 0$. By applying this procedure the maximum of the emitted light is found to occur at temperature T* where T* satisfies the following relation:

$$\frac{\beta E}{kT^{*2}} = s \exp\left(-\frac{E}{kT^*}\right) \qquad (10)$$

T* is known as the peak temperature, and it is clear from equation 10 that it depends on the heating rate β.

Equation 2 can be used to obtain the rate of decay of the number of trapped electrons at a constant temperature T. Assuming n_o is the number of trapped electrons in traps of depth E per unit volume, then the number of electrons remaining at a time t at a given constant temperature T is:

$$n = n_o \exp\left(-s t \exp\left(-\frac{E}{kT}\right)\right) \qquad (11)$$

From equation 11 the time required to drain half of the filled traps (the half-life of the trapped electrons) is found to be:

$$\tau_{\frac{1}{2}} = \frac{\ln 2}{s} \exp\left(\frac{E}{kT}\right) \qquad (12)$$

Equation 12 shows clearly the strong dependence of the half-life of the trapped electrons on the trap depth E and the storage temperature. This temperature dependency is an important characteristic upon which the method of TL dating is based. For a phosphor stored at room temperature, half-lives for shallow traps can be found to be as short as a few seconds, while for the deepest traps the half-life can be as long as many millions of years.

The chief characteristics of the variation of thermoluminescence with temperature equation 9 when E is single valued, are summarised by Garlick

and Gibson as follows:

1. For given values of s, n_o, and β the peak temperature T^* at which the maximum emission occurs is proportional to the trap depth E.

2. For given n_o and E, the peak maximum T^* moves to higher temperatures as s decreases or β increases. This also makes the peak sharper and therefore higher.

3. In all cases the area under the emission-temperature curve is proportional to the number of electrons initially trapped before warming begins (n_o). However, the actual shape of the emission curve is independent of n_o which also means that the height of the curve at any point is proportional to n_o.

4. The initial rise of the TL curve is exponential with temperature following the simple relation:

$$I = n_o s \exp(-E/kT) \qquad (13)$$

This is the basis of the initial-rise method for trap depth E determination and has been used in this work (see Chapter VI).

1.2.2 Garlick-Gibson theory.

In this theory the retrapping effect was considered and second-order kinetics used. The theory assumes that the electrons, freed from their traps by warming the phosphor, can either be retrapped or may recombine during their movement in the crystal of the luminescent phosphor. Also, according to this theory, an electron escaping from a trap has the same probability of being retrapped as it has of recombining with an empty luminescence centre. This theory deals with traps of single energy depth E and one type of emission centre at which recombination occurs.

If the number of trapped electrons is n per unit volume and the total

number of traps is N, then there will be (N-n) empty traps available for re-trapping and n empty luminescence centres also available for recombination (the number of electrons in the conduction band at any instant is assumed to be small compared with n during the thermoluminescence). Hence, the probability that an escaping electron will recombine with an empty luminescence centre and not be retrapped is given by:

$$\frac{n}{(N - n) + n} = \frac{n}{N} \tag{14}$$

and

$$I(T) = -\frac{dn}{dt} = \frac{n}{N} \cdot n\, s \exp(-E/kT) \tag{15}$$

where the rate of escape of trapped electrons from the traps during thermoluminescence process is the same as in the first order kinetics, namely $n\, s \exp(-E/kT)$.

Using equation 15, the decay of TL at a fixed temperature is found to be:

$$I = n_o^2\, s \exp(-\frac{E}{kT}) / N \left[1 + (\frac{n_o}{N})\, s t \exp(-\frac{E}{kT}) \right]^2 \tag{16}$$

where n_o is the original number of trapped electrons, i.e. the value of n at t = 0. The equation is simplified if the traps are saturated at the commencement of decay. That is, if $n_o = N$, the equation 16 becomes:

$$I = N s \exp(-\frac{E}{kT}) / \left[1 + s t \exp(-\frac{E}{kT}) \right]^2 \tag{17}$$

If the phosphor is warmed at a uniform rate β after excitation at low temperature, then the TL variation with temperature, in the case when the retrapping effect is considered, is given by:

$$I = n_o^2\, s \exp(-\frac{E}{kT}) / N \left[1 + \frac{n_o}{N} \int_o^T \frac{s \exp(-\frac{E}{kT})}{\beta} dT \right]^2 \tag{18}$$

The properties of equation 18 have been summarised by Garlick and

Gibson (1948) as follows:

1. For fixed values of s, n_o, and β the temperature at which the emission reaches its maximum is proportional to the electron trap depth E. For saturation of the traps ($n_o = N$) and the same values of s, equations 9 and 18 give maxima at the same temperature.
2. For given n_o and E, the peak temperature T^* increases as β increases or s decreases, in the same way as for the case when retrapping is absent.
3. In all cases the area under the emission-temperature curve is proportional to the number of electrons (n_o) initially trapped. However, the actual shape of the curve is dependent on n_o as shown by equation 18. This is essentially different from the case when retrapping is negligible.
4. The initial rise of the curve before peak emission is reached is given by the following relation which can be derived by setting the integral part in equation 18 equal to zero, namely:

$$I = \frac{n_o^2}{N} s \exp\left(-\frac{E}{kT}\right) \qquad (19)$$

Comparing this equation with equation 13 it is seen that the power of n_o is different in the two equations, the exponential term being identical. This provides a further means of experimental correlation with theory.

The retrapping has important effects on the applications of TL for dosimetry and dating purposes. Due to the retrapping, the peaks shift towards higher temperatures and peak half-widths are increased. Furthermore, the peak height is not linearly dependent on the number of filled traps. Retrapping also affects the decay of the TL peak at constant temperature, with the decay becoming non-exponential and slower. Because of these effects the TL peak height or glow area versus dose curves used in dating

and dosimetry will be inaccurate, so that extrapolated doses will also be inaccurate. This can be more complicated when there are more than one kind of trap with different number densities and cross sections for charge carrier capture and subsequent recombination. This is usually the case in materials which are commonly used in dating and dosimetry.

1.3 Methods for the determination of TL parameters.

Knowledge of the thermoluminescence parameters, namely the trap depth E(eV) and the frequency factor s(sec^{-1}) are vital (see Chapter VI). Several methods have been developed for the determination of these parameters which are described in various papers (see, for example, Braünlich, 1968). In this section three commonly used methods for the determination of E and s values are described, with the emphasis given to the initial-rise method.

1.3.1 Hoogenstraaten's method.

This method (Hoogenstraaten, 1958) depends upon the relationship which exists between E, s, the peak temperature T^*, and the heating rate β. The relation between these variables was found to be (see equation 10):

$$\frac{E}{kT^{*2}} = \frac{s}{\beta} \exp\left(-\frac{E}{kT^*}\right)$$

and hence:

$$\ln\left(\frac{T^{*2}}{\beta}\right) = \frac{E}{kT^*} - \ln\frac{sk}{E} \qquad (20)$$

Thus a plot of $\ln\frac{T^{*2}}{\beta}$ versus T^{*-1} is linear and has a slope $\frac{E}{k}$. The frequency factor s can be determined from the intercept of this line on the $\ln\left(\frac{T^{*2}}{\beta}\right)$ axis. The intercept is equal to $-\ln\frac{sk}{E}$, where k is the Boltzmann Constant.

This method is applied for glow peaks obeying the first order kinetic

only since it is based upon the theory of Randall and Wilkins (1945).

The experimental procedure is to monitor the change in the peak temperature T^* as a result of the change in the heating rate β. This method is limited by the capacity of the TL apparatus, since to change the peak temperature by a measurable amount requires varying the heating rate over a wide range. Also, even assuming that the equipment available can provide a wide range of heating rates, the method cannot achieve accuracy better than 20 or 30% in E. This is due to the fact that the peak temperature varies very slowly with the heating rate (Curie, 1963) and overlapping of different peaks makes the method impossible to use in most materials.

1.3.2 Isothermal decay method.

This method is also based on the first order kinetics theory of Randall and Wilkins (1945). From this theory we can have (see equation 11):

$$n(t) = n_o \exp(-s\,t \exp(-\frac{E}{kT}))$$

where n_o is the initial number of trapped electrons immediately after the irradiation is ended (i.e. at $t = 0$). $n(t)$ is the surviving number of trapped charges after keeping the phosphor at a constant annealing temperature, T, for time t.

Equation 11 can be written as follows:

$$\frac{-\ln n/n_o}{t} = s \exp(-\frac{E}{kT}) \qquad (21)$$

The left-hand term of the above equation is equivalent to the decay constant λ of a simple nuclear decay, that is:

$$\lambda = \frac{1}{\tau} = \frac{-\ln n/n_o}{t} \qquad (22)$$

Then equation 21 can be re-written as:

$$\ln\left[\frac{-\ln n/n_o}{t}\right] = \ln s - \frac{E}{kT} \qquad (23)$$

or

$$\ln \lambda = \ln s - \frac{E}{kT} \qquad (24)$$

The experimental procedure of this method involves the determination of the ratio n/n_o for different holding periods at a constant annealing temperature. The same procedure is then repeated for other annealing temperatures. The ratio n/n_o can then be plotted against the storage time t for each annealing temperature on a semi-log scale. The half-life of the trapped electrons can be determined from the slope and hence the mean-life time τ at that temperature can be determined. The decay constant λ can then be calculated for each temperature and λ plotted against $\frac{1}{T}$ on a semi-log scale to give a straight line, the slope of which is equal to-E/k; the y intercept will give s.

The isothermal annealing decay method for the determination of TL parameters has the following disadvantages.

1. It is a lengthy method. It also requires the control of more than one variable such as the annealing temperature and the annealing time and also the calculation of E depends upon the experimental determination of the mean-life values which might give rise to error.
2. It requires a large amount of material which is not always available, particularly in the case of lunar and meteorite samples.
3. It is highly dependant on the order of kinetics for the decay of a peak. Since the order of kinetics is usually not easy to determine, the decay curves cannot be readily used for E determination.

1.3.3 Initial-rise method.

The initial-rise method was first suggested by Garlick and Gibson (1948)

as a means of determining the energy depths of the traps of a TL phosphor. Since then this method has been used successfully to measure the energy depths of the traps for a large number of materials such as lunar and meteorites Christodoulides, 1972; Durrani et al, 1972a; Wintle, 1974).

This method is based on the fact that at temperatures far below the peak temperature T^*, the initial rise of the TL intensity is found to be proportional to the factor $\exp(-\frac{E}{kT})$. This result is found to be true regardless of the order of the kinetics involved. Provided the temperature T is much lower than T^* (peak temperature as given by equation 10), the integral part of equations 9 and 18 which account for the fraction of traps emptied as a result of heating the sample up to temperature T, can be neglected. Then equation 9, which is based on the first-order kinetics (Randall and Wilkins, 1945), reduces to:

$$I(T) = -\frac{dn}{dt} = n_o s \exp(-\frac{E}{kT}) \qquad (25)$$

Similarly equation 18 which was derived from the second-order kinetics reduces to:

$$I(T) = \frac{n_o^2}{N} s \exp(-\frac{E}{kT}) \qquad (26)$$

In both the above cases a plot of Log I versus $\frac{1}{T}$ yields a straight line with slope of $-\frac{E}{k}$ from which the E value can be determined.

The experimental procedure involves a subsequent heating followed by cooling to room temperature, which leads to a series of initial rise curves. Each initial rise curve is plotted on a logarithmic scale against $\frac{1}{T}$. The linear part of each curve has a slope of $-\frac{E}{k}$. The values of E found from the slopes can be plotted against the average temperature of the range used for finding the energy. The initial rise method should yield E values which

form groups corresponding to the number of glow peaks constituting the glow curve (see Figures 6.8a and 6.8b, Chapter VI). The temperature of each peak can be determined by a separate experiment such as the thermal cleaning which has been used to resolve the peaks of the lunar samples glow curves (Nicholas and Woods, 1964). Knowing E, T^*, and β, equation 10 can be used for the determination of the frequency factor s, assuming first-order kinetics. The advantages of the initial rise method, which has made it highly competitive as a means of determining the energy depths of the traps, are:-

1. The evaluation of E is independent of the order of the kinetics involved.
2. Quite a large number of energy measurements can be made on as much material as needed for one glow curve.
3. The method can be used for the determination of E values regardless of the heating rate, linear or not.

For these advantages the initial-rise method was chosen during this work for the determination of the energy depths of the traps in some lunar samples (see Chapter VI).

CHAPTER II

APPARATUS AND EXPERIMENTAL PROCEDURE

2.1 TL Appartus.

The thermoluminescence measurement equipment consists of three major parts. These parts are: heating system, light detection system and recording system. A block diagram of the apparatus is shown in Figure 2.1.

2.1.1 Heating system.

In this work, samples were heated on a tantalum strip of dimensions 14 cm x 2.5 cm x 0.025 cm. The choice of the material for the heating strip was governed by restrictions placed upon the amount of available power. Calculations made for tantalum as well as for other possible materials, e.g. copper, nickel, iron and graphite, (Prachyabrued, 1972), revealed that the power consumption of a tantalum strip was well within the range available. The strip is enclosed in a light-tight cylindrical chamber. The chamber is made of brass. The radius and the height of the chamber are 10 cm and 5 cm respectively. During measurements, oxygen-free nitrogen at constant pressure is flushed through the chamber in order to avoid chemiluminescence and oxidation of the tantalum strip (Aitken et al, 1967).

The temperature of the strip is measured by a nickel-chromium/nickel-aluminium thermocouple, spot-welded on its under side.

The temperature of the strip can rise from room temperature to about 600^{o}C by passing an electric current through it. The heating rate can be varied from 0.1^{o}C/sec to 90^{o}C/sec with consistent linearity better than 3%. The heating rate which was used throughout this work was 3.6^{o}C/sec. The

Block Diagram of the TL Apparatus

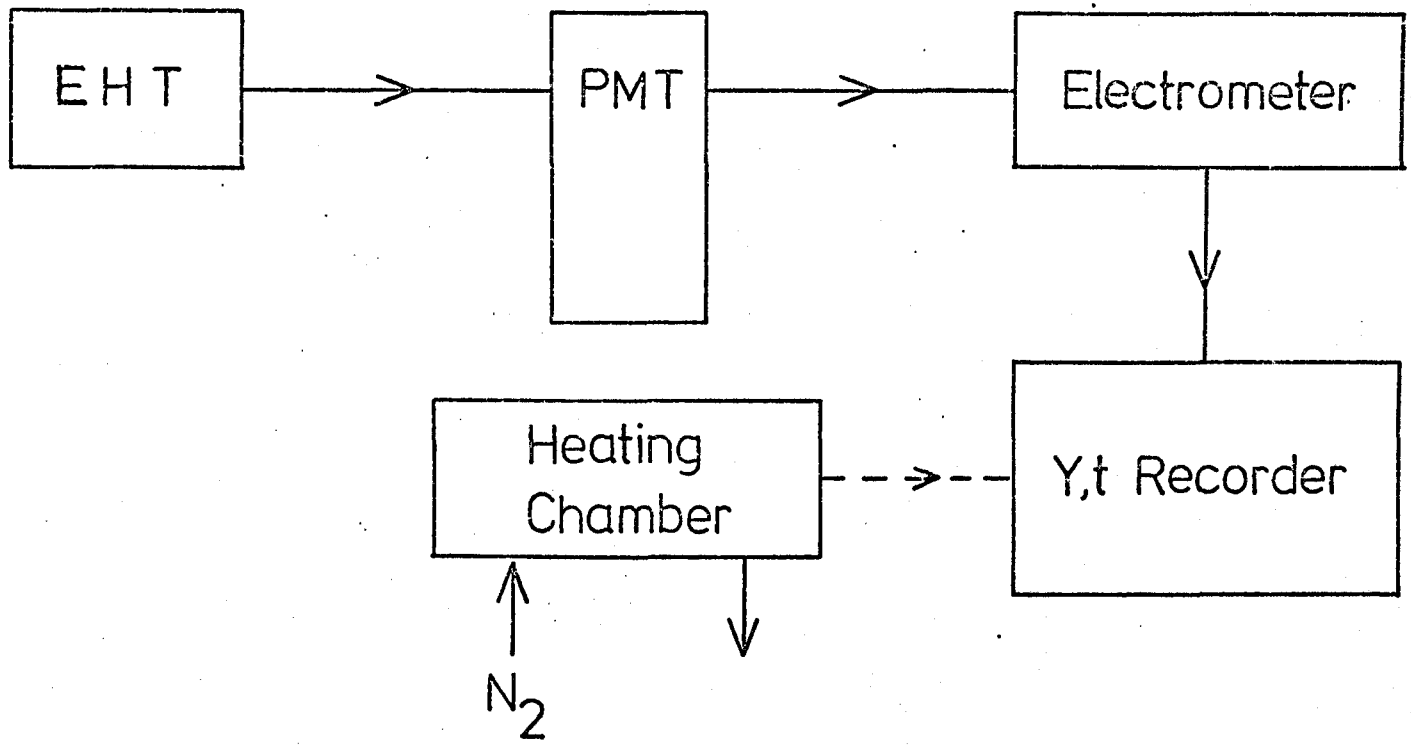

Fig 2·1

linear heating rate was maintained automatically by a comparator amplifier. The e.m.f. developed across the thermocouple is compared by means of an operational amplifier with a reference voltage from a ramp generator. The difference between the thermocouple e.m.f. and the reference voltage is amplified and subsequently used to activate a thyristor firing unit which in turn fires a 'triac' for an appropriate duration of time to supply the necessary power to the heating strip. The system is described in detail, together with the electrical circuits, in Prachyabrued, 1972. A schematic diagram of the temperature controller is shown in Figure 2.2.

2.1.2 Light detection system.

The thermoluminescence light which is emitted from the sample was usually detected, during the course of this work, by means of EMI photo-multiplier (P.M.) tubes, types 6256SQ and 9804QB. Both P.M. tubes were supplied with quartz windows. These tubes were selected for their low dark current at room temperature which is typically 0.5nA. The P.M. tube is housed in a thermoelectrically cooled P.M. tube housing unit type TE-102TS, Serial No. 1-70-2, (Products for Research Inc., 78 Holten Street, Danvers, Massachusetts 01923.) The housing unit was designed to cool the P.M. tube cathode to at least -20°C, stable to $\pm$ 0.50°C, in a maximum ambient temperature of 22°C. This allows one to work with very low signal levels where the signal currents are of the order of nA(10^{-9}A). The tube operates with its photocathode at a potential of -1200V in the case of the 6256SQ type and -1000V in the case of the 9804QB type with respect to common earth. The potential difference developed across a resistor, due to the flow of anode current through it, was amplified by a sensitive electrometer (model 600B, Keithley Instruments Ltd.). The electrometer

Block Diagram
of the Temperature Controller

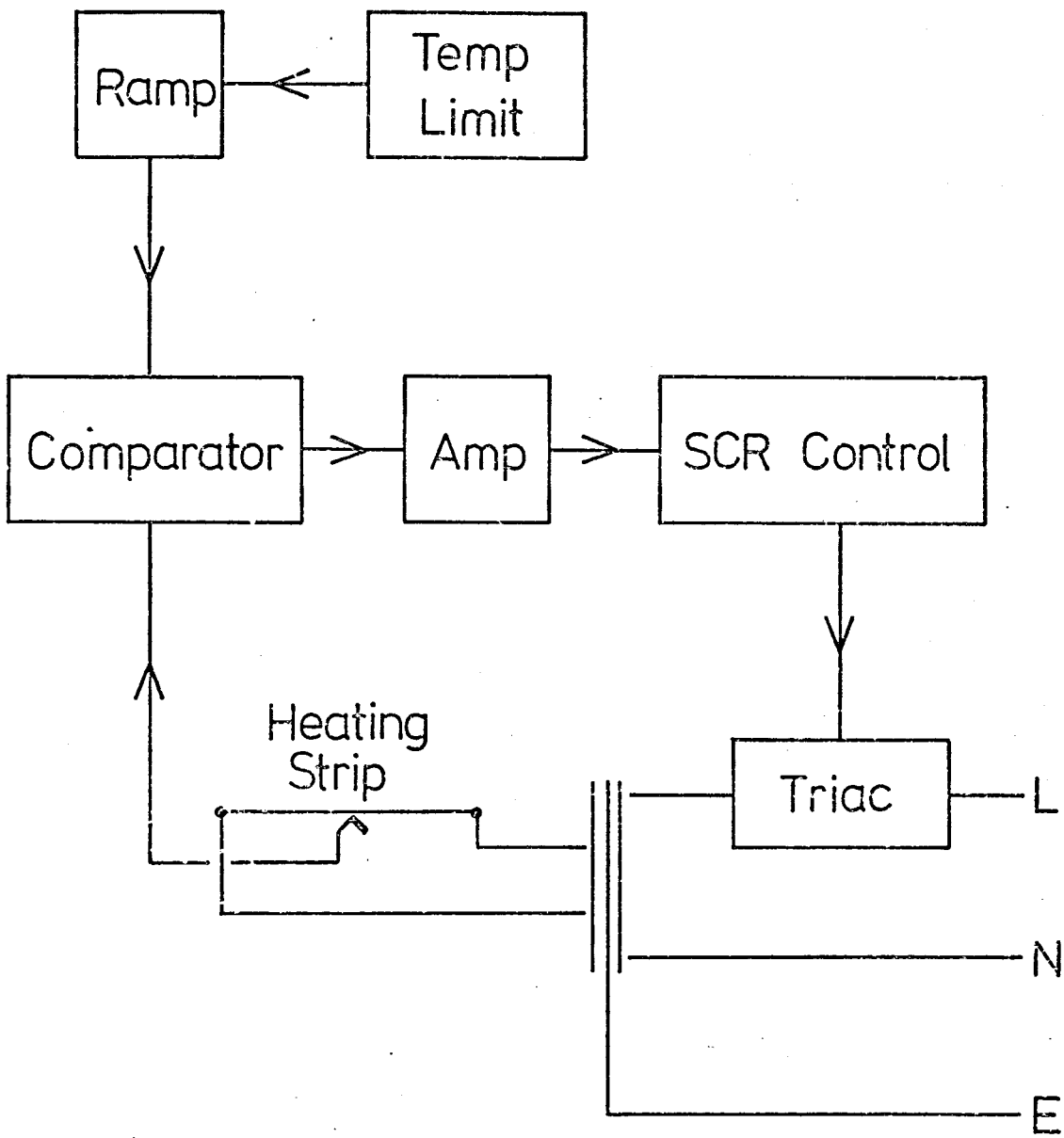

Fig 2·2

output was fed into a two-channel potentiometric chart recorder. The recorder registers the electrometer output as a function of time. A silica window and Ilford "Bright Spectrum Blue" filter No. 622, transmission band (375-530 nm) were inserted between the photomultiplier tube and the sample to protect the P.M. tube from the heat and to reduce interference from black-body radiation. A polished aluminium reflecting cone open at both ends and positioned over the sample was used to limit the amount of black-body radiation received by the photomultiplier tube by limiting the area of the strip visible. From the time to time the P.M. tube gain was checked by utilising a betalight source which consists of a sealed glass tube coated internally with a zinc sulphide and filled with tritium gas. The source was embodied inside a perspex disc to avoid damage and permit easy handling. The betalight source was made by SRDL (Saunders-Roe Development Ltd., Hayes, Middlesex, England) and encapsulated in perspex by K. Stammers. For the purpose of obtaining the TL emission spectra of some phosphors, a set of 'BALZERS' B-40 interference filters was occasionally used. The transmission characteristics of these filters together with the quantum efficiency of the P.M. tubes 6256SQ and 9804QB versus light wavelength are shown in Figures 2.3 and 2.4.

2.1.3 Recording system.

The P.M. tube current output was measured by a Keithley 600B electrometer. The electrometer provides an output of 1 volt for full-scale deflection. The recorder used was a y-t two-channel potentiometric recorder Servoscribe 2 (Smiths Industries Ltd.). The time was plotted along the t axis and the P.M. tube output along the y axis. As the temperature is known to be changing linearly with time, it was possible, therefore,

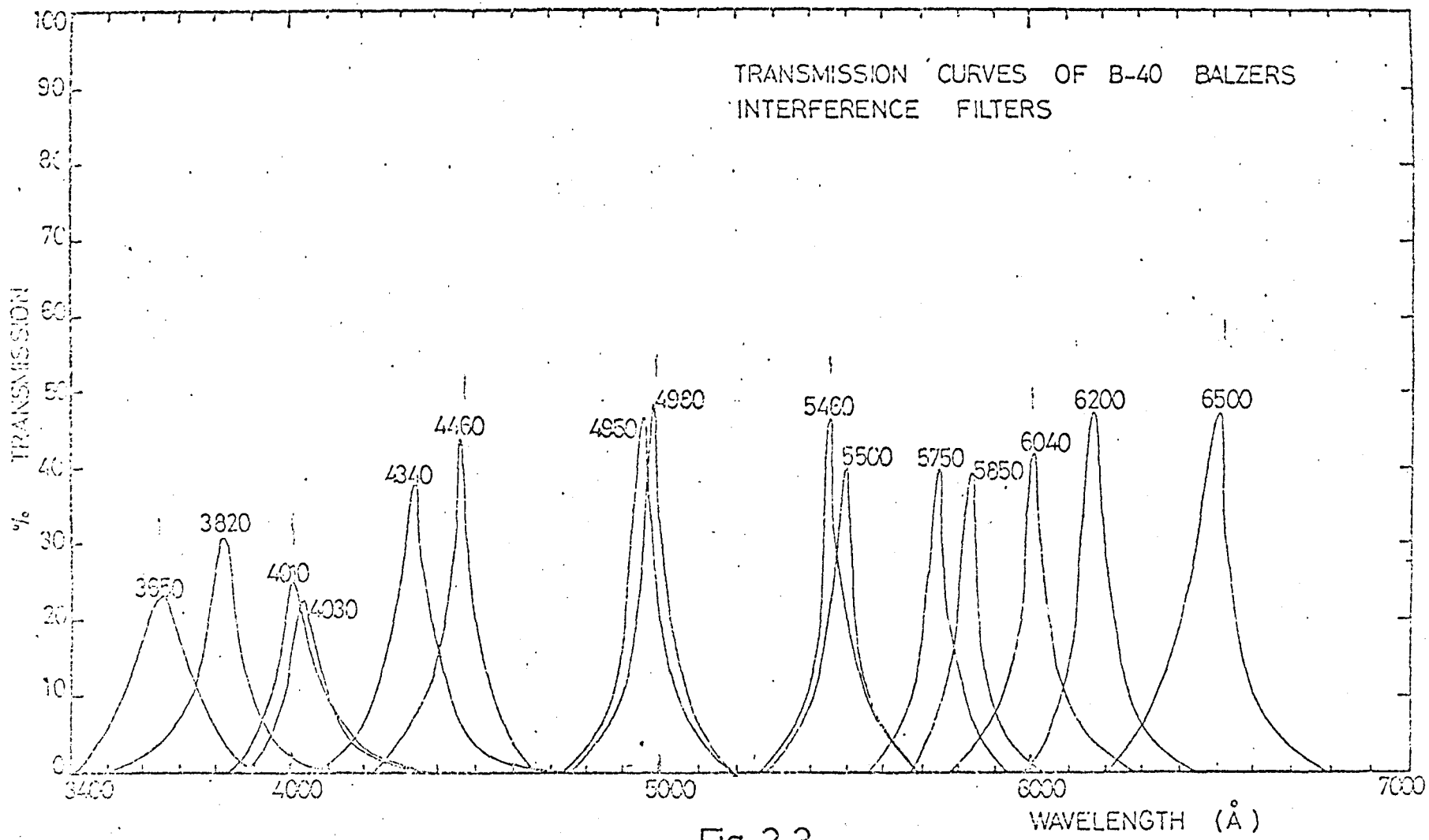
TRANSMISSION CURVES OF B-40 BALZERS
INTERFERENCE FILTERS
% TRANSMISSION
100
90
80
70
60
50
40
30
20
10
0
3400
4000
5000
6000
7000
WAVELENGTH (Å)
3650
3820
4030
4340
4460
4950
4980
5460
5500
5750
5850
6040
6200
6500

Fig 2·3

PM Tube Responses

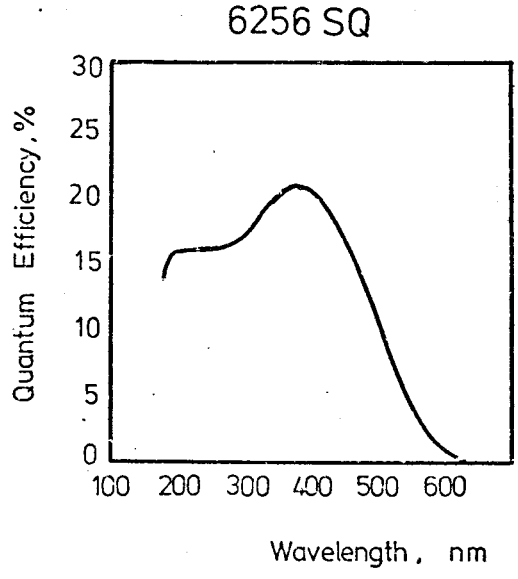

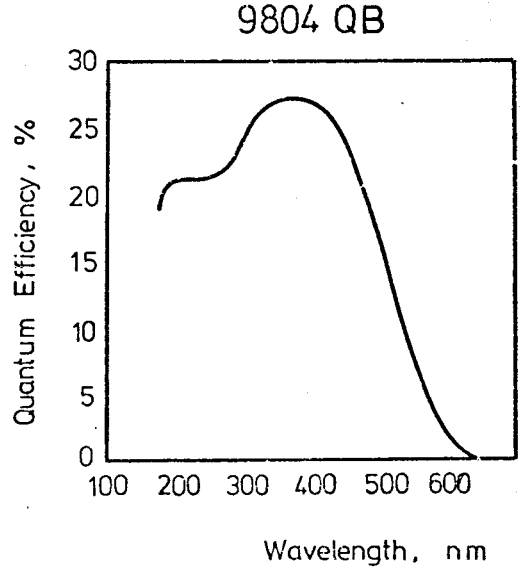

From EMI publication ref. p001S/a72

Fig 2·4

to have an indirect plot of TL output versus temperature.

2.2 Irradiation Facilities.

2.2.1 Beta irradiation.

Irradiation with beta particles during this project was performed using a 0.5 Curie Strontium-90 beta source. The source was made and calibrated by the Radiochemical Centre, Amersham, England, the Strontium-90 powder being uniformly rolled between two silver plates. The thicker plate of the sandwich source is used for backing support and the thinner one of 0.04 mm thickness is used as the front surface of the source to cut off the weak beta particles emitted from the Strontium-90. This plane source has an active area 1 x 2 cm^2. The isotope Strontium-90 is a pure beta emitter with a maximum energy of 0.54 MeV. Its daughter nuclide, Yttrium-90, emits beta particles with energies up to 2.27 MeV.

The source is mounted at a fixed position inside a 0.625 cm thick brass box with a shutter which is made of the light alloy, duralumin. Samples can be irradiated at a known distance from the surface of the source. This set-up can be seen in Figure 2.5.

The dose rate at four different distances from the surface of the source was determined (Hwang, 1972) using film badges as dosimeters, for the purpose of the dose rate determination. The film badges were analysed by the Radiological Protection Service Unit and the dose rate was measured by the darkening of the emulsion (see Figure 2.6).

The beta source has also been calibrated independently by Dr. K.V. Ettinger (Hwang, 1972) using a miniature ionization chamber. The results were found to be in excellent agreement with the film badge results.

Beta Source Container

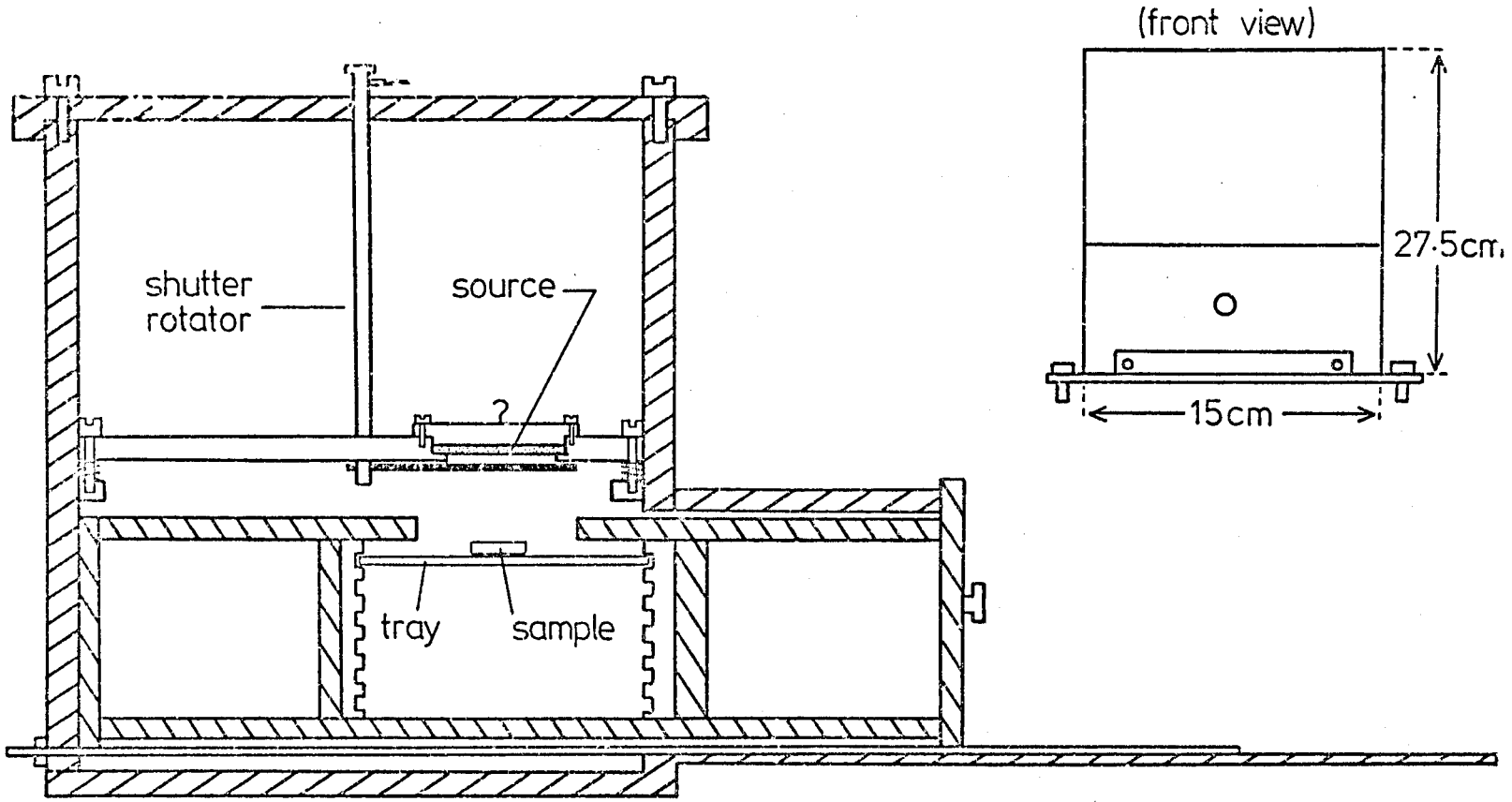

Fig 2·5

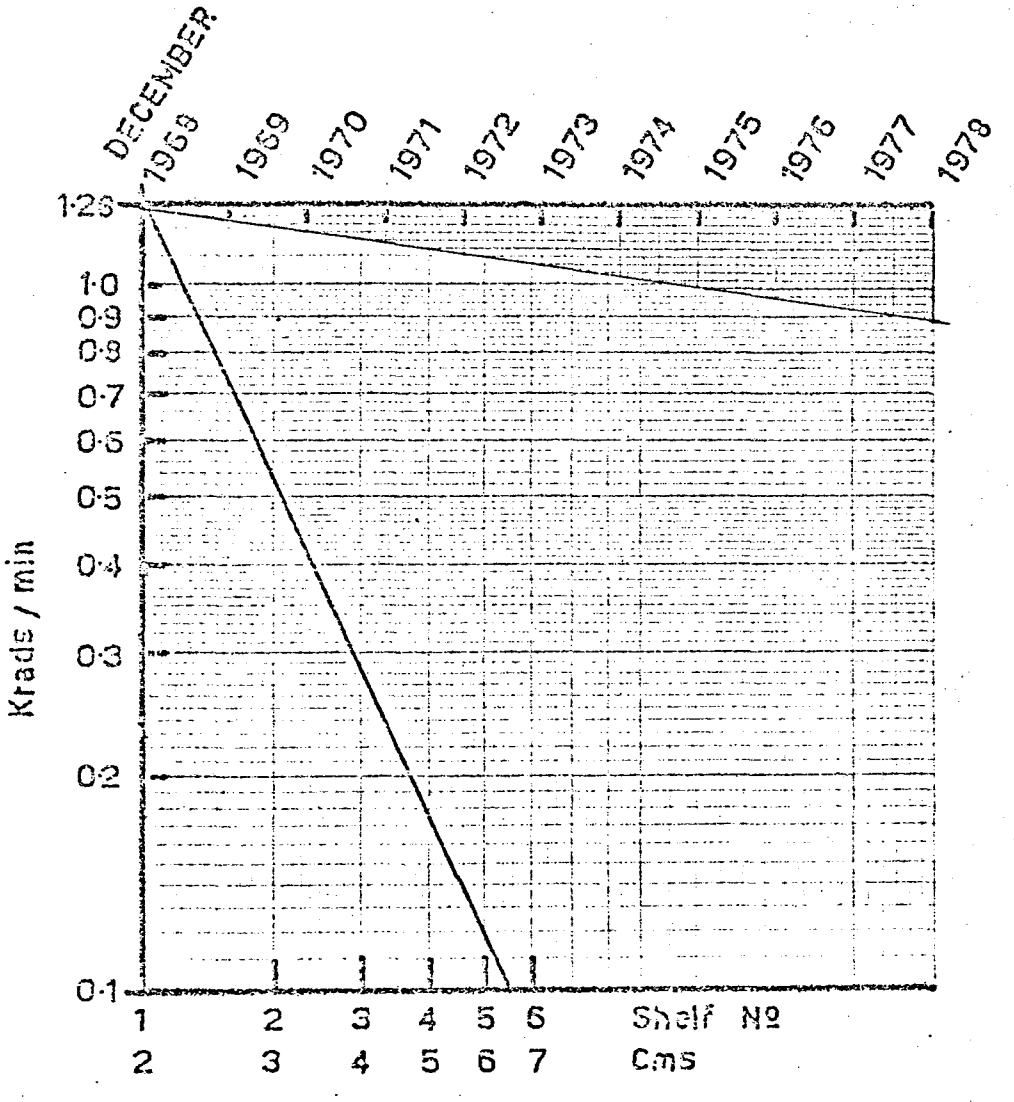

β Source Dose Rate

Fig 2·6

2.2.2 Gamma irradiation.

Gamma irradiation was used extensively during the course of this work. The irradiation with gamma-rays was performed with the aid of a ^{60}Co gamma source situated in the Radiation Centre, University of Birmingham. The strength of the ^{60}Co source used was 5000 Curies in September 1973, reduced to 3500 Curies in July 1976 through decay.

The dose rate measurements were made by Dr. P. Fowles of the Radiation Centre. These measurements were done at various distances from the source along the axis of the irradiation chamber situated in the centre of the source unit. The dose rates varied considerably with the distance from the source. According to the dose rate measurements made on 1st July, 1976, the dose rates vary from 2Mrad/hr at 0.5 cm from the source to $\sim$ 27krad/hr at 38 cm. The dose rates used during the course of this project ranged from 800krad/hr to 500krad/hr. Lower dose rates were occasionally used for the purpose of studying the effect of dose rates upon the TL sensitivity of quartz.

The irradiation with gamma-rays gives rise to the problem of achieving electronic equilibrium throughout the irradiated sample. For irradiation with ^{60}Co gamma-rays (1.25 MeV average), a minimum of 450 mg/cm^2 build-up thickness must be placed before the target to build up the free electron density to its equilibrium value inside the target (Johns, 1961). Consequently, if a TL sample without the necessary amount of build-up material is irradiated by a photon beam (x-rays, γ-rays), the average dose received is somewhat less than it would be under equilibrium conditions.

To obtain electronic equilibrium, all samples were irradiated in cylindrical aluminium containers of wall thickness 3.3 mm and internal

diameter of 6.2 mm. This thickness of 900 mg/cm^2 reduces the dose rates by 5% (Christodoulides, 1972).

2.2.3 X-ray irradiation.

The X-ray irradiation was carried out using the X-ray set located in the Radiation Centre, University of Birmingham. The X-ray set is a Pantak constant potential industrial radiography unit modified to reduce output fluctuations by stabilising the main supply and the tube current. Both voltage and current are continuously variable up to maxima of 300kV and 12mA. The set also includes a three-range automatic timer and an automatic exposure shutter. The latter permits the operator to set voltage and current before exposing the sample. The shutter can be removed in the case of a very high dose rate requirement for samples small enough to go into the unshielded re-entrant region of the tube shield.

The tube generates up to 3.6 kW and is cooled by circulating oil through the tube shield and an oil-to-water heat exchanger. The cooler is on a separate mains supply so as to allow the cooling of the tube for a minute or so after completion of an experiment.

The sample table provided is aligned horizontally to a good degree of accuracy. The table slides up to approximately 2 metres to allow for a range of exposure distances. The radiation output obeys the inverse square law and can be expressed (Fowles, 1976) by:

$$R = \frac{R_o}{(x + d)^2}$$

where R_o (Roentgen min^{-1}) is the exposure rate at one metre from the focus, d is the distance (m) from the shutter front plate and x is the distance (m) of the focus from this plate (= 17.8 cm by extrapolation). The equation

gives central axis exposure rates (Roentgen min^{-1}) in air, which can be converted to rads by using the appropriate multiplying factor. The maximum dose rate which can be obtained with unfiltered radiation by removing the shutter is about 700krad/hr.

2.2.4 Proton and Helium-3 irradiation.

Protons and Helium-3, at energies of 10 and 30MeV respectively, were used during the course of this project (see Chapters III and V). The irradiations were carried out using the Department of Physics 1.50m Nuffield cyclotron. The cyclotron is capable also of providing deuterons and alpha particles at energies of 10MeV per nucleon. The Nuffield cyclotron is capable also of producing fast neutrons of maximum energy of 7MeV by bombarding a lithium target with 10MeV protons. The mean energy is about 2.2MeV and the yield is $\sim 2 \times 10^{10}$ n μA^{-1} sec^{-1}. Bombarding a beryllium target with 30MeV Helium-3 particles will yield about 6×10^{10} n μA^{-1} sec^{-1}, with a mean energy of $\sim$ 8MeV and with a maximum of 35MeV.

A charged particle current of 2μA was used in both proton and Helium-3 irradiations. All the irradiations were carried out in vacuum and the sample holder was cooled by circulating water.

2.3 X-ray Techniques for Structural and Compositional Studies.

2.3.1 The production of X-rays.

X-rays are generated when electrons, travelling at high speeds, collide with the atoms of a target. Broadly speaking, two types of interaction occur and these result in two types of X-ray spectra: continuous and characteristic (Nuffield, 1966).

The characteristic spectra are produced when the bombarding electrons have sufficient energy to penetrate to the interior of the atoms of the target and to strike and displace a tightly bound electron deep in the atom near the

nucleus, thereby ionising the atom. When a particular inner shell of an atom has been ionised in this manner, an electron from an outer shell may fall into the vacant place, with the resulting emission of X-rays characteristic of the atom involved.

A high-speed electron may be slowed down in passing through the strong electric field near the nucleus of an atom. The decrease in energy ΔE of the electron appearing as an X-ray photon of frequency ν as given in Einstein's equation:

$$h\nu = \Delta E$$

in which h is Planck's constant. In this case, the produced X-radiation is independent of the nature of the atom being bombarded and appears as a band of continuously varying wavelength whose lower wavelength limit is a function of the maximum energy of the bombarding electron. Hence, a continuous spectrum is produced.

2.3.2 X-ray fluorescence technique.

The content of the major elements in Oklo materials (see Chapter V) were determined by using the X-ray fluorescence technique. The basis of X-ray fluorescence and its use for elemental analysis is as follows.

The absorption of X-rays by an element gives rise to the excitation of the atoms of that element which is followed by the generation of secondary radiation. The secondary radiation is characteristic of the absorbing element. When an element is generating X-radiation in this manner it is said to be fluorescencing; the secondary radiation is usually called fluorescent radiation.

The fluorescence is a useful tool in X-ray spectroscopy. In this method of elemental analysis the sample is bathed in a beam of X-radiation. The

K and/or L spectra of the elements are thereby excited and the sample fluorescences. It remains only to determine the wavelength of the characteristic peak in the radiation emitted by the sample and their intensities to identify the elements and to estimate their abundance.

Theoretically if the mass absorption is constant, then a simple linear relationship will exist between fluorescence intensity and element concentration. Following this assumption, the nature of a certain element could be found by using the linear calibration of a 'standard' of the same absorption coefficient. The wide variation in mass absorption coefficients of the Oklo samples made the simple linear calibration unsuitable. This difficulty was overcome by adopting the fusion technique (West et al, 1974).

The Oklo samples were fused in sodium tetraborate with an oxidising agent, sodium nitrate, added. All the fusions were performed in platinum plus gold crucibles in an electric muffle furnace. The apparatus used for bead preparation consisted essentially of a duralumin plunger mounted on a hot plate into which was recessed a duralumin mould. The melt was poured into the mould and the plunger brought down forming a thin bead (0.8 mm thick). The fusion mixture consisted of 0.2 gm sample, 0.4 gm sodium nitrate and 2.5 gm flux. It was thoroughly mixed in a platinum + 5% gold crucible which was then placed in a muffle furnace at 1150°C. After ten minutes, the crucible was quickly transferred to a blast burner (maintained at 1150°C), given a vigorous stir to ensure homogeneity in the melt, and the contents poured into the mould of the bead-making apparatus. The stability of the beads was ensured by annealing for ten minutes at 240°C.

The induced X-ray fluorescence from the beads was collimated and passed on to the analysing crystal which was orientated in such a way that

only the K_a emision of the element to be measured in the specimen was diffracted into the detector. The content of certain elements in the bead was determined by comparing the fluorescence intensity with that of the standard using the calibration lines.

A Philips PW-1212 automatic spectrometer was used in the X-ray fluorescence analysis. The machine is situated in the Department of Geology, University of Birmingham. The machine is connected to an on-line computer and a print-out machine; therefore the analysis is fully automatic after the calibration. This technique is able to detect concentrations of a few parts per million with an accuracy of better than 0.1% for most elements.

2.3.3 X-ray diffraction technique.

The phenomenon of X-ray diffraction by crystals results from a scattering process in which the X-rays are scattered by the electrons of the atoms without change in wavelength (coherent or Bragg scattering). The X-ray diffraction can be produced only when certain geometrical conditions are satisfied which may be expressed in the form of the Bragg law:

$$n\lambda = 2d \sin\theta$$

where λ is the wavelength of the reflected X-radiation, d is the spacing of the reflection planes, θ is the angle of reflection, and n is the order of the diffraction.

The X-ray diffraction pattern of a substance is unique to that substance. For the identification of minerals in Oklo materials, such as quartz, feldspar, etc., the fine powder technique was used. In the case of a mixture of substances each substance produces its pattern independently of the others, so that the photograph obtained with a mixture is the superimposition of the

Page 25 is missing in this thesis.

of that line was calculated by applying the Bragg law. This value of d was compared with those in standard tables which led to the identification of the unknown elements in the sample. The results obtained by this method also showed that there is no evidence of crystalline quartz in the core samples in contrast to the samples from outside the core (see Chapter V).

2.4 The High Temperature Annealing System.

Isothermal annealing at temperatures as high as 900°C was carried out by the aid of the high temperature annealing system available in the thermoluminescence laboratory, Department of Physics, University of Birmingham. The system for high temperature annealing consists of a tubular furnace which is fitted with a vacuum tube relay and controlled by the thermocouple. The whole furnace was made by Johnson, Matthey and Co., England. The tube, which is made of fired clay, is about one foot long and $1\frac{1}{4}$" in diameter. The heating element is a coil wound around the tube and embedded in a good electrical insulator. The power consumption of the heating element is 2,000 Watts and it provides a maximum working temperature of 1350°C. The heating current is controlled by a Ni-Cr/Ni-Al thermocouple which is inserted into the tube with its tip at about the mid-point of the tube. The thermocouple is connected to a temperature indicator and an automatic relay, type 17-90B, both made by Ether Ltd., England, for maintaining the temperature to an accuracy of $\pm$ 2°C.

To avoid inaccuracies due to the temperature gradient which forms along the length of the tubular furnace, the samples were always put at the same position next to the tip of the thermocouple. Also, during the actual annealing period both ends of the furnace were sealed with aluminium foil to prevent temperature fluctuation resulting from draughts.

2.5 The Design and Construction of Low Temperature TL Readout Apparatus.

Following the finding of the effect of the temperature of irradiation on the sensitivity of quartz (Khazal et al, 1975), a TL apparatus was designed and constructed capable of reading out thermoluminescence from samples irradiated at temperatures far below room temperature. The apparatus was designed by the author and constructed in the main workshop in the Department of Physics, University of Birmingham. The newly designed machine is a modified version of the one used at Harwell to study the low temperature thermoluminescence of lunar samples, induced by 160 MeV proton beam (Jahn, 1971). The modifications centred on the sample holder as well as the size and capacity of the machine to maintain the sample at low temperature for a reasonable period of time if needed. In the Harwell-designed apparatus the sample was held in a vertical position to suit the irradiation facilities.

The newly designed apparatus was able to overcome all the disadvantages inherent in the old version; in particular the sample holder was arranged horizontally. It was intended to use this apparatus to study the low temperature TL characteristic of phosphors other than quartz, such as meteorite and lunar samples, feldspar, flint, etc., as well as the effect of the temperature of irradiation upon the TL sensitivity of these minerals (Khazal et al, 1975). The size of the apparatus as well as the small volume of the irradiation chamber in the gamma-ray irradiation unit limited the source of inducing TL to the X-ray set which could be aligned so that the beam is directed at any angle.

A cut-away view of the apparatus is shown in Figure 2.7. It consists

Sectional View of the Low Temperature TL Apparatus

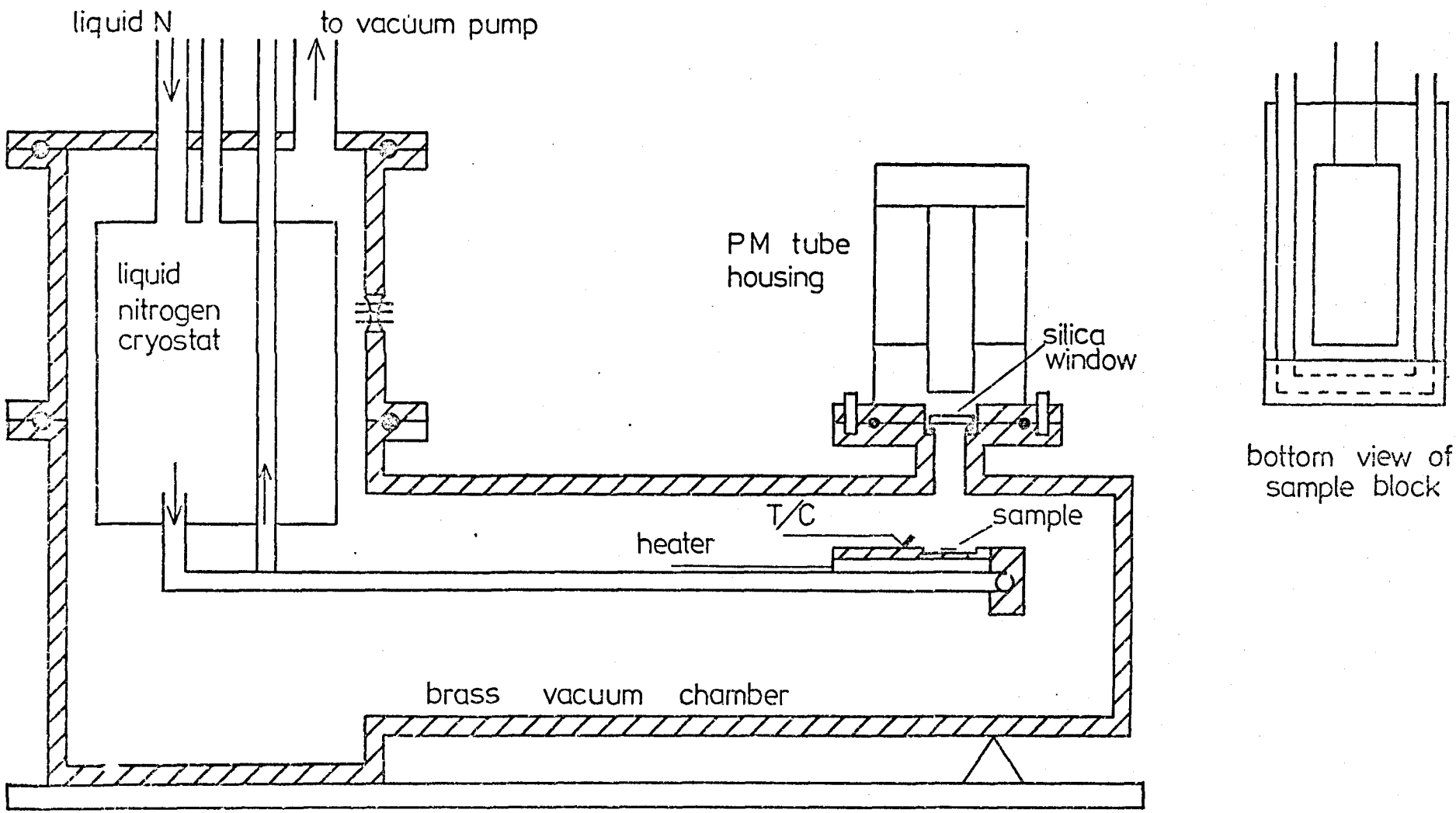

bottom view of
sample block

Fig 2·7

of a liquid nitrogen cryostat and sample holder assembly held inside a vacuum chamber. The cryostat and the pipes which carry the liquid nitrogen are made of stainless steel. The vacuum chamber is made of brass. The cryostat volume is 3.7 litre, which gives liquid nitrogen retention of a few hours to allow the sample to receive a reasonable amount of irradiation if a high dose is needed. It was found that $\sim$ 5 minutes were enough to cool the sample to temperatures as low as -160°C. The cooling of the sample to such low temperatures was achieved by an arrangement which allowed liquid nitrogen to flow through the two stainless steel pipes brazed on to the rear of the copper sample block. On the top surface of the copper sample block a recess of 1 cm in diameter and 0.2 mm deep was cut, into which a sample container could be placed when powder samples were being used. In the case of a sliced sample, the sample was put in contact with a copper block in the middle of the recess. A chromel-alumel thermocouple was soldered next to the groove in order to monitor the temperature of the sample. Between the cooling pipes and beneath the copper sample block a 60 watt heating element was fitted to warm up the sample for the TL readout from the irradiation of $\sim$ -160°C to +300°C. The heating element was connected to a mains rheostat by which the power to the element could be controlled to maintain a given heating rate.

Electrical connections were made to the outside of the vacuum chamber by means of a set of metal pins electrically isolated from each other. The pins unit was soldered to the wall of the part of the vacuum chamber containing the cryostat. This arrangement of the electrical connections enabled one to inspect the sample holder unit when it was needed by taking it out together with the cryostat unit without the need of disconnecting any of the electrical

connections.

On the top of the sample position a P.M. tube, type EMI 9804QB, was located for the detection of the TL light from the sample when the sample was heated. The P.M. tube views the sample through a window 5 cm in diameter covered by a silica disc to seal the chamber during evacuation. Optical filters of dimensions 2" x 2" could be used with the silica disc to select certain wavelengths of the TL light. These filters were rested in a special groove made for this purpose. The output of the P.M. tube was amplified by a sensitive electrometer, model 600B (Keithley Instruments Ltd.) and fed into a single pen recorder, model Oxfored Series 3000, and recorded on chart paper.

The chamber was evacuated to $\leq 5 \times 10^{-2}$ torr by means of a rotary pump, type Speedivac, single stage ISI50, to prevent an ice layer forming on the sample holder and on the chamber surface due to the presence of water vapour. The pressure inside the vacuum chamber was monitored by means of a mercury-filled pressure gauge, model Edwards 'Vacustat'.

CHAPTER III

THE VARIATION OF THE TL SENSITIVITY OF NATURAL QUARTZ WITH RADIATION DOSE USING GAMMA-RAYS AND PROTON IRRADIATIONS

3.1 Introduction and Theoretical Background.

One of the many problems confronting investigators using thermoluminescence (TL) as a means of archaeological and geological dating has been the phenomenon of sensitization of the TL signal by radiation dose, particularly when the TL phosphor being studied in the dating process is quartz (Aitken, 1968; Tite, 1968). The mechanisms of such sensitization are not perfectly understood despite substantial studies of the TL properties of quartz (Yokato, 1953; Medlin, 1963; Schlesinger, 1964; McMorris, 1969 and 1971).

One usually considers that the incident electromagnetic radiation (X- or γ-ray) excites electrons and holes within the crystal. A proportion of these charge carriers is then captured by existing traps. As the radiation dose is increased it follows that the subsequent TL intensity (due to the thermally stimulated radiative recombination of the electrons and holes) will increase until such time as the existing traps become filled and the TL intensity reaches saturation level.

Some results have been obtained, however, which are not in accord with these expectations in as much as the predicted saturation level is not reached. This points to the possibility of the creation (and subsequent filling) of new traps by the incident radiation (Ichikawa, 1968). Such an increase in the concentration of trapping centres beyond the original concentration will result in an increased TL sensitivity for the sample. Further-

more, it has been suggested that extremely high doses of radiation will, after an initial increase in sensitivity, give rise to a sensitivity decrease (Durrani et al, 1975; Shekhmametev, 1973).

The extent to which quartz exhibits TL is related to the presence of impurities within the material giving rise to trapping centres (electron traps) and recombination centres (hole traps) (Schlesinger, 1964; Ichikawa, 1968; Batrak, 1958). The smoky colour induced by radiation in all types of quartz has been shown to be intimately related to the presence of aluminium substitutionally incorporated into the quartz lattice in place of silicon (Halperin, 1963).

O'Brien (1955) was the first to describe this centre in detail. The trivalent Al, substituting for a Si, results in an unpaired electron on an adjacent O atom (Figure 3.1). This unpaired charge is compensated for by the presence of a monovalent positive ion (usually an alkali ion, Na^+ or Li^+) which is in an interstitial position in close proximity to the Al atom. Upon irradiating the sample, electron-hole pairs are created and a hole is localised by the oxygen atom with the unpaired electron, so that the alkali ion is now free to migrate away. The alkali ion migrates along one of the structural channels (e.g. the c-axis [Chentsova, 1956]) until it reaches a captured electron which has become localised at a nearby electron trap (such as substitutional Ge, [Schlesinger, 1964]). In this position the alkali ion now stablises the trapped electron. Upon heating the sample the electron is freed to recombine radiatively with the trapped hole. This results in the characteristic blue TL emission near 300°C, and the Al/alkali centre is reformed.

In this way the Al/alkali centre can be seen to be acting as a recombina-

The Al/Alkali Centre in Crystalline Quartz

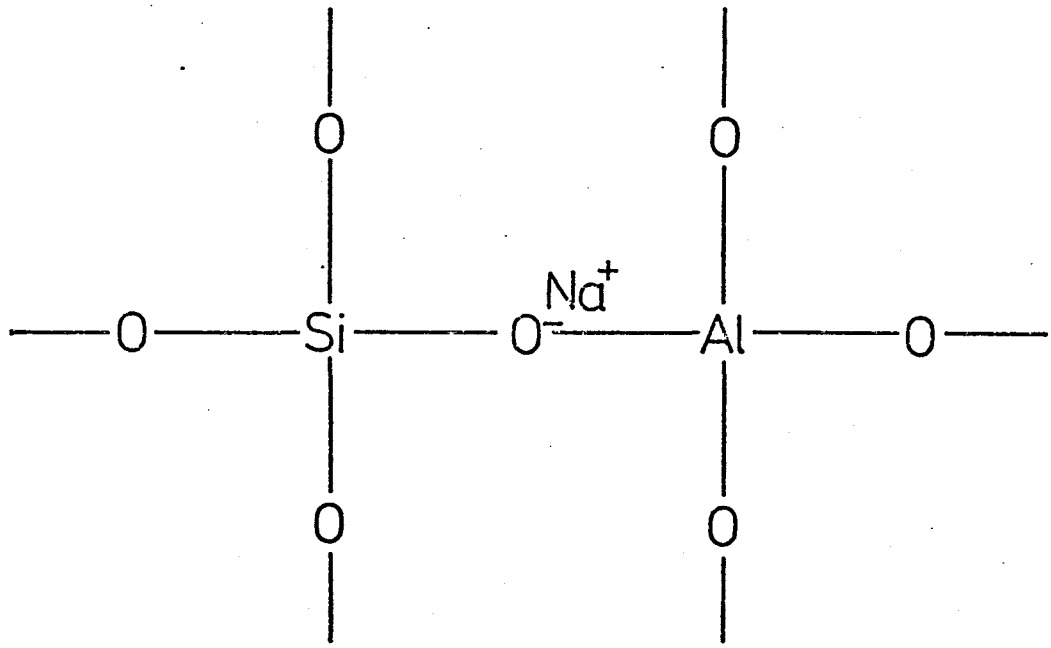

Fig 3·1

tion centre for the electron and the hole. This sequence of events has been confirmed, notably by Mackey (1963) who used Electron Paramagnetic Resonance studies to support the work of Halperin and Ralph (1963) and O'Brien (1955), and it has now become the generally accepted mechanism for TL in quartz (see review by Lell et al, 1966).

Questions arising from these TL studies of quartz include considerations as to how the sensitivity is affected by radiation dose when the traps and recombination centres are associated with impurities. Furthermore, if the radiation is causing structural damage, how is this damage produced by purely electromagnetic radiation such as X-rays or γ-rays ?

It is in the context of these problems that further investigations were undertaken into the TL properties of quartz with a view to understanding the mechanisms of TL sensitisation by dose.

The part of this project which will be described in this chapter was initiated by the finding which will be discussed inChapter V (see also Durrani et al, 1975), namely the failure of some of Oklo samples (core samples) to retain their natural TL and to produce TL artifically by irradiation. This was explained by the radiation damage hypotheses put forward by the author (see Chapter V) which led to a thorough investigation of the change of the sensitivity of natural quartz over a wide range of radiation dose.

3.2 Samples and Sample Preparation.

The samples used in this work were of different types of natural Brazilian quartz (rose, smoky and clear crystals) supplied by Kernowcraft, Truro, Cornwall, England. To achieve a reproducible geometry of the sample, the samples used were in slice form (Göksu and Fremlin, 1972). The slices of 0.5 mm thick were cut from a lump of natural quartz using a

diamond wheel mounted on a Macrotome 2 built by Metals Research Ltd., Melbourne, Royston, Herts., England. The slices were then ground to a thickness of about 150μm using a slurry of 400 grade Carborundum (silicon carbide). All the slices were annealed (unless otherwise stated) at 500°C in an open-tube furnace (see Section 2.4) for one hour to remove their natural TL. After annealing, the slices were polished on both faces using diamond dust on a cloth lap to improve the transmission of the TL emitted from the interior. The polished slices were then cleaned with acetone to remove any grease or dirt marks. Finally, the large clean slices were broken carefully into small pieces of 1-2 mg in weight, which were ready for experimental use.

3.3 General Experimental Procedure.

The apparatus used (see Section 2.1 for details) consisted essentially of a brass chamber in which the samples were heated, in an oxygen-free nitrogen atmosphere, on a 0.025cm thick tantalum heating strip. The constant heating rate (3.6°C/sec) was accurately controlled by a programmable temperature controller.

For normal work the TL output was transmitted through a (375 - 530nm) broad band blue filter and detected by an EM19804QB photomultiplier tube. The output from this was monitored by a Keithley 600B electrometer and graphically displayed on the y-axis of a y-time pen recorder.

For the determination of the emission spectra of the TL light output, the broad-band blue filter was replaced by narrow band Balzer interference filters.

Two methods for obtaining the TL intensity were adopted in this work: namely, measurements of peak height and of the area under the glow curve.

In each case the measured TL output was divided by the sample weight to give the TL intensity in arbitrary units of peak height or glow area per unit sample weight.

When peak heights are used for the TL intensity, it is necessary to isolate each peak appearing in the TL spectrum. The method adopted for this was the technique of 'thermal cleaning', described in detail in Nicholas and Woods (1964). Briefly, the method consists of systematically emptying the traps, the shallowest first, and thus obtaining the rising portions of the individual glow peaks corresponding to each succeeding trap.

In order to define the area under the glow curve when the alternative method of measuring the TL output is used, the area under the glow curve from 240°C to 480°C was taken. (The lower temperature was chosen to reduce any possible effects of thermal fading and the upper temperature was generally where the black-body radiation became appreciable).

Gamma irradiations were performed using the 3500 Curie ^{60}Co gamma source in the Birmingham Radiation Centre, University of Birmingham (see Section 2.2.2). The proton irradiations were carried out on the Nuffield cyclotron in the Department of Physics; the cyclotron provides beams of 10MeV protons.

3.4 Gamma-ray Irradiations.

A typical glow spectrum for gamma-irradiated quartz is seen in Figure 3.2. At least four peaks are evident at approximately 200°C, 260°C, 300°C and 360°C. When this spectrum is resolved by thermal cleaning into its peak components the glow curves of Figure 3.3 are obtained. Four definite peaks are seen at 200°C, 255°C, 275°C and 355°C. The four peaks shown were found to be reproducible in position and relative size. The

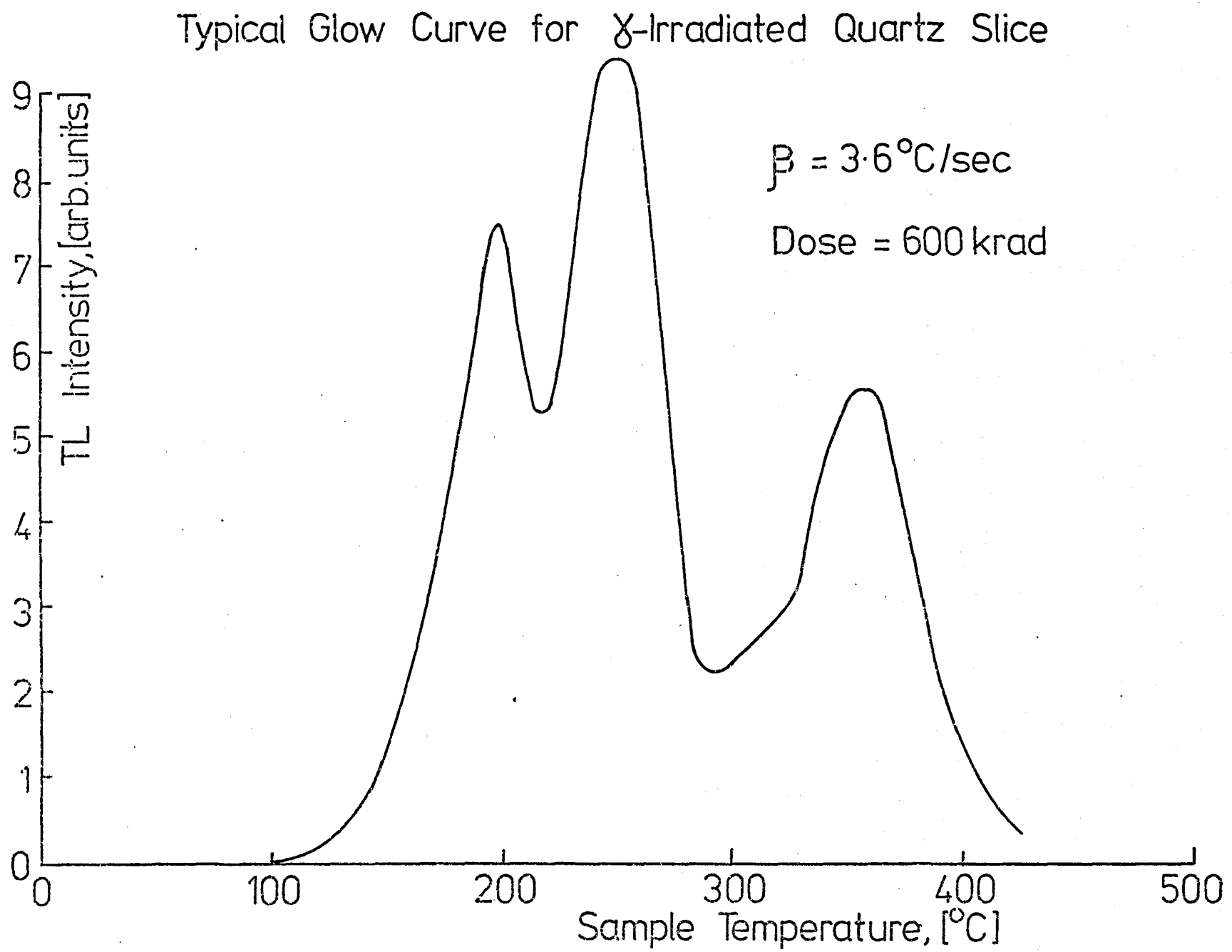
Typical Glow Curve for γ-Irradiated Quartz Slice
β = 3·6°C/sec
Dose = 600 krad
TL Intensity, [arb.units]
0
1
2
3
4
5
6
7
8
9
0
100
200
300
400
500
Sample Temperature, [°C]

Fig 3·2

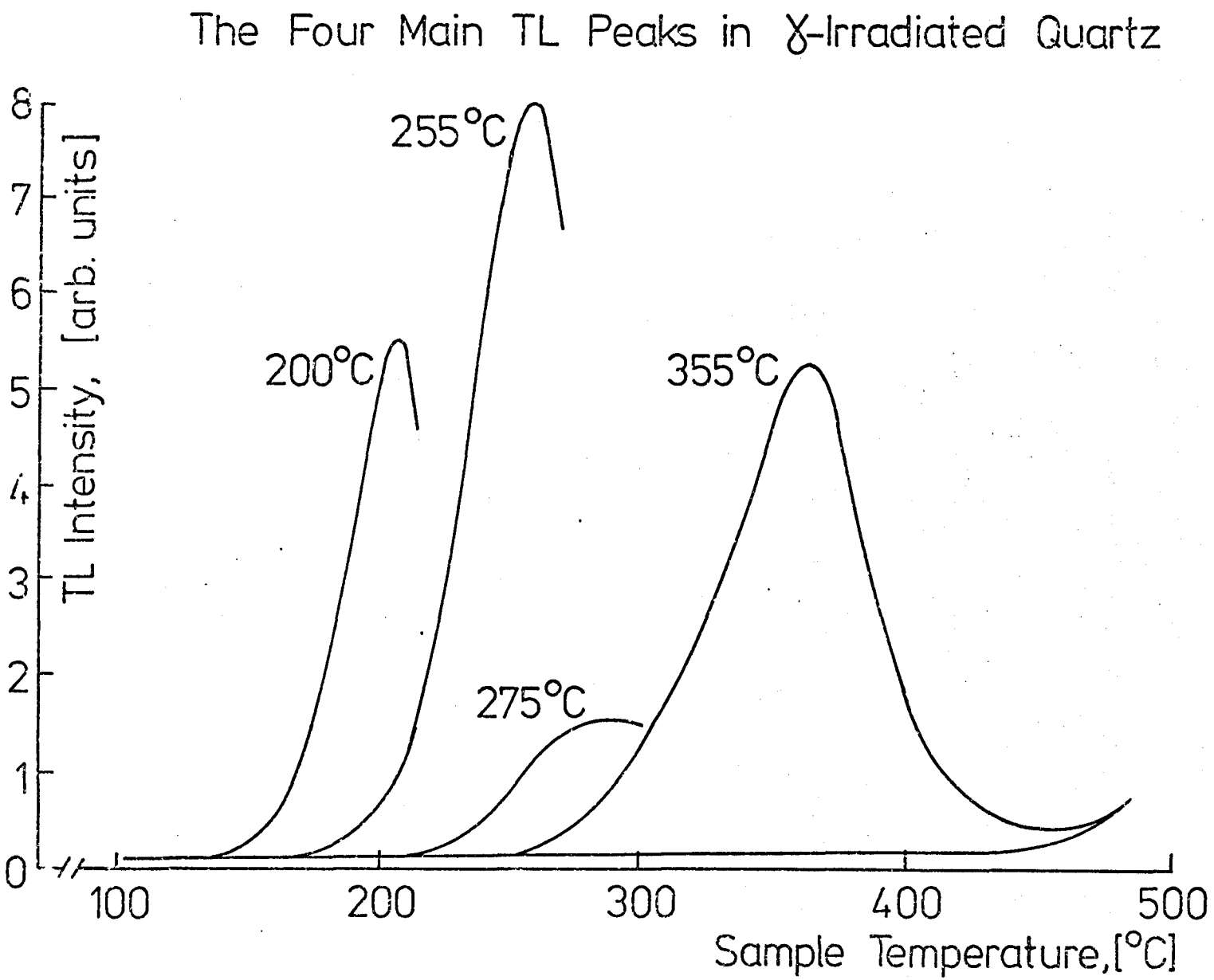
The Four Main TL Peaks in γ-Irradiated Quartz
TL Intensity, [arb. units]
0
1
2
3
4
5
6
7
8
255°C
200°C
355°C
275°C
100
200
300
400
500
Sample Temperature,[°C]

Fig 3·3

355°C peak sometimes appeared to be composed of at least two peaks, but these were found to be extremely difficult to resolve and in all the following results the 355°C peak is treated as a single peak.

Owing to the inhomogenous distribution of impurities within the quartz samples, the slices were found to exhibit appreciable differences in TL sensitivity. To correct for this, each sample was given an initial test dose of 15krad of beta irradiation at room temperature from a ^{90}Sr source (see Section 2.2.1) and its sensitivity was then defined as 'the TL response per unit sample weight to 15krad β'. Having determined the 'intrinsic' sensitivity of each sample in this way, their response to subsequent gamma-irradiations could be normalised and direct comparisons of the responses were made. Furthermore, in order to prevent any changes in sensitivity due to thermal cycling of a sample (Durrani et al, 1972a) each sample was only used once so that each point on the emission spectra, dose response and sensitivity curves to follow was taken from a different sample.

In Figure 3.4 are shown the growths of the TL glow for the four TL peaks with increasing gamma dose. All four curves exhibit a similarity, with a fast initial growth up to $\sim 2 \times 10^6$ rads. Of interest here is the observation that the 255°C peak shows a noticeable decrease in response for doses $\geq 2 \times 10^6$ rads whilst the other three curves exhibit properties akin to reaching a saturation level. The sensitivity changes induced by these large gamma doses are shown in Figure 3.5. Here, all four curves show an increase in sensitivity up to a dose of 10^6 rads, followed by a lessening of the increase with the sensitivity apparently reaching a steady level at doses of $\sim 10^7$ rads.

From Figures 3.4 and 3.5 it can be seen that all four peaks behave in a

Response to Gamma Irradiation

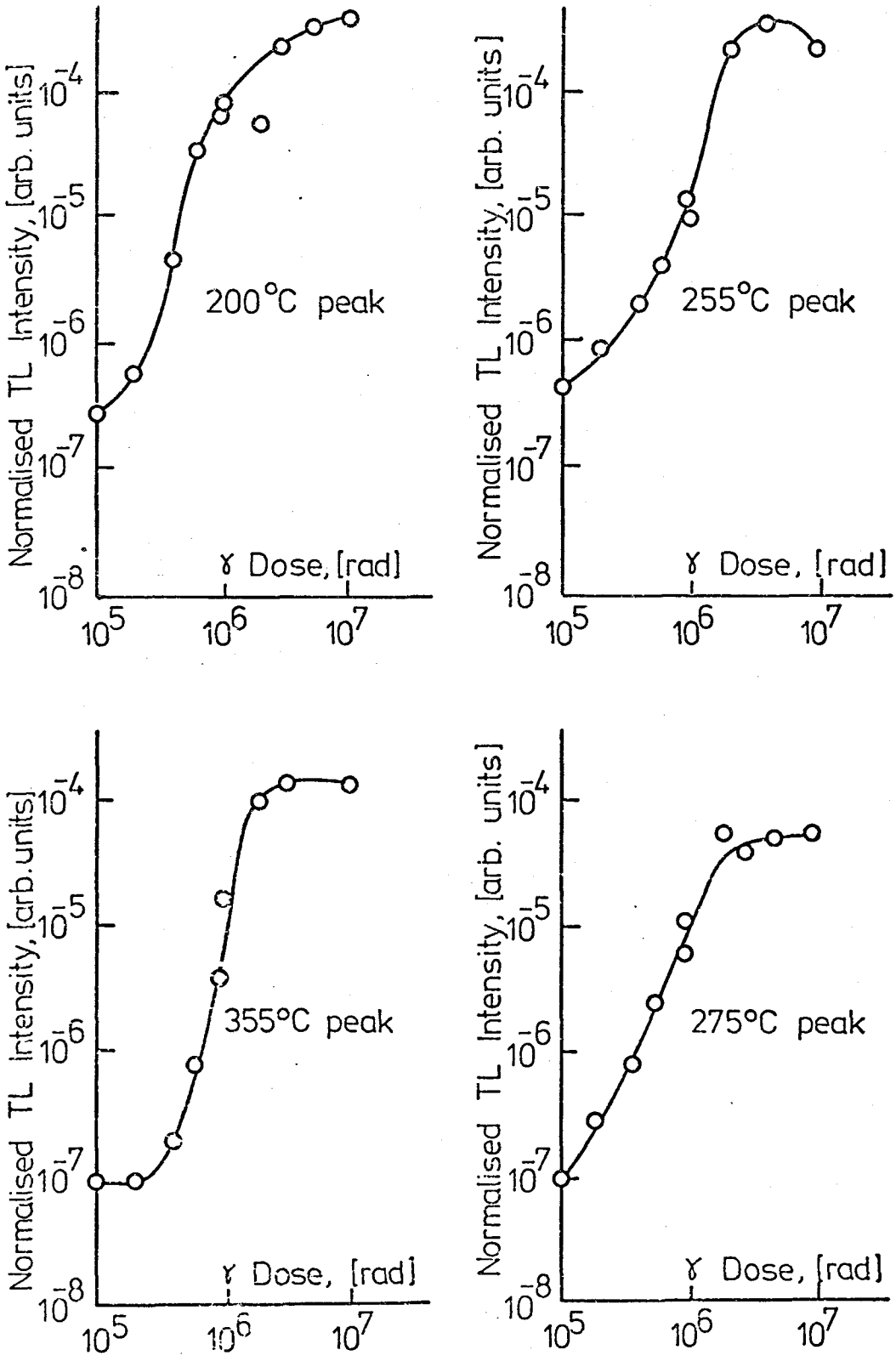

Fig 3·4

Sensitivity Changes Following γ-Irradiation

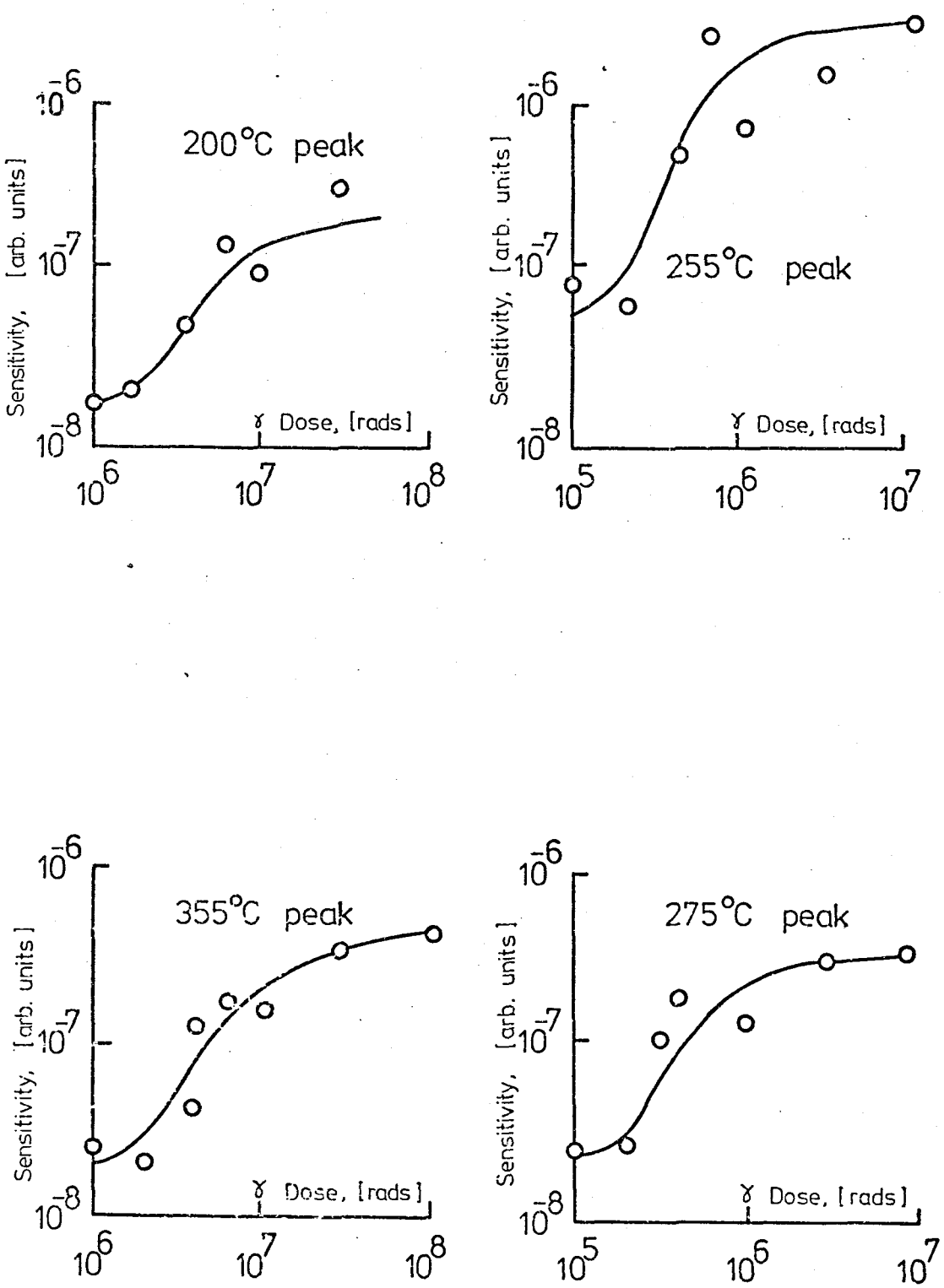

Fig 3·5

similar fashion, i.e. the gamma-rays are apparently affecting each peak in the same way. It will be shown in the next section that the common factor between the four traps is the recombination centre, which is being affected in a uniform (but as yet unknown) fashion by the radiation, giving rise to the observed curves of Figures 3.4 and 3.5

3.5 TL Emission Spectra.

Figure 3.6 shows the emission spectrum of each peak in the quartz TL glow. For these curves a series of Balzers narrow-band interference filters (types R-UV and B-40) were used during TL readout after giving each sample a gamma-ray dose of 310krad. The photomultiplier output at any given temperature of readout is a function of the emitted TL intensity $I(\lambda)$, the transmission characteristics $F(\lambda)$ of the filter in use and the quantum efficiency $Q(\lambda)$ of the photomultiplier at the pass-band wavelength λ of the filter. The differences in $F(\lambda)$ and $Q(\lambda)$ for each filter can be compensated for by a process of normalisation in order that the true variation in normalised $I(\lambda)$ can be determined. Figure 3.6 shows the variation in normalised $I(\lambda)$ (corrected for the different sample sensitivities) with λ. As can be seen, all four curves exhibit broadly the same shape, peaking in the blue region near 470nm (compared with 450nm as reported by Batrak, 1958). The important information gleaned from Figure 3.6 is that each of the four different electron traps responsible for the observed four TL peaks uses the same recombination centre. Once thermally liberated from the traps into the conduction band, the freed electrons are no longer dependent upon the nature of the traps. The TL emission wavelength is dependent only upon the position of the recombination (luminescence) level in the energy band diagram of the material, which in turn is dependent solely upon the nature of

Emission Spectra
for the 200°C & 255°C Quartz Peaks

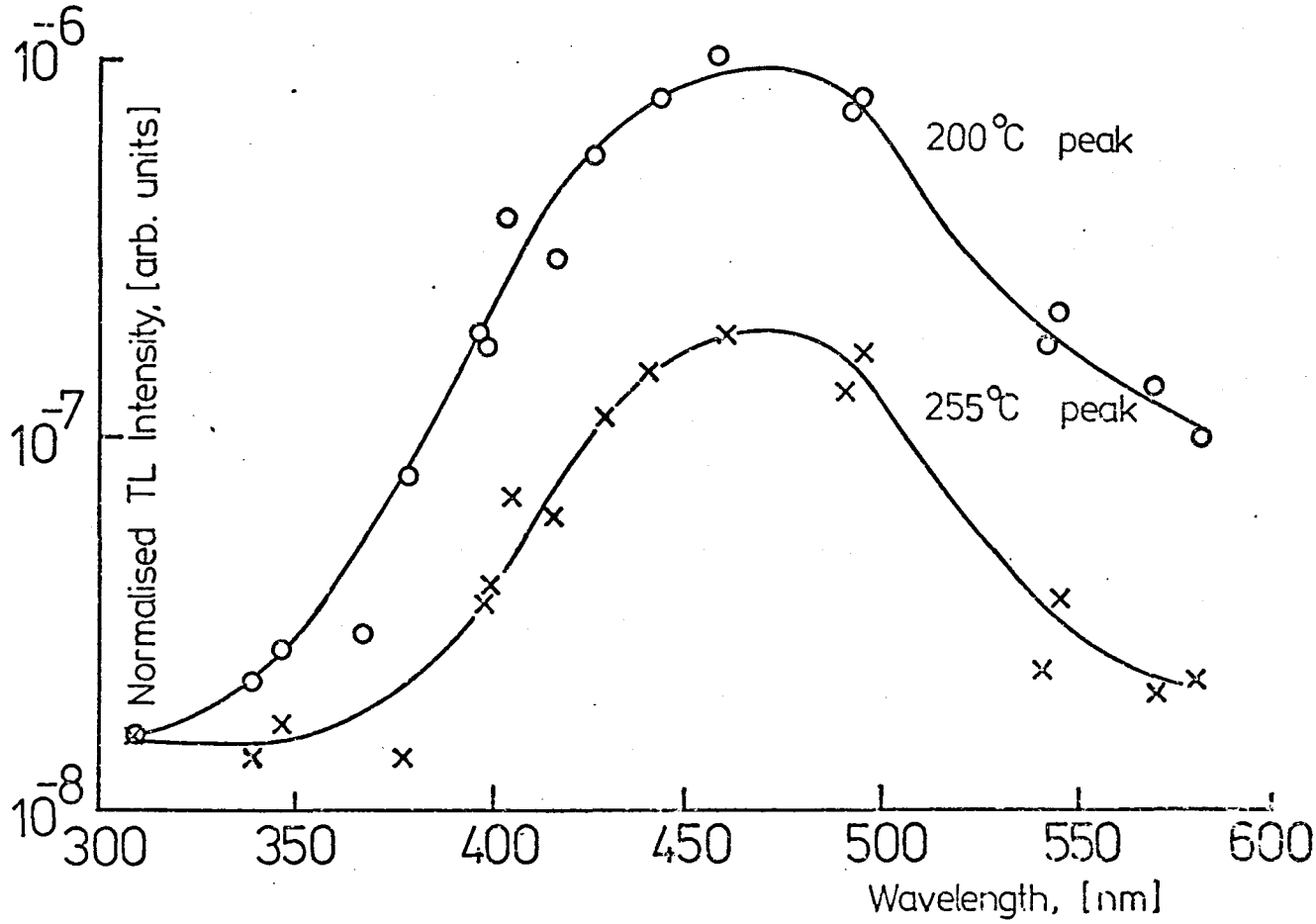

Fig 3·6(a)

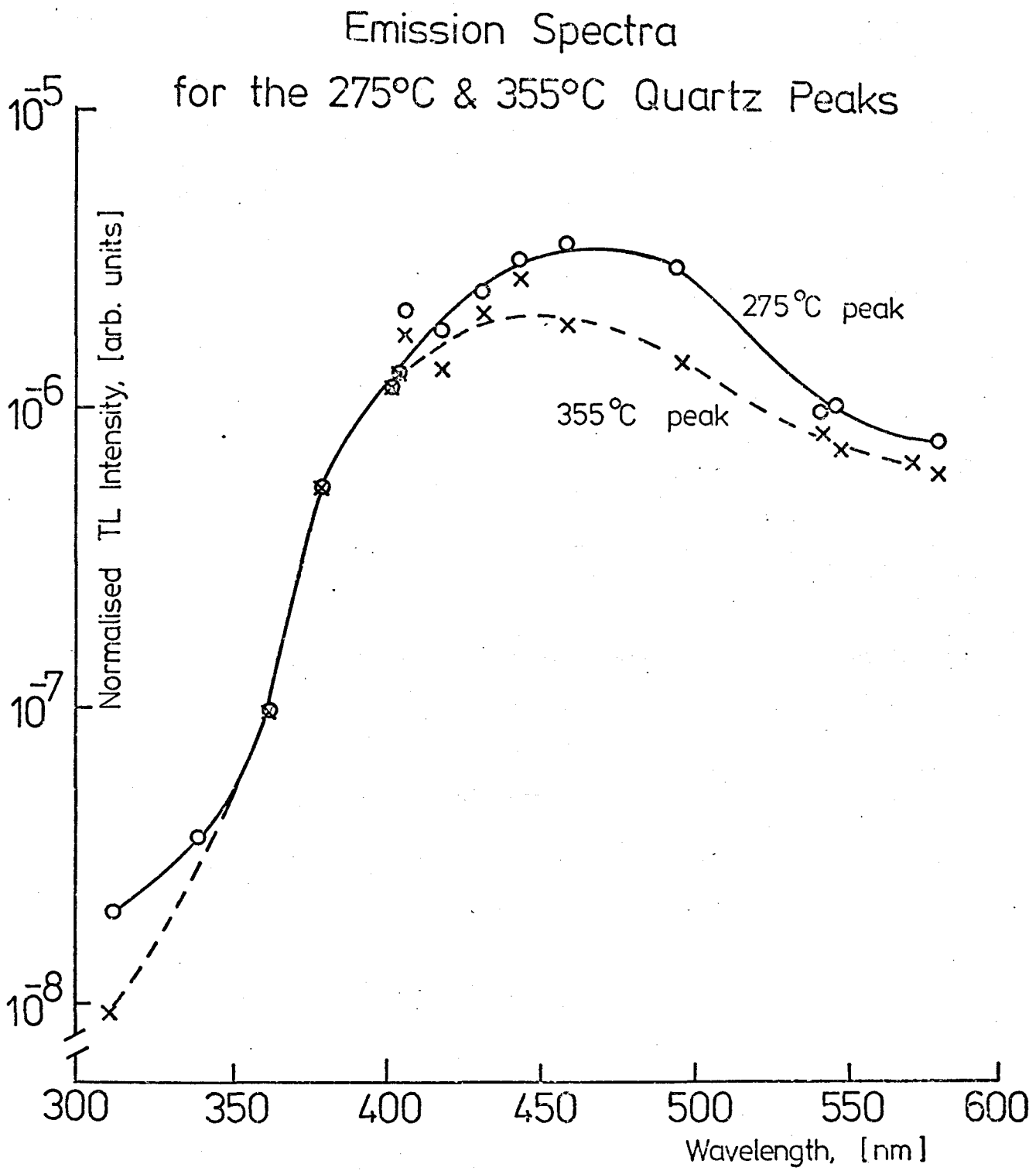
Emission Spectra
for the 275°C & 355°C Quartz Peaks
Normalised TL Intensity, [arb. units]
10⁻⁵
10⁻⁶
10⁻⁷
10⁻⁸
275°C peak
355°C peak
300
350
400
450
500
550
600
Wavelength, [nm]

Fig 3·6(b)

the centre itself.

3.6 Bulk Test.

This test was carried out to see whether or not the sensitisation of the quartz following a radiation dose was a surface effect. The test was made by preparing two slices: one of them ground to a thickness of about 150μm , the other to 250μm. The initial sensitivity of each slice was measured by using a test dose of 30krad of beta particles, then the induced TL readout and the areas under their glow curves in the temperature range 240°C to 480°C were measured as the glow intensity. Both slices were then given a gamma dose of 1.5Mrad followed by TL readout. The 250μm thick slice was then ground down to 150μm by removing 50μm from each face. After this procedure both slices were given the 30krad beta test dose followed by the readout of the TL and the new sensitivity determined. The results of this experiment showed that both slices were sensitised by the 1.5Mrad gamma dose to the same degree. This experiment proved clearly that sensitisation is a bulk effect.

3.7 The Effect of Isothermal Annealing on the Dose-Created Sensitisation.

It was noticed by the author that annealing of quartz, previously sensitised by gamma-radiation at 500°C for one hour, did not re-install the original sensitivity. This result indicates that the entities responsible for the observed increase in sensitivity were thermally stable at this temperature. This led to the study of the effect of annealing at higher temperatures. The experiment was performed on polished slices of 150μm thick and about 2mg in weight. For the purpose of normalisation, all slices were first given a 30krad beta dose and the TL from each sample normalised to a unit of weight and dose, this being defined as the original sensitivity of each slice.

These slices were then sensitised by giving each sample a gamma dose of 600krads followed by TL readout. The samples were then given a dose of 30krad beta and the area under the glow curve between 240°C and 480°C, normalised to a unit weight and dose, designated n_o. Annealing was carried out for various times at each of the constant annealing temperatures. After the annealing period the sample sensitivity was tested by using the standard dose of 30krad beta, and the new sample sensitivity designated n. The ratio of the sensitivity of the sample after a certain annealing time to the sensitivity of the sample corresponding to a zero time of annealing (i.e. n/n_o) was calculated and plotted against the annealing time. This procedure was repeated for five temperatures: 540°C, 550°C, 560°C, 570°C and 580°C. The results of this experiment are shown in Figure 3.7.

For each annealing temperature the 'decay curve' can be broken into two linear components, each component representing the logarithmic decay of the entity which was created by the high gamma-ray dose and also responsible for the sensitisation. A 'half-life', $\tau_{\frac{1}{2}}$, can be defined for each component as in the case of a simple nuclear decay. The term $\frac{\ln(n/n_o)}{t}$, equivalent to the 'decay constant' (λ) of the corresponding component, is plotted against $\frac{10^3}{T}$ (where T is the annealing temperature in °K). The result is shown in Figure 3.8.

Annealing of a previously sensitised quartz sample (by 15Mrad of gamma-ray dose) at 900°C was also carried out. The results of this investigation showed that annealing for two hours at 900°C was capable of removing the sensitisation effect and the sensitivity of the sample returned within a factor of 5 of the original. A similar annealing procedure was carried out upon an unsensitised (virgin) sample of natural quartz, the results

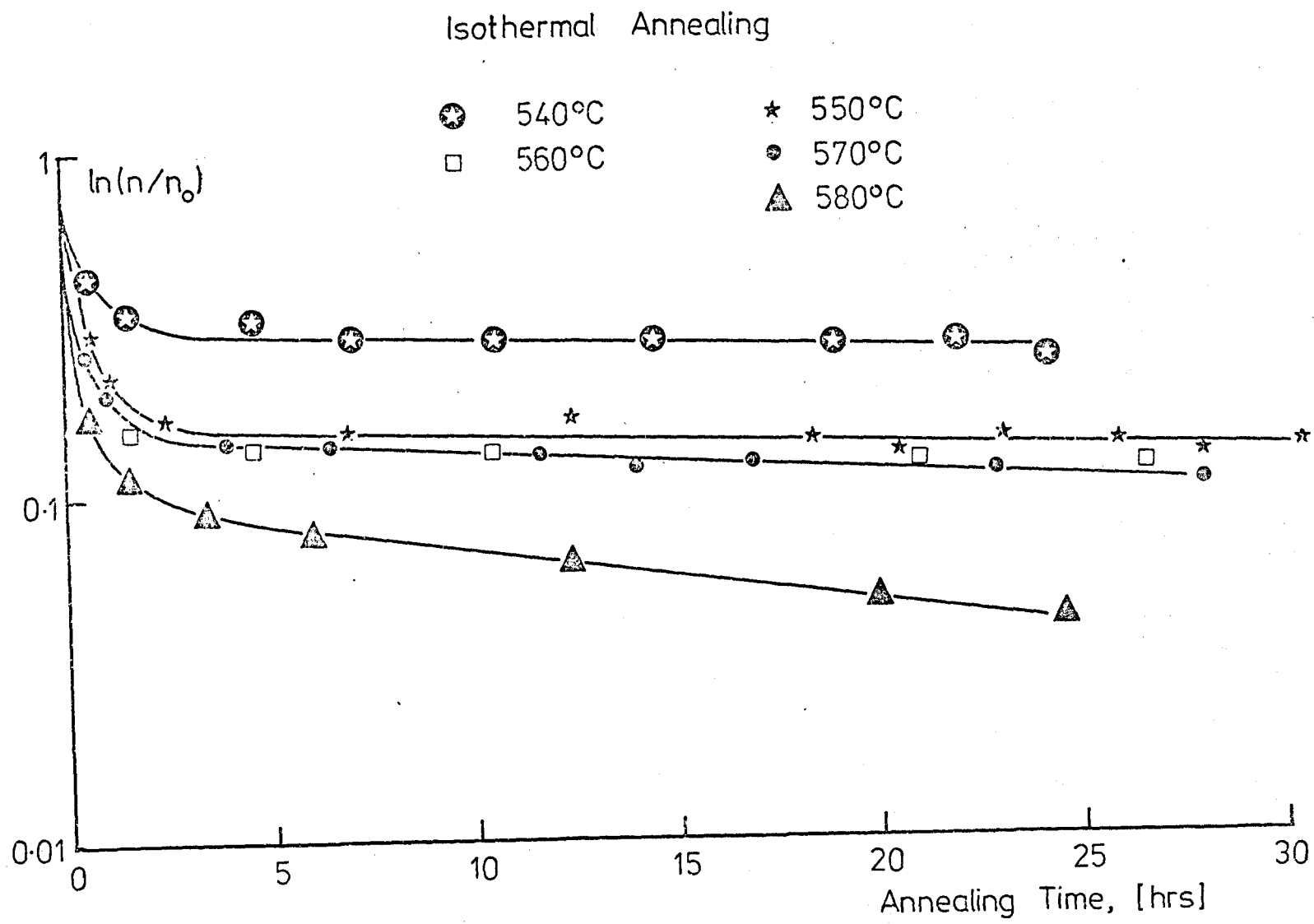
Isothermal Annealing
540°C
550°C
560°C
570°C
580°C
ln(n/n$_o$)
1
0·1
0·01
0
5
10
15
20
25
30
Annealing Time, [hrs]

Fig 3·7

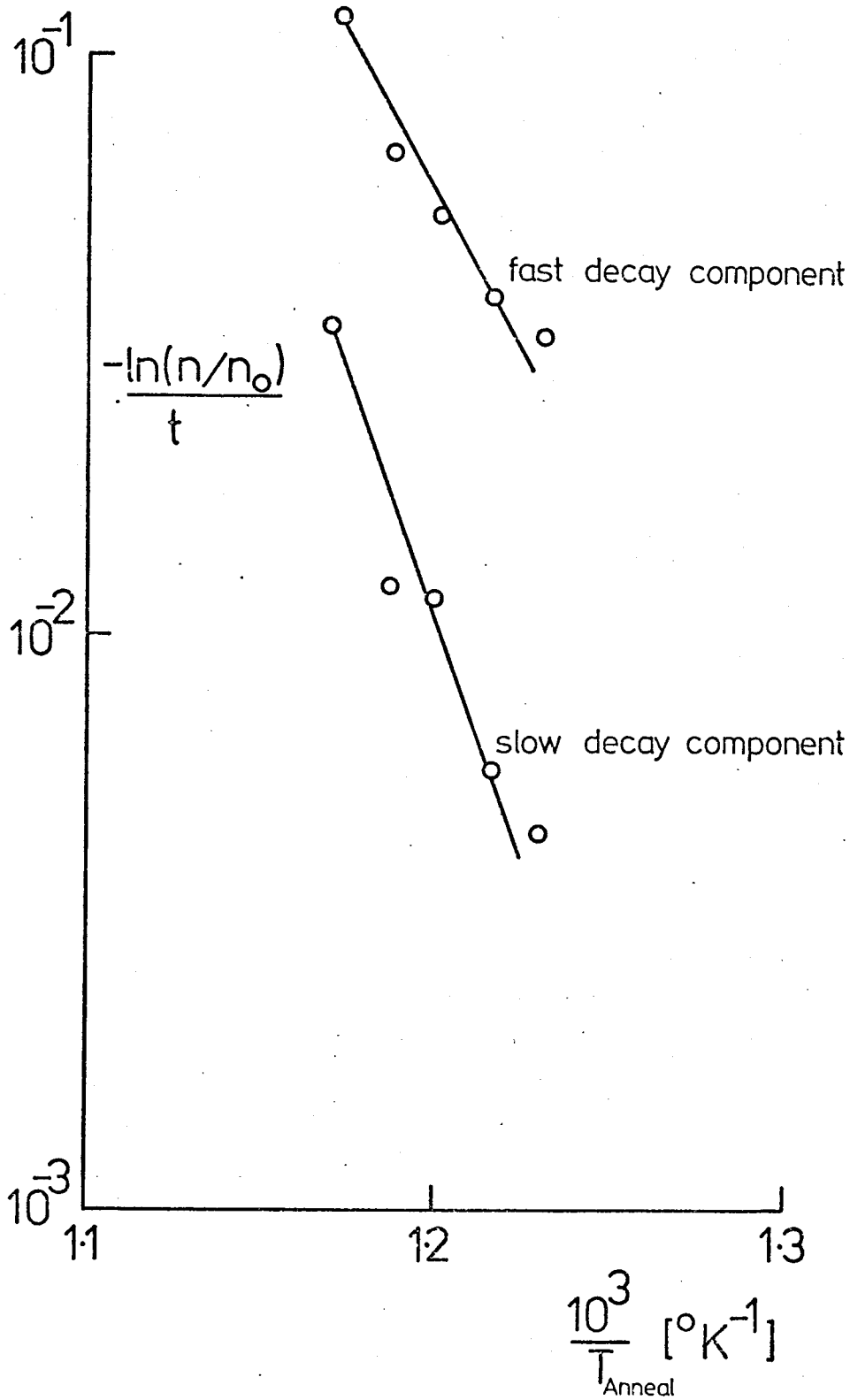
10^{-1}
10^{-2}
10^{-3}
$-\frac{\ln(n/n_o)}{t}$
fast decay component
slow decay component
1·1
1·2
1·3
$\frac{10^3}{T_{Anneal}}$ [°K^{-1}]

Fig 3·8

of which showed that annealing at 900°C for 20 hours followed by slowly cooling to room temperature increased the sensitivity of the sample by a factor of 5.

In Figure 3.9 the results of annealing of two previously sensitised quartz samples by a dose of 600krad of gamma- and X-rays respectively at two annealing temperatures (530°C and 580°C) are shown. For the purpose of this experiment two quartz slices were prepared. One slice was sensitised by ~ 600krad gamma-rays and the second slice was sensitised by 600 krad of 300keV X-rays. The sensitivity of each slice as a result of the 600krad was determined using a test dose of 30krad beta. The samples were then annealed first at 530°C for different lengths of time and the sensitivity after each annealing time was determined using a 30krad beta test dose. This was followed by raising the annealing temperature to 580°C and the sensitivity after each annealing time calculated following the procedure described above. A conclusion can be drawn from Figure 3.9: the sensitisation created by X-rays is thermally less stable compared with that created by gamma-rays.

The effect of successive heating (by TL machine, i.e. 20°C to ~ 500°C) on the gamma-dose-induced sensitisation in natural quartz was studied using two samples prepared by following the procedure described in Section 3.2. They were first heated (by TL machine to ~ 500°C) to eliminate their natural TL, then the intrinsic sensitivity of each sample was determined by using a 15krad test dose of beta particles. After this, one sample was given repeatedly 15krad of beta and the TL area/mg between the temperature range 240°C to 480°C after each step determined. The second sample was given 150krad in one irradiation and the TL due to this dose was eliminated by heating the sample in the TL apparatus. After this the sensitivity of the

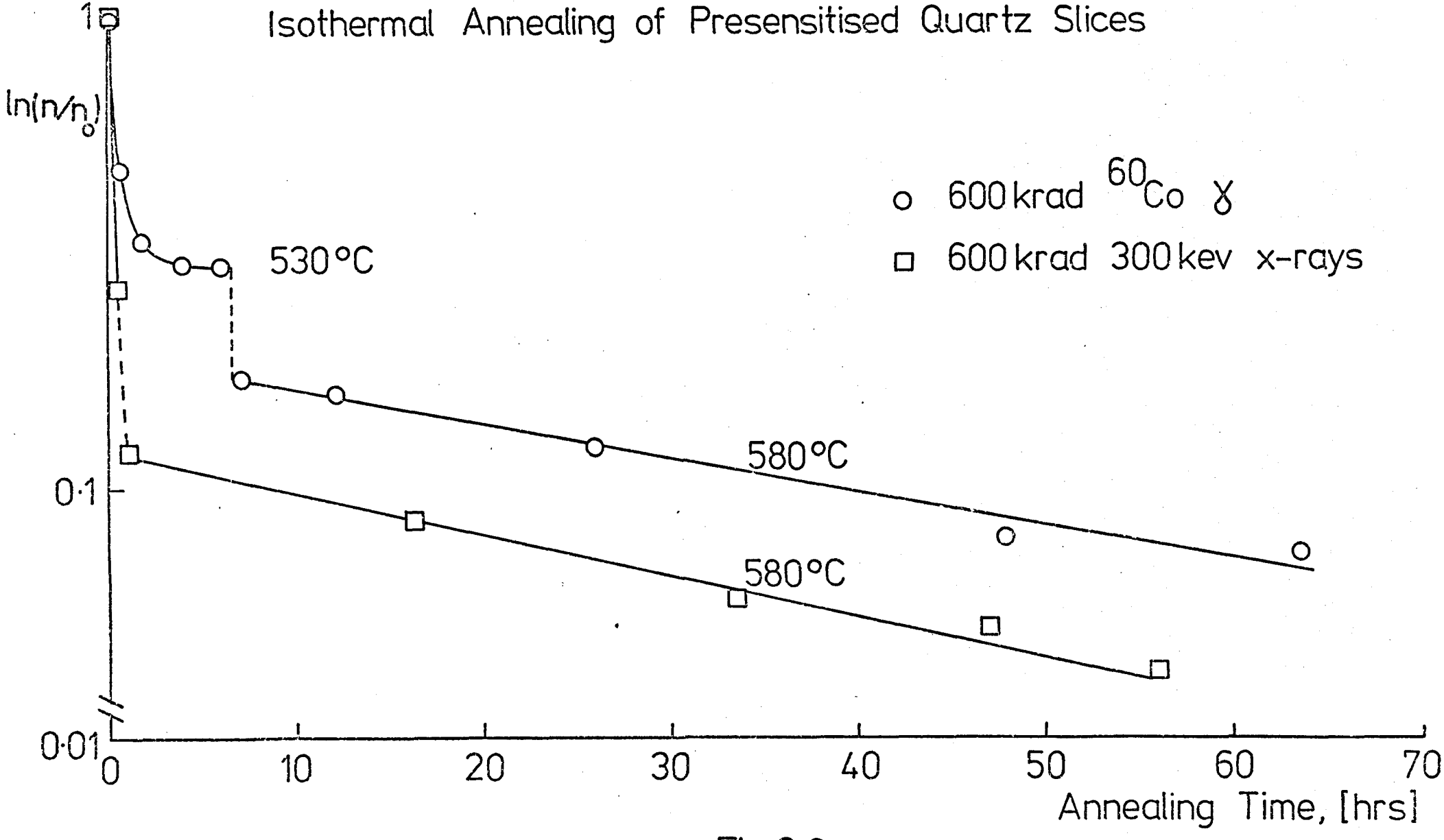
Isothermal Annealing of Presensitised Quartz Slices
1
ln(n/n₀)
0·1
0·01
530°C
580°C
580°C
600 krad ⁶⁰Co γ
600 krad 300 kev x-rays
0
10
20
30
40
50
60
70
Annealing Time, [hrs]

Fig 3·9

sample was determined by using the 15krad test dose. Since the total dose received by both samples was the same and was equal to 180krad of beta, the difference in sensitisation between the two samples (see Figure 3.10) could be explained by the fact that the first sample was heated (by TL apparatus) many times more than the second, giving rise to the desensitisation of the quartz sample.

3.8 The Variation of the TL Sensitivity of Quartz with Dose-rate.

In this section the effect of the gamma-dose rate upon the sensitivity of quartz in the region of the glow curve between 240°C and 480°C is studied. Slices of natural quartz 150μm thick and 1-2mg in weight (prepared by following the procedure described in Section 3.2) were used in this investigation. A test dose of 15krad of ^{90}Sr betas was used to determine the initial sensitivity of each slice for the purpose of normalisation. The variation of the normalised TL glow area, induced by a dose of 50krad, between 240°C and 480°C with the dose rate is shown in Figure 3.11. The figure shows that for dose rates greater than 500krad hr^{-1} there was no change in TL sensitivity with the dose rate, while for dose rates between 500krad hr^{-1} and 60krad hr^{-1} the sensitivity varied by a factor of $\sim$ 4. As a result of this finding a dose rate of $\sim$ 600krad hr^{-1} was used in the TL studies reported in Chapters III and IV to avoid any dose-rate effect.

3.9 Proton Irradiation.

Figure 3.12 shows a typical glow-curve following a dose of 10^7 rads of 10MeV protons. As can be seen, the glow-curve shape is similar to that obtained from the gamma-irradiated quartz (cf. Figure 3.2), with the previously discussed four peaks being apparent.

Owing to restrictions placed upon the gamma dose rate, it was not

Effect of Heating

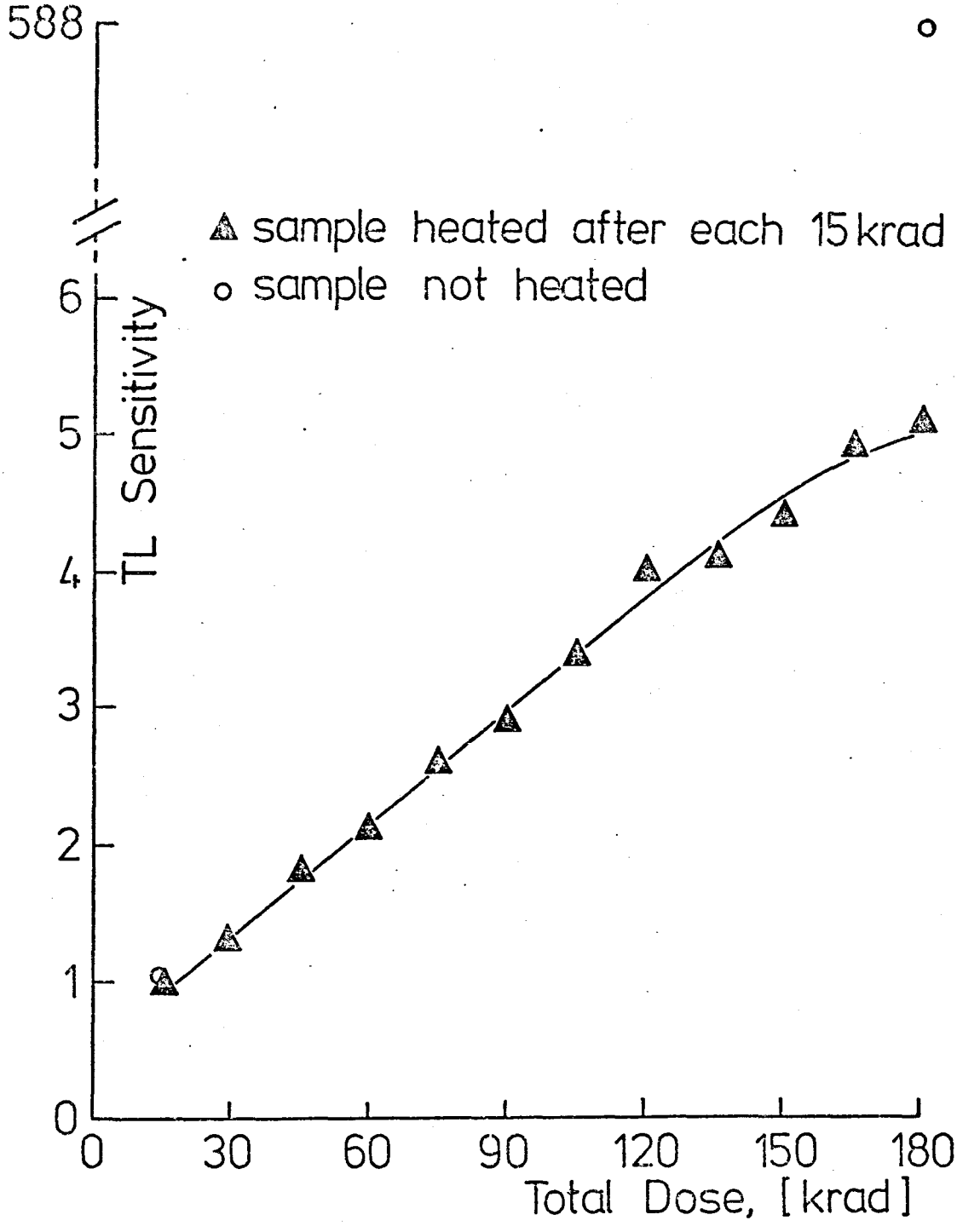

Fig 3-10

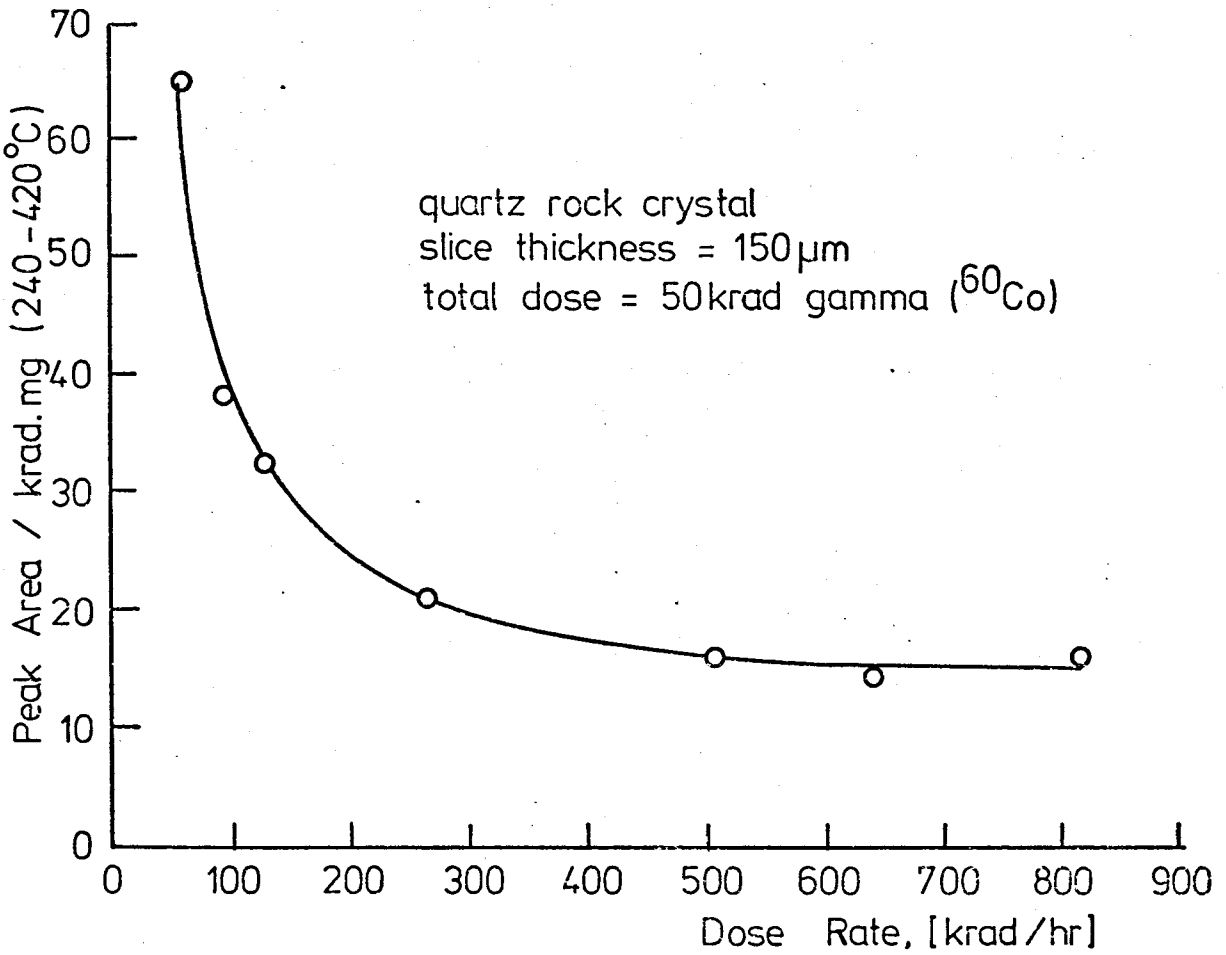
70
60
50
40
30
20
10
0
Peak Area / krad.mg (240-420°C)
quartz rock crystal
slice thickness = 150 µm
total dose = 50 krad gamma (^{60}Co)
0
100
200
300
400
500
600
700
800
900
Dose Rate, [krad/hr]

Fig 3·11

Typical Glow Curve
for Proton-Irradiated Quartz Slice

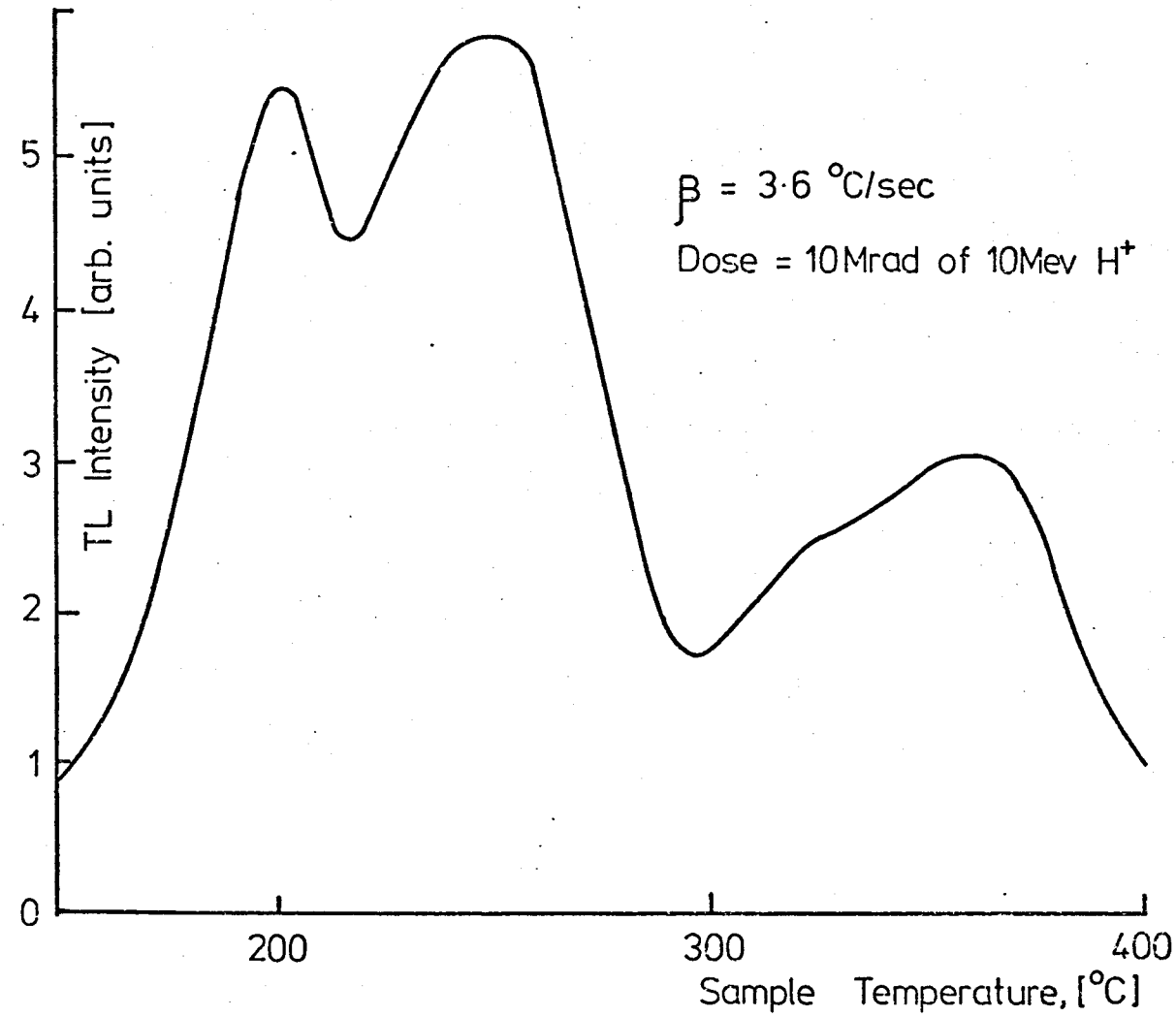

Fig 3·12

possible to obtain gamma-doses of greater than 5×10^7 rads. With proton irradiation, however, much larger doses were available. With these larger doses changes became evident in the glow-curve shape. The glow in the region 200°C to 300°C became less significant, with the result that the main glow appeared in the region of 350°C. This is demonstrated in Figure 3.13, where the glow-curve obtained after a proton dose of 2×10^{10} rads is illustrated. Only one peak is immediately obvious and it proved extremely difficult to resolve the glow-curve into any further components. For this reason the TL intensity was defined as the area under the glow-curve from 240°C to 480°C.

Using this definition of glow intensity it was possible to produce curves exhibiting changes in the TL response and TL sensitivity as increasing doses of proton irradiation were imparted to the sample. Figure 3.14 illustrates these curves. Here one again sees the initial growth of TL up to doses of $\sim 10^7$ rads, followed by a tendency to saturate, similar to that seen by gamma-irradiation. However, it can be seen in Figure 3.14 that as the dose is increased further a sharp decrease in both the TL response and sensitivity is observed. This decrease occurs at doses greater than 10^9 rads and is followed by a region in which the sensitivity and the response remain reasonably stable (at doses of $\sim 10^{11}$ rads) before apparently decreasing again at higher doses (10^{12} rads). Although the areas under the glow-curve between 240°C and 480°C at doses of 10^7 rads and 10^{11} rads are approximately equal, the shape of the glow curve has changed considerably, as is evident by reference to Figures 3.12 and 3.13.

It is interesting to note that the initial increase in sensitisation due to proton irradiation is less than that induced by the gamma-irradiation. This

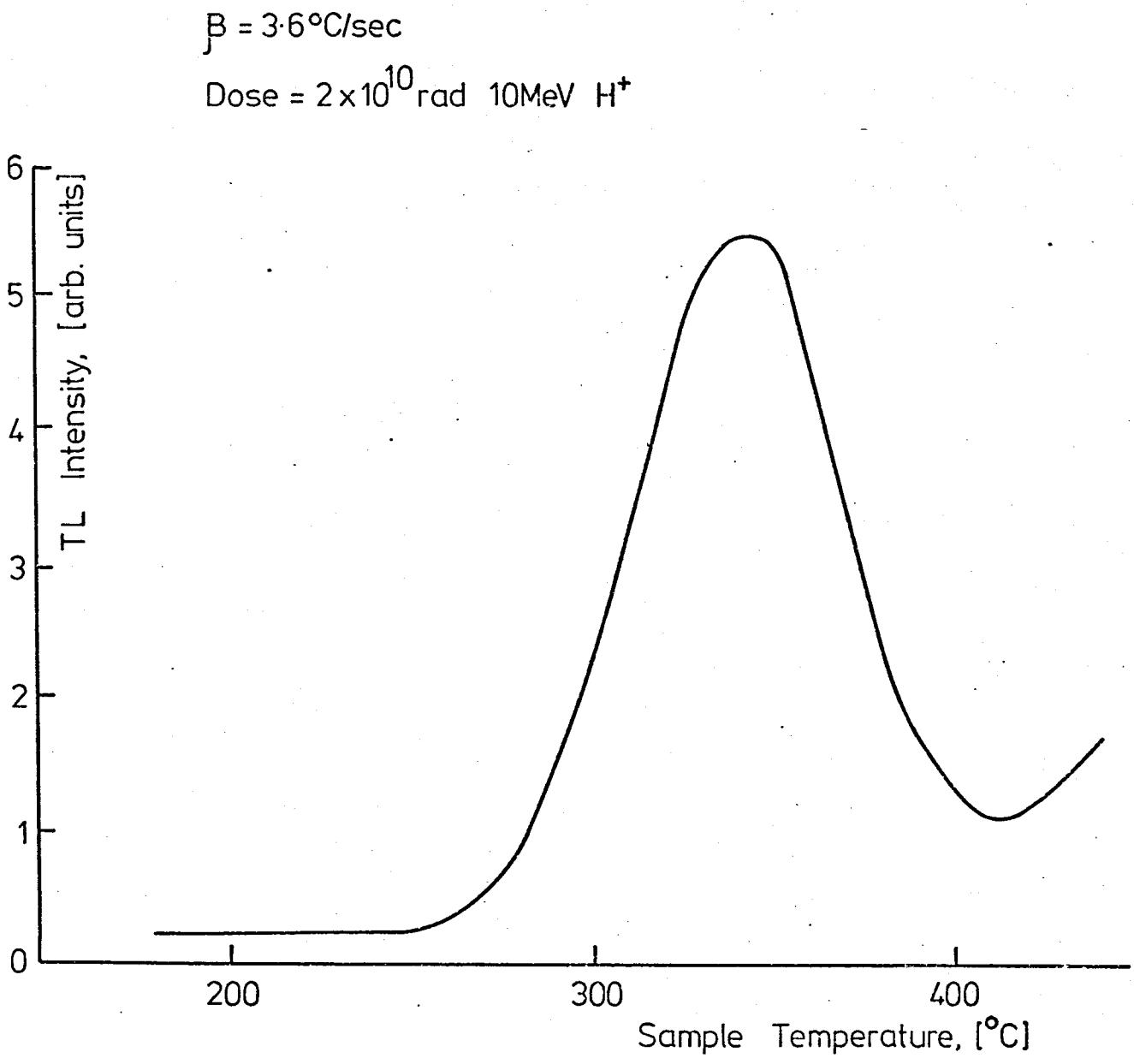
β = 3·6°C/sec
Dose = 2 x 10^10 rad 10MeV H+
TL Intensity, [arb. units]
0
1
2
3
4
5
6
200
300
400
Sample Temperature, [°C]

Fig 3·13

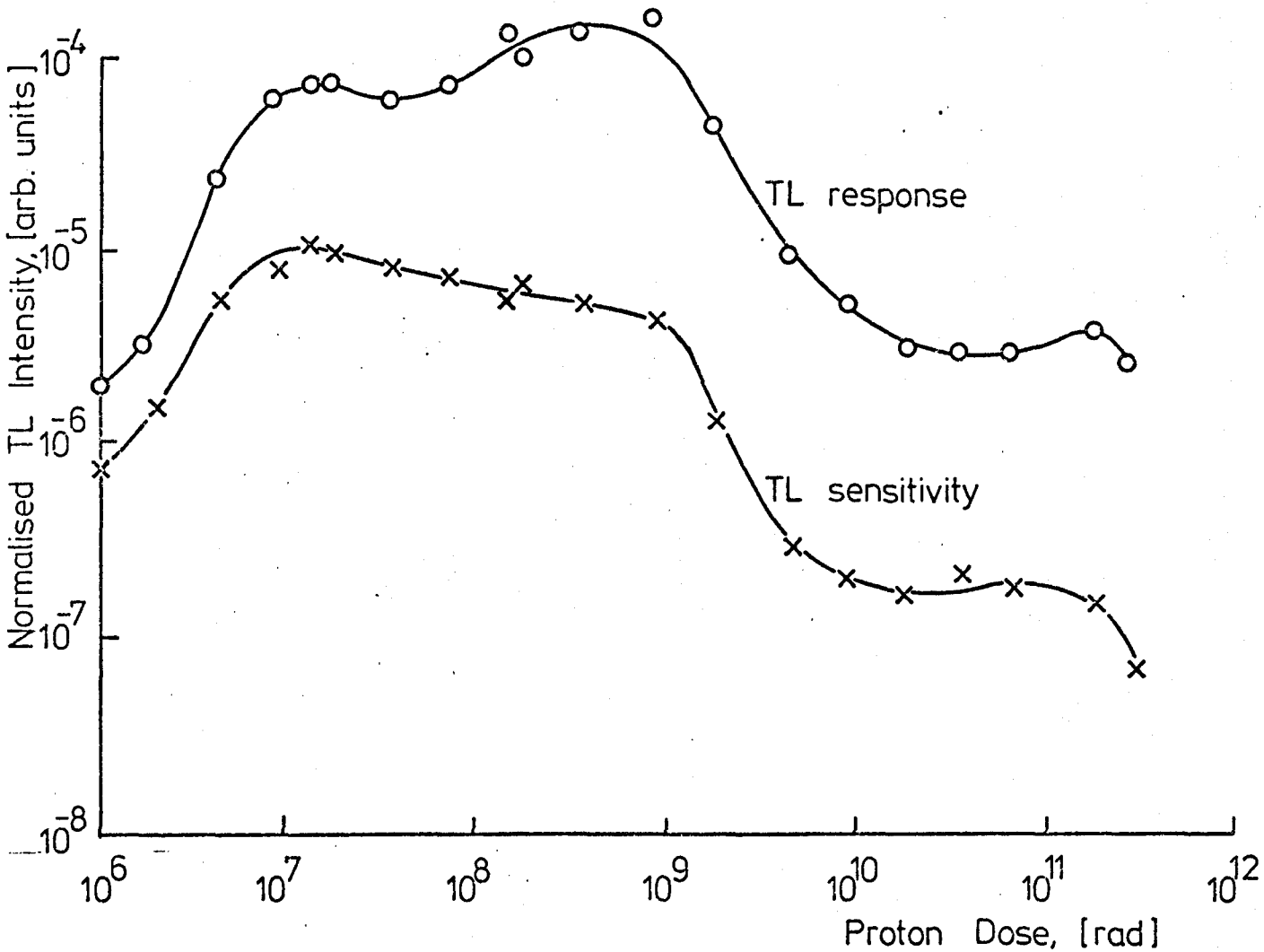
Normalised TL Intensity, [arb. units]
10^{-4}
10^{-5}
10^{-6}
10^{-7}
10^{-8}
TL response
TL sensitivity
10^{6}
10^{7}
10^{8}
10^{9}
10^{10}
10^{11}
10^{12}
Proton Dose, [rad]

Fig 3·14

is illustrated in Figure 3.15 where the sensitisation induced by gamma irradiation is compared with that induced by proton irradiation. In this figure the TL intensity for the gamma-irradiated samples is taken as the area under the glow-curve from 240°C to 480°C, as is the case for the proton-induced TL intensity, in order that direct comparison of the effects of the two types of irradiation can be made.

3.10 Discussion.

The Al/alkali centre described in the introduction (cf. Figure 3.1) is the predominant hole trap in crystalline quartz. Electron traps in natural 'as received' samples also result from the presence of impurities. Schlesinger (1964) has shown the importance of substitutional Ge as an electron trap in smoky quartz, whilst Wright et al (1963) have indicated that substitutional Ti is a significant electron trap in rose quartz. Alkali impurities in quartz break up the Si —— O bonds, thereby introducing non-bridging oxygens which can also act as electron traps. Although usually associated with Al impurities (to form the hole traps) the alkali ions have been observed without the nearby presence of Al (Lell et al, 1966), and Batrak (1958) reports the observation of TL peaks arising from the presence of Li and Na alone.

There is some evidence, however, to indicate that the total number of possible electron traps is insufficient to match the total number of Al/alkali hole trapping centres present (Bambauer, 1961). The implication here is that if extra electron traps were to be created (by, say, raidation damage effects) there would be sufficient hole traps (recombination centre) initially present to compensate for them.

Although predominantly a covalent compound, quartz does have some

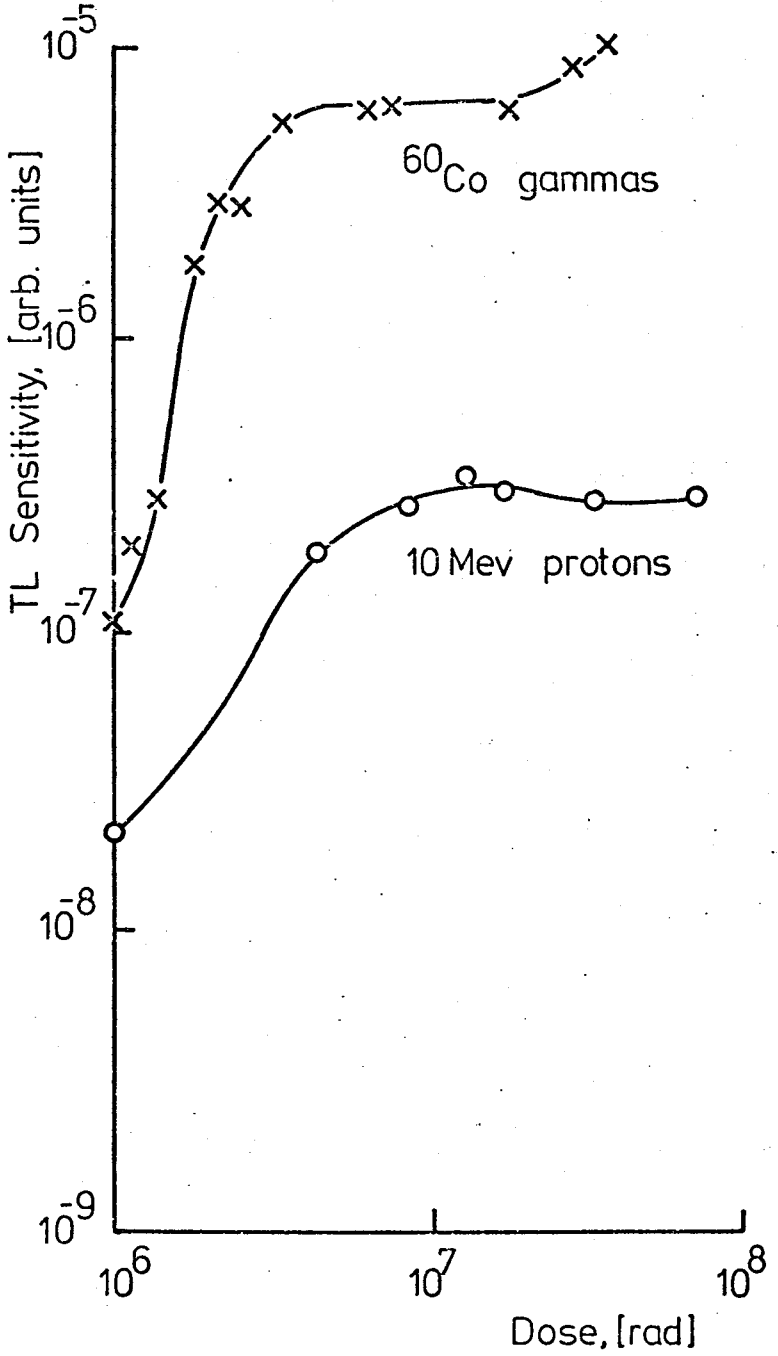
TL Sensitivity, [arb. units]
10^{-5}
10^{-6}
10^{-7}
10^{-8}
10^{-9}
^{60}Co gammas
10 Mev protons
10^{6}
10^{7}
10^{8}
Dose, [rad]

Fig 3·15

degree of ionic character. Evans (1964) estimates the Si —— O bond to be 60% covalent and 40% ionic. However, in contrast to a metallic or a purely ionic bond, a predominantly covalent bond is highly directional with a well-defined bond length giving rise to a rather rigid lattice structure. Point defects and dislocations do exist, but their usually complex structures are not well known in any great detail although they are usually found to be intimately associated with the presence of impurities, substitutional or interstitial. Similarly, any lattice damage induced by radiation absorbed by the sample is also likely to be associated with impurities due to the relative ease with which bonds can be broken in these strained lattice regions. This latter point is thought to be certainly true of electromagnetic (ionising) radiation (Lell et al, 1966). Although calculated energies of γ- and X-rays appear sufficient to dislodge oxygen atoms in unstrained regions of the quartz lattice, very few such examples have been observed with any degree of certainty. Structural faults of this nature usually require irradiation of the sample with high energy particles.

The present work indicates that structural changes are occurring within the quartz lattice when irradiated with a sufficiently high dose of either gamma-ray or protons. The structural changes give rise to the observed changes in TL sensitivity. The evidence presented also suggested that structural changes are centred upon the recombination centres which, owing to the high concentration of Al impurities in all types of quartz, are thought to be the Al/alkali centres (McKeever, 1976).

Because this damage can be induced by electromagnetic radiation (gamma-rays), even at relatively low doses (cf. Figure 3.5), it is suggested that the damage takes the form of a broken bond rather than a direct 'knock-on' dis-

placement. In order to produce vacancies by a direct displacement process the gamma-irradiation would have to give rise to energetic secondary electrons which would then displace the oxygen from its normal lattice site. Arnold and Compton (1959) calculate that if the binding energy of a lattice atom were 24eV then an electron energy of 0.16MeV would be required to produce a displacement by elastic collision. Although this is possible, they suggest the most likely mechanism would be to break a strained Si — O bond, a process which requires far less energy and can result from simple ionisation.

It is suggested here that the latter process is occurring at the Al/alkali centre. The ionising radiation will simply be required to break the strained bond between the silicon and the oxygen atom which is associated with the alkali ion. This will result in an oxygen vacancy and an oxygen interstitial. Although it is not clear what will happen to the alkali ion, it can be seen that the result of this damage would be that the recombination centre is destroyed and, furthermore, that electron traps are likely to be created at its expense. As it is assumed that, initially, the concentration of electron traps is less than the concentration of recombination centres, this would result in an increased TL sensitivity for relatively low gamma and proton doses (see Figures 3.4, 3.14 and 3.15).

In materials with an atomic number $\leq$ 30, the number of direct displacements caused by gamma-irradiation is 5 orders of magnitude lower than that caused by alpha particles (Levy, 1968). Hence, if the mechanism of increasing the sensitivity at these low doses was due to direct displacement then one would expect protons to produce far greater sensitisation than gamma rays. Figure 3.15 shows this not to be the case.

The process of electron-trap creation at the expense of the recombination centres is illustrated phenomenologically in Figure 3.16. In this figure, N_{to} and N_{ro} represent the initial concentration of electron traps and recombination centres respectively, where $N_{ro} > N_{to}$. As the amount of radiation absorbed by the sample is increased the concentration of recombination centres decreases, giving rise to an increase in concentration of electron traps. When the dose is less than D_c, $N_r > N_t$ and hence as N_t increases the TL sensitivity increases also. At dose D_c, $N_t = N_r$ and hence the TL sensitivity reaches a limiting value. Finally, for doses greater than D_c, $N_r < N_t$ and the TL sensitivity begins to decrease. The general shape of the sensitivity curve shown in Figure 3.16b has been observed experimentally in Figure 3.14 for large proton doses. Also, a decreased TL response is evident for the TL peak at 255 when gamma rays are used (cf. Figure 3.4). The curve of Figure 3.14 is seen to have more structure than the theoretical curve would suggest. This is taken to be due to the contributions from the different peaks; one peak reaching its 'sensitivity limit' before another one.

Any oxygen interstitials created by direct collision when large proton doses are used will tend to fill up the interstitial channels along which the alkali ions migrate, thereby restricting the movements of these ions and inhibiting the trapping of holes at the Al/alkali centres. This, therefore, removes the effectiveness of this defect as a recombination centre. This may be an additional factor in the desensitisation when using proton irradiation, and may explain how the protons sensitised the samples less strongly than the equivalent gamma dose (cf. Figure 3.15).

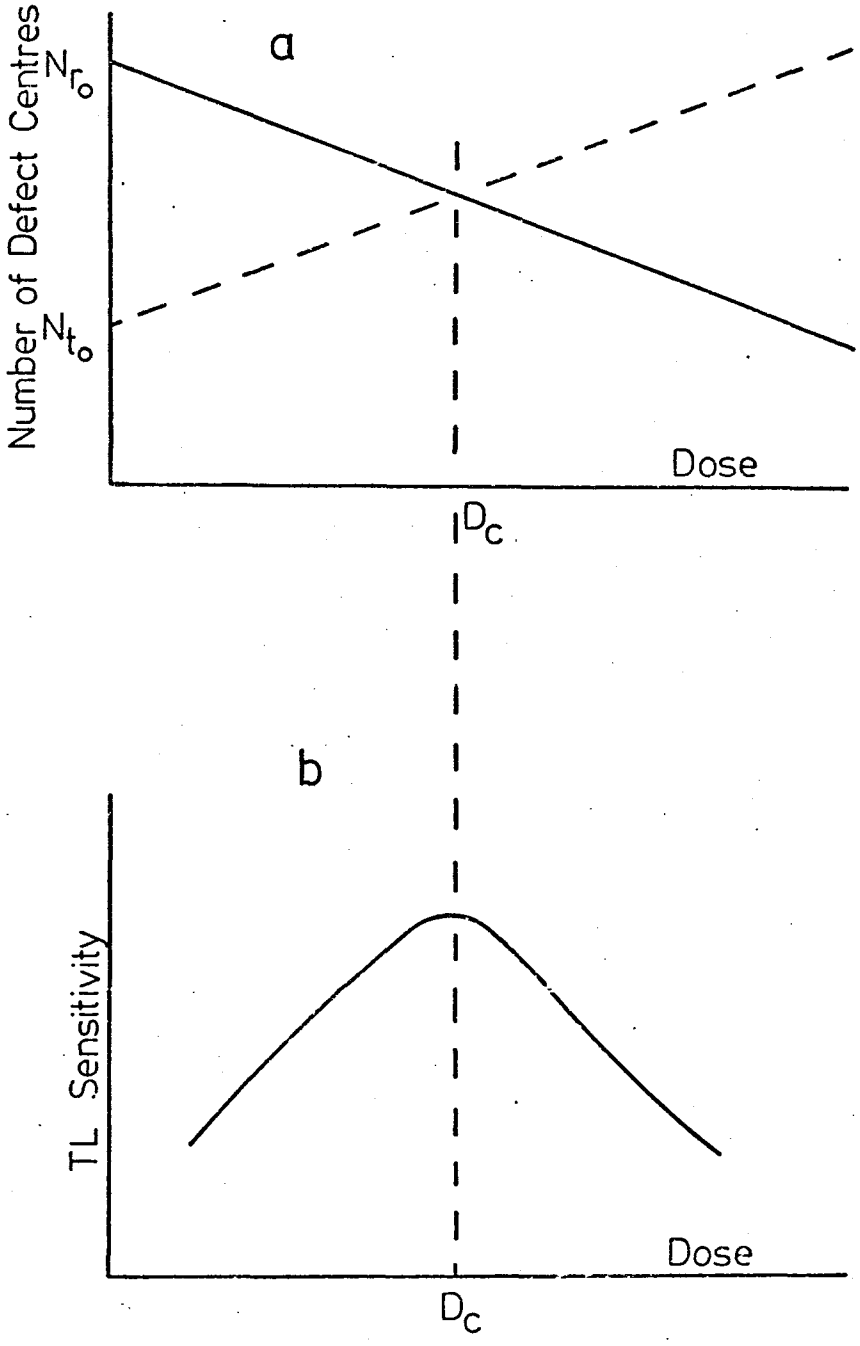
a
Number of Defect Centres
N_{r_o}
N_{t_o}
Dose
D_c
b
TL Sensitivity
Dose
D_c

Fig 3·16

3.11 Conclusion.

The present work has indicated that TL sensitisation by radiation dose in crystalline quartz occurs by radiation damage of the Al/alkali recombination centre. The sensitivity changes can be induced by purely electromagnetic, ionising radiation, such as gamma-rays. Indeed, the gamma-irradiated samples show a greater increase in sensitivity than the samples irradiated with the equivalent protons dose. This points to the occurrence of damage by means of the breaking of a strained Si —— O bond, rather than by direct displacement of an oxygen atom. Such damage can be induced by simple ionisation processes and requires far less energy than direct displacement of an atom. The breaking of the strained Si —— O bond and the subsequent formation of the oxygen vacancy and interstitial result in the destruction of the Al/lakali recombination centre, whilst at the same time giving rise to the creation of further electron traps. If, initially, the concentration of the recombination centres is taken to be greater than the concentration of the electron traps, the damage will first result in an increase in TL sensitivity. As the dose to the sample is increased further, however, a point will be reached at which the electron trap concentration becomes greater than the recombination centre concentration and, hence, a decrease in TL sensitivity results.

CHAPTER IV

THE EFFECT OF THE TEMPERATURE OF IRRADIATION UPON THE TL SENSITIVITY OF QUARTZ

4.1 Introduction

Thermoluminescence has become a generally accepted method for dating archaeological and geological materials, both terrestial and extra-terrestial (e.g. Aitken, 1968; Durrani and Christodoulides, 1969; Christoldoulides et al, 1970). A commonly occurring thermoluminescent phosphor found in nearly all types of pottery and geological samples is quartz and this material plays an important role in the process of age determination by TL.

In certain instances, however, the conditions reproduced in a laboratory during the TL dating procedure are far from those experienced by the sample in its natural environment. If, for example, the TL output depends upon the temperature at which the sample was irradiated (Khazal et al, 1975), this factor must be taken into account. Most energy absorption by a meteorite sample or a lunar sample collected from the shadow of a lunar boulder (see Chapter VI) (say) occurs at low temperatures in space. Since the artificial TL required for calibration purposes is usually imparted by irradiating the sample at room temperature, large errors may be introduced. Similarly, specimens from a fire-site in the Australian desert ought to be treated cautiously if the calibration procedure is being performed in the relative cool of a laboratory.

In this chapter the finding by the author, i.e. the variation of the TL sensitivity of natural crystalline quartz with the temperature of irradiation, is reported and discussed. The results are discussed in the light of the known solid-state defect structure of quartz (see Chapter III), and it is felt

that such work may lead to a better understanding of the phenomena of TL sensitisation, supralinearity and the damage effect of radiation in this material. The radiations used in the experiments are X- and gamma-rays.

4.2 The Effect of the Temperature of Irradiation upon the Sensitivity of Quartz using X-rays.

The X-ray irradiation was carried out by using the X-ray set available in the Birmingham Radiation Centre which was a Pantak constant potential 300kV source (see Section 2.2.3). Figure 4.1 shows a schematic representation of apparatus B which was designed specifically by Dr. S. W. S. McKeever for reading out the TL glow below room temperature and also to enable the sample to be irradiated 'in situ' with X-rays at whatever irradiation temperature was required (see Section 2.5). The sample is heated, in a vacuum environment (10^{-5} torr) by a 75 watt Solon heating element which is fixed to the end of copper 'cold-finger' which extends outside the vacuum chamber. The sample may be cooled to the required temperature by immersing the cold finger into a dewar containing a suitable freezing mixture (e.g. liquid nitrogen; solid CO_2 in acetone; ice and salt). Heating rates of up to 6°C/sec can be employed. The samples were irradiated by X-rays through a 30μm aluminised mylar film, whilst viewing of the sample (for TL readout) was via a 1mm thick Lexan window. A photomultiplier tube (EMI9804QB) was used with this set to monitor the TL readout. This set has been described in detail in Groom (1977).

A typical glow curve obtained on apparatus B (the low temperature set) after irradiating a small slice $\sim$ 200μm thick and $\sim$ 2mg in weight, of natural Brazilian clear quartz with 5krad of X-rays at 293°K is shown in Figure 4.2 (curve A). The main glow appears in the readout region 570°K to 650°K. Also shown (curve B) is the glow curve obtained by irradiating

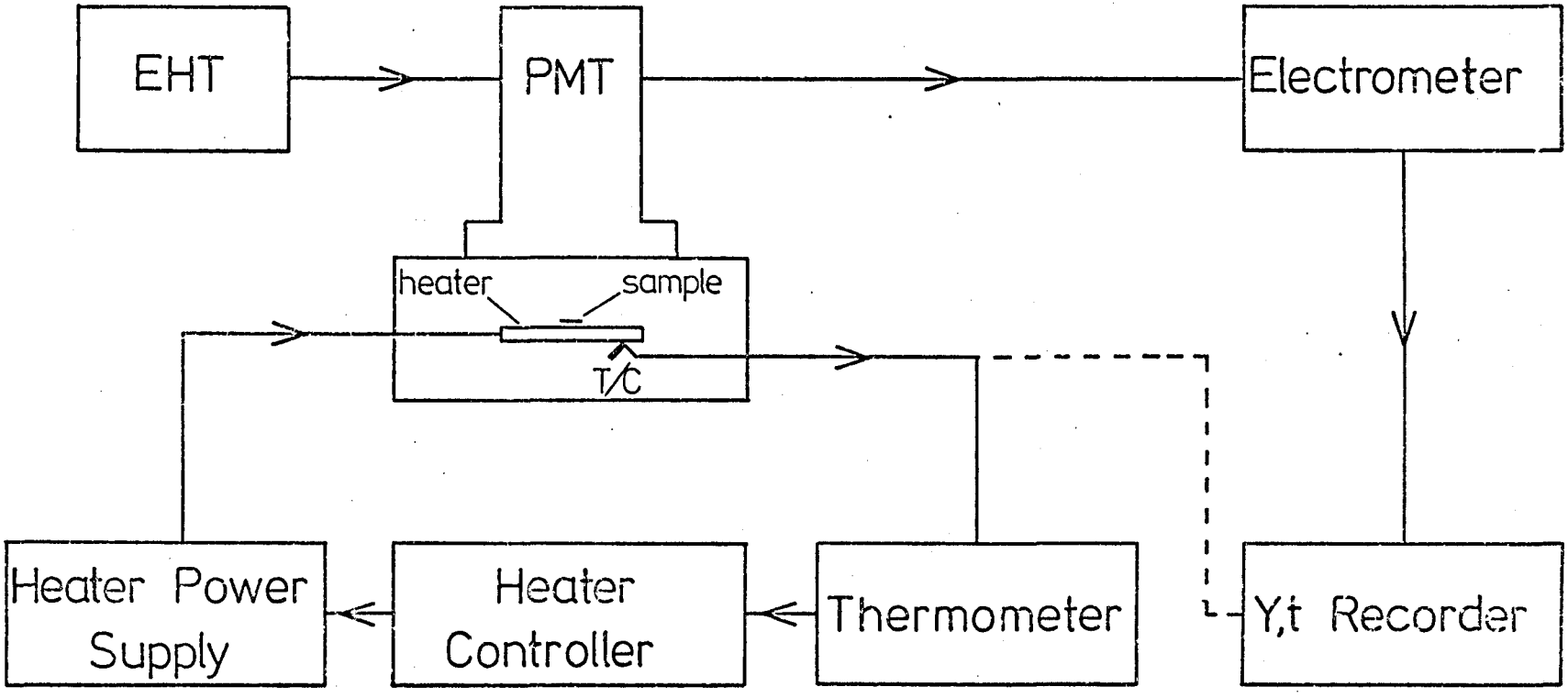
EHT
PMT
Electrometer
heater
sample
T/C
Heater Power Supply
Heater Controller
Thermometer
Y,t Recorder

Fig 4·1

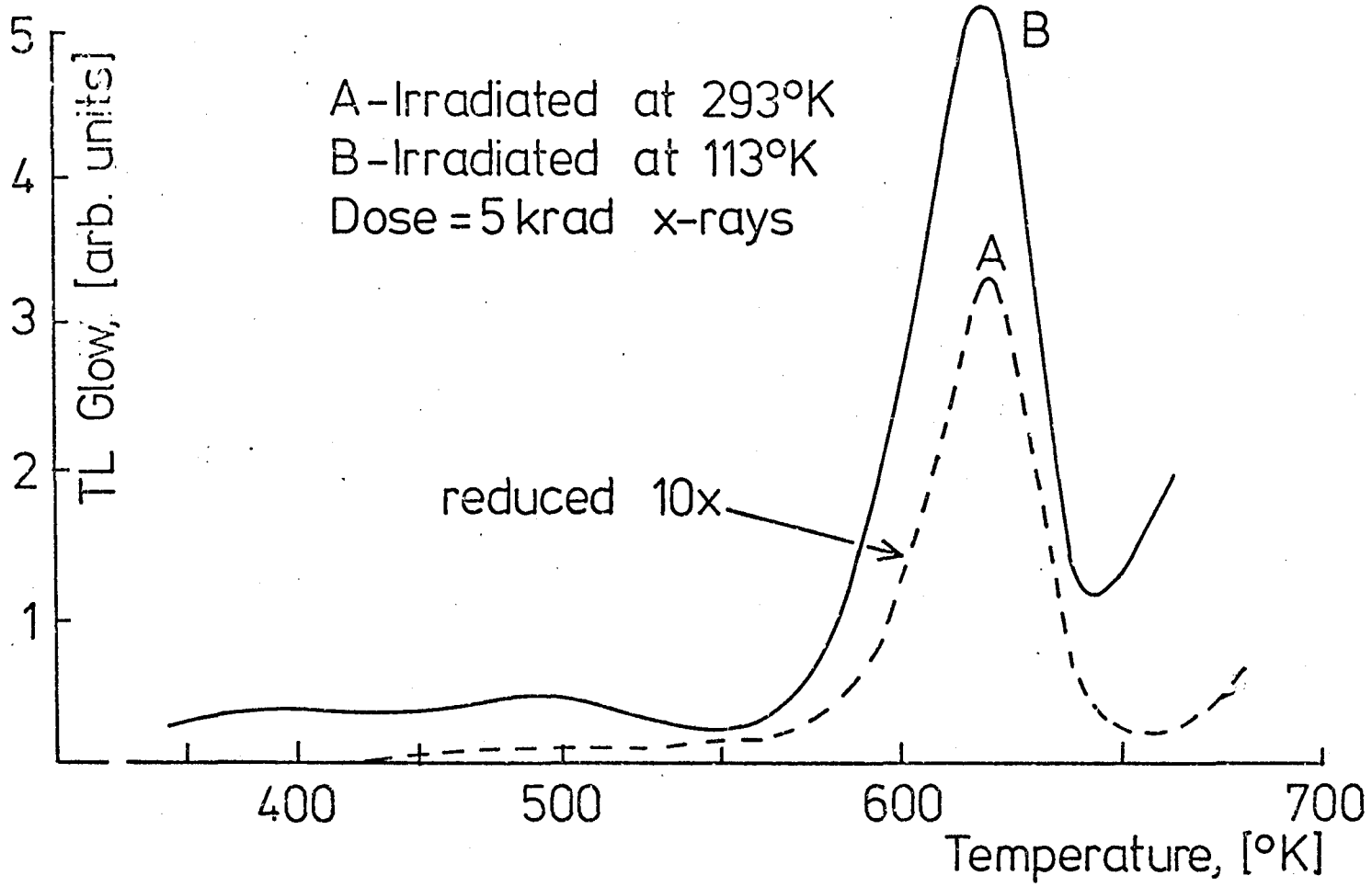

Fig 4·2 (after Groom, 1977)

a similar slice at 113°K with 5krad of X-rays (note: curve A has been reduced by a factor of 10 in the figure). Again the main glow is in the readout region 570°K to 650°K. In order to prevent changes in sample sensitivity induced by either thermal cycling (i.e. repeated heating and cooling; see Section 3.8), or repeated irradiations of the sample, a fresh sample was required for each TL readout. Because of the inhomogenous distribution of impurities within quartz each slice was found to have different initial TL sensitivity, making direct comparison of the glow curve intensities invalid. In order to overcome this problem each sample was given a test dose of 5krad of X-rays at 293°K and the TL response per unit sample mass to this dose was noted. The initial sensitivity of each sample was then defined as the TL response per unit sample mass to this test dose. The response of each sample to subsequent irradiations could then be normalised by dividing the TL output by the sample's sensitivity.

Figure 4.3 shows the variation in normalised TL response with temperature of irradiation (T_{irr}), plotted as ln(TL) versus T_{irr}^{-1}, for an X-ray dose of 5krad. As can be seen, the normalised TL intensity varies by a factor of $\sim$ 5 over the T_{irr} range from 293°K to 113°K. In order to obtain a reliable measure of the TL output, the area under the TL glow curve from 513°K to 693°K was taken in all cases.

Figure 4.4 shows the ln(TL) versus T_{irr}^{-1} plots for quartz samples irradiated with X-ray doses of 10krad, 60krad and 120krad at different temperatures. Unfortunately, only three values of T_{irr} could be maintained for the necessarily long periods required for the larger doses, the dose rate at the sample being estimated at 1krad/minute. Nevertheless, it is evident from Figure 4.4 that a far greater variation in TL intensity is observed when

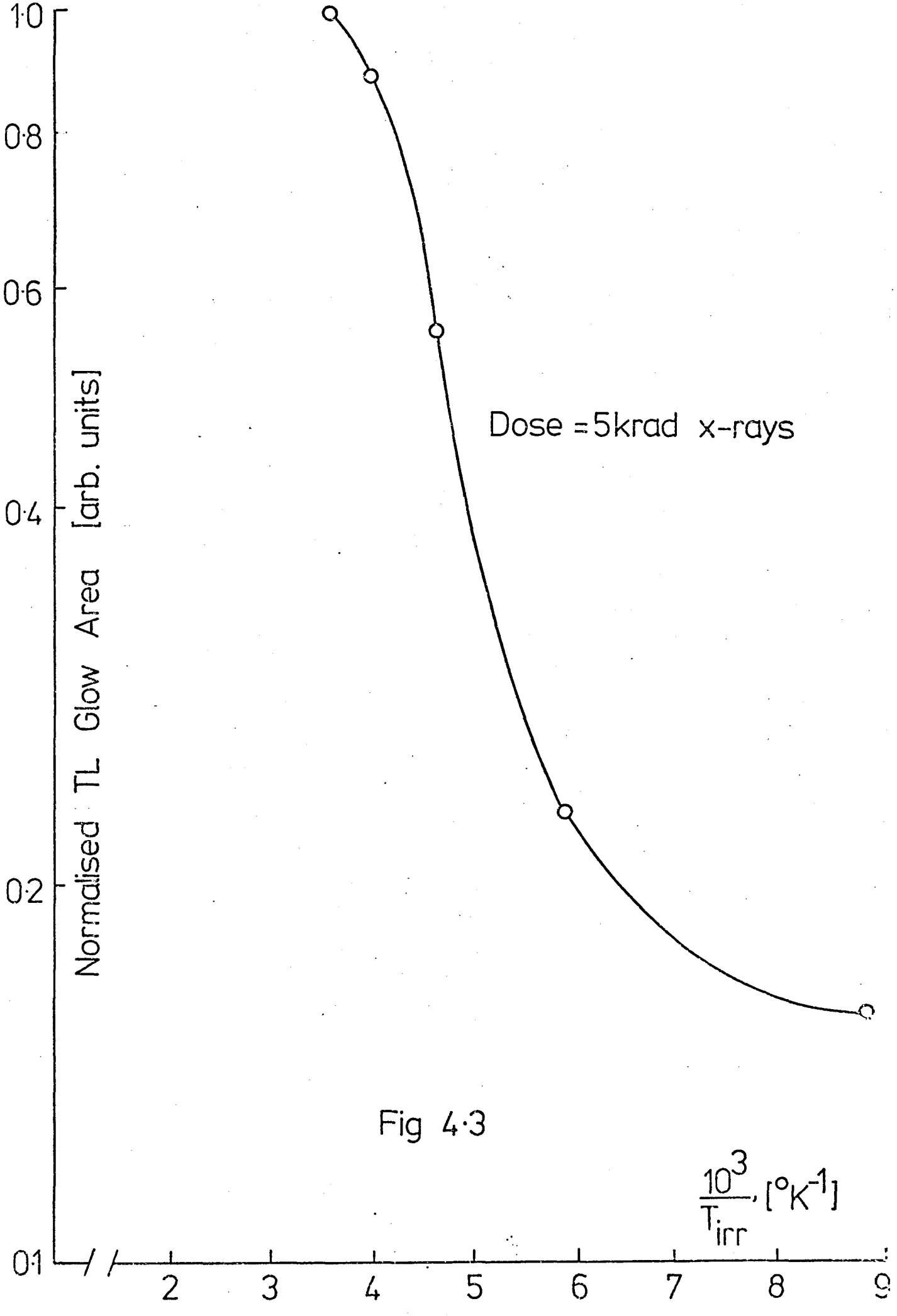
1·0
0·8
0·6
0·4
0·2
0·1
Normalised TL Glow Area [arb. units]
Dose = 5krad x-rays
2
3
4
5
6
7
8
9
$\frac{10^3}{T_{irr}}$, [°K^{-1}]

Fig 4·3

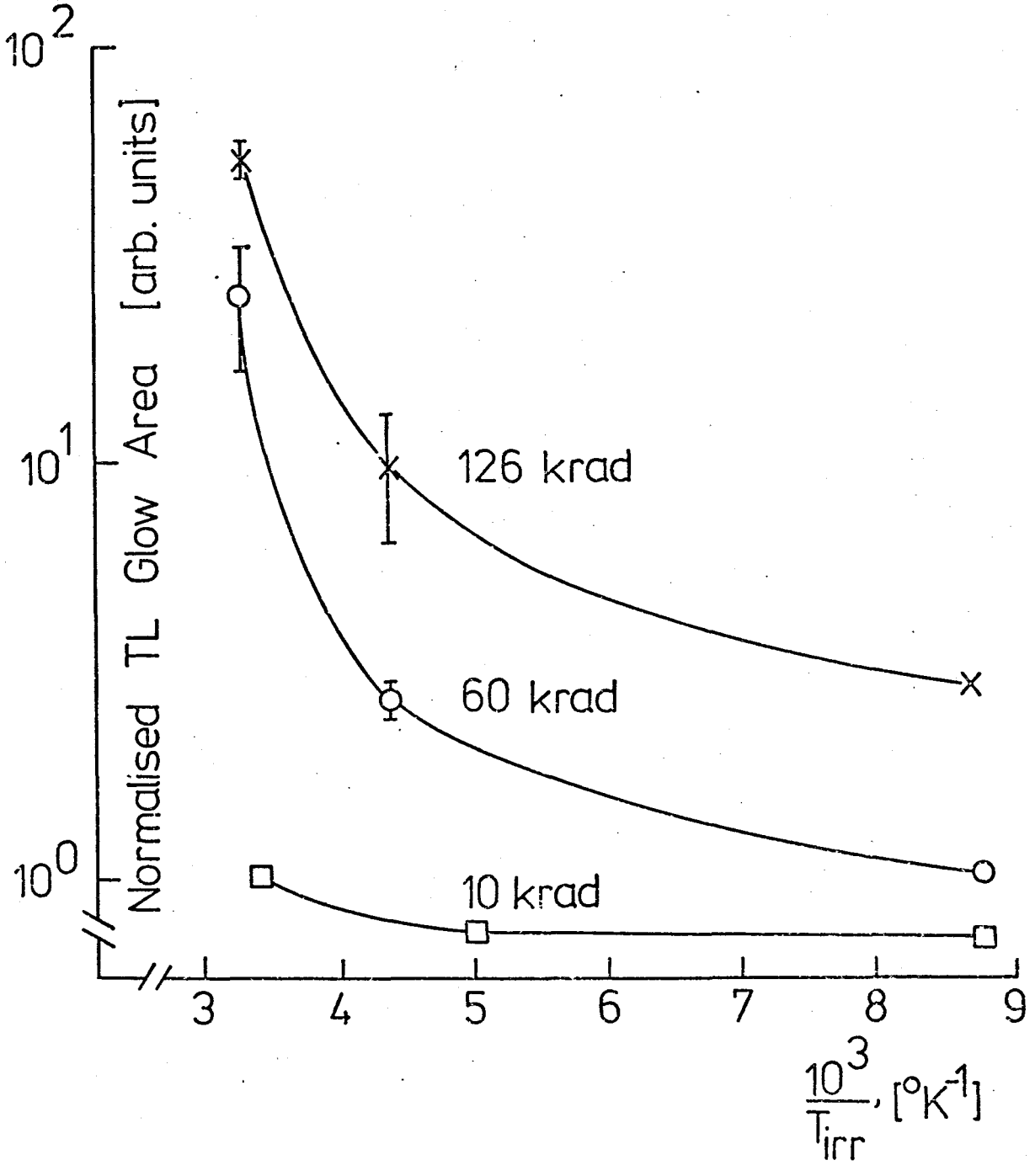
10^2
10^1
10^0
Normalised TL Glow Area [arb. units]
126 krad
60 krad
10 krad
3
4
5
6
7
8
9
$\frac{10^3}{T_{irr}}$, [°K^{-1}]

Fig 4·4

the samples are irradiated with the larger X-ray doses.

Following each of the primary irradiations represented in Figure 4.4, the sample was re-irradiated with the 5krad test dose at 293°K in order to ascertain whether any changes in sample sensitivity had occurred following the large X-ray doses. The results are shown in Figure 4.5 where it can be seen that no noticeable changes in sensitivity have occurred following the 10krad primary dose. The 60krad dose induces sensitivity changes at $T_{irr} > 218^{o}K$, whilst the 120krad dose induces sensitivity changes at all values of T_{irr} except 113°K. The error bars shown in Figure 4.4 and 4.5 represent the scatter of results obtained by repeating the experiment several times on different samples.

4.3 The Effect of the Temperature of Irradiation upon the Sensitivity and Saturation Level of Quartz, using Gamma-rays.

The gamma-irradiations were performed using the 3500 Curies ^{60}Co source available in the Birmingham Radiation Centre, University of Birmingham (see Section 2.2.2), the dose rate in this experiment being 620krad hr^{-1}. The TL induced by gamma-irradiation was read out using the apparatus described in detail in Section 2.1.

The samples used in this work were different types of natural quartz (i.e. smoky, rose, rock and clear crystal) together with synthetic quartz made and supplied by Cathodeon Crystals Ltd., Linton, Cambridge, England. The samples were prepared following the procedure described in Section 3.2.

4.3.1 The variation of the quartz TL response with the irradiation temperature.

Irradiation with gamma-rays at different temperatures was achieved by placing the sample slice in a small, thin, sealed polythene container which itself was immersed into a suitable freezing mixture inside a vacuum flask to give the desired irradiation temperature. The five temperatures

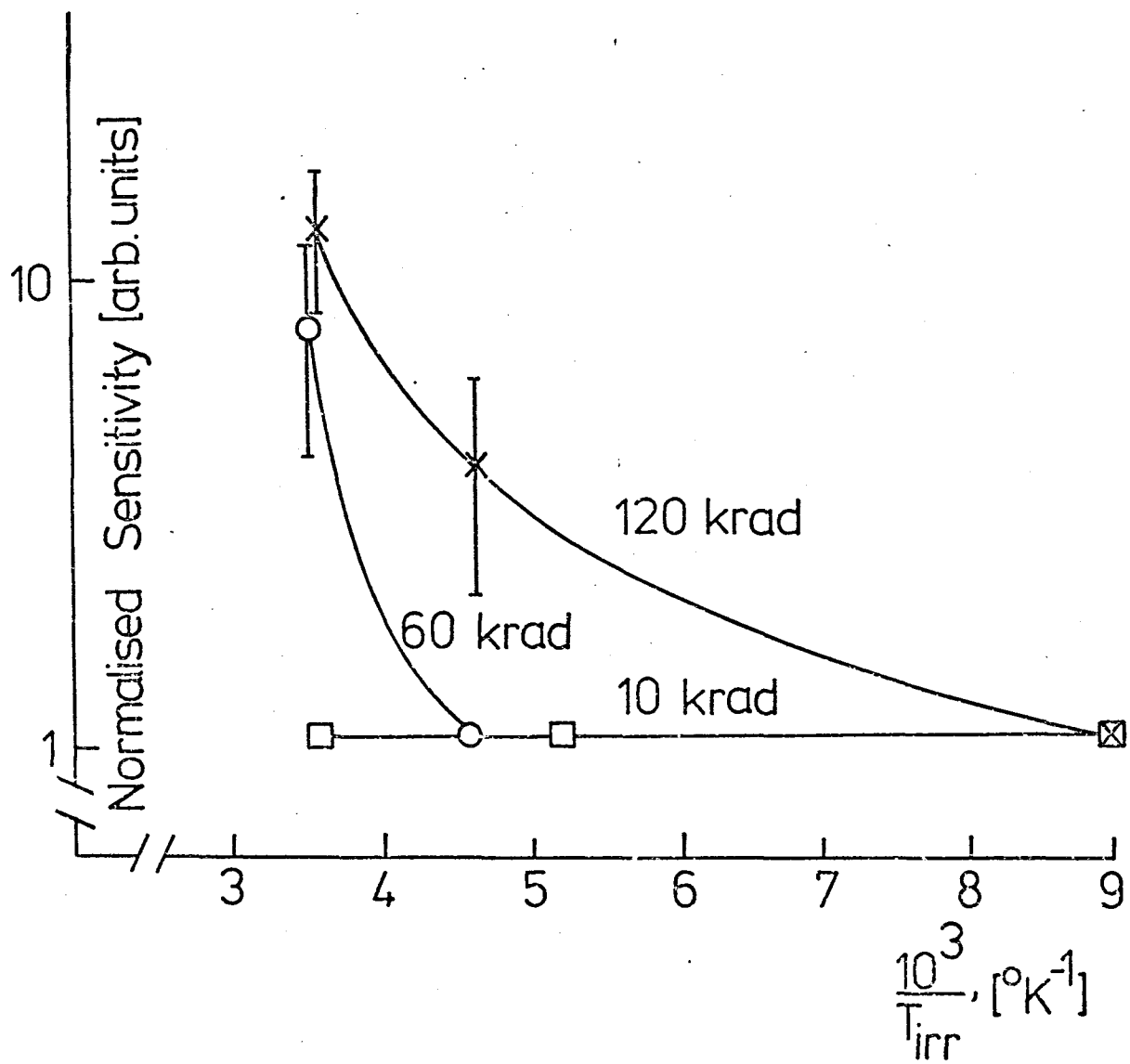
Normalised Sensitivity [arb. units]
10
1
120 krad
60 krad
10 krad
3
4
5
6
7
8
9
$\frac{10^3}{T_{irr}}$, [°K^{-1}]

Fig 4·5

used in this work were 293°K, 273°K, 248°K, 195°K and 178°K. These are the temperatures of room temperature, ice + water, solid brine, solid CO_2 and solid acetone respectively. The solid brine was prepared by saturating boiling water with NaCl, leaving it to cool down to room temperature, and then freezing by mixing it with solid CO_2. Solid acetone was prepared by mixing the acetone gently with liquid nitrogen. The sample in its container was kept in the coolant for several hours prior to the irradiation in order to ensure that it had reached the desired temperature. Each sample (in the coolant) was then given a 600krad dose from the ^{60}Co source and left to warm to room temperature. Following transfer to apparatus A (see Section 2.1) the TL glow was recorded in the usual manner. A typical glow curve from the gamma-irradiated clear quartz is shown in Figure 4.6. More glow peaks are apparent in the 513°K to 693°K region than in the glow curve obtained from an X-irradiated sample. Figure 4.7 shows the variation in normalised TL glow with irradiation temperature for the five different types of quartz. It is evident from Figure 4.7 that in contrast to the lower doses of X-rays, the relatively high dose gamma-irradiation produces a far greater variation with temperature, the TL glow intensity falling by over three orders of magnitude over the temperature range 293°K to 178°K. It was also noted that when gamma-irradiation was used the observed TL glow in the readout interval from room temperature to 423°K was unaffected by the changes in irradiation temperature. It may be noted from Figure 4.7 that the synthetic quartz which is expected to have the lowest impurity content of the samples used, yields the lowest TL glow.

4.3.2 The variation of the quartz sensitisation with the temperature of irradiation.

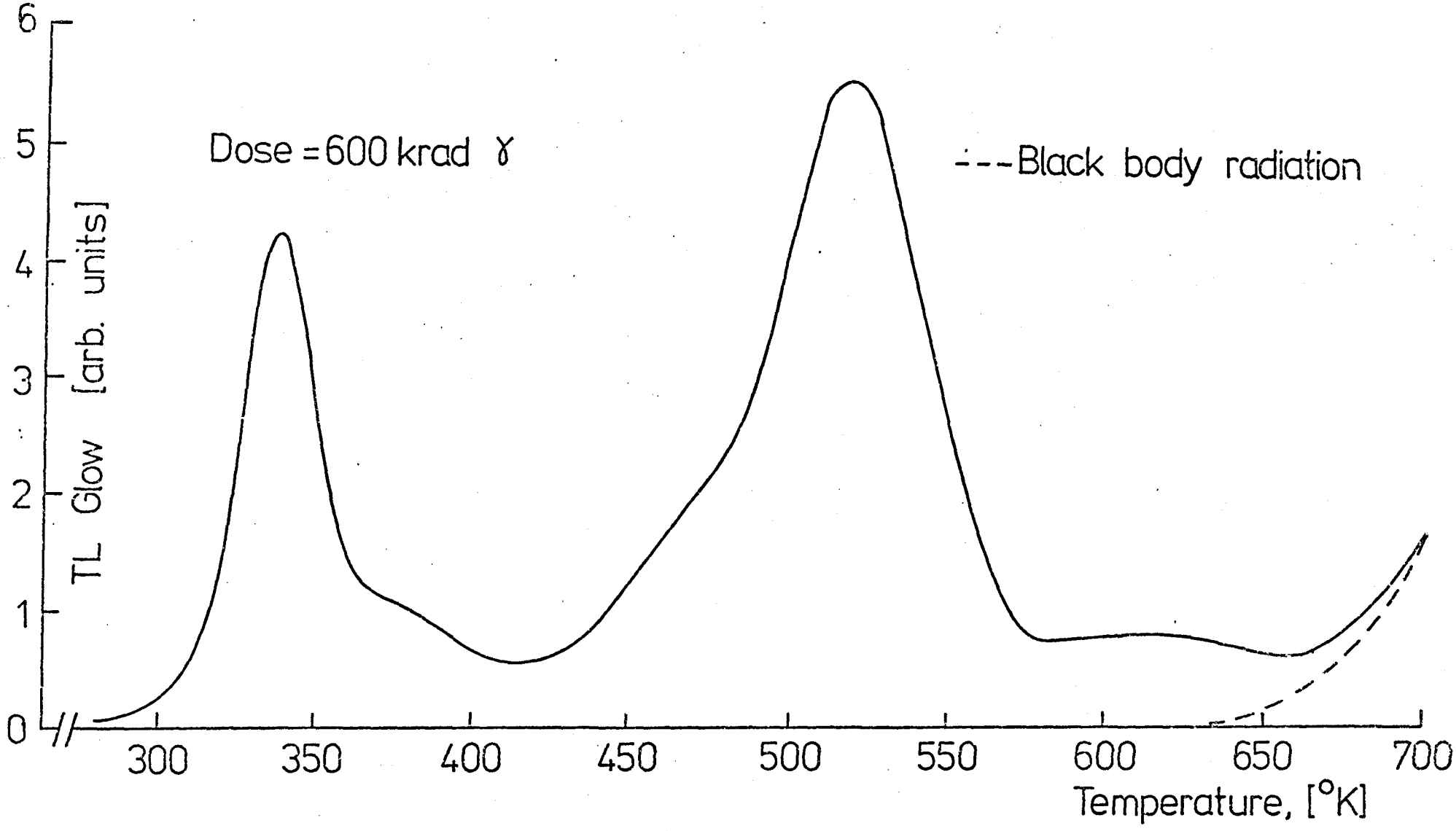
Dose = 600 krad γ
---Black body radiation
TL Glow [arb. units]
0
1
2
3
4
5
6
300
350
400
450
500
550
600
650
700
Temperature, [°K]

Fig 4·6

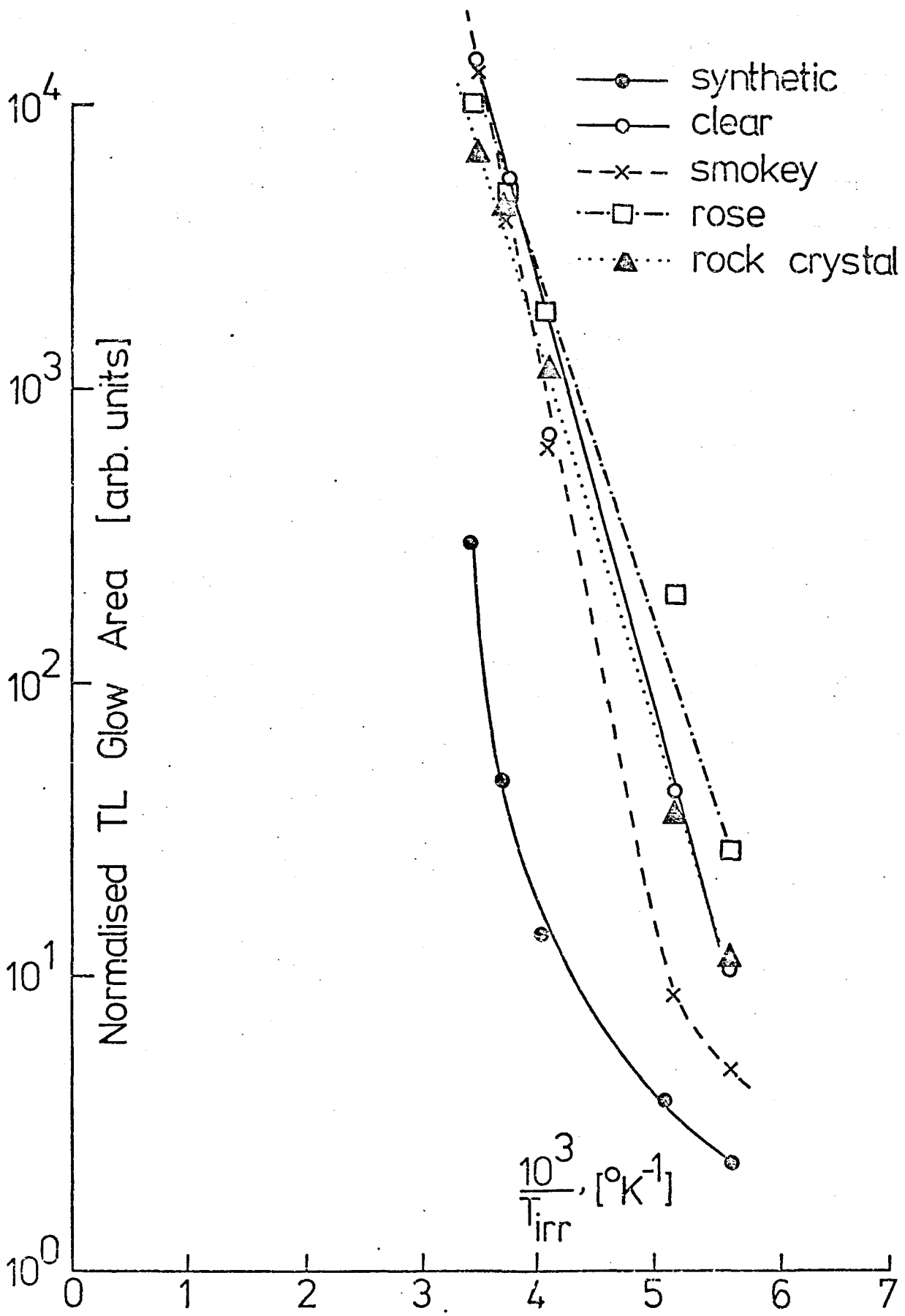
synthetic
clear
smokey
rose
rock crystal
Normalised TL Glow Area [arb. units]
10^4
10^3
10^2
10^1
10^0
0
1
2
3
4
5
6
7
$\frac{10^3}{T_{irr}}$, [°K^{-1}]

Fig 4.7

The variation of the sensitisation of natural quartz with the temperature of irradiation was studied using slices of 200μm thickness and about 2mg in weight. These slices were first given a beta test dose of 30krad from a ^{90}Sr source and the initial sensitivity (S_o) of each slice, for the purpose of normalisation, was determined. The slices were then given a gamma dose of 600krad under different temperatures of irradiation. Four temperatures of irradiation were used for the purpose of this investigation (i.e. 293°K, 273°K, 248°K and 195°K), two fresh slices being used for each temperature of irradiation. The gamma irradiation was followed by reading out the induced TL. The slices were again given the test beta dose of 30krad and their new sensitivity (S) determined for each temperature of irradiation. In all the TL measurements the glow area over the temperature interval 513°K to 693°K was measured. The ln of the ratio $(\frac{S}{S_o})$ for each of the temperatures of irradiation used was plotted versus $\frac{10^3}{T_{irr}}$, where T_{irr} is the temperature of irradiation in degrees Kelvin. The results of this experiment are shown in Figure 4.8. The results show the sensitization of natural quartz falling by three orders of magnitude over the temperature range 293°K down to 195°K.

4.3.3 The variation of the saturation level with the temperature of irradiation.

Figure 4.9 shows the variation in normalised TL glow area from 489°K to 813°K with imparted gamma-dose for quartz irradiation at (A) room temperature (293°K) and (B) solid CO_2 temperature (195°K) - curve A has been reduced by a factor of 10^3 in the plot. The maximum glow of the room temperature curve (A) is seen to be nearly 10^3 times that for curve B, which is reached with a larger dose of ~ 8Mrad. Furthermore, the saturation level of this latter curve appears to remain constant at higher doses whilst

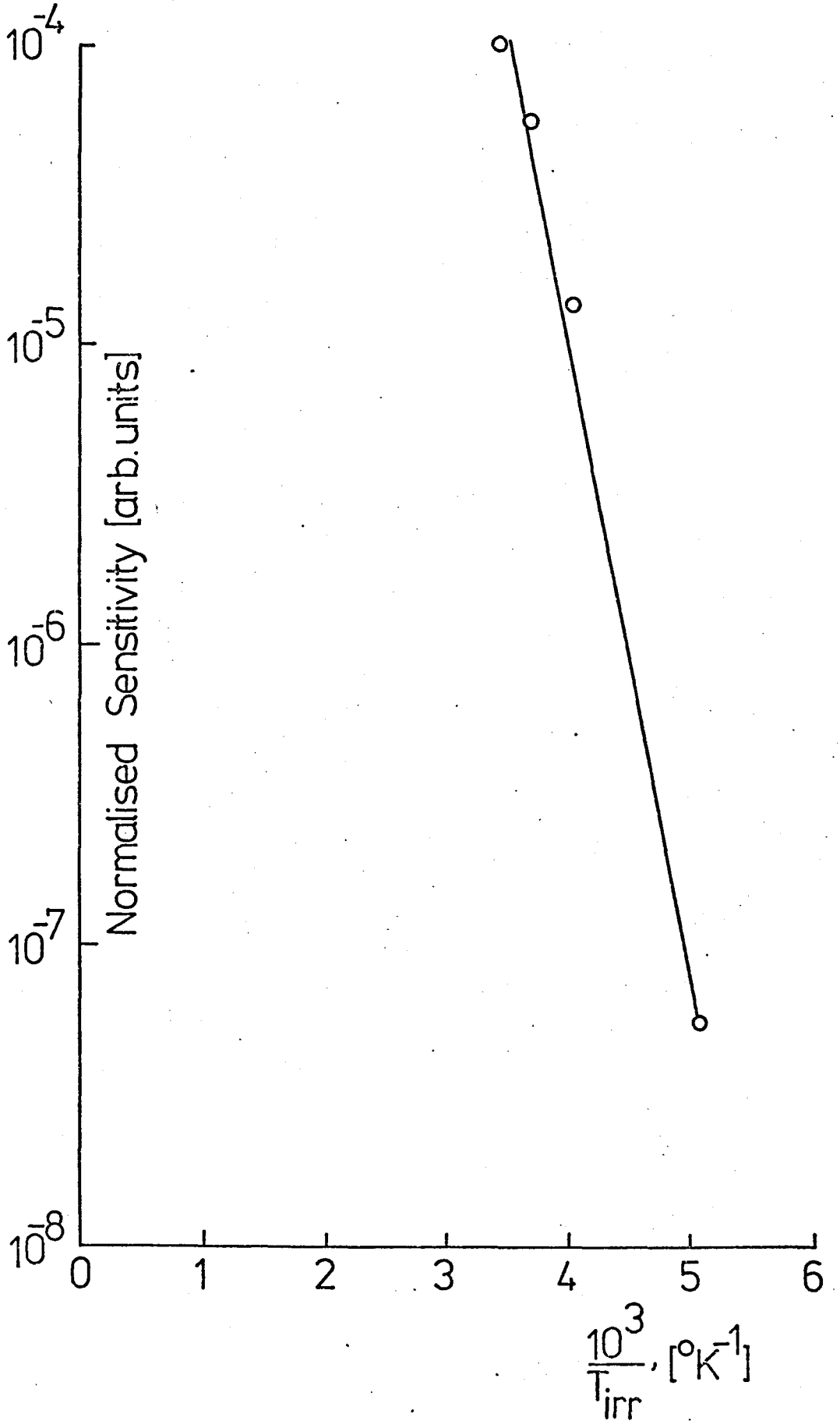
10^{-4}
10^{-5}
10^{-6}
10^{-7}
10^{-8}
Normalised Sensitivity [arb.units]
0
1
2
3
4
5
6
$\frac{10^3}{T_{irr}}$, [°K^{-1}]

Fig 4·8

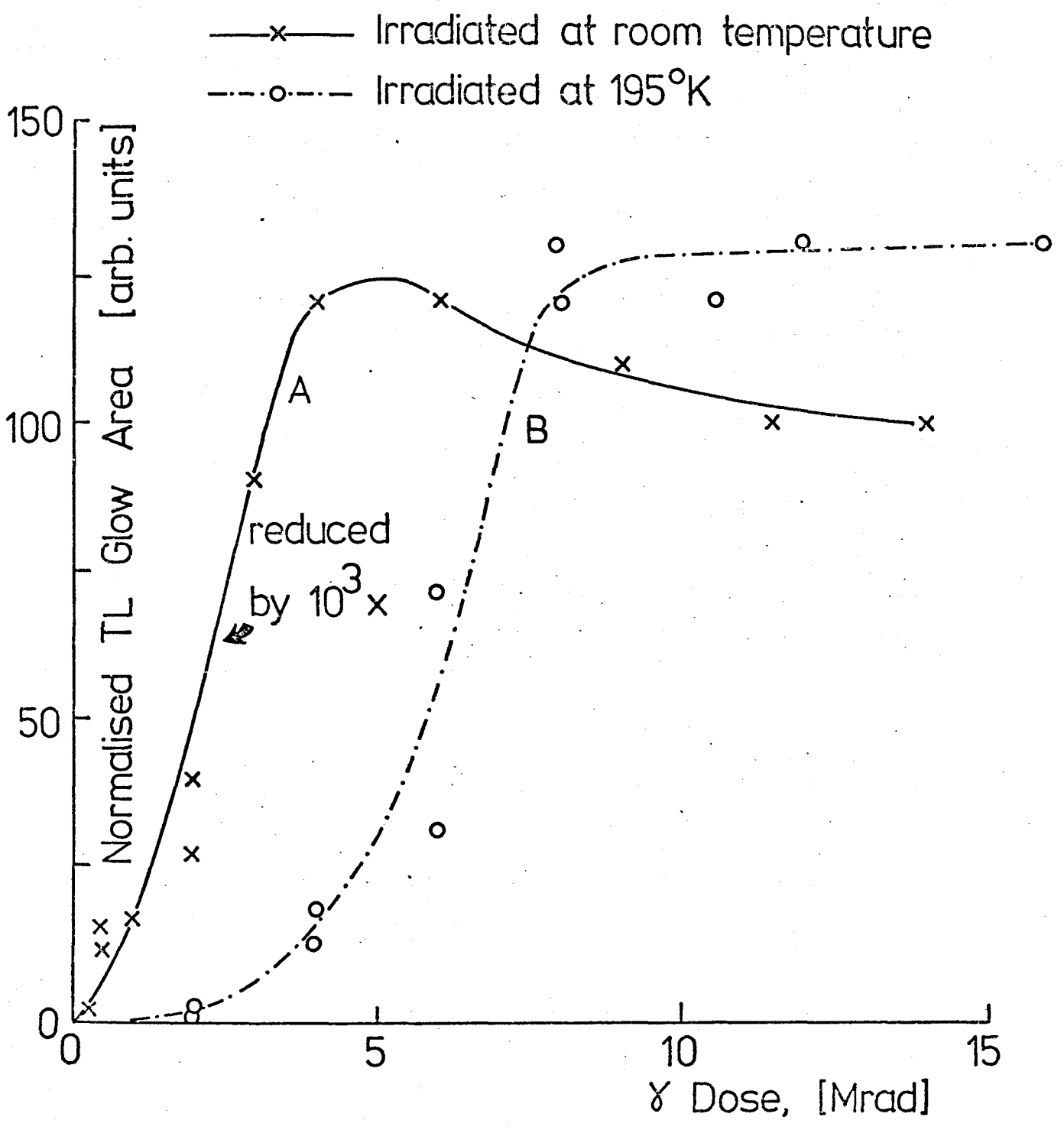
Irradiated at room temperature
Irradiated at 195°K
150
100
50
0
Normalised TL Glow Area [arb. units]
A
B
reduced
by 10^3 x
0
5
10
15
γ Dose, [Mrad]

Fig 4·9

the room temperature curve shows a decrease beyond ~ 6Mrad.

4.4 Discussion.

4.4.1 Low doses - no structural damage.

The TL glow from quartz in the readout interval 470°K to 670°K is known to be directly associated with the presence of impurities within the quartz lattice (Batrak, 1958; Schlesinger, 1964; Ichikawa, 1968). The blue emission in this region of the glow curve is due to the radiative recombination of thermally released electrons at luminescence centres. These centres are thought to consist of a hole localised at a defect site resulting from the presence of substitutional Al and an interstitial alkali ion (see Section 3.1). The trivalent Al substitutes for a host Si atom. The unpaired electron on the adjacent oxygen atom is charge-compensated by the presence of a monovalent interstitial alkali ion. When hole-electron pairs are created within the sample by irradiation with, say, X-rays, the hole becomes localised at the oxygen site, enabling the alkali ion to migrate away along the interstitial channels within the quartz lattice. This trapped hole centre can now act as a recombination centre for the electron which has become localised elsewhere within the crystal. Thermal stimulation in a TL experiment liberates the electron which radiatively recombines with the hole, thus allowing the alkali ion to migrate back to the Al site and reform the Al/alkali centre.

Obviously the effectiveness of the Al/alkali centre in acting as a recombination centre is reflected in the ability of the centre to capture a hole. This, in turn, is dependent upon the mobility of the alkali ion (McKeever, 1976). Hence, the most abundant type of alkali ion found at such centres is Li^+ or Na^+; the larger K^+ ion is too big to migrate easily along the inter-

stitial channels. Furthermore, if the Li^+ or Na^+ ions were prevented from moving, no hole trapping would take place and, hence, no TL would result. If, therefore, the sample is irradiated with X-rays at very low temperatures, little or no TL will be seen in this part of the glow curve since the alkali ion will not possess enough thermal energy to migrate away. Such a temperature dependence has been confirmed by Halperin and Ralph (1963) and Mackey (1963) using optical absorption and electron spin resonance techniques.

Consider a sample with N available electron traps, of energy depth E below the conduction band, irradiated at a dose rate r whilst being held at a temperature T_{irr}. If p is the probability per unit dose of a trap being filled, then the total number of traps filled at time t is:

$$n = \frac{N}{1 + \frac{s}{rp} \exp\left(\frac{-E}{k T_{irr}}\right)} \left[1 - \exp\left(-rpt\left(1 + \frac{s}{rp} \exp\left(\frac{-E}{k T_{irr}}\right)\right)\right)\right] \quad (1)$$

where s is the 'attempt-to-escape' frequency factor for the electron trap. If the total dose in time t is D = rt and T_{irr} is low enough so that thermal drainage of the traps can be ignored, then equation (1) reduces to:

$$n = N\left(1 - \exp\left(-Dp\right)\right) \quad (2)$$

In the case of the Al/alkali centre the probability of this centre capturing a hole is directly dependent upon the rate at which the alkali ion can move away. As the number of trapped electrons must equal the number of trapped holes (for charge neutrality) one can say that the probability of an electron being trapped is also directly dependent upon the mobility of the alkali ion, assuming there is just one type of hole-trapping centre. Approximating the motion of the interstitial alkali ion by an Arrhenius type equation (McMorris, 1971), the following equation is obtained:

$$rp \propto \tau_o^{-1} \exp\left(\frac{-H}{kT_{irr}}\right) \qquad (3)$$

where τ_o^{-1} is a characteristic frequency factor and H is the activation energy for movement of the interstitial ion.

Using the first-order kinetics of Randall and Wilkins (1945) the TL intensity I(T) can be expressed by:

$$I(T) = C n s \exp\left(\frac{-E}{kT}\right) \qquad (4)$$

where C is a recombination constant. The number of filled traps, n, is usually independent of irradiation temperature - provided that T_{irr} is low enough to prevent thermal drainage. However, combining equations 2 and 3 gives rise to the following equation:

$$n = N\left[1 - \exp\left(-\frac{D\alpha}{\tau_o r} \exp\left(\frac{-H}{kT_{irr}}\right)\right)\right] \qquad (5)$$

where α is a proportionality constant. From equation 5 it can be seen that n is dependent upon T_{irr}, provided:

$$\exp\left(\frac{-H}{kT_{irr}}\right) > \exp\left(\frac{-E}{kT_{irr}}\right)$$

i.e. $E > H$; there is some evidence that this latter proviso is valid. Stevels and Volger (1962) use dielectric loss measurements to determine the activation energy for interstitial alkali ion movement within the interstitial channels in quartz. They find an activation energy of 0.089eV for Li^+ and 0.055eV to 0.14eV for Na^+. Using $E = 25\,kT^*$ (T^* is the temperature of a particular glow peak) values for E from 1.01 to 1.35eV for the TL peaks in the region 470°K to 670°K have been calculated.

Substituting equation 5 into equation 4 gives:

$$I(T) = C\,N_s \exp\left(\frac{-E}{kT}\right)\left[1 - \exp\left(\frac{-D\alpha}{\tau_o r}\exp\left(\frac{-H}{k\,T_{irr}}\right)\right)\right] \qquad (6)$$

when $n = N$, $I = I_o = C\,N\,s\exp\left(\frac{-E}{k\,T}\right)$ (saturation level).

Hence:

$$I(T) = I_o\left[1 - \exp\left(\frac{-D\alpha}{\tau_o r}\exp\left(\frac{-H}{k\,T_{irr}}\right)\right)\right] \qquad (7)$$

The curve of $\ln(I(T))$ against T_{irr}^{-1} is shown in Figure 4.10. The family of curves shown has been plotted with arbitrary values for I_o, $\frac{D\alpha}{r\tau_o}$ and $\frac{H}{k}$. H is the variable parameter. The purpose of plotting the curves of Figure 4.10 is to show the general shape of the function expressed in equation 7.

In the present work, for samples irradiated with 5krad of X-rays, the TL intensity has been shown to vary by a factor of ~5 over the irradiation temperature range 293°K to 113°K and the curve shape (Figure 4.3) can be seen to exhibit a general similarity with the theoretical curves of Figure 4.10. With low doses no observable sensitisation and, therefore, no significant structural changes have taken place, as is evident from the 10 krad curve of Figure 4.5. Therefore, under these conditions of no sensitisation, it is concluded that the predominant effect of varying the temperature of irradiation is to alter the probability of trap filling, in accordance with equation 7.

4.4.2 Large doses - effect of structural damage.

The derivation of equation 7 obviously requires that the total number of traps N is a constant, i.e. it is independent of both dose D and temperature T_{irr}. The introduction of a non-constant N would invalidate equation 7. When irradiated with large X-ray doses, i.e. 60krad and 120krad, sensitisa-

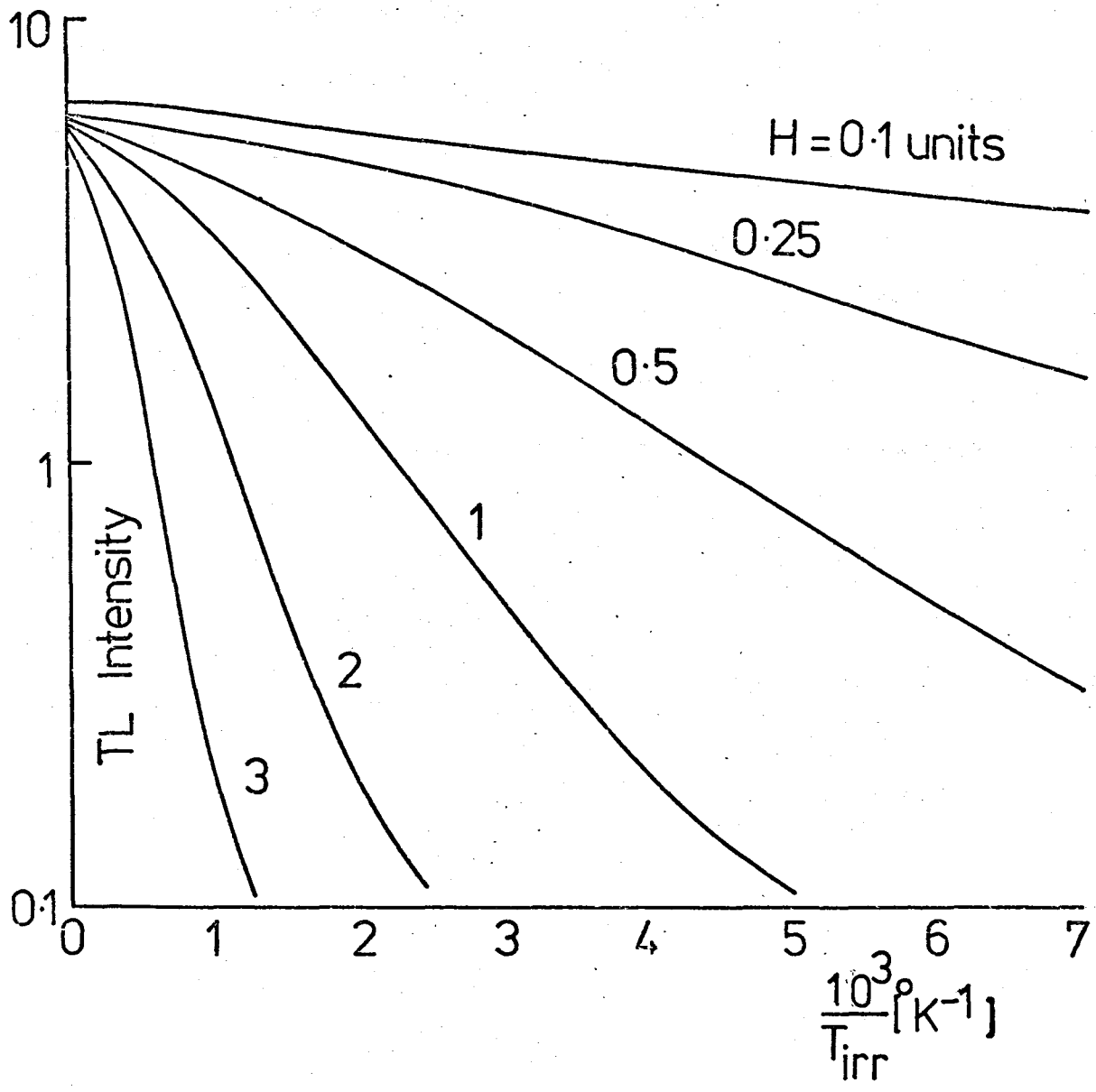

Sketch of equation 7, with I_o = 10 units, $\frac{Da}{r\tau_o}$ = 1 unit and k = 1 unit. H is the variable parameter.

Fig 4·10

tion of the sample occurs (Figure 4.5) and a larger variation in the TL intensity with T_{irr} results (Figure 4.4). The latter point is even more forcefully illustrated when large (600krad) gamma-doses are used (Figure 4.7). It is postulated here that the sensitisation changes occur as a result of permanent structural changes which result from sample irradiation. These structural changes manifest themselves by a breaking of the strained Si —— O bond at the Al/alkali centre. The results of this breakage is to produce an oxygen vacancy and an oxygen interstitial. The damage, therefore, destroys the hole-trapping Al/alkali centre and creates extra electron traps (Ichikawa, 1968). If one assumes that, originally the number of Al/alkali centres present in most forms of quartz is greater than the number of potential electron traps (Bambauer, 1961) then, as the damage proceeds, an increase in the TL sensitivity of the sample will initially result. This is because extra electron traps are created whilst there are still sufficient Al/alkali centres remaining to complement them. The migration of the alkali ion and the formation of the oxygen vacancy and interstitial will be temperature dependent. One would expect that at low temperatures the oxygen interstitial would be in close proximity to the oxygen vacancy, which would result in a shielding of the charge on the vacancy and thus little or no electron capture. This, in turn, would lead to a reduced TL intensity. As the temperature is increased the interstitial and vacancy can separate farther apart, giving rise to increased trapping and, therefore, a larger TL intensity. These features give rise to the curves of Figures 4.4 and 4.5.

The appearance of this temperature effect in different types of quartz supports these postulates. The quartz samples used for Figure 4.7 all

have Al/alkali centres as their main recombination centre for TL emission over the readout interval 470°K to 670°K. The impurity content of synthetic quartz can be expected to be less than that of the other natural samples and so one might expect the TL output to be lower, as is seen to be the case in Figure 4.7.

4.4.3 Combined effect of irradiation temperature (T_{irr}) upon trap filling and trap creation.

The curves of Figures 4.7 and 4.4 are the result of the combined effect of T_{irr} upon the rate of trap filling and of trap creation. The effect upon trap creation alone can be seen in Figure 4.5. The effect that the variation of T_{irr} has upon the TL response, as increasing radiation doses are imparted to the sample, is seen in Figure 4.9, the shape of the curves in this figure being best explained by reference to Figure 4.11. In Figure 4.11a the result of changing T_{irr} when no trap creation is occurring is shown. T_{irr} merely affects the dose D_o at which the saturation level I_o is reached. When T_{irr} affects trap creation only and does not affect the probability of trap filling, Figure 4.11b will result. Here only the magnitude of I_o is affected. The result of combining the two effects is seen in Figure 4.11c. Here both I_o and D_o are dependent upon T_{irr}. From Figure 4.3 it can be seen that the TL intensity per unit dose changes by a factor of $\sim$ 4 over the temperature range 293°K to 195°K when trap filling alone is affected by T_{irr}. In Figure 4.9 it can be seen that the dose required to reach saturation also changes by a factor of $\sim$ 4 when T_{irr} is changed from room temperature to 195°K. Furthermore, from Figure 4.7 it can be seen that the TL intensity changes by a factor of $\sim 10^3$ over the temperature range 293°K to 178°K when trap creation is occurring. Also, the saturation level differs by a factor of $\sim 10^3$ when T_{irr} is changed from room temperature to 195°K, as

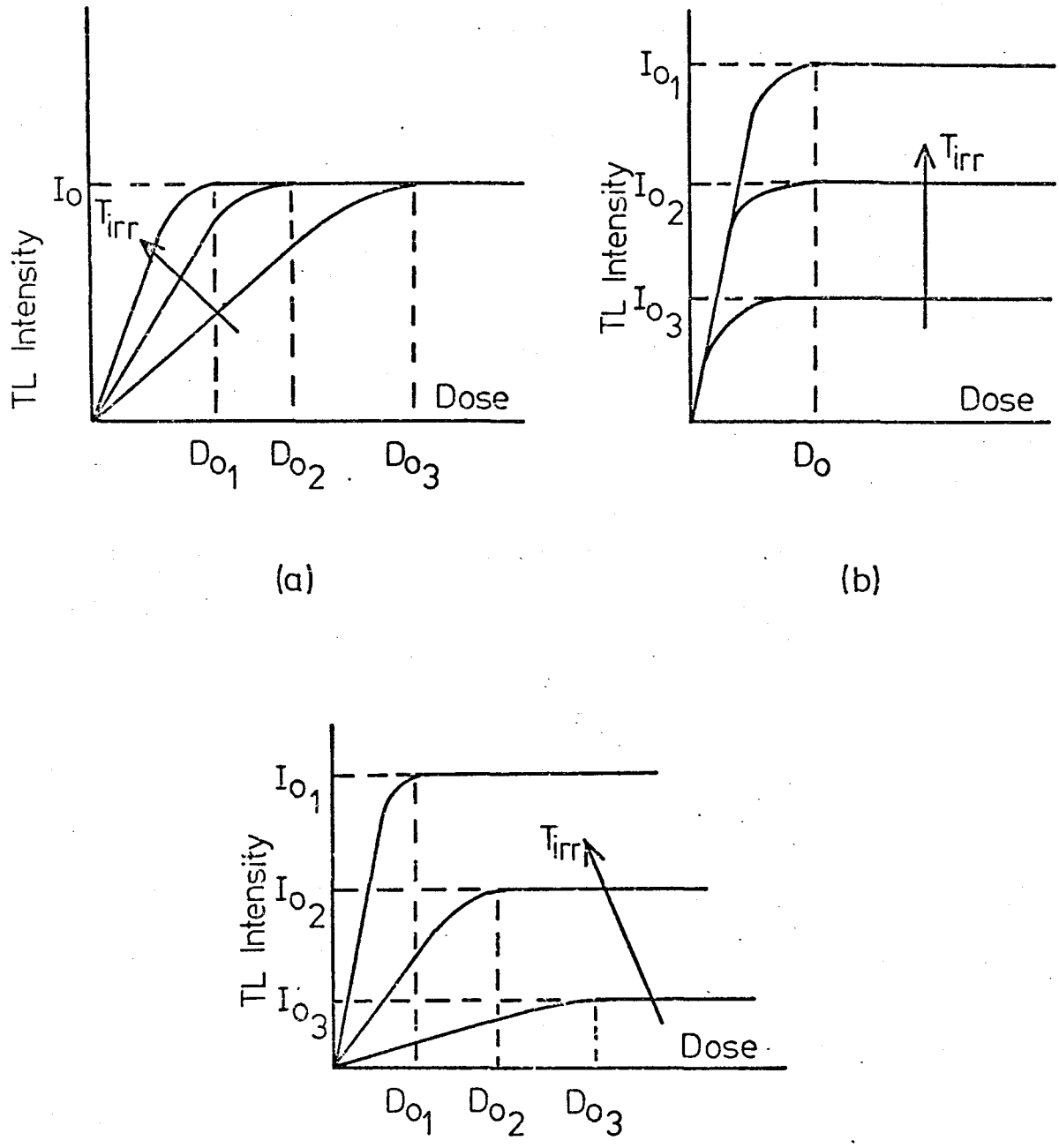
TL Intensity
Io
Tirr
Dose
Do1
Do2
Do3
(a)
Io1
Io2
Io3
Tirr
TL Intensity
Dose
Do
(b)
Io1
Io2
Io3
Tirr
TL Intensity
Dose
Do1
Do2
Do3
(c)

Fig 4·11

can be seen from Figure 4.9.

The room temperature curve in Figure 4.9 does not attain a fixed saturation level. This is the result of increased damage upon the recombination centre at high radiation doses. Because the damage takes the form of destruction of the Al/alkali recombination centres, there comes a point at which the concentration of recombination centres is less than the total concentration of electron traps. This results in a decrease in TL intensity. The observation that this decrease in TL intensity does not occur when irradiated at 195^{o}K is further confirmation of the hypothesis.

4.5 Summary and Conclusion.

This chapter reports upon the finding of a dependence of the TL output upon the temperature of irradiation in quartz. Both X-irradiation and gamma-irradiation were employed in this work and the evidence presented suggests that two distinct processes are responsible for this temperature dependence.

When low dose X-rays are used, only a small variation in TL with T_{irr} is evident. This variation is postulated to arise from the dependence of the probability per unit dose of a hole being captured at an Al/alkali centre. The result of this is a variation by a factor of $\sim$ 5 in the TL glow intensity over the T_{irr} range from room temperature down to 113^{o}K with an X-ray dose of 5krad.

A much larger variation in TL with T_{irr} is noted with higher dose irradiations. The evidence presented suggests that this arises from the dependence of sensitisation (i.e. electron trap creation) upon T_{irr}. This results in a variation in TL intensity by a factor of $\sim 10^{3}$ over the T_{irr} range from room temperature down to 178^{o}K with a gamma dose of 600krad.

The finding reported in this chapter, namely the effect of the temperature of irradiation upon the TL sensitivity and the sensitisation of quartz, has serious implications for dating practice. The specimen calibration in dating procedure by adding alpha, beta or gamma doses before and after the readout of the natural TL may no longer be valid. This conclusion arises from the fact that the traps already existing cannot be differentiated from those created by laboratory radiations. The results of this chapter also imply that although soft X-ray and U.V. irradiations are still subjected to the effect of irradiation temperature on sensitivity, small doses of such low energy radiations do not create traps to an appreciable degree, thus avoiding the complication of the strong temperature dependence of trap creation by high energy radiation in the calibration of quartz specimens. The temperature effect also implies that careful consideration should be given to the temperature of burial of the specimen in any dating procedure. As an example, specimens, say, from the Aboriginal fire sites in the Australian desert, or sherd recovered from sub-zero environment, should be treated cautiously if the separated mineral is quartz and the calibration is going to be carried out at a temperature different from that of the burial. From the results given in this chapter, it is estimated that the TL intensity of a quartz sample irradiated at, say, $-5^{\circ}C$ (average winter temperature) is about 40% of that irradiated at $20^{\circ}C$ (average summer temperature) for a gamma dose of 600krad. Although the dose used here was far higher than that in a normal dating calibration routine, the effect is found to be the same for lower doses of gamma-rays, energetic beta particles (^{90}Sr) and X-rays.

From the above discussion it is concluded that the effect of the temperature of irradiation could be corrected for either by carrying out the irradiation

of the quartz sample during the calibration procedure at a temperature identical to that of burial or by using a sensitivity versus temperature of irradiation graph similar to that of Figure 4.7 obtained for that particular type of quartz with a radiation dose not far from the natural dose received by the sample, since the temperature effect varies with the dose received by the sample.

The work reported in this chapter shows not only that the TL sensitivity but also the saturation level of quartz varies with the temperature at which the irradiation is carried out. These results suggest that one can use the sensitivity or the saturation level versus the temperature of irradiation graph as a thermometer to determine the environmental temperature of a specimen if the separated mineral is quartz. This result would be of vital importance in the TL studies of extraterrestrial materials such as meteorites and lunar samples collected from, say, a shadow of boulder where the aim of TL studies for these materials is to gain information concerning their thermal and radiation history. This last conclusion is applicable if these materials show such a temperature effect.

CHAPTER V

THERMOLUMINESCENCE AND FISSION-TRACK STUDIES OF THE OKLO FOSSIL REACTOR MATERIALS

5.1 Historical Background of Oklo Phenomenon.

The starting point in the discovery of the phenomenon was the finding of an unusual isotopic abundance in a sample of natural uranium. This discovery was made in June 1972 by a team working under the direction of Dr. H. V. Bouzigues (Naudet, 1974) at the French Commissariat a l'Energie Atomique (CEA) service laboratory at Pierrelatte in France.

During the certification of a secondary standard of UF_6 by the gas diffusion method, a marked anomaly in the abundance of the uranium-235 isotope was noticed ($0.7171 \pm 0.0006\%$). However, the difference was very small although the isotopic composition of uranium should be exactly the same everywhere on earth and even on the moon.

It was thought initially that the marginal difference in uranium abundance could be a result of a measuring or handling error. Such a possibility was excluded by rechecking the analytical procedure which showed, to the contrary, that this was a large-scale isotopic degradation.

The question of an artificial contamination was also excluded by a systematic analytical campaign which was started right from the production of UF_6 at Pierrelatte, through the Malvesi and Gueugnon factories, up to the preconcentrates supplied by the Compagnie des Mines d'Uranium de Franceville (C.O.M.U.F.) which works the two neighbouring deposits of Mouana and Oklo in Gabon. It was concluded from this campaign that a natural ore with unusual content existed. It was also found that the source of the mineral responsible for the anomalies was the northern end of the

Oklo deposit.

Large depletions of uranium-235 isotope were discovered (down to 0.621%, and eventually to 0.296%) in uranium samples which were traced back to the Oklo deposit. It was also established that all the uranium shipped (from Mouana concentration plant) between December 1970 and May 1972 had an isotopic abundance lower than usual. This anomaly involved over 700 tonnes of uranium having entered the industrial circuits. This was therefore a phenomenon of considerable size.

5.2 The Principal Characteristics of Oklo Deposit.

The Oklo deposit is of the sedimentary type. The tip of the uraniferous layer, which is 5 to 8 metres thick, is inclined of the order of 45^{o}. The mining is carried out in the tip by cutting successive horizontal sections (Naudet, 1974).

The anomalies are located in three zones in the northern part of the Oklo ore deposit (Figure 5.1). Zone 1 and zone 2 are separated by 30m and have respectively $150m^2$ and $130m^2$ of area. At 40m in the south, zone 3 has been discovered by drilling but has not yet been reached by the mine working. The area of the worked part of zone 1 and zone 2 is the same order of magnitude as that of the unworked part. It has been confirmed that zone 1 is irregular, the distribution of the uranium content being often haphazard. Zone 2, on the contrary, is more regular and more compact. The richest part in these zones is 50cm to a metre thick with an average uranium content greater than 15 to 20% which is at least 40 times more than the average mineral. It is believed that there may be other zones not yet brought to light which may exist in the deposit.

Figure 5.2 shows a map of the uranium content on the outcropping of

Northern Extremity of the Oklo Quarry

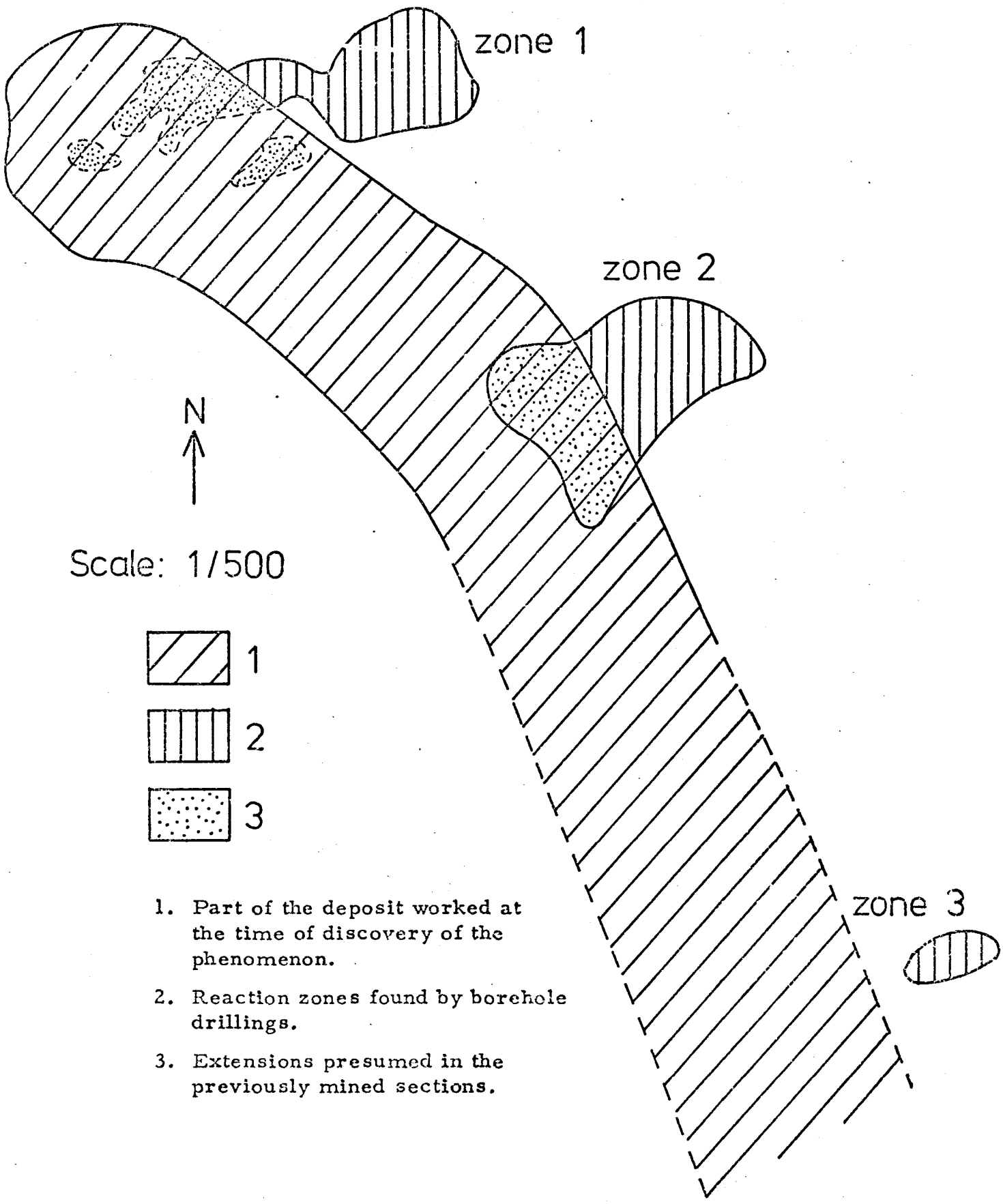

1. Part of the deposit worked at the time of discovery of the phenomenon.
2. Reaction zones found by borehole drillings.
3. Extensions presumed in the previously mined sections.

Fig 5·1

Outcropping of Reaction Zone 2

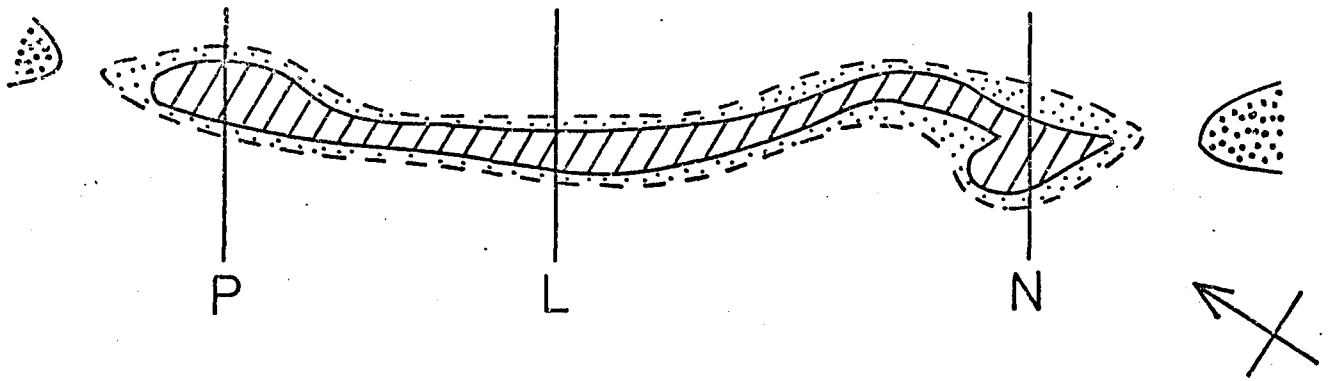

The richest mineral forms a compact mass. At the two extremities the lens of rich mineral adjoins lenses of conglomerate.

Fig 5·2

zone 2 which is far from the richest part. It is found that minerals with a concentration larger than 20% form a continuous horizontal section which is about 14m long and about 1m wide. Inside this mass a large fraction of the mineral has a content greater than 40%. In the surrounding area the concentration decreases very rapidly; often dropping below 5% and then 1% at less than 10cm.

Inside these zones uranium is strongly depleted and reaches its normal concentration further away. It was found that the depletion of U-235 in these zones becomes larger as the uranium content and the thickness of the rich zone increases.

5.3 The Hypothesis of Fossil Nuclear Reactor.

The hypothesis of the occurrence of a chain reaction was confirmed by the finding of fission products in the ore recognisable because isotopic compositions at the end of a radioactive decay chain are generally very different from thoseof natural elements. For some isotopes, significant deviations were noticed; increase in Nd-144 offsetting an equal reduction of Nd-143. Likewise Sm-148 against Sm-147 or Sm-150 against Sm-149, the latter having almost completely vanished. These deviations could be explained by the neutron capture effect, thus confirming the existence of a very high integrated neutron flux at some points exceeding 1.5×10^{21} n cm^{-2}. A correlation between the uranium content and the isotopic degradation of the uranium, as well as with the quantities of fission products, was confirmed. Also it was found that the number of fissions were a hundred thousand times greater than the spontaneous fission of uranium-238 in two billion years. This means that the neutrons responsible for the fission had been strongly thermalised and that the reactions were spread over a very long period of time. Such high number of fissions could

only have been achieved by chain reactions maintained for a long time.

A detailed study of the Oklo deposit (Naudet, 1974) revealed the existence of three vital conditions for the starting of a fission chain reaction. These conditions are (i) high concentrations of uranium, (ii) the absence of strongly neutron-absorbing elements, and (iii) the presence of water as a moderator. Also, concentration of uranium-235 in natural uranium in the remote past was much higher than it is now (3.65% two thousand million years ago as against 0.72% now). This percentage is not far from the percentage used in the present water reactors.

Finally, all these facts made the belief in the occurrence of such fossil nuclear reactor plausible.

5.4 Thermoluminescence Studies of the First Set of Oklo Samples.

5.4.1 Samples and sample preparation.

Two series of samples were used during the course of this work. The first one included samples $2P_1$ to $2P_{15}$ (Nos. 430 to 444 according to Dr. R. Naudet's code) from the outcrop of zone No. 2, picked every 10cm along a line going out from reaction zone 2 and traversing the width of the ore-rich lens. From $2P_1$ to $2P_5$ the samples are still in the 'reactor core'; those beyond are from the low-grade ore. The second group of samples included four samples from the site numbered 1304-1326 from the vertical drilling core SC20 which crosses reaction zone No. 1 at a depth of between 5.30m and 6.40m. The four samples used are No. 1310 (2.00m to 2.20m), No. 1312 (2.40m to 2.60m), No. 1318/1 (3.60m to 3.70m) and No. 1326 (4.80m to 4.90m).

The matrix material from each sample was sieved and grains of diameter between 106 and 180μm were selected for TL studies.

5.4.2 Natural and induced thermoluminescence.

The TL from samples $\sim$ 2mg in weight was read out following the procedure in Section 2.1. Figure 5.3 shows the natural glow curve from sample $2P_{11}$, chosen here as an example. For comparison, also shown is the result of irradiating the same sample with 6Mrad of ^{60}Co gamma rays before the readout. It is clear from the figure that little natural TL has survived below $\sim$ 200°C whereas a prominent peak at $\sim$ 220°C, as well as another one at $\sim$ 140°C, exists in glow curve from the artifically irradiated sample. More stable peaks appear at $\sim$ 350°C and 475°C.

Figure 5.4a shows the variation in the glow areas normalised to a unit of weight (mg) (integrated over the temperature interval 180 to 340°C) under the TL curves resulting from heating natural samples $2P_1$ to $2P_{15}$. Also shown are the TL 'saturation values' (integrated over the same temperature interval) for these samples, achieved by imparting a 6Mrad ^{60}Co γ-ray dose to the natural samples prior to readout. Figure 5.4b shows the glow areas integrated over the (more stable) high-temperature interval 340 to 500°C for the same samples.

Two important features are evident in Figure 5.4. The first is that, in samples $2P_6$ to $2P_{15}$ saturation seems to have been reached in nature in the high-temperature TL (340 to 500°C; Figure 5.4b), whereas fading (i.e. thermal drainage) has reduced the natural TL in the less stable region (180 to 340°C; Figure 5.4a). Since the surviving TL represents the dynamic equilibrium value reached as a result of competition between the radiation filling and the thermal draining of the TL traps in a geological sample, and this equilibrium level is not much affected by the massive dose-rate (up to $\sim$ 2Mrad/hr) employed in the artifical irradiation, this implies that the

Natural and Artificially Induced TL in Sample $2P_{11}$

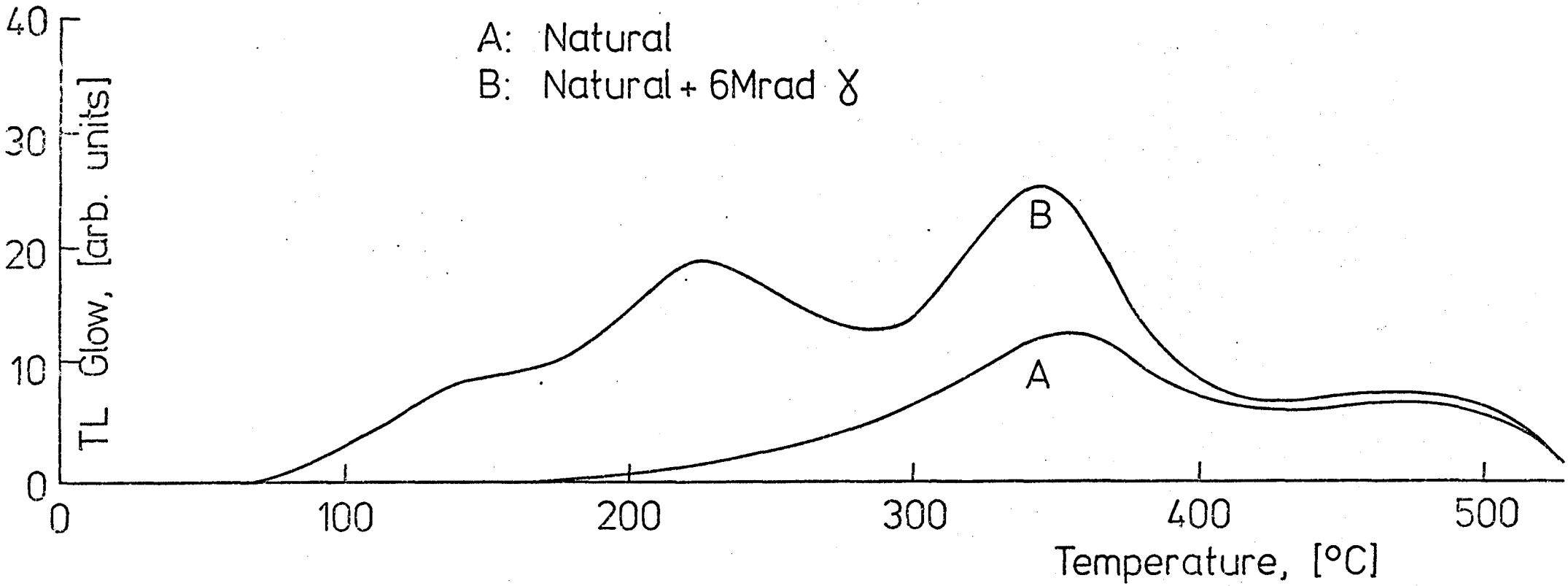

Fig 5·3

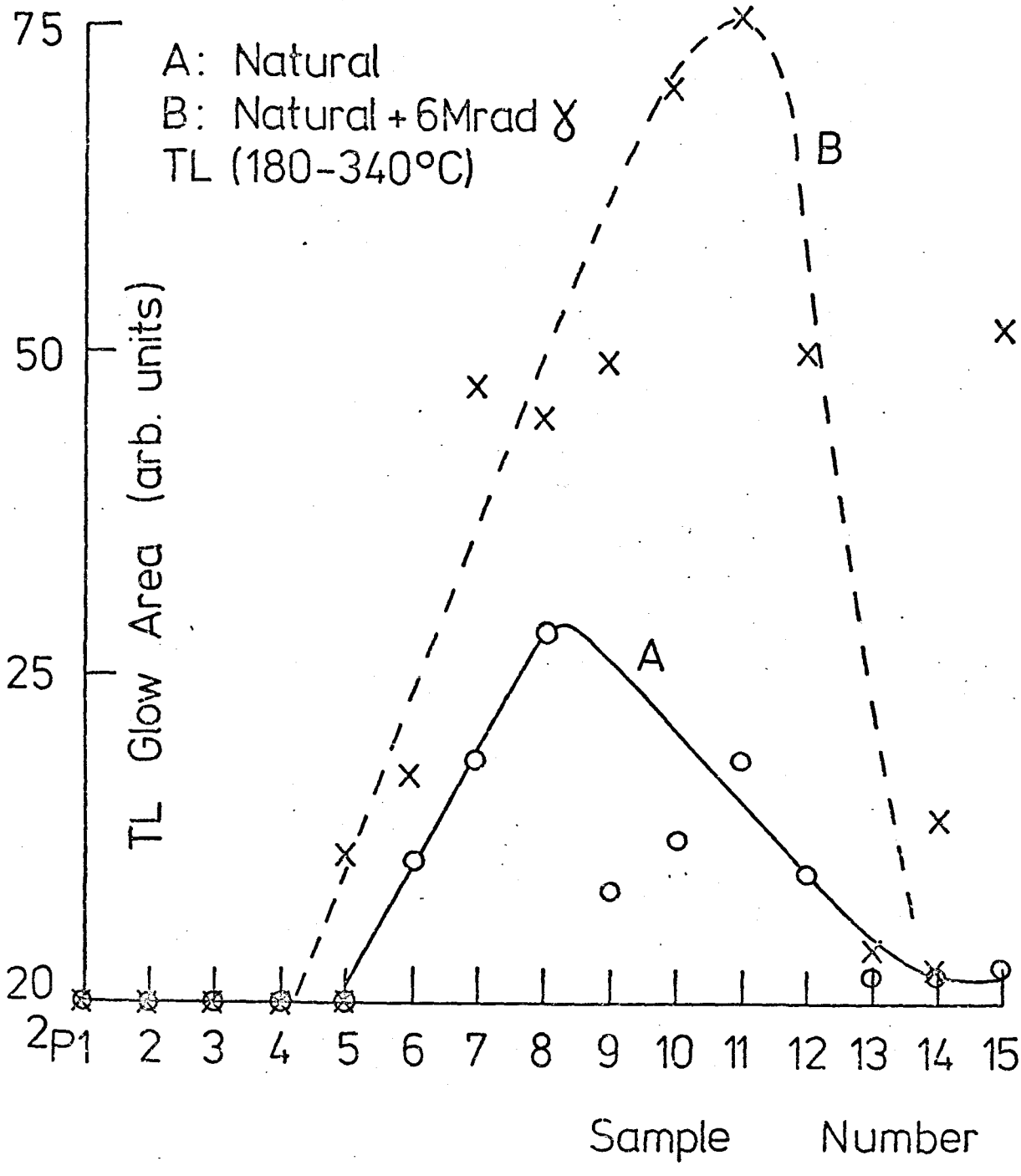
75
50
25
20
A: Natural
B: Natural + 6Mrad γ
TL (180-340°C)
TL Glow Area (arb. units)
A
B
2P1 2 3 4 5 6 7 8 9 10 11 12 13 14 15
Sample Number

Fig 5·4(a)

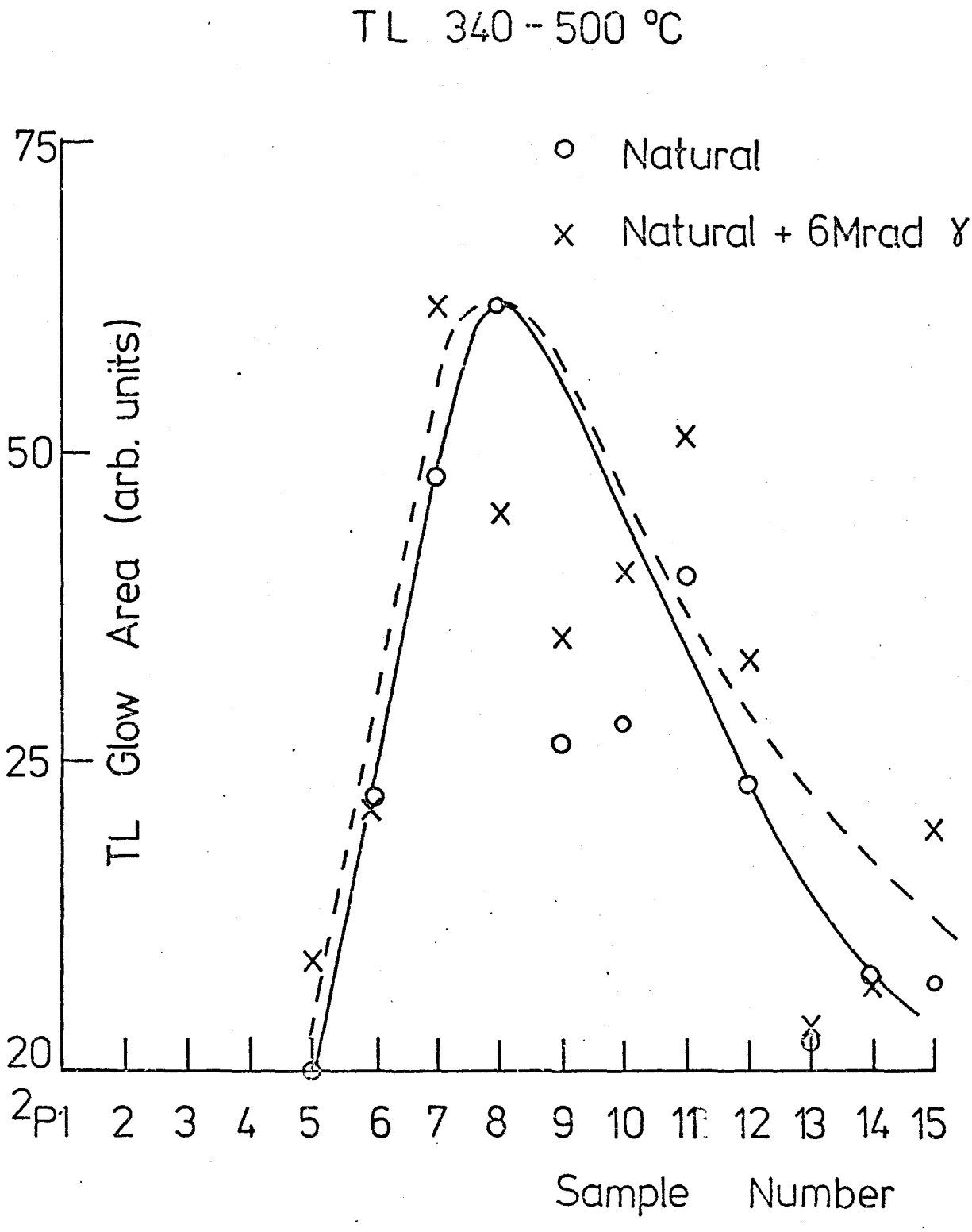
TL 340 - 500 °C
Natural
Natural + 6Mrad γ
TL Glow Area (arb. units)
75
50
25
20
2P1
2
3
4
5
6
7
8
9
10
11
12
13
14
15
Sample Number

Fig 5·4(b)

dose rate in nature must have been quite high (as would be expected from the substantial uranium content of the samples).

The second, and most significant, feature of Figure 5.4 is the striking difference in the natural TL output from samples $2P_1$ to $2P_5$ from inside the reaction zone in comparison with that from samples $2P_6$ to $2P_{15}$ from outside the reaction zone. This feature indicates a qualitative difference in the TL properties of the core versus the outer samples.

5.4.3 Determination of the TL sensitivity of the samples.

Since the output of TL from a sample depends on the amount of TL phosphors (and activators) present in it, in addition to the dose received by the sample, it is necessary to determine the TL sensitivity of the various samples. This was done by giving each sample an artificial dose of 150 krad of ^{60}Co γ-rays after first having drained it of its natural TL by heating to $\sim$ 500°C. In Figure 5.5 is plotted the TL sensitivity (in terms of the 340 to 500°C glow area per mg per krad) against the sample number. Figure 5.5 shows the complete insensitivity of the core samples ($2P_1$ to $2P_4$) to artificial dose while the sensitivity of the samples from outside the core increased with distance (samples $2P_5$ to $2P_7$) and then dropped (samples $2P_{13}$ to $2P_{15}$) to a value not far from that of sample $2P_5$. Assuming that the soil is homogeneous (in mineral composition) and that the source of radiation is of constant strength, one would expect to get an increase in TL sensitivity with distance from the core until it reaches either a constant value or the initial sensitivity of the soil before the irradiation.

The gradual decrease in sensitivity of samples $2P_7$ to $2P_{15}$ could be explained by the possible existence of another pocket of activity near to sample $2P_{15}$.

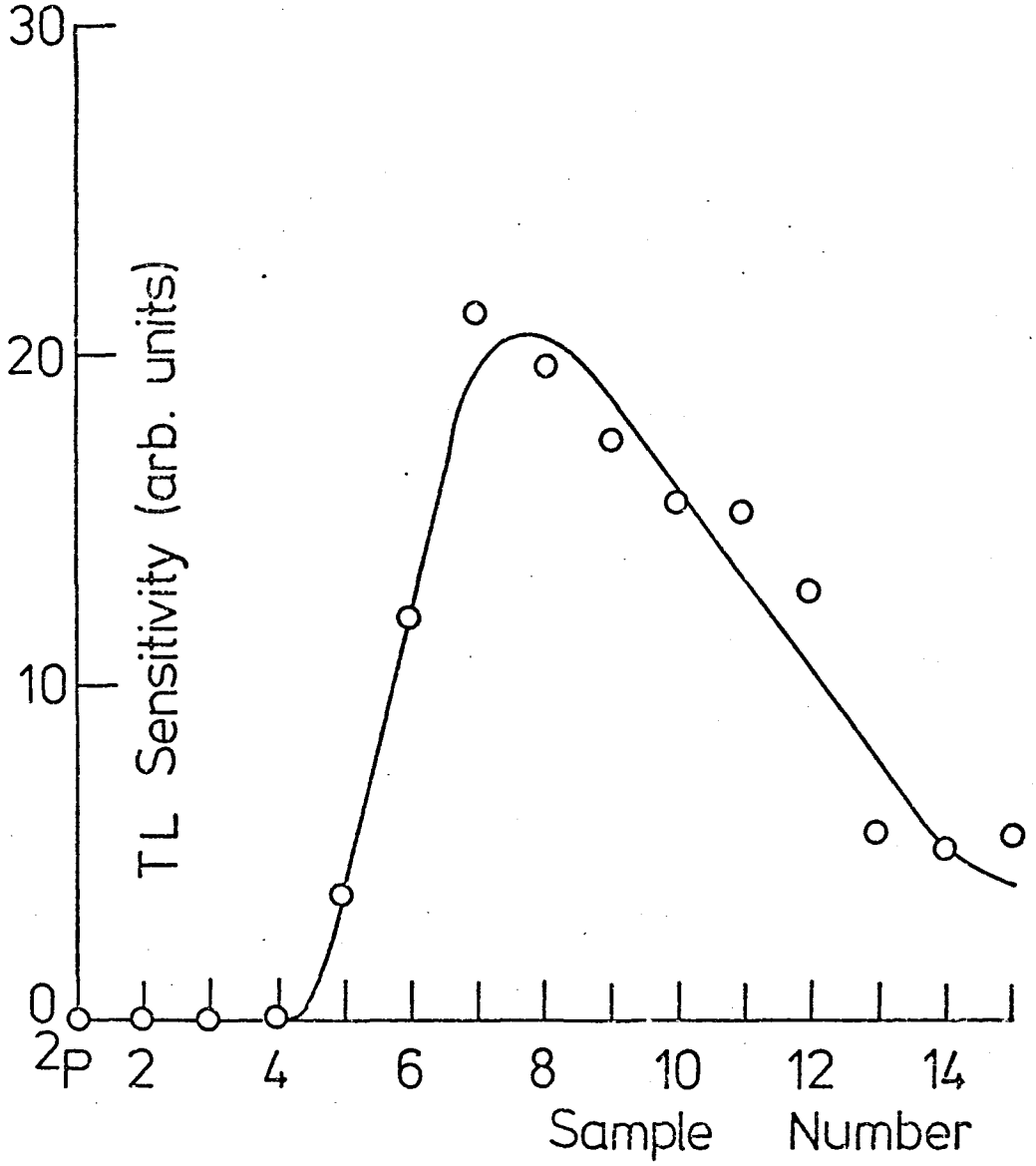
30
20
10
0
TL Sensitivity (arb. units)
2P
2
4
6
8
10
12
14
Sample Number

Fig 5·5

5.4.4 Normalisation of the natural TL.

By dividing the natural TL of each sample by its TL sensitivity, one obtains the 'normalised' TL from different samples. This provides a more meaningful comparison (and, if the dynamic equilibrium plateau had not been reached in the TL glow, the normalised values would have yielded the 'effective' radiation doses received by the samples). The normalised natural TL output of the various samples is shown in Figure 5.6.

Two features of Figure 5.6 are of particular interest. The first is the approximately equal natural TL (after normalisation) in a majority of the samples $2P_6$ to $2P_{15}$, indicated by a notional straight line fitted to the experimental points; the scatter probably represents the inhomogeneities in the distribution of TL phosphors in the aliquots used for the measurement of natural and induced glows (at 150krad). The error shown in the figure is the mean error of all points, based on two TL readouts for each sample. It is interesting to note that the three outer samples ($2P_{13}$, $2P_{14}$ and $2P_{15}$) showing markedly low natural TL as well as TL sensitivity, are all remarkably deficient in K_2O (see Table 5.1), which may indicate a deficiency in their feldspar content usually the chief source of TL in geological samples.

The second and much more important feature of Figure 5.6 is the total absence of TL glow in the core samples $2P_1$ to $2P_4$ (and the very small anount for sample $2P_5$). The same absence of natural glow in samples $2P_1$ to $2P_5$ has already been noted in discussing Figure 5.4. The absence of induced glow in these samples is also evident in Figure 5.5. There are two possible explanations for this extraordinary result, namely, the failure to induce any TL in the core material (samples $2P_1$ to $2P_4$) by artificial irradiation. Either the core samples do not now contain, and never have

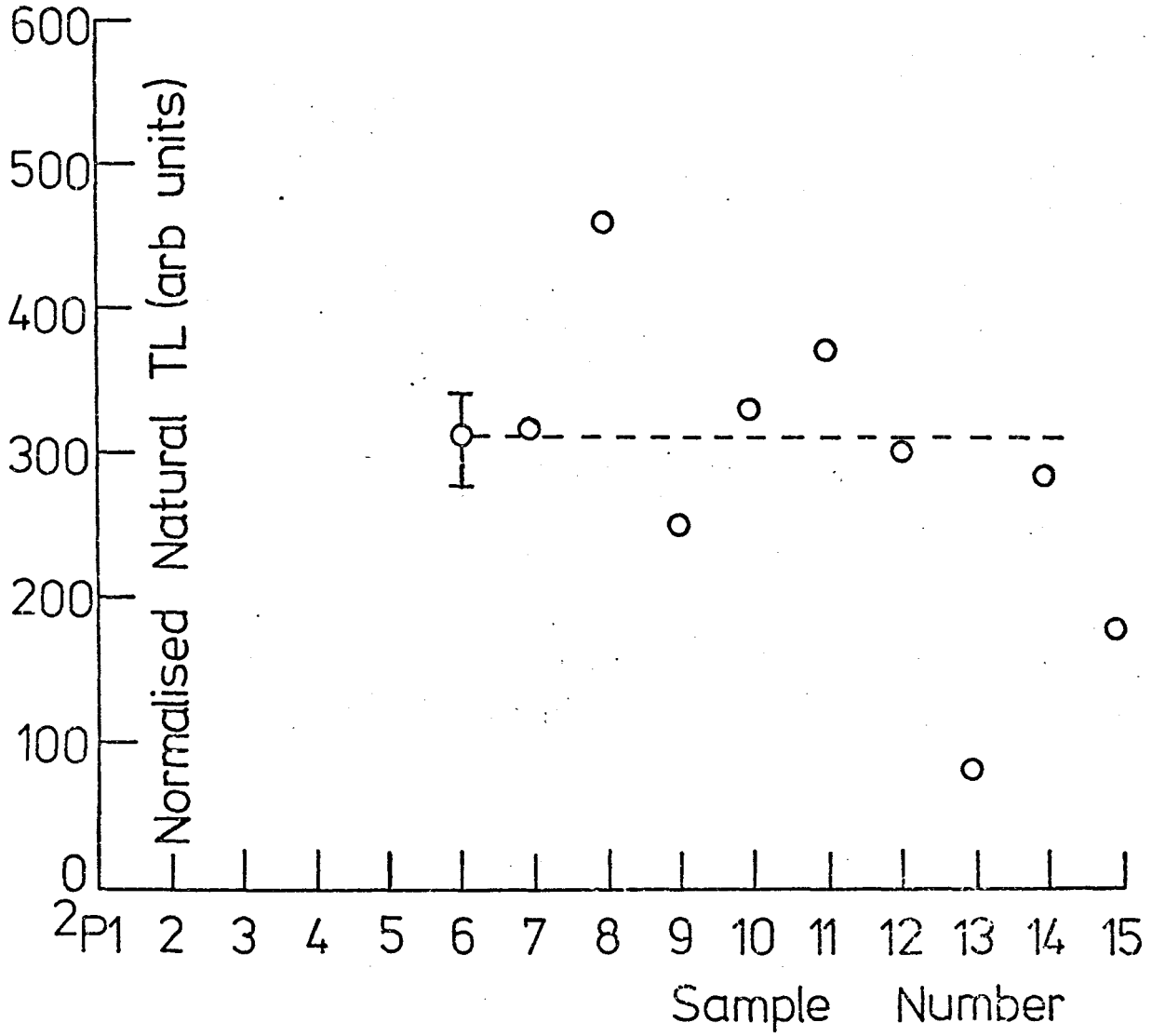
600
500
400
300
200
100
0
Normalised Natural TL (arb units)
2P1 2 3 4 5 6 7 8 9 10 11 12 13 14 15
Sample Number

Fig 5·6

contained, TL-producing phosphors (feldspars, quartz, etc., with appropriate activator impurities); or, if they originally did contain them, they have become highly radiation-damaged, presumably as a result of the chain reaction.

5.5 Structural and Compositional Studies of Samples.

To examine the causes of the striking differences between the TL from the core samples and that from the outer samples, the material from two samples from within the core and another two from outside the core were analysed uxing X-ray diffraction and fluorescence techniques. The structural study of the samples was done by using two different methods - the X-ray powder camera (Debye-Scherrer) and an X-ray powder diffractometer. These experiments were carried out in the Geology Department of the University of Birmingham. The samples used in this analysis were $2P_1$, $2P_4$ (samples from the core), and $2P_8$, $2P_9$ (samples from outside the core).

Figures 5.7a and 5.7b show the X-ray diffraction patterns for samples $2P_1$ and $2P_9$ chosen as examples. These patterns were analysed using the Bragg law:

$$n\lambda = 2d \sin\theta$$

where d is the spacing of the reflection planes and θ is the angle of reflection and λ the wavelength of reflected X-ray radiation. From the above formula the d value was calculated using the known value for λ ($\lambda_{Cu} = 1.542\,\text{Å}$) and the value of θ which was calculated from the position of each line. The calculated values of d were compared with the known d values of the compounds expected to be present which are listed in tables (powder diffraction file published by the Joint Committee on powder diffraction

X-ray Diffraction Pattern of Sample $2P_1$

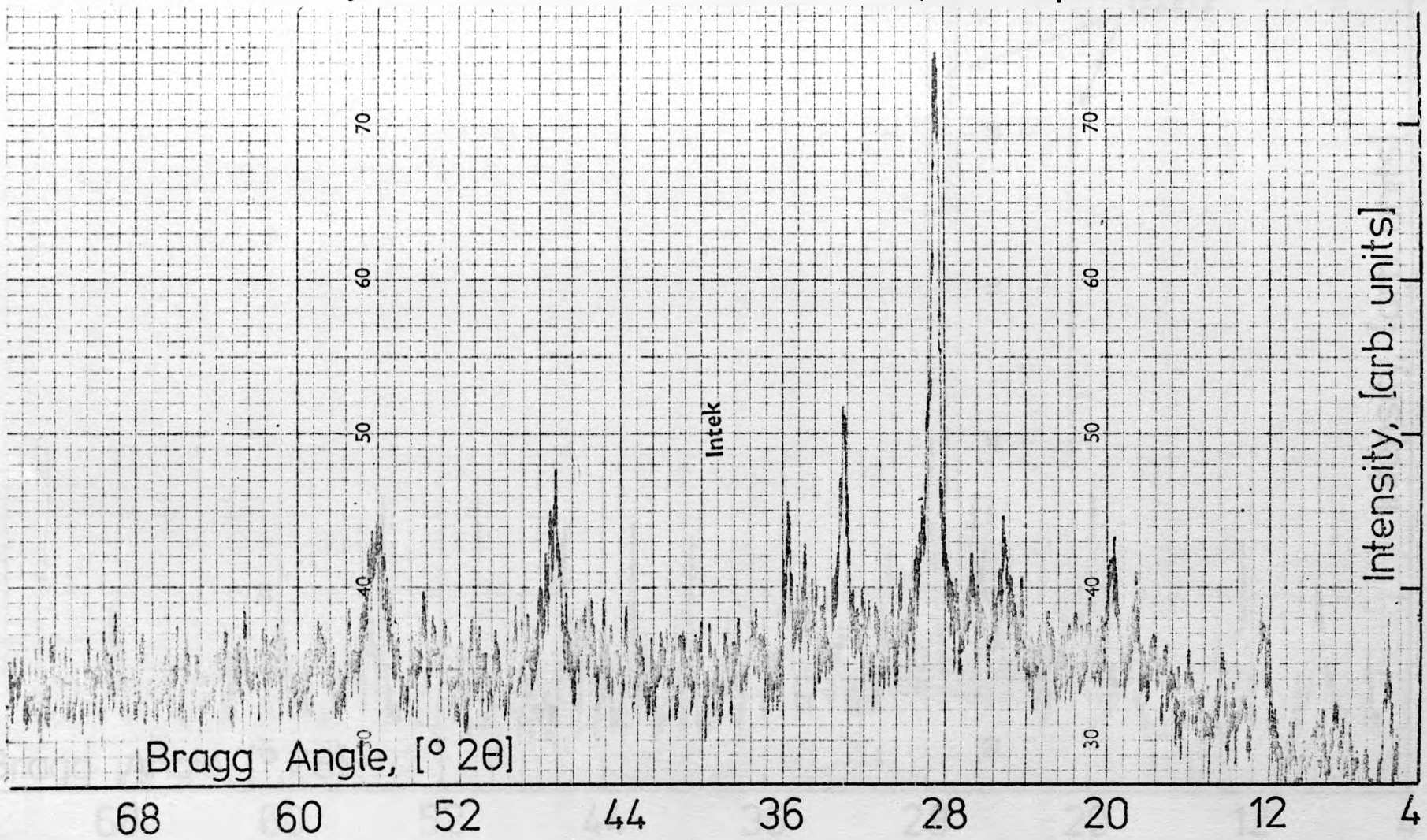

Fig 5·7(a)

X-ray Diffraction Pattern of Sample 2P9

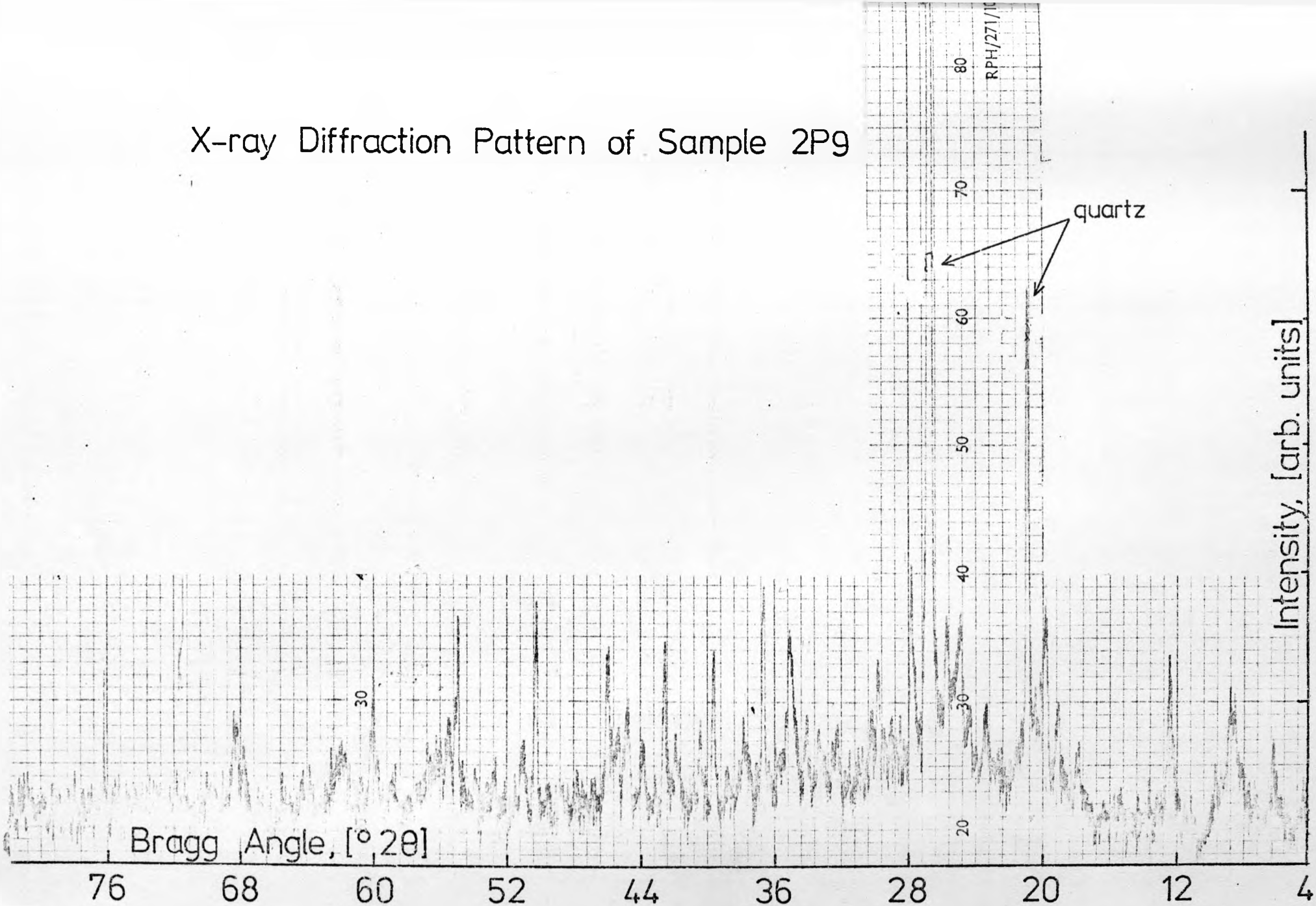

Fig 5·7(b)

Standards, 1601 Park Lane, Pennsylvania 19081, U.S.A.) and from this comparison it was possible to identify most of the interesting compounds existing within the samples.

In the case of the experiments using the X-ray powder camera the value of d was calculated for each of the curved lines on the film by measuring the distance D between each two corresponding lines as they appeared on the film. The distance D for each line pair for the type of camera used in these experiments was related to θ by:

$$D(mm) = 4\theta\ (degree)$$

$$\text{or} \qquad \theta = \frac{D}{4}$$

Then the d spacing for each line on the film was found using the Bragg equation, as with the X-ray diffractometer experiments. The values of d were used to identify compounds of interest, for example, quartz, feldspar, using the tables mentioned above.

The results of the analysis of the four samples have shown that in samples $2P_8$ and $2P_9$ quartz and feldspar crystals (probably orthoclase) were identified. Samples $2P_1$ and $2P_4$ (core samples), however, failed to yield lines corresponding to these crystals.

There are two possible explanations for these results. First, the core material contained, from the beginning, no crystalline material whatsoever. This would result either from the assumption that regions of high uranium content had, at the outset, a very fine phyllitic matrix from which quartz was excluded, or that the secondary silica, produced during diagenesis prior to the nuclear reaction. occurred around but not in the heavily mineralised pockets.

The second explanation is that a high degree of radiation damage has

metamictized the in-core material and reduced it to an amorphous state (as happens on the moon under high solar-flare irradiation conditions, according to the work of Dran et al, 1972). The very fine phyllitic matrix within the core would then be a result of the radiation damage and would not pre-date it.

The elemental composition studies of all Oklo samples were carried out using the X-ray fluorescence technique. These experiments were carried out in the Geology Department by Dr. G.L. Hendry. The results of this analysis are listed in Table 5.1. Both silicon dioxide and potassium oxide were found in all the samples. By correlating the X-ray diffraction results with those of X-ray fluorescence one can say that the silicon and potassium compounds found in the core samples were in amorphous states and that this was produced by the heavy radiation damage, since quartz, receiving a massive radiation dose, would yield non-crystalline SiO_2 which is found in all the core samples. Also potassium oxide, which was found in the core samples, could have been part of potassium feldspars originally present in the core samples as well as the outer samples (e.g. the orthoclase found in $2P_8$ and $2P_9$). Naudet (1974) reported that zircons were absent in the reaction zone even though they are very common in the surrounding ore (zircons are particularly sensitive to irradiation). He also reported that it seems certain that radiation doses were such that primitive crystalline structures were strongly 'bludgeoned'. This observation by Naudet as well as the results of the X-ray analysis for the samples support strongly the hypothesis that heavy radiation damage occurred in the core region.

TABLE 5.1

X-ray fluorescence analysis of Oklo samples*

Sample	UO_2 %	ThO_2 %	PbO %	K_2O %	CaO %	Al_2O_3 %	SiO_2 %
$2P_1$	41.8	0.13	4.4	1.2	0.6	7	13
$2P_2$	52.8	0.30	6.4	1.0	-	7	13
$2P_3$	29.0	0.23	5.2	1.5	-	15	22
$2P_4$	10.6	0.13	2.4	2.0	0.2	21	30
$2P_5$	50.8	0.41	8.5	1.5	-	7	14
$2P_6$	1.3	0.01	0.8	1.9	0.1	21	42
$2P_7$	0.8	nd	0.8	3.1	nd	17	68
$2P_8$	3.9	0.03	4.0	3.9	0.1	22	48
$2P_9$	0.2	nd	0.2	7.9	-	25	53
$2P_{10}$	0.1	0.02	0.7	3.3	nd	13	78
$2P_{11}$	0.3	0.03	3.8	1.9	nd	10	79
$2P_{12}$	1.3	0.01	0.8	1.5	nd	28	40
$2P_{13}$	0.2	nd	0.03	0.01	-	22	32
$2P_{14}$	0.05	nd	nd	0.02	nd	21	32
$2P_{15}$	0.11	0.01	0.2	0.2	-	24	30
1310	6.5	nd	0.03	3.8	nd	20	59
1312	0.1	nd	0.2	8.6	nd	32	46
1318/1	4.9	0.01	1.0	0.9	0.1	25	30
1326	14.6	0.02	1.0	2.0	0.1	24	31

nd indicates values below the sensitivity of the method.

- indicates 'not attempted'.

* The values of oxides of radioactive elements and some other major components are expressed as percentages.

5.6 Radiation Damage Experiments.

If the lack of natural TL in the core samples ($2P_1$ to $2P_5$) is to be attributed to radiation damage, it is necessary to test the effects of high doses of radiation on crystals which are normally good TL phosphors. Simulation experiments have, therefore, been carried out on a sample of natural geological quartz (from Brazil) as well as on a quartz crystal from position $2P_{11}$ at Oklo. Thin slices ($\sim$ 250μm) of these two types of quartz were prepared for these experiments.

The TL sensitivity of these quartz slices to a test dose of 10krad of β-particles (from Sr-90 source) was measured at three successive stages: (a) in their natural state (after having first been annealed to drain their natural TL); (b) after giving them a fairly large γ-ray dose (some megarads); and (c) after having imparted a massive dose of protons, which is expected to produce large radiation damage in the crystals. A dose of 10^{11} rad of 10MeV protons from the Nuffield cyclotron, Department of Physics, University of Birmingham, was used in this damage experiment.

The results are shown in Table 5.2. It is clear from the results on the Brazilian quartz that a large pre-dose of γ-rays (from ^{60}Co) sensitizes the crystal by a factor of $\sim$ 600 in its response to the beta-particles test dose (Khazal et al, 1975; see Chapter III). A subsequent massive dose ($\sim 10^{11}$ rad) of energetic protons, however, destroys this sensitization and brings back the β-sensitivity to roughly its original value (within a factor of $\sim$ 2). It is interesting to note that, in contrast, the addition of a large γ-ray pre-dose (up to $\sim$ 30Mrad) to the Oklo quartz fails significantly to enhance its beta-sensitivity. A further addition of a massive proton dose ($\sim 10^{11}$ rad) dose, however, results in a marked reduction (by a factor of

TABLE 5.2

Effect of large pre-dose on the TL sensitivity of quartz samples from Brazil and from the Oklo site (position $2P_{11}$)[a]

Sample	Step	Dose (and radiation)	TL glow[b] (180-500°C area/mg)	TL sensitivity (180-500°C area/mg · krad)
A. Brazilian quartz	1[c]	10 krad (β)	148	14.8
	2	2.5 Mrad (γ)	1.95×10^5	-
	3	10 krad (β)	8.7×10^4	8700
	4[d]	$\sim 10^{11}$ rad (P)	8.6×10^3	-
	5	10 krad (β)	350	35
B. Oklo quartz ($2P_{11}$)	1[c]	10 krad (β)	100	10
	2	370 krad (γ)	2.7×10^3	-
	3	10 krad (β)	180	18
	4	1.48 Mrad (γ)	3.8×10^3	-
	5	10 krad (β)	160	16
	6	30 Mrad (γ)	4.0×10^3	-
	7	10 krad (β)	220	22
	8[d]	$\sim 10^{11}$ rad (P)	3.2×10^3	-
	9	10 krad (β)	20	2

a. The sensitivity values refer to a test dose of 10 krad β-particles at each stage.

b. The glow area units are the same as those used in Figures 5.3 and 5.4.

c. The first test dose of 10 krad (β) is given after draining the natural TL of the sample. All artificial doses are given sequentially to the same quartz slice.

d. Dose of 10MeV protons.

10) in the beta-sensitivity of the sample.

The interpretation of the above observations is that (i) a massive radiation damage greatly reduces the TL sensitivity of quartz crystals (see Chapter III) and (ii) the reason that a large γ-ray pre-dose does not significantly sensitize the Oklo quartz is, probably, that it had already received a massive dose of radioactivity because of its uranium content. It was calculated that a uranium content of 0.50% (a reasonable value in the region of low-grade ore), situated adjacent to a quartz crystal and distributed uniformly, will impart to it a dose of $\sim 10^{12}$ rad in 2×10^{9} yr. from the alpha-decay of the Uranium-238 nuclei alone. There is experimental evidence, therefore, that massive radiation dose ($\sim 10^{11} - 10^{12}$ rad) can destroy the TL properties of quartz crystals. It is thus possible that the lack of natural and induced TL output from the core samples ($2P_1$ to $2P_5$) is a result of the huge radiation damage received by these samples both from their uranium content (up to $\sim$ 50%, which would yield an α-dose of $\sim 10^{14}$ rad) and from the chain reaction with its neutron and γ-ray doses.

5.7 TL Studies of the Second Set of Oklo Samples.

5.7.1 Purpose of the study.

The main purpose of the study of these samples, which are mineralogically equivalent to the core samples material but are located far away from the reaction zone, is to compare the TL characteristics (sensitivity, natural TL, induced TL, etc.) with those of the core sample which would be a crucial test of the damage hypothesis. If they display both natural and induced TL glow, in contrast to the core material, this would be strong evidence that the absence of TL in the core samples is indeed a consequence of the extreme radiation damage suffered by them.

5.7.2 Samples and sample preparation.

Four samples were used in this study, the sample numbers being 762, 1943, 2321 (KN259) and 2266 (KN228). The sample numbers are as defined by Dr. R. Naudet (Naudet, 1975). The first two samples had a clay matrix very similar to the ore of the core; that is to say similar to the samples $2P_1$ to $2P_4$. These samples were located one to three metres from the core. They have been picked out from the surface after geological examination.

The last two samples are made of rich ore but with a very low reaction rate.

The samples were prepared for TL studies by sieving the matrix of each sample, and grains of diameter between 106 and 180 μm were selected.

5.7.3 Natural and induced TL.

The natural TL glow curve from sample 1943, chosen as an example, is shown in Figure 5.8. Also shown in the figure is the artificial glow curve induced by irradiating the sample with 6Mrad of ^{60}Co gamma irradiation before the readout (curve B). Two stable peaks appear, at 324°C and 423°C, which are enhanced by artificial irradiation - Figure 5.8. The remains of a peak around $\sim$ 220°C can also be seen, whereas little natural TL has survived below $\sim$ 200°C. Artificial irradiation was able to induce the low temperature peaks at 100°C and 220°C (curve B).

All samples showed natural TL in the temperature interval 180 to 500°C. The absence of natural TL below 180°C could be explained in terms of fading, in particular thermal. In all samples it was possible to induce TL artificially by gamma irradiation.

The results listed in Table 5.3 indicate clearly that samples 2266,

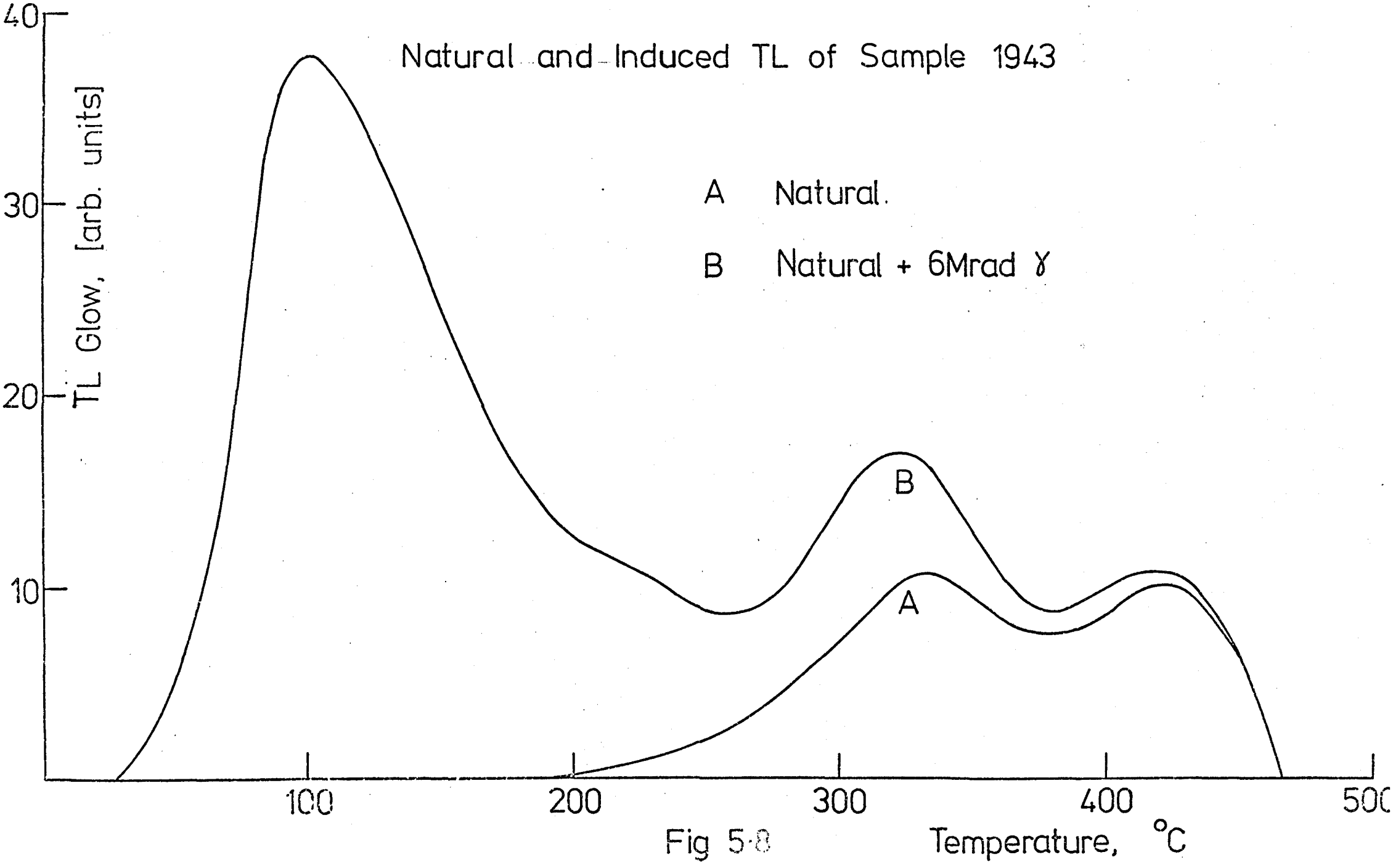
Natural and Induced TL of Sample 1943
A Natural.
B Natural + 6Mrad γ
TL Glow, [arb. units]
40
30
20
10
B
A
100
200
300
400
500
Temperature, °C

Fig 5·8

TABLE 5.3

Thermoluminescence characteristics of the second set of Oklo samples

Sample No.	Area II (180-340°C)		Area III (340-500°C)			
	Natural TL	Natural +6Mrad(γ)	Natural TL	Sensitivity x 10^{-2}	Normalised Natural TL	Natural +6Mrad(γ)
762	15.6	28.8	26.2	12.2	214.8	32.7
1943	14.9	61.8	23.2	20.0	116	44.5
2266	4	18.5	4.5	2.4	187.5	11.85
2321	6.6	33.4	10.6	7.4	143.3	20

2321 from the rich ore have considerably little natural TL as well as a low sensitivity compared with the other samples (762, 1943) which were selected from an area undepleted in Uranium-235. This difference could be explained by the fact that the depletion of Uranium-235, which occurred as a result of the occurrence of a chain reaction, gave rise to a very high radiation dose as well as dose rate (of neutrons, fission product, etc.), which in turn damaged the TL-sensitive phosphors and this gave rise to the reduction of TL sensitivity. Furthermore, the results listed in Table 5.3 show that there is a distinct difference between the natural TL and sensitivity of samples 762 and 1943 and of $2P_1$ to $2P_4$ despite the similarity in their mineral composition. This difference implies that the failure of the core samples to retain their natural TL as well as the failure of TL to be induced artificially was not a result of a lack of TL phosphors but a result of radiation damage which destroyed the crystalline structure of the phosphors and changed it to an amorphous state.

5.8 Fission Track Studies of Oklo Samples.

5.8.1 Fission track phenomenon.

The passage of a heavy ion in an electrical insulator creates a narrow trail of radiation damage in the material known as a latent track or, simply, a track. These latent tracks were first observed by Silk and Barnes in 1959 when they were able to observe these tracks in thin sections of mica, irradiated by fission fragments, using a high voltage electron microscope. In 1962 it was found by Price and Walker that these tracks could be enlarged and made permanent by immersing the irradiated solid in a suitable chemical reagent, usually called an etchant. This important breakthrough added a new dimension to the potential of these track registering solids or, as they

are usually called, Solid State Nuclear Track Detectors (SSNTDs). There are other dielectric solids capable of storing tracks which can be chemically etched - examples are plastics, glasses and the most important of all from the radiation history studies point of view are the mineral crystals (e.g. quartz from Oklo deposit).

The etchant and the experimental conditions under which the etching is performed are already established for some track-registering solids (e.g. glasses, plastics, crystals) (Lal et al, 1968; Krishnaswami et al, 1971). For others the etching procedure is still a matter of trial and error. Glasses are best etched with hydrofluoric acid solutions in concentrations of 10-48% at room temperature. Plastics are most commonly etched in solutions containing 25 grams of NaOH to 75 grams of water at a temperature of 50-60°C. Crystals are mainly etched in boiling concentrated NaOH solutions containing typically 60% NaOH by weight. A successful etchant should be able, under suitable experimental conditions, to etch the general surface with a uniform velocity over the whole area and should produce the minimum number of background etch pits possible. Also, the etchant must be able to etch the tracks with a preferential velocity V_T (the velocity of the etchant in the damage region) which is greater than the general velocity V_G (the velocity of the etchant in the bulk material). One of the important parameters governing the shape of the track is θ_c, the critical angle of etching (the angle below which particles falling on the detector surface will not be revealed by etching) of the material for a particular particle of specified energy determined under specified experimental conditions. The critical angle θ_c of a detector is related to the velocities V_T and V_G, defined above, by $\sin\theta_c = \frac{V_G}{V_T}$ (Somogyi et al, 1970). From

Figure 5.9 the relation between V_G, V_T and θ can be derived. The letter t in the figure represents the etching time.

The SSNTDs have certain features (Malik, 1973) such as insensitivity to light (cf. nuclear emulsion), geometric flexibility and simplicity of construction and use (i.e. crystals, mica, glass and plastic sheet). These features have made the SSNTDs highly competitive with other kinds of detectors in the field of particle identification, such as the detection of light-charged nuclei (i.e. ^{1}H, ^{2}H, ^{3}H, ^{3}He and ^{4}He) (Somogyi et al, 1966; Somogyi, 1968), and have led to rapid advances in their applications. The ability of track registering solids in general and geological crystals in particular in storing the tracks for long periods of time under various environmental conditions of temperature, humidity, mechanical vibrations and pressure opened a new field of application to the SSNTDs. This important property of the SSNTDs has made possible the study of the radiation history as well as the determination of the age of these materials such as lunar glasses and quartz crystals from Oklo deposit and for other geological crystals.

5.8.2 The theory of the method of age determination.

The spontaneous fission of the Uranium-238 nuclei leaves latent trails of damage in a crystal which may be enlarged by a suitable etchant so that they can be examined under an optical microscope (OM)or a scanning electron microscope (SEM). The amount of uranium in the sample can be determined by irradiating the sample (after annealing out the natural tracks by heat treatment) in a reactor and producing induced fission in the Uranium-235 component. The induced fission fragments can be observed either in the primary material, i.e. the crystal itself, or in an auxiliary

Track Geometry with V_T and V_G Constant and with Vertically Incident Particle

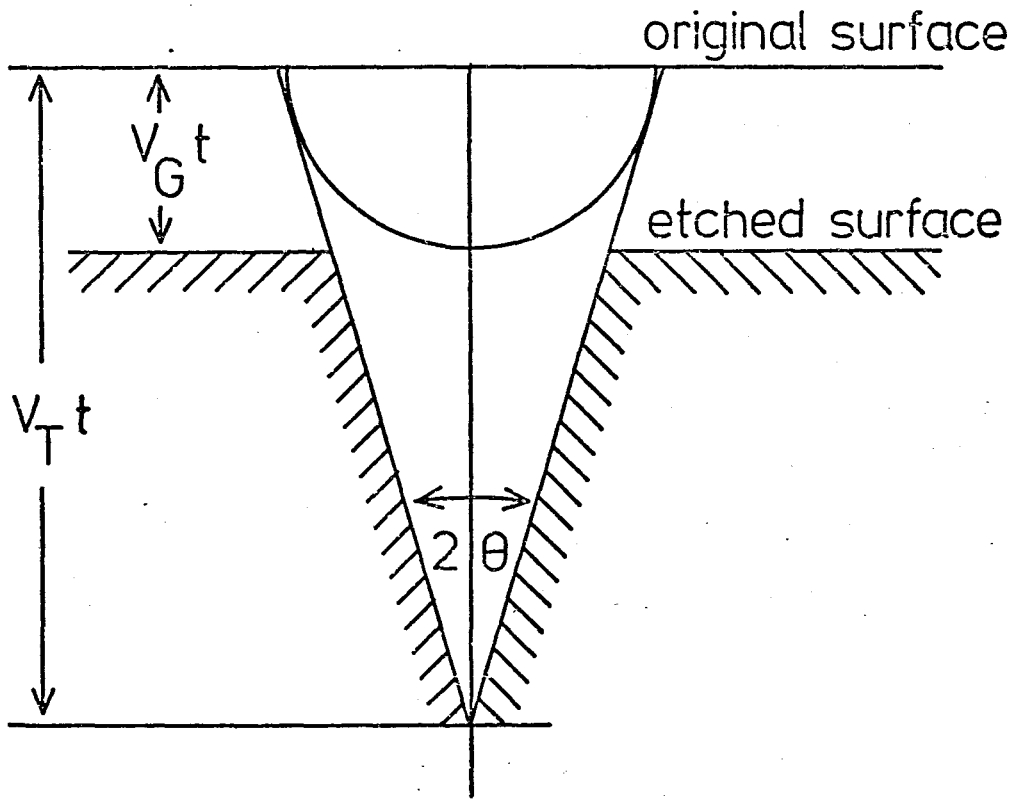

Fig 5·9

detector, e.g. a plastic foil placed in close contact with the crystal during reactor irradiation. Then, since the fission decay constant of uranium is well known, the age of the formation of the crystals can be calculated from the observed density of sponteneous-fission tracks in the crystal using the following equation (see Fleischer et al, 1975; Khan et al, 1972, and Durrani et al, 1970).:

$$A\ (\text{years}) = \frac{N_5}{N_8}\ \frac{\sigma_f}{\lambda_f}\ \left(\frac{\rho_s}{\rho_i}\right) F\ ,\ \left(\frac{N_5}{N_8}\ \frac{\sigma_f}{\lambda_f} = 5.0\times10^{-8}\right) \quad (1)$$

where:

A is the age of formation (or last severe heating) of the Oklo crystals;

N_5, N_8 are the number of Uranium-235 and Uranium-238 atoms respectively per unit volume, $\left(\frac{N_5}{N_8} = 7.20 \times 10^{-3}\right)$;

λ_f and σ_f are the spontaneous-fission decay constant of Uranium-238 and the thermal-fission cross section of Uranium-235, ($\lambda_f = 8.42\times10^{-17}$ yr^{-1}; $\sigma_f = 586 \times 10^{-24} cm^2$);

ρ_s and ρ_i are the spontaneous- and induced-fission track densities respectively;

and F is the thermal neutron fluence responsible for ρ_i.

Equation 1 needs to be modified for the alpha-decay of the Uranium-238 content (half-life 4.5×10^9 yr.) over the $\sim 1.8 \times 10^9$ yr. This factor is found to be equal to 0.875 (Durrani et al, 1975), so that the corrected age is

$$A'\ (\text{corrected}) = 0.875A = 4.375 \times 10^{-8} \left(\frac{\rho_s}{\rho_i}\right) F\ \text{yr.} \quad (2)$$

Since no crystals or glasses were found in the core samples, no worthwhile track studies could be made within the reaction zone. An X-ray diffraction experiment (see Section 5.5), however, established that a

significant proportion of quartz crystals was present in samples $2P_7$ and $2P_{11}$ (roughly 20 and 60cm respectively away from the boundary of the reaction zone). It was decided to try to date the formation (or the last severe heating) of these quartz crystals by the fission-track analysis method.

The age A' (corrected) of formation (or last severe heating) of the Oklo crystals is worked out using equation 2. The corrected age of the six quartz crystals from samples $2P_7$ and $2P_{11}$, listed in Table 5.4, yield remarkably consistent values. The simple mean age of the formation of Oklo quartz is found to be $(1.73 \pm 0.14) \times 10^9$ yr, where the error shown is the 'internally consistent' statistical standard deviation. This error takes into account all the random measurement errors indicated in the table.

The mean age of the Oklo quartz obtained by the fission-track method, namely $(1.73 \pm 0.14) \times 10^9$ yr, agrees well with the geological age of rocks in the Franceville formation found by other methods (Lancelot et al, 1975), and justifies the application of fading corrections (Storzer et al, 1969; Mehta et al, 1969) based on tektite data (see Figure 5.10; Durrani et al, 1970) to fossil-track densities in Oklo quartz, and ignoring any induced-fission contribution, made by the chain reaction, to the fossil-track density in quartz crystals studied (which were located at $\sim$ 20cm and 60cm respectively from the edge of the reaction zone). This implies that the fall-off of the thermal neutron flux outside the reaction zone is very fast. The presence of neutron-absorbing elements (e.g. boron) in the surrounding soil in sufficient quantities could, for example, account for such a decline in the thermal flux. The fact remains, however, that ignoring the induced fission of Uranium-235 at distances of $\sim$ 20cm from the reaction zone gives

TABLE 5.4

Ages of the formation of Oklo quartz by the fission-track method

Sample No.[a]	Fluence F(thermal n·cm^{-2}) ±8%	Induced fission-track density ρ_i (cm^{-2}) ±10%	Uranium content (Cu ppm) ±14%	Fossil-track density ρ_s (cm^{-2})	Formation age of the quartz crystal (yr)
$2P_7$ (a)	1.19×10^{13}	7.05×10^5	1499	$(2.28 \pm 0.23) \times 10^9$	$(1.67 \pm 0.27) \times 10^9$
$2P_7$ (b)	1.15×10^{14}	9.26×10^5	204	$(3.50 \pm 0.42) \times 10^8$	$(1.89 \pm 0.33) \times 10^9$
$2P_7$ (c)	1.48×10^{12}	1.24×10^5	2128	$(3.13 \pm 0.74) \times 10^9$	$(1.62 \pm 0.43) \times 10^9$
$2P_{11}$ (x)	1.19×10^{13}	3.42×10^5	727	$(1.10 \pm 0.22) \times 10^9$	$(1.66 \pm 0.40) \times 10^9$
$2P_{11}$ (y)	1.48×10^{12}	7.29×10^4	1244	$(1.92 \pm 0.26) \times 10^9$	$(1.70 \pm 0.32) \times 10^9$
$2P_{11}$ (z)	1.48×10^{12}	4.61×10^3	79	$(1.33 \pm 0.13) \times 10^8$	$(1.85 \pm 0.30) \times 10^9$

a. Letters a - z in parentheses are code numbers of different crystals from the two locations, both of which are outside reaction zone 2.

Mean age = $(1.73 \pm 0.14) \times 10^9$ yr.

Relationship between the Residual Track Density, ρ, and the Reduction in Mean Etch-Pit Diameter

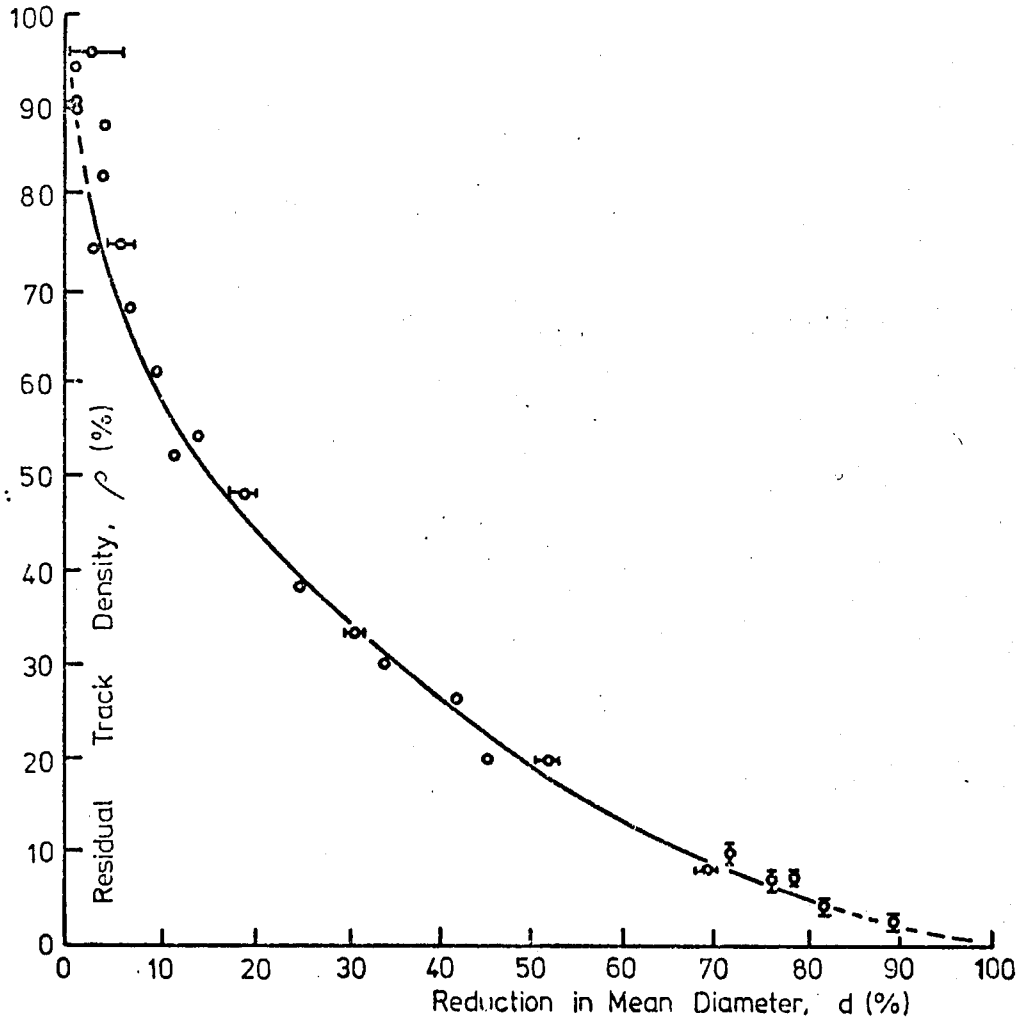

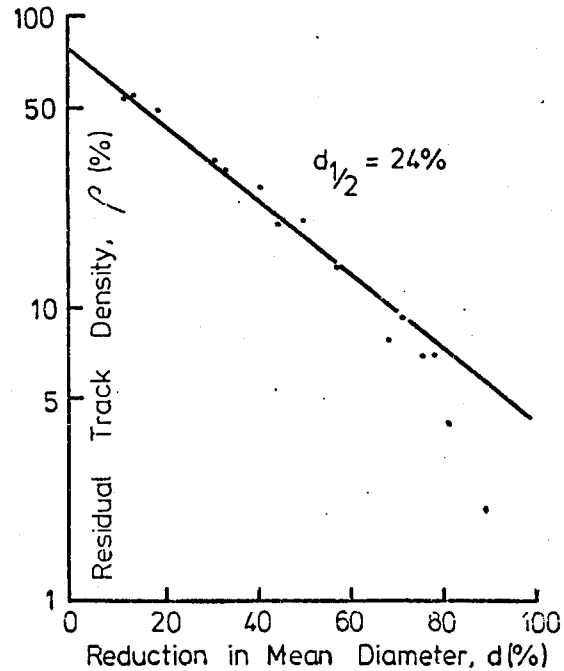

Fig 5-10

acceptable values for the age of the Oklo quartz.

5.9 Conclusion.

There is a striking difference in the natural and induced thermoluminescence between the samples inside the reaction zone and those outside. This was attributed to a high degree of radiation dose suffered by the core material. This conclusion was confirmed by the TL studies made upon samples similar to the core material but situated far away from the reaction zone. These samples were able to retain their natural TL and to produce it by artificial irradiation in contrast to the core samples.

The age of formation of the Oklo quartz is found by the fission-track method to be $\sim 1.73 \times 10^9$ yr, which agrees well with the geological age of rocks in the Franceville formation found by Naudet (1974) and Lancelot et al (1975).

CHAPTER VI

DETERMINATION OF THE TEMPERATURE AND DURATION OF SOME APOLLO 17 BOULDER SHADOWS

6.1 Introduction.

The main purpose of the thermoluminescence studies of the lunar samples is to gain information about the thermal and radiation histories of these samples and of the moon's surface. It has been reported (Hoyt et al, 1970; 1971; Dalrymple and Doell, 1970; Durrani et al, 1972a) that the natural TL in a lunar sample depends significantly upon the depth from which the sample has been collected. These results were explained (Durrani et al, 1974; Hoyt et al, 1971) by the decrease in the thermal drainage of the trapped charge in the sample owing to the attenuation of the diurnal heat wave with depth on the one hand, and shielding against the radiation flux in space provided by the lunar soil on the other. Durrani et al (1972b, 1973) were able to estimate the effective storage temperature on the surface of the moon and consequently countercheck the depth from which the specimens had been collected. TL studies of some lunar samples (Durrani et al, 1974) collected from various known depths and brought back by the Apollo 17 mission, offered an excellent opportunity to check the previous TL findings and to estimate the actual magnitude of the thermal wavelength of the diurnal heat wave.

In this chapter the results of some interesting TL studies of some lunar samples, brought back by the Apollo 17 mission, are described. The TL from soil samples collected from inside the shadows of certain boulders on the lunar surface is compared with the TL of soil samples taken from an adjacent sunlit area. The samples studied here are 76240 'shaded sample',

76260 'sunlit sample' and 72320 'partially shaded' sample. The natural and artifically induced TL in these samples is described. Also, the methods adopted to calculate the surface temperature in the lunar shade, as well as the duration of that shade are described.

6.2 Samples and Sample Preparation.

The samples used in this study had been collected from two locations at the Apollo 17 site. These locations are shown in plate 6.1 (a, b). From station 6 (see plate 6.1a) came the permanently shadowed soil sample 76240 which was collected from a position 0.5 to 1 metre under the north overhang of a 5 x 4 x 3m boulder (Astrogeology (73, 72), ALGIT, 1975). The boulder in question (boulder No. 4) is believed to have originated from the North Massif and appears to have been moving downhill on an 11^{o} slope to the south. For comparison a 2cm deep skin soil sample (76260) was collected from just outside the shadow. From the second location, namely station 2, only one sample (72320) was collected; this was a surface soil from about 20cm under an east-west overhang of a 2m boulder No. 2 lying in a strewn boulder field on the lower slopes of the South Massif (plate 6.1b). This sample is occasionally referred to as the partially shaded sample. No sunlit sample from an adjacent area was available for comparison in this case.

The two shadowed samples were each subdivided into two parts. One part of these samples was very kindly kept in deep freeze (at $\sim -20^{o}C$) by the staff of the Lunar Receiving Laboratory at the request of Dr. S.A. Durrani to limit thermal fading (Durrani, 1972). This refrigeration lasted from 11th January, 1973 (i.e. about three weeks after the Apollo 17 splash-down) to 22nd March, 1974, when these samples were brought to England in dry ice (CO_2 snow) packing. Since that date these samples have been kept

Plate 6.1a

Pre-sampling view on the north side of Boulder 4, showing the east-west split between Boulders 3 and 4 on the south slope of the North Massif (Station 6). Boulder 4 was 5 x 4 x 3m in size, and the "permanently shadowed" soil sample 76240 (the sample (A) was collected from about 0.5 to 1m "in under the north overhang" of this boulder. The sample B (76260), a "2cm deep skim soil", was collected from just outside the shadow, as marked in the photograph. NASA Cat. No. 141-21605.

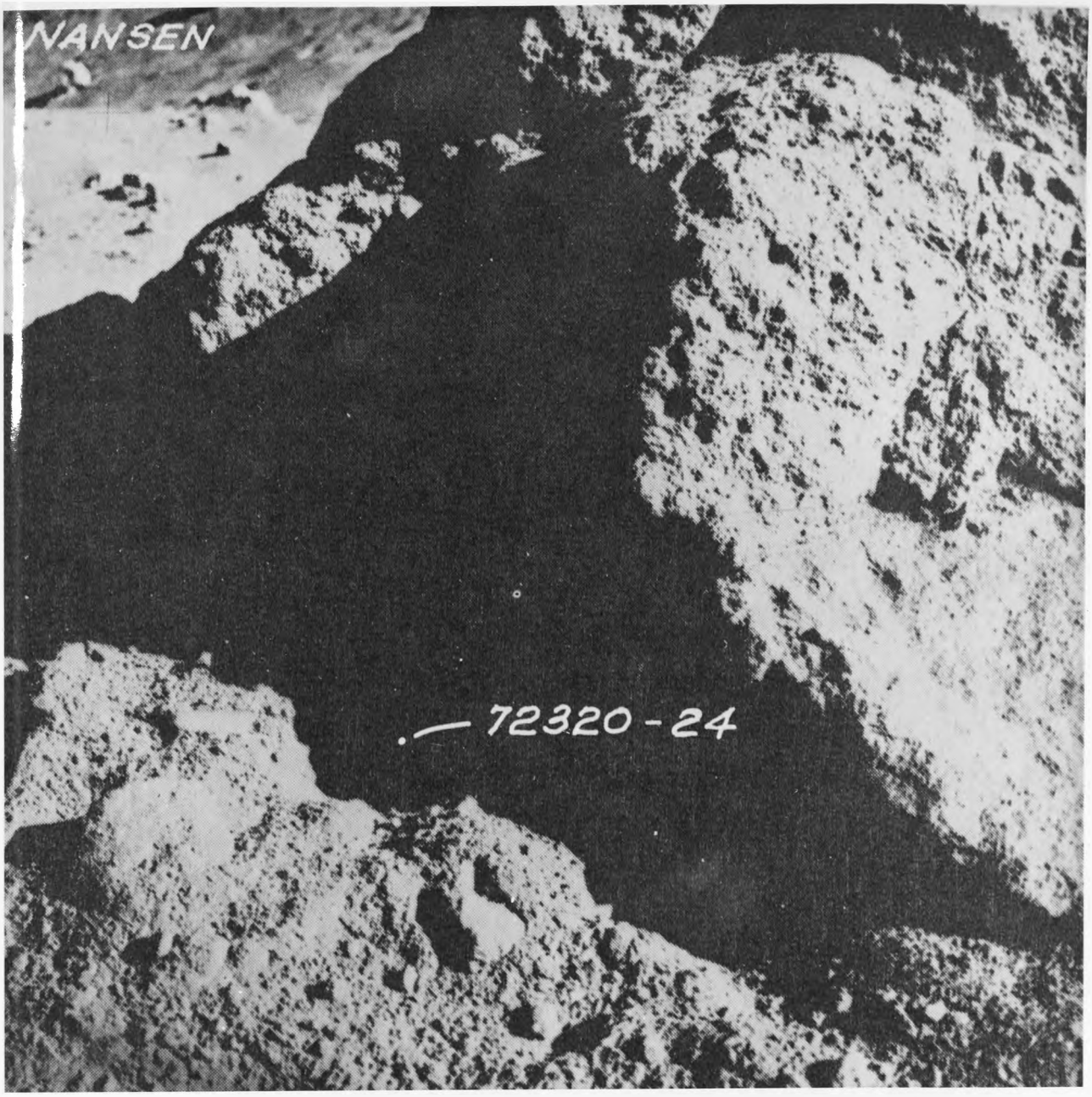

Plate 6.1b

Post-sampling view, looking north, showing the location of the shadowed soil sample 72320 collected from "about 20cm under an overhang of 2m boulder" (no. 2 at Station 2), on lower slopes of South Massif. This sample is referred to in the text as the "partially shaded sample". NASA Cat. No. 137-20925.

in the laboratory at the temperature of either dry ice (-78.5°C) or liquid nitrogen (-196°C) in an effort to preserve as much of the natural TL of the shaded lunar soil as possible.

The refrigerated portions are referred to here as the 'freezer samples' (76240,22 and 72320,4). The non-refrigerated portions kept at room temperature are terms the 'freezer counterparts' (76241,23 and 72321,3 respectively). The 'sunlit sample' from the first location (76261,25) has also been stored at room temperature (with no freezer counterpart).

6.3 General Experimental Procedure.

The samples used in this work, and mentioned in the previous section, were unsorted fines. These fines were sieved using a set of sieves available only for lunar sample uses. This was in order to prevent contamination of the samples with other materials. The sample grain sizes used during this study were always between 45 and 106μm. The apparatus used was described in Section 2.1. Samples of ~ 1-2mg were heated on a tantalum strip in an oxygen-free nitrogen atmosphere at a heating rate of 3.6°C/sec. The TL output, normally transmitted through an Ilford 'Broad Spectrum Blue' filter No. 622 (375-530nm transmission band) by a specially selected quartz-window photomultiplier (EMI6256SQ) in a thermo-electrically cooled housing. The P.M. tube output, measured by a sensitive electrometer, was registered on the y-axis of a y-t chart recorder.

The artificial TL was induced by a ~ 3500 Ci ^{60}Co gamma-ray source, the dose rate (of up to ~ 800 krad hr^{-1}) having an uncertainty of ~ ± 3%. The irradiated samples were usually read out within 15 minutes after the end of irradiation in an attempt to avoid any fading of TL. Other experimental details are given at appropriate points in the following sections.

6.4 Natural and Induced Glows.

The natural TL glow-curve from the shaded samples was found to be very much different in both intensity and structure from that of the sunlit samples. The natural TL from the two (shaded) 'freezer samples' 76240,22 and 72320,4, as well as that from the sunlit sample 76261,25, is shown in Figure 6.1. It is clear that the shaded samples from 1 m inside the shadow 76240 exhibits the most natural glow, followed by the one from 20cm inside the shaded 72320, with the least preserved glow being in the sunlit sample 76261. Moreover, the glow starts at successively and appreciably higher temperatures of readout as one goes from the 'permanently shadowed' samples 76240 ($\sim$55°C) to the 'partially shadowed' sample 72320 ($\sim$110°C) and finally to the sunlit sample 76261 ($\sim$180°C). It was concluded that sample 72320, which was $\sim$20cm inside the shadow when collected, had not been adequately shaded on the moon and had thus remained at a higher effective temperature than the permanently shadowed sample 76240.

In order to see the shape of the original undrained TL glow-curve, artificial TL was induced in the samples (using the room temperature 'counterparts' in the case of the shaded samples). Figure 6.2 shows a typical induced-TL glow-curve, produced by subjecting the natural sample to a gamma-ray dose of 90krad, in which the naturally drained low-temperature peaks in the sunlit sample 76261 have been restored. The structure of the induced TL curves for the nearby shaded sample is similar to that for the sunlit sample, which suggests a similarity of mineralogical composition. This similarity is further supported by the closeness of the trap depth (E) and frequency factor (s), for these samples, as will be discussed in the following sections.

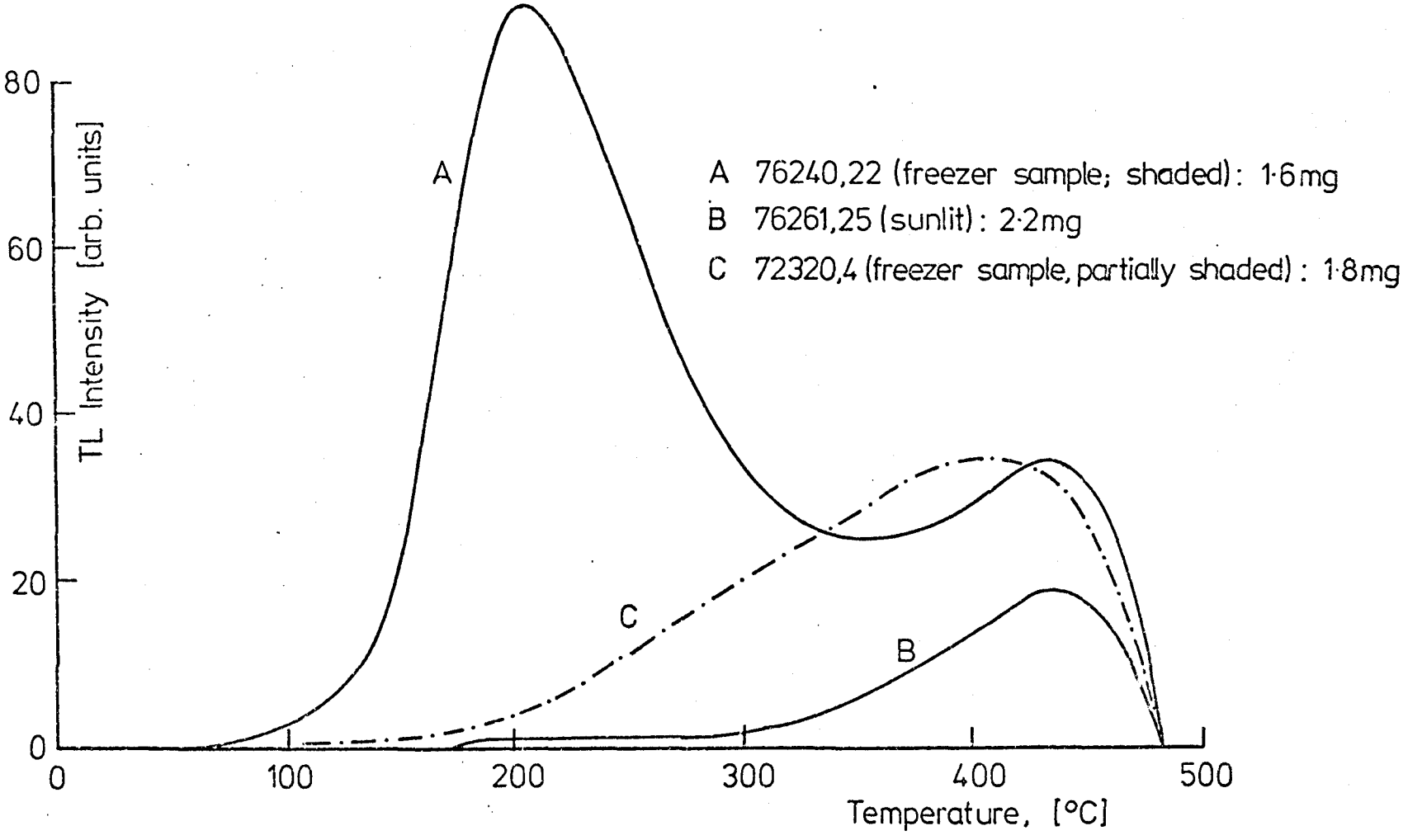
80
60
40
20
0
TL Intensity [arb. units]
A
C
B
0
100
200
300
400
500
Temperature, [°C]
A 76240,22 (freezer sample; shaded): 1·6mg
B 76261,25 (sunlit): 2·2mg
C 72320,4 (freezer sample, partially shaded): 1·8mg

Fig 6·1

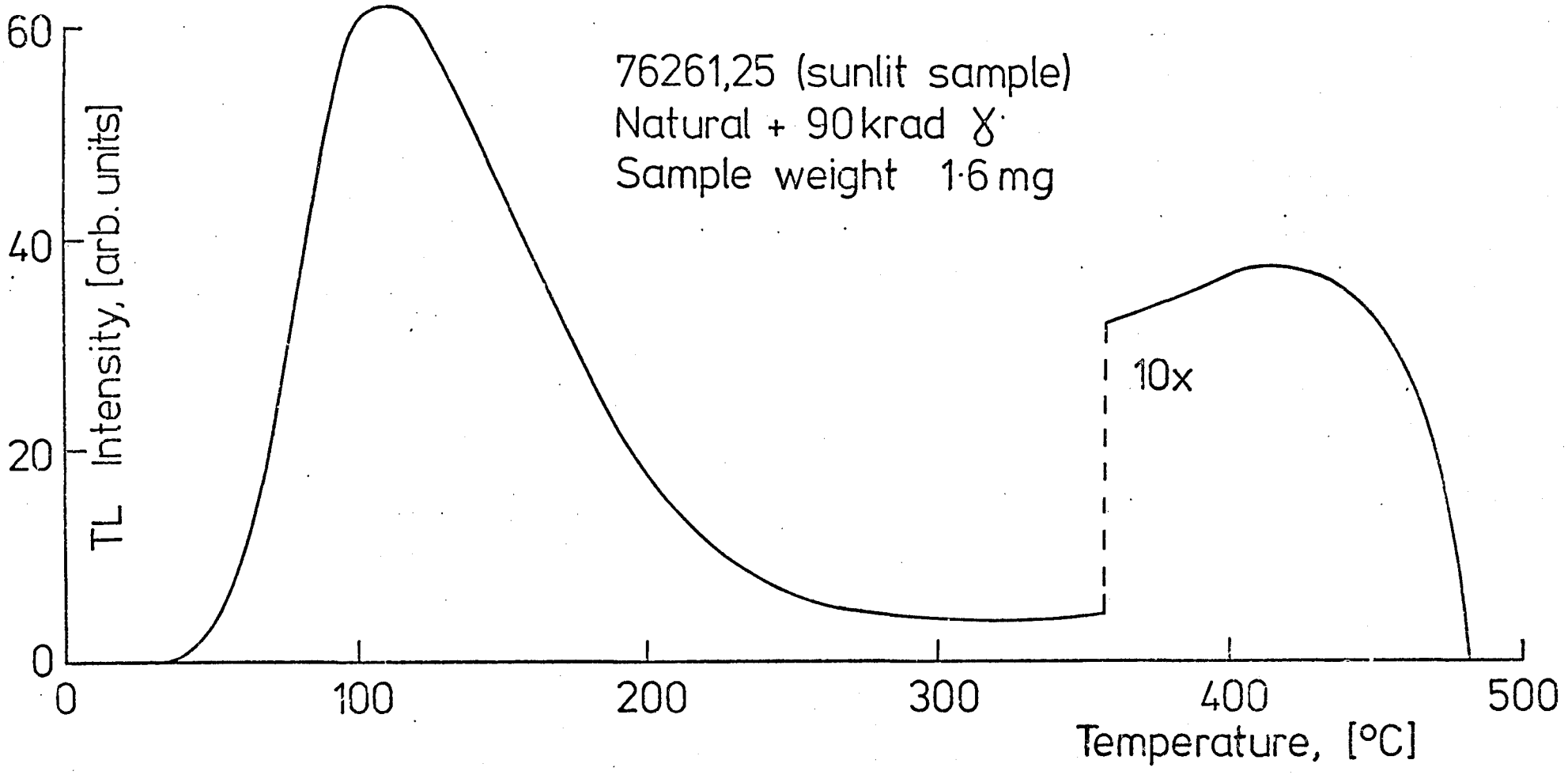
60
40
20
0
TL Intensity, [arb. units]
76261,25 (sunlit sample)
Natural + 90 krad γ
Sample weight 1·6 mg
10x
0
100
200
300
400
500
Temperature, [°C]

Fig 6·2

6.5 Dose Response and Inferred Natural Dose.

Powder samples of grain sizes between 45 and 106μm and 1-2mg in weight were used in this study. Fresh samples were used for successive runs in order to avoid temperature and dose sensitization effects (Durrani et al, 1972a). The samples were subjected to artificial gamma-ray doses up to 3Mrad at a dose rate of 800krad hr^{-1}. Figures 6.3a and 6.3b show the dose-response curves for the shaded sample counterpart 76241, 23 (hereinafter called 'sample A') and the sunlit sample 76261, 25 ('sample B') respectively. In each curve the TL output has been integrated over three consecutive temperature intervals (corresponding to different peaks or trapping levels as discussed below), namely: 216 - 306°C (area I), 306 - 378°C (area II) and 378 - 486°C (area III). These integrated TL glow areas were normalised to a unit of sample weight (mg) and the normalised values were plotted against the gamma-ray dose. By extrapolating these curves backward it is possible to infer, to a first approximation, the natural dose retained by the two samples in each temperature interval.

By examining the growth curves, shown in Figures 6.3a and 6.3b one can also graphically determine the 'half-dose' $R_{\frac{1}{2}}$, so termed from analogy with half-life in a growth-to-saturation curve in radioactivity (Durrani et al, 1972b). This is the dose required to fill half the remaining traps at any stage of irradiation (in the absence of thermal decay), assuming the growth law:

$$n = N\left(1 - e^{-0.693R/R_{\frac{1}{2}}}\right) \qquad (1)$$

where n is the number of filled traps for a total dose R (including the natural dose) and N is the total number of available traps of a given energy depth. The values of $R_{\frac{1}{2}}$ for the various trapping depths (corresponding to various

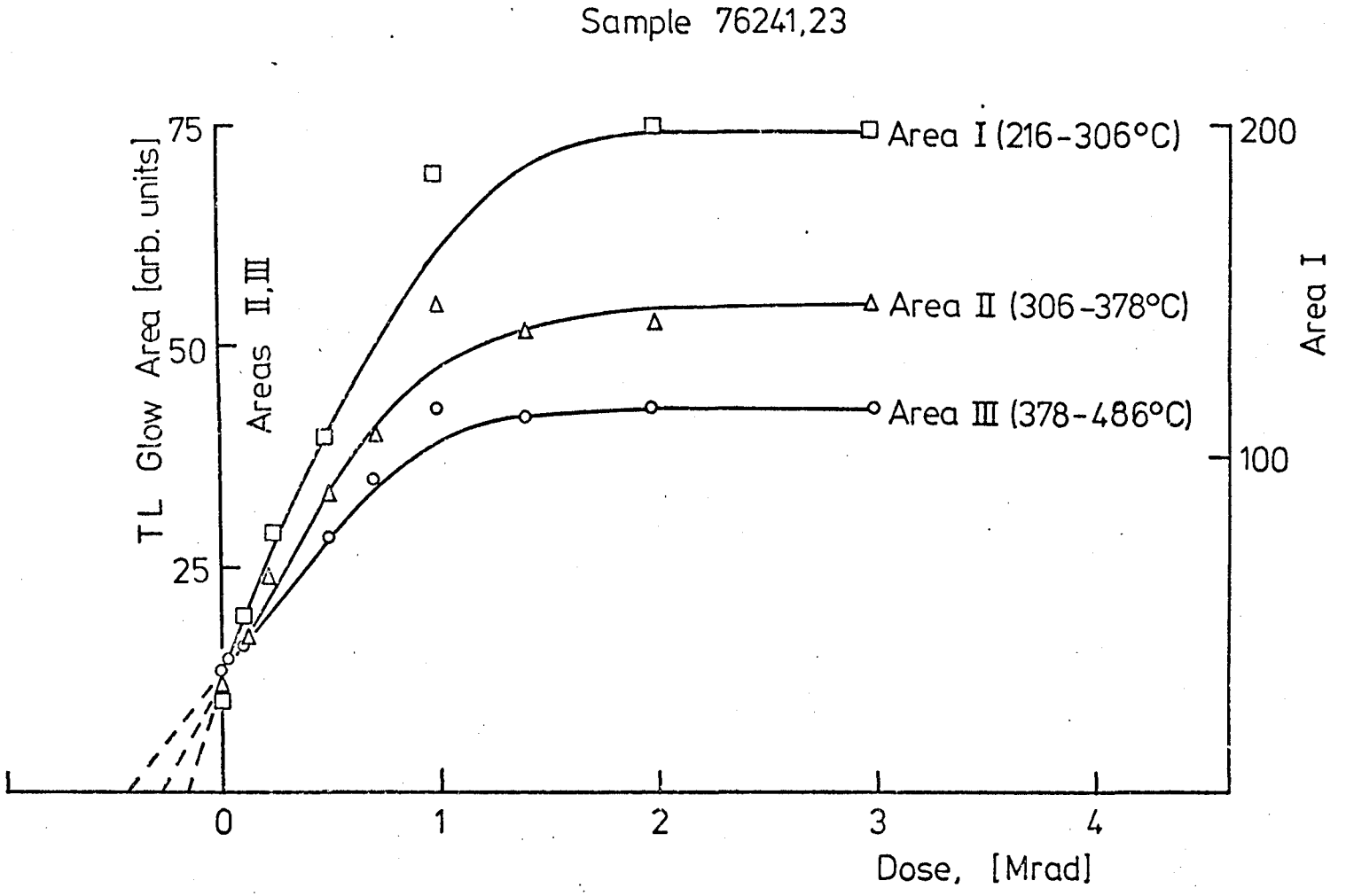
Sample 76241,23
TL Glow Area [arb. units]
Areas II, III
Area I
75
50
25
200
100
0
1
2
3
4
Dose, [Mrad]
Area I (216-306°C)
Area II (306-378°C)
Area III (378-486°C)

Fig 6·3(a)

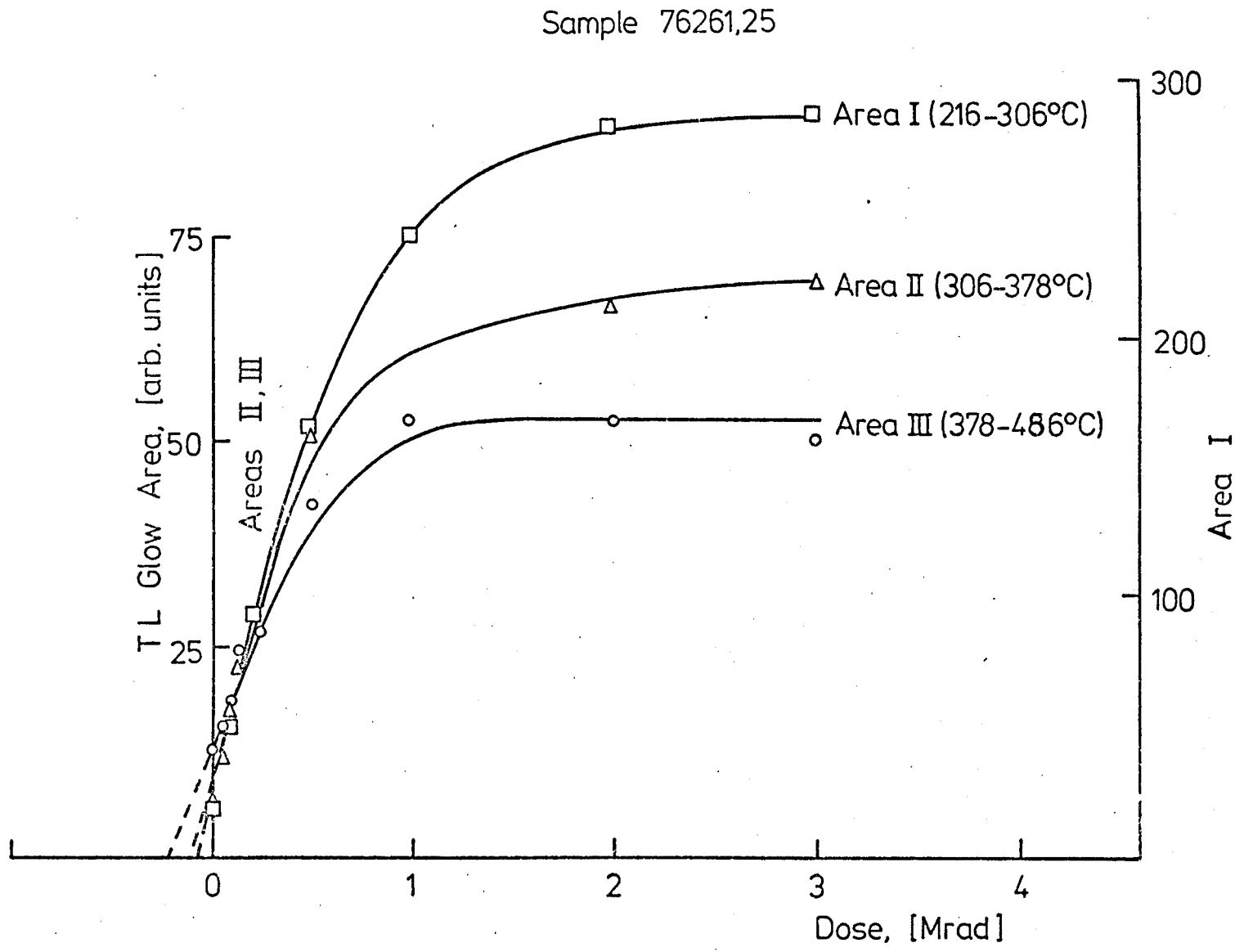
Sample 76261,25
Area I (216-306°C)
Area II (306-378°C)
Area III (378-486°C)
TL Glow Area, [arb. units]
Areas II, III
Area I
Dose, [Mrad]
75
50
25
300
200
100
0
1
2
3
4

Fig 6·3(b)

readout temperature-intervals) are shown in Table 6.1 along with other relevant data.

6.6 TL Emission Spectra.

The TL emission spectra from the sunlit sample 76261,25 (sample B) and the shaded sample 'freezer counterpart' 76241,23 (sample A) were determined using a set of interference filters (Filtraflex B40 and R-UV, made by Balzers, typical transmission band width at half-height $\sim$ 10nm) after irradiation with 1Mrad of ^{60}Co γ-rays. The samples which were used for the determination of the emission spectra were previously drained of their natural TL by heating to 500^{o}C using the TL apparatus described in Chapter II. The heating rate used in this study was 3.6^{o}C/sec. Also, the TL output was normalised to a unit of weight (mg) and corrections were made for the quantum efficiency of the quartz-window photomultiplier tube (6256SQ.) and the transmission characteristics of the filters. The filter with transmission peak 365nm was arbitrarily chosen as the reference and all the results obtained with other filters were normalised with respect to it.

In Figures 6.4(a,b) and 6.5(a,b) the TL emission spectra of both samples at temperatures corresponding to the temperatures of the glow peaks which are present in the glow curves (see Section 6.8), are shown. The main conclusion drawn from these curves is that the TL emission spectra from the two samples, the shaded and the sunlit, are similar. These results, together with the similarity of the artificial TL glow curves and the trap depths of both samples, indicates that the mineral composition of both samples is similar. Also, the TL emission spectra for both samples show clearly a dominant blue peak (with a maximum at $\sim$ 410nm), decreasing in intensity as the temperature of emission rises. The figures also show that

TABLE 6.1

Values of useful parameters for the shaded sample A and the sunlit sample B related to calculations for the temperature and duration of the boulder shadows.

Parameter	Sample A (76241,23; "freezer counterpart") TL area I (216-306°C)	TL area II (306-378°C)	TL area III (378-486°C)	Sample B (76261,25) TL area III (378-486°C)
Trap depth E(ev)	1.046 ± 0.05	1.134 ± 0.07	1.439 ± 0.06	1.72 ± 0.06
Frequency factor s(sec^{-1})	$\sim 5 \times 10^{8}$	$\sim 2 \times 10^{8}$	$\sim 1 \times 10^{9}$	$\sim 2 \times 10^{11}$
Peak temperature T* (°C) (± 10°)	279	351	450	441
N/n_{eq} (or N/n) (± 10%)	7.41	4.58	3.31	3.85
Half-dose $R_{\frac{1}{2}}$ (± 10%) (krad)	500	520	520	340
Storage temperature T_1 (°K) (± 15°K)	256 (calculated)	256 (from area I)	256 (from area I)	371 (calculated)
Length of storage t_1 (yr)	-	3.98×10^{4} (assuming 48% fading)	5.65×10^{4} (assuming 43% fading)	∞
Mean life τ (T_1) (yr)	2.44×10^{4}	3.50×10^{6}	7.16×10^{11}	3.85×10^{4} (at T_1 = 371°K)
Mean life τ (20°C) (yr)	62	5.9×10^{3}	1.49×10^{8}	6.48×10^{10}

Sample 76241,23

(freezer counterpart)

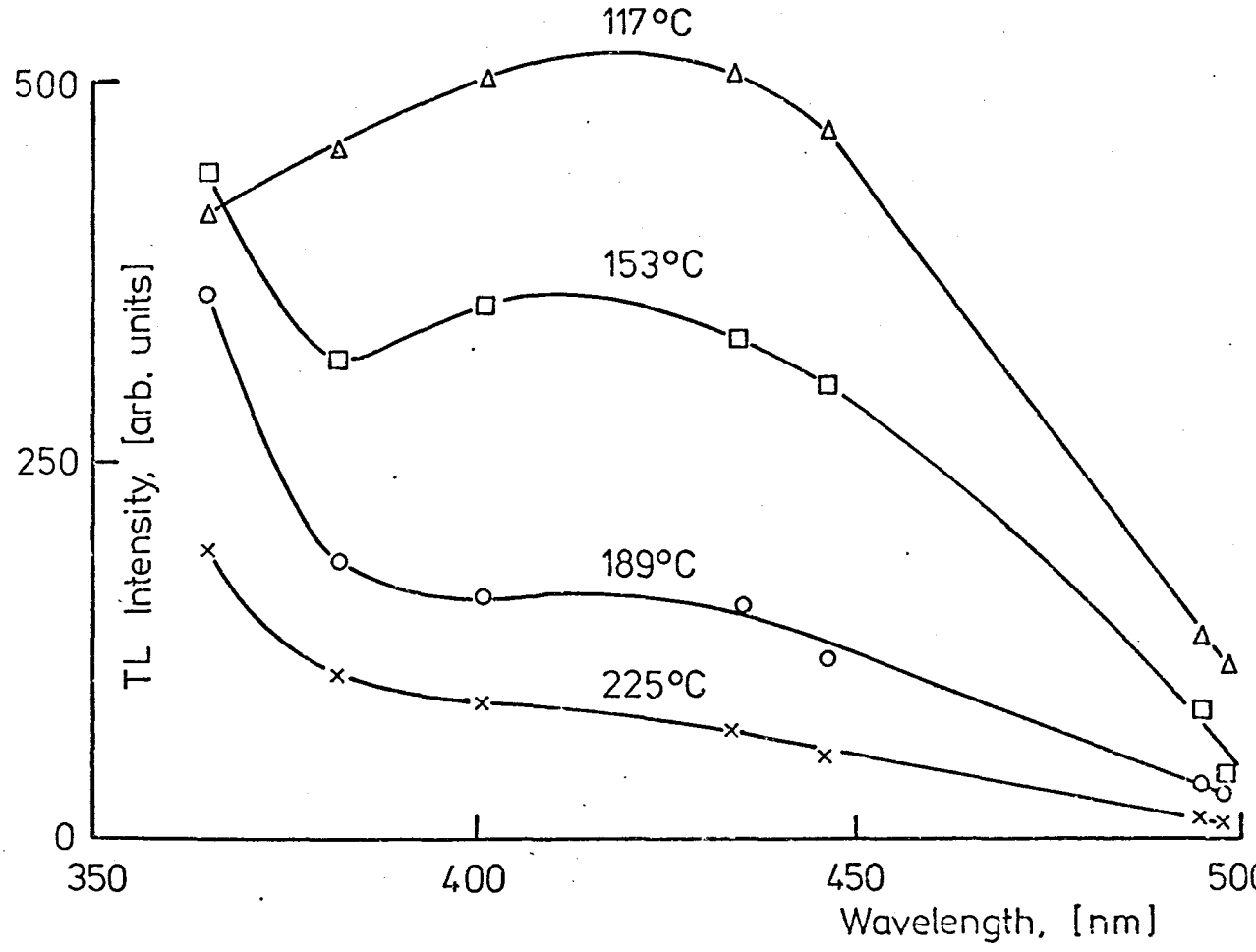

Fig 6·4(a)

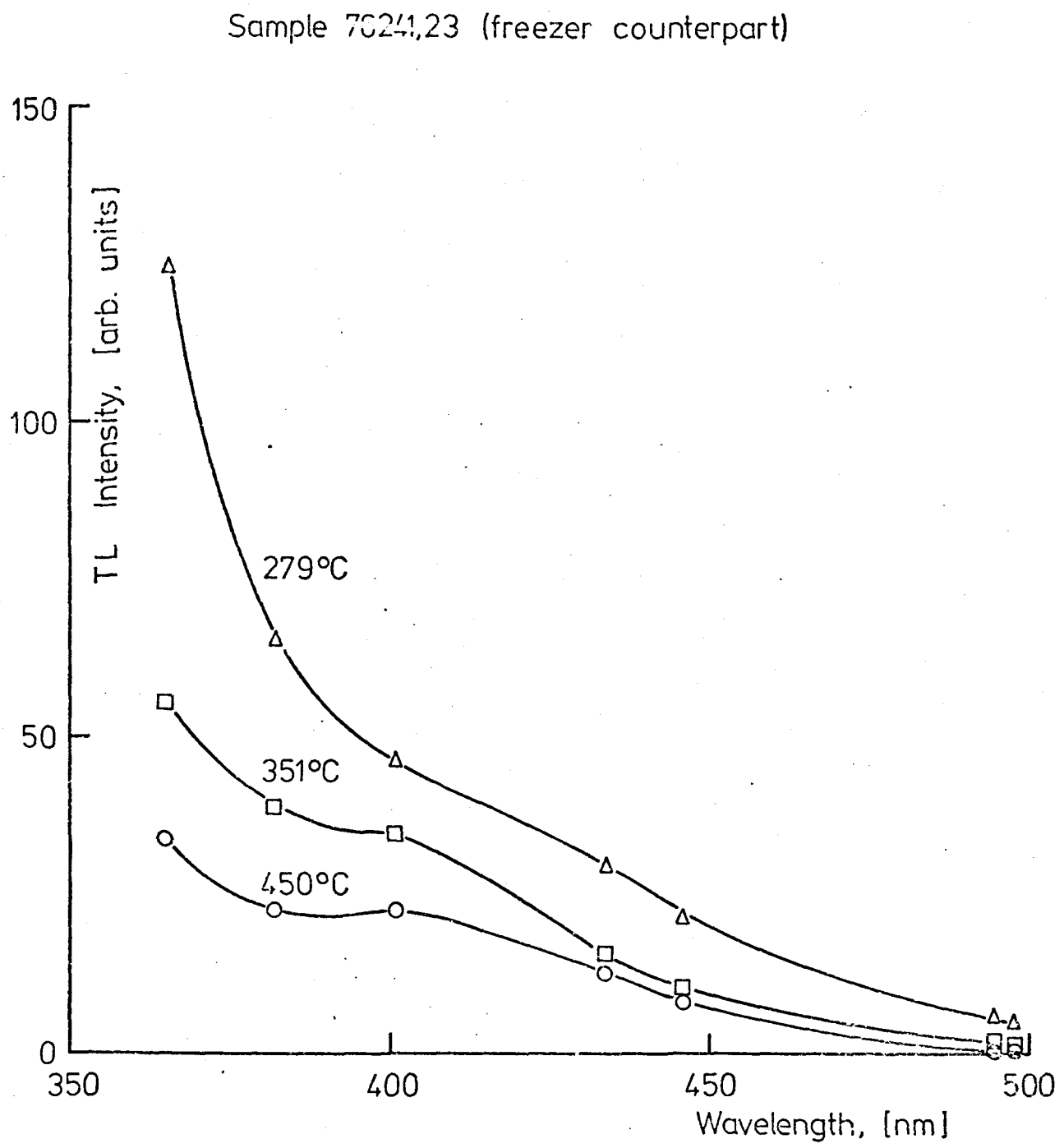
Sample 70241,23 (freezer counterpart)
150
100
50
0
TL Intensity, [arb. units]
279°C
351°C
450°C
350
400
450
500
Wavelength, [nm]

Fig 6·4(b)

Sample 76261,25 (sunlit)

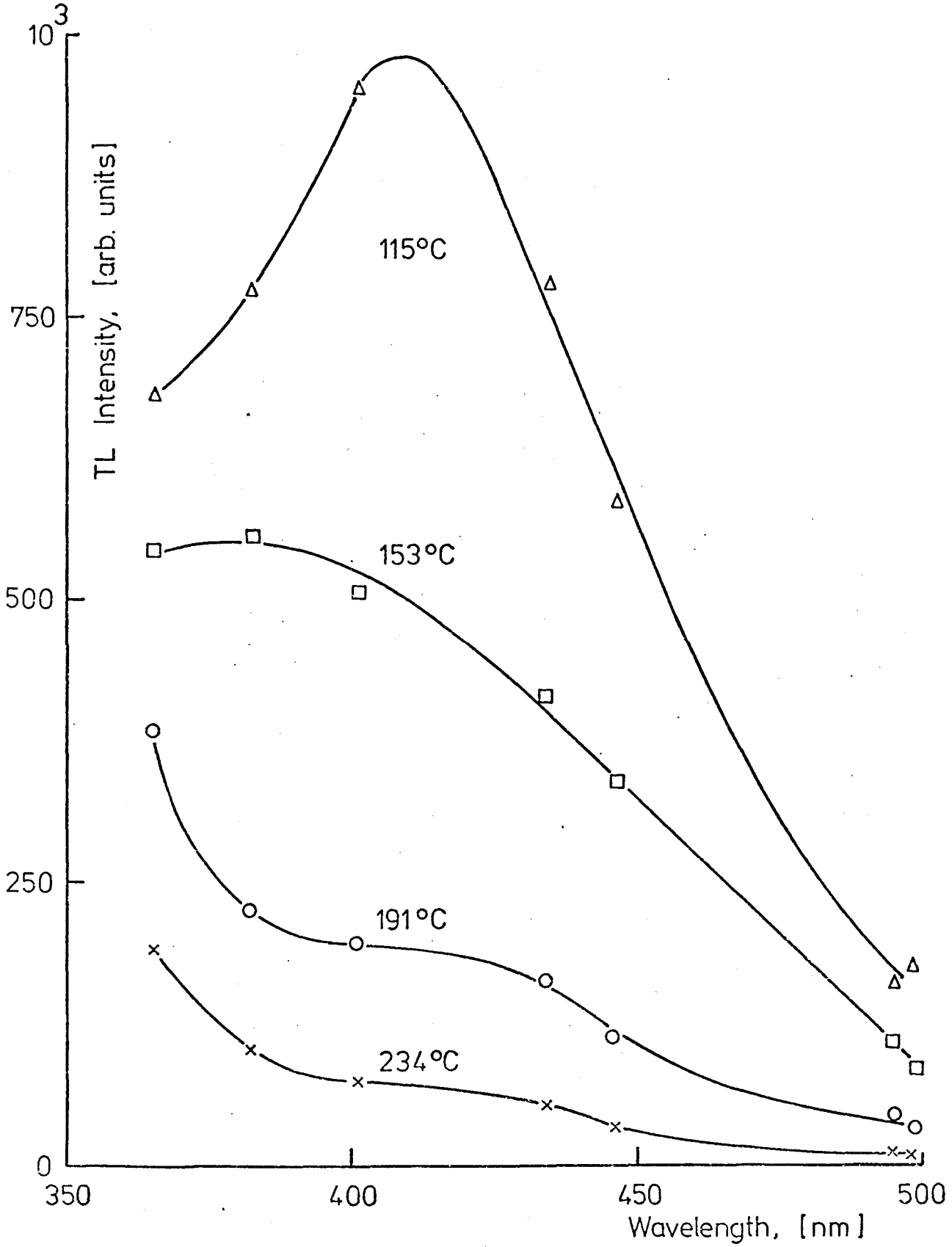

Fig 6·5(a)

Sample 76261,25 (sunlit)

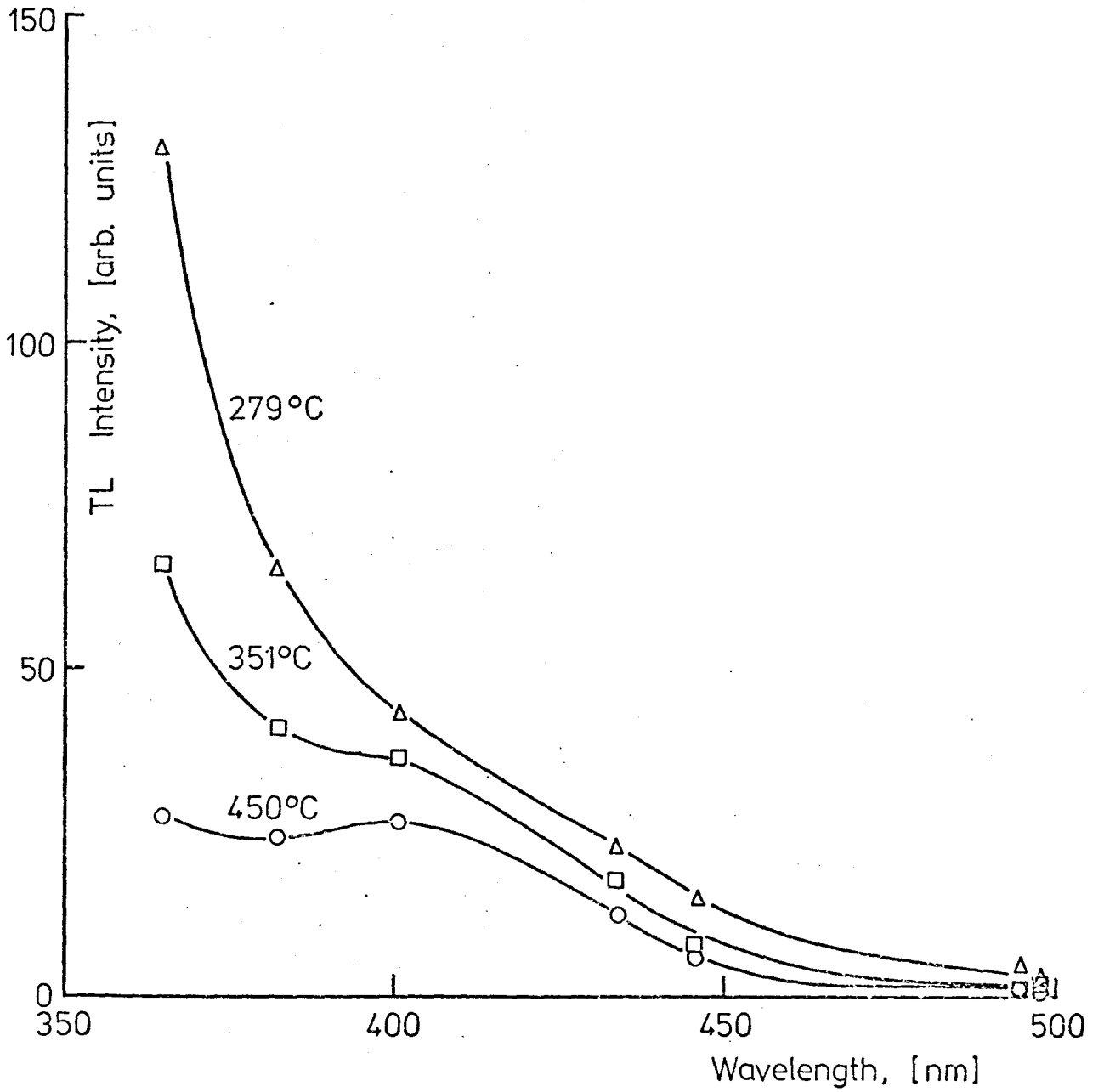

Fig 6·5(b)

the contribution from wavelengths beyond ~ 500nm is almost nil in particular at high emission temperatures (~ 280°C and greater).

6.7 Fading and Isothermal Annealing Studies.

To investigate the effect of room-temperature storage of the 'freezer counterpart' samples over the last ~ 3 years, natural fading and isothermal annealing studies were carried out on the various samples. In Figure 6.6a are shown the natural TL outputs at the beginning of 1976 from the freezer sample (76240) and its room-temperature counterpart (76241). Similarly, natural TL curves for the freezer sample (72320) and its room-temperature counterpart (72321) are shown in Figure 6.6b. In Figure 6.6a a total fading (corrected for sample weights) of ~ 49% over the whole temperature range is observed in the counterpart sample as a result of room-temperature storage for ~ 3 years. The degree of fading (~ 40%) in the high temperature region (360 - 486°C) is surprisingly high and suggests anomalous fading (Garlick and Robinson, 1972). Recorded in Table 6.2 is the degree of fading observed in the two counterpart samples 76241 and 72321, after three years of storage at room temperature, which is determined by comparing the natural TL surviving in three consecutive temperature intervals of interest to the determination of the temperature and duration of the boulder shadows (namely 216 - 306°C, 306 - 378°C and 378 - 486°C) with the corresponding amounts in the freezer samples 76240 and 72320. The fading that may have taken place in the freezer samples themselves during their first ~ 3 weeks of storage in the Lunar Receiving Laboratory has been ignored.

In order to examine the effect of lunar day-time temperature on the natural TL of samples (whether during the sample collecting or during the

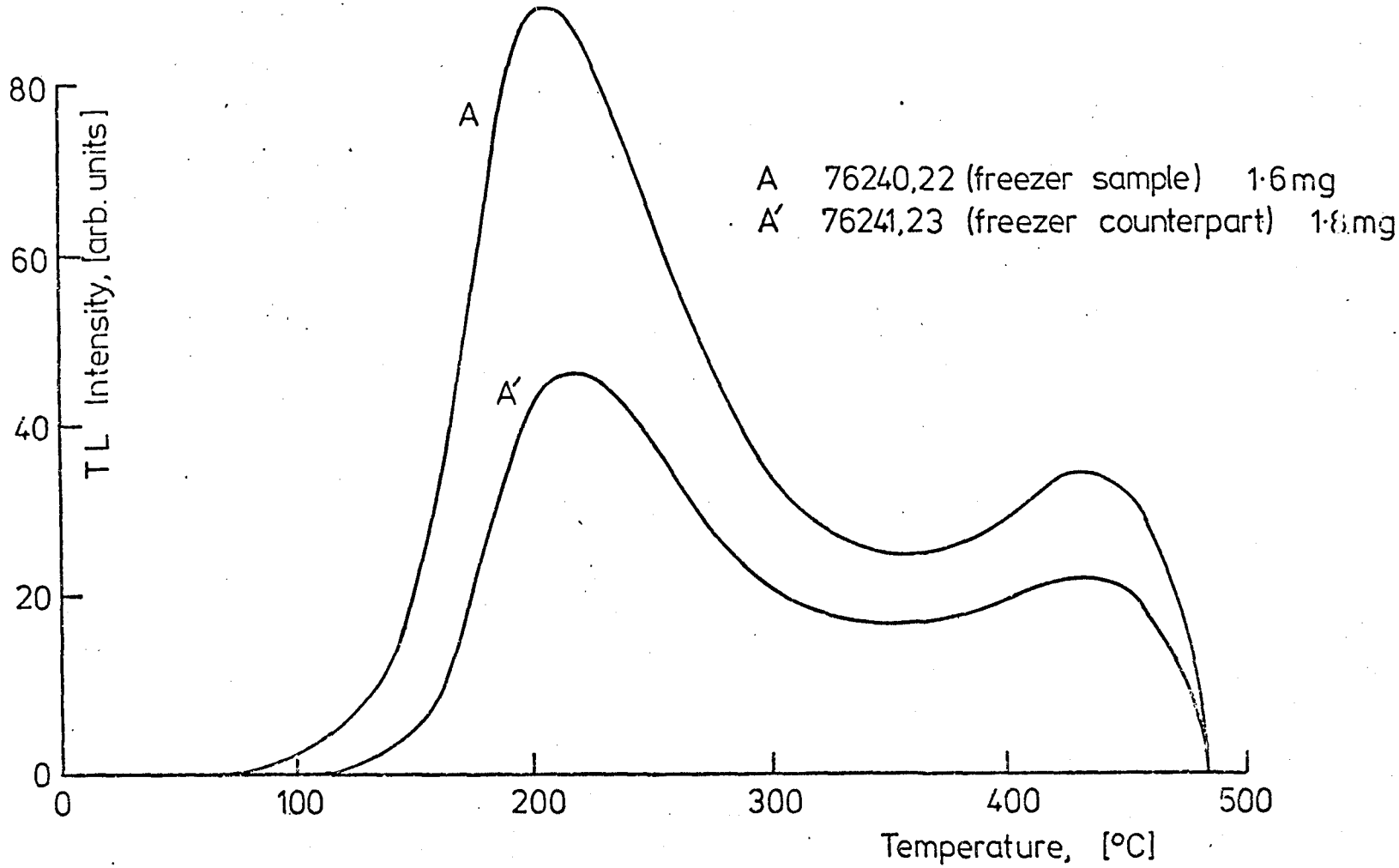
80
60
40
20
0
TL Intensity, [arb. units]
A
A'
A 76240,22 (freezer sample) 1·6 mg
A' 76241,23 (freezer counterpart) 1·8 mg
0
100
200
300
400
500
Temperature, [°C]

Fig 6·6(a)

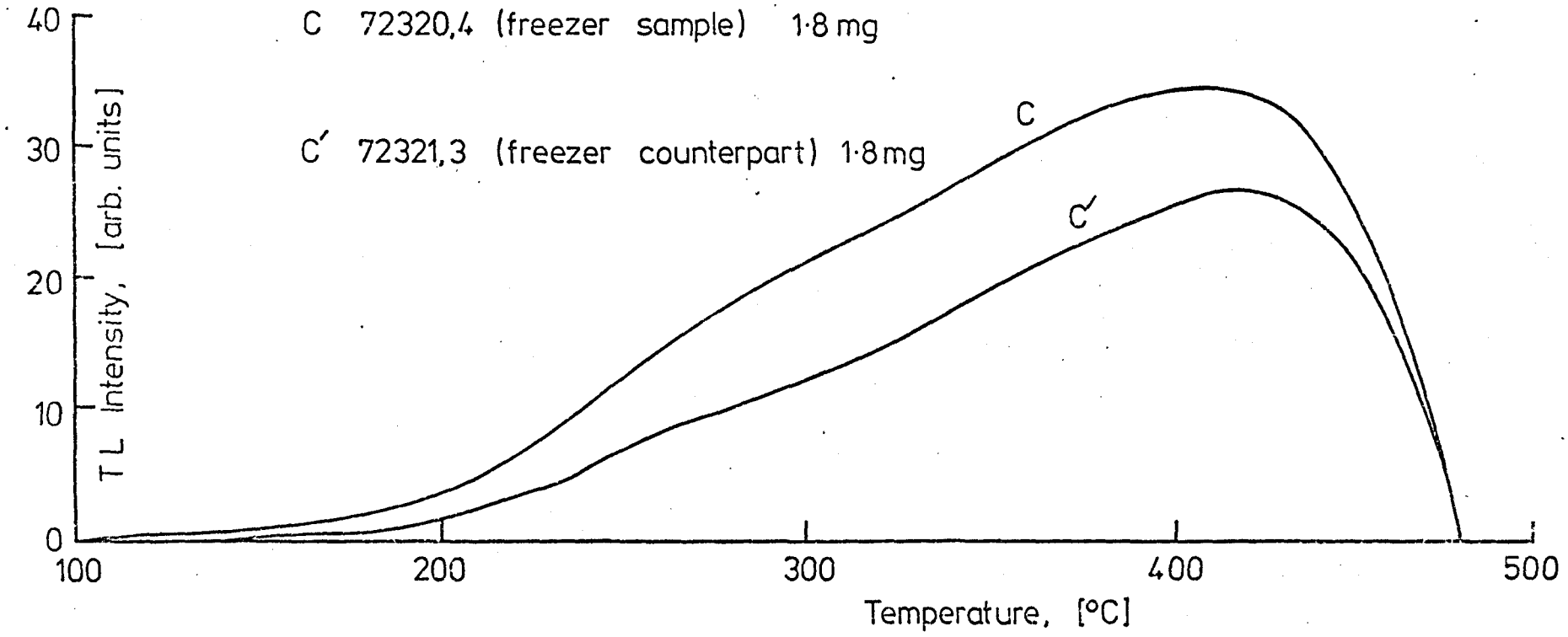
C 72320,4 (freezer sample) 1·8 mg
C′ 72321,3 (freezer counterpart) 1·8 mg
C
C′
T L Intensity, [arb. units]
Temperature, [°C]
0
10
20
30
40
100
200
300
400
500

Fig 6·6(b)

TABLE 6.2

Fading of TL in the room-temperature "counterparts" over a period of 3 years by comparison with the "freezer samples".

Sample	Area I (216 - 306°C)		Area II (306 - 378°C)		Area III (378 - 486°C	
	TL/mg*	Fading	TL/mg*	Fading	TL/mg*	Fading
76240,22 ("freezer sample")	37.5		15.0		22.5	
76241,23 ("counter-part")	20	47%	7.8	48%	12.8	43%
72320,4 ("freezer sample")	7.2		11.7		18.9	
72321,3 ("counter-part")	4.45	38%	8.3	29%	14.5	24%
76261,25 (sunlit sample)†	0.68		1.82		7.27	

* TL (integrated over the temperature interval in each case) is expressed in arbitrary units, but has been normalised for sample weight.

† The values for the sunlit sample are recorded for completeness.

exposure of the 'partially shaded' sample 72320 to the sun), isothermal annealing experiments were performed on the counterpart sample 76241. Figure 6.7 shows the results of annealing the natural sample at 120°C (roughly comparable with the lunar maximum surface temperature) for varying lengths of time up to 196 hours. Isothermal annealing was also studied at dry-ice (-78.5°C) and 20°C temperatures (Durrani and Khazal, 1976). These studies were performed by irradiating a fresh amount of the sample 76241 with a gamma dose of 1120krad. The irradiated powder was divided into two parts; one part was kept at room temperature (20°C) for fourteen days and the other half kept at dry-ice temperature (-78.5°C) for three weeks. Fading of $\sim$ 10-20% in the sample kept at 20°C was observed over the period of 14 days in the readout intervals 306 - 378°C and 378 - 486°C, and of 25% in the interval 216 - 306°C. Dry ice storage (-78.5°C) over the three weeks showed no fading in areas II (306 - 378°C) and III (378 - 486°C), and a fading of 5% in area I (216 - 306°C). The effects of fading on the calculation of temperature and duration of boulder shadows are discussed in Section 6.10.

It is clear from the fading studies that the refrigeration of the shaded samples by NASA and by the TL group at the Department of Physics, University of Birmingham, over the last three years has been a worthwhile exercise and is justified (Durrani, 1972).

6.8 Determination of TL Parameters.

For the determination of the effective storage temperature of various samples in their lunar environment one needs to know the trapping parameters E (trap depth, usually in eV) and s (frequency factor, in sec^{-1}) of the trapping levels responsible for the observed TL. These parameters

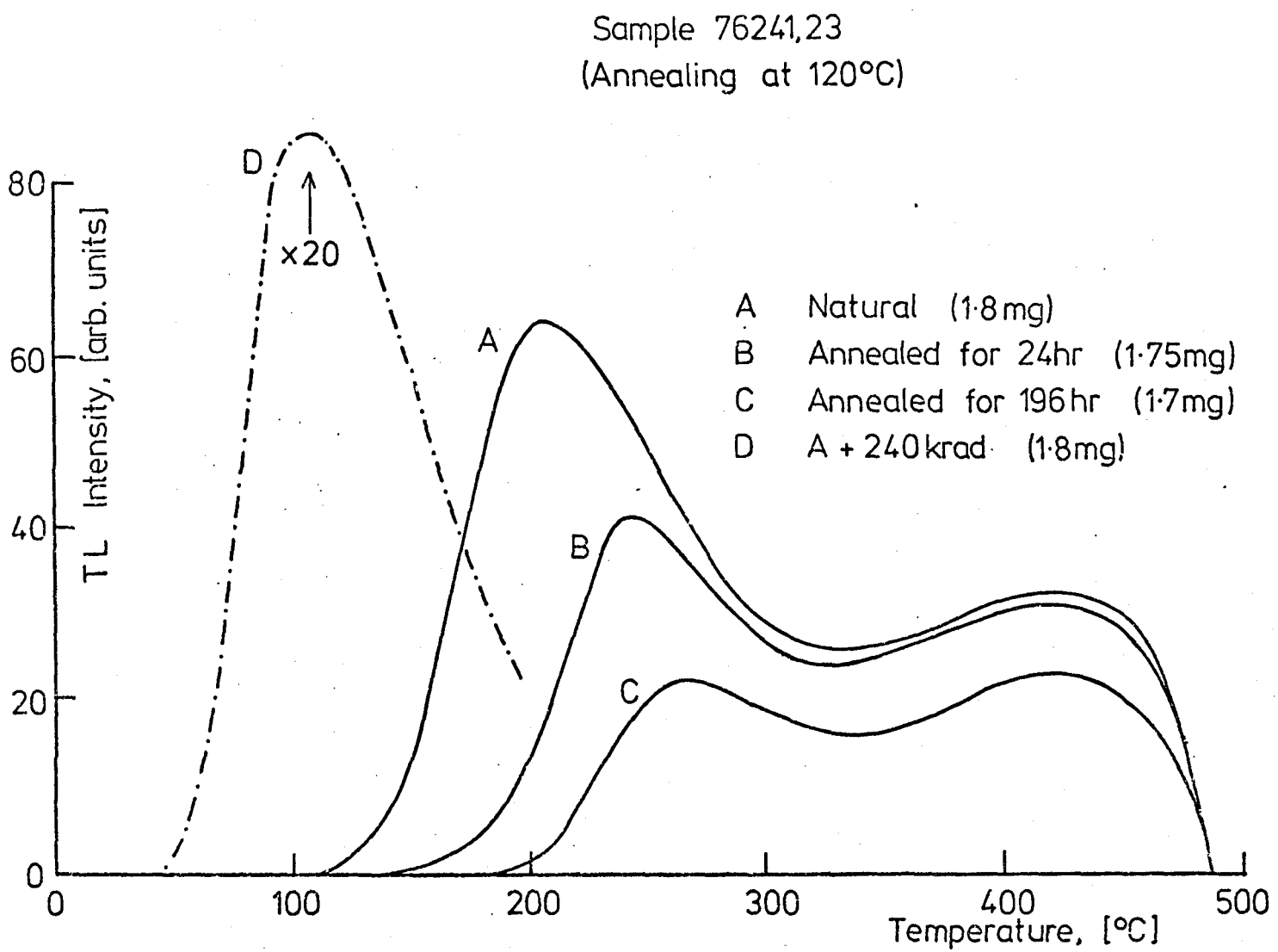
Sample 76241,23
(Annealing at 120°C)
D
×20
A
B
C
A Natural (1·8mg)
B Annealed for 24hr (1·75mg)
C Annealed for 196hr (1·7mg)
D A + 240krad (1·8mg)
TL Intensity, [arb. units]
80
60
40
20
0
0
100
200
300
400
500
Temperature, [°C]

Fig 6·7

were determined by using the 'initial-rise method' of Garlick and Gibson (1948), which is independent of the recombination kinetics of the thermally released electrons and also of the rate of heating, β, employed. This method is based on the fact (see Section 1.3.3) that, at temperature T sufficiently below the 'peak temperature' T^* for a given trap, the TL intensity I(T) rises with temperature as $e^{-E/kT}$. On plotting lnI against T^{-1} the initial part of the glow curve, thus yields a straight line with slope $\frac{-E}{kT}$. This method is described in detail in Chapter I.

The experimental procedure for the determination of the trap depth (E) and consequently the frequency factor (s) for the various peaks in the samples 76241 ('freezer counterpart, sample A) and 76261 (sunlit, sample B) can be summarised as follows. Samples $\sim$ 3mg in weight were given an artificial dose of 2.4Mrad ^{60}Co gamma rays, in addition to their natural dose, to induce as much TL from the samples as possible which is an important factor for the success of this method - see Section 1.3.3. The samples were then heated at a heating rate (β) of 3.6°C/sec to successively increasing terminal (or interruption) temperatures followed by cooling to room temperature. Figures 6.8a and 6.8b show the resulting E values, obtained by plotting lnI against T^{-1}, plotted against the temperature of interruption for the shaded sample counterpart (76241, sample A) and the sunlit sample (76261, sample B) respectively. The horizontal clusters correspond to the trap depths for the various glow peaks, which have been obtained by a separate experiment involving the 'thermal cleaning' of peaks. The values of T^* have an uncertainty, generally, of $\sim \pm 10^{\circ}$C. Other peaks at lower temperatures T^* in each sample are not shown in the figure. These peaks were, for sample A: $\sim$ 234°C, 191°C, 153°C

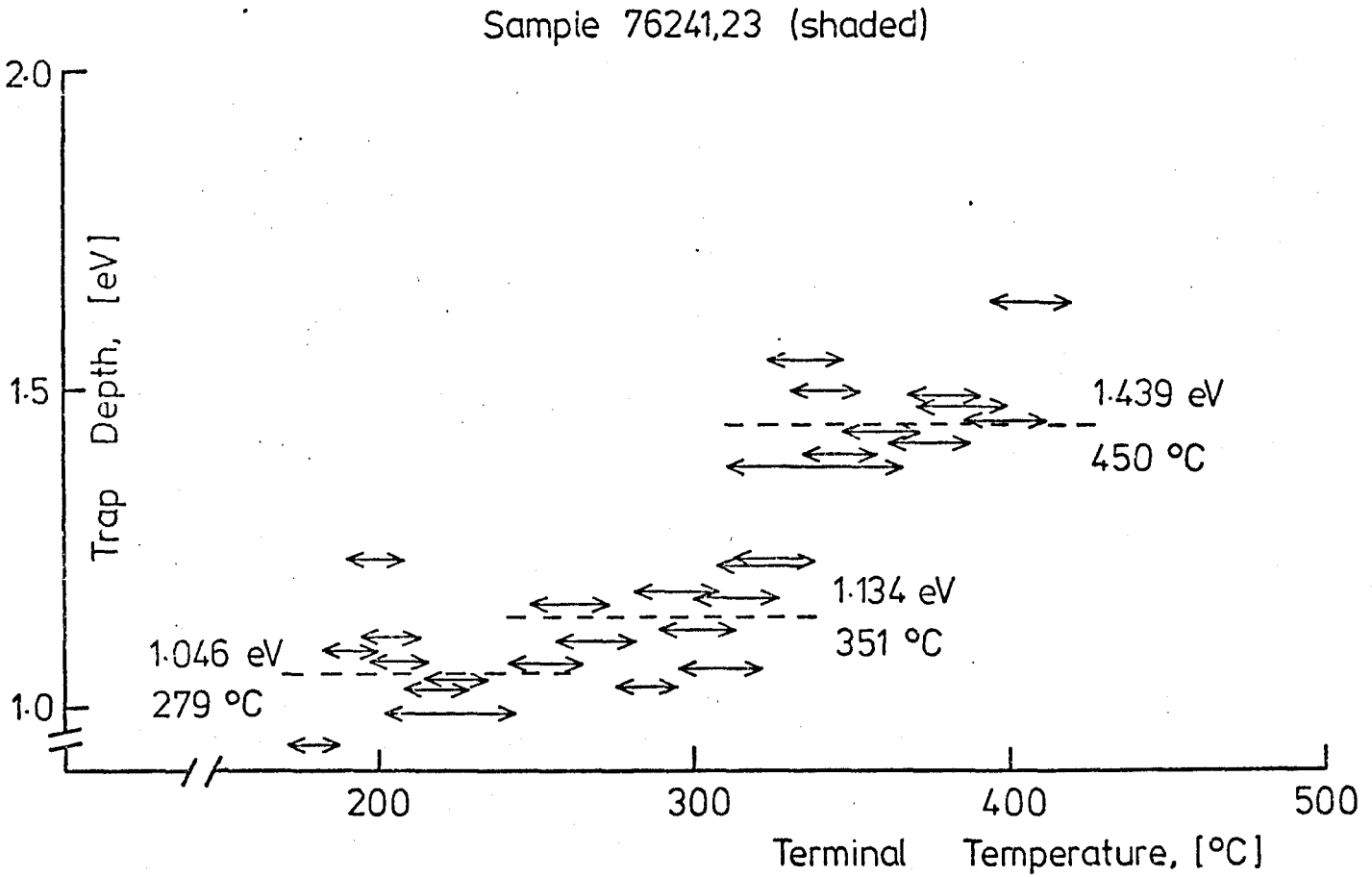
Sample 76241,23 (shaded)
2·0
1·5
1·0
Trap Depth, [eV]
1·439 eV
450 °C
1·134 eV
351 °C
1·046 eV
279 °C
200
300
400
500
Terminal Temperature, [°C]

Fig 6·8(a)

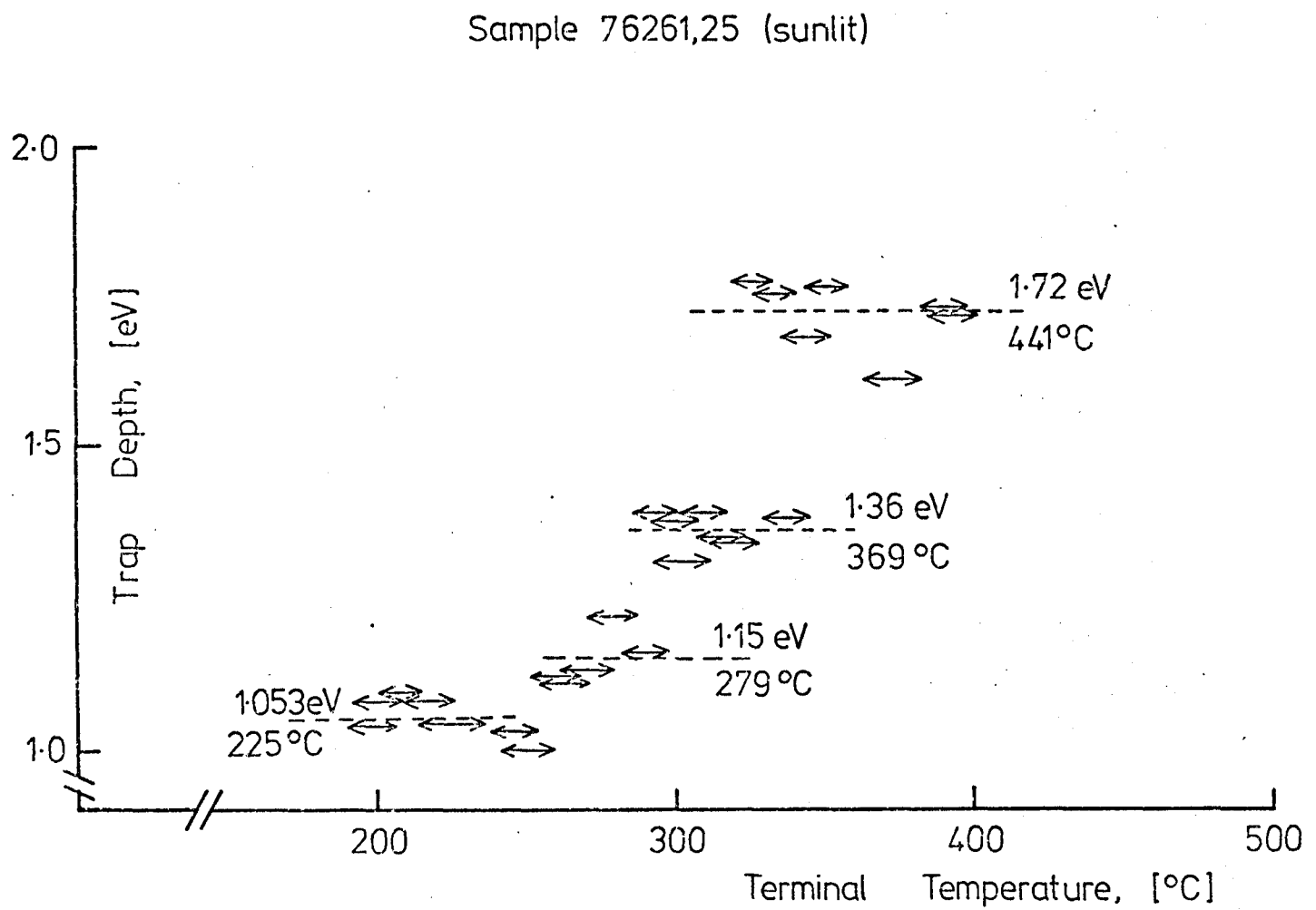
Sample 76261,25 (sunlit)
2·0
1·5
1·0
Trap Depth, [eV]
1·72 eV
441°C
1·36 eV
369 °C
1·15 eV
279 °C
1·053eV
225 °C
200
300
400
500
Terminal Temperature, [°C]

Fig 6·8(b)

and 115°C; and for sample B: ~189°C, 153°C and 117°C. The s factor is then calculated from the first-order kinetics relation:

$$s = (\beta E/kT^{*2}) \cdot \exp(E/kT^{*}) \qquad (2)$$

where k is Boltzmann's constant and T^{*} is in °K.

6.9 Determination of the Temperature and Duration of the Boulder Shadow.

6.9.1 General remarks.

The data obtained in the previous sections, namely the trapping parameters, the inferred natural dose, the half-dose $R_{\frac{1}{2}}$, and the saturation level achieved by various samples upon artificial irradiation, were used to calculate both the temperature inside the boulder shadows and the duration of the shade. In these calculations it was assumed that the trap-filling process obeyed the first-order kinetics of Randall and Wilkins (1945). The thermal and radiation characteristics of the samples studied played an important role in laying down the theoretical framework as well as in conducting a meaningful discussion of the results obtained from the experiments on the shaded and sunlit samples.

6.9.2 Theoretical framework.

Consider a sample with a total of N traps, each of depth E and frequency factor s, irradiated with a dose-rate r while being held at an absolute temperature T. The following equation holds for the radiative filling and the thermal drainage of traps with time:

$$dn/dt = -\lambda n + (N - n)r\,p \qquad (3)$$

where n is the number of filled traps at time t, λ is the decay constant at temperature T, and p is the probability per unit dose of filling one of the above traps. The following relations exist for parameters λ and p:

$$\lambda = s \exp(-E/kT) \qquad (4)$$

or $$\lambda = \tau^{-1} = 0.693/\tau_{\frac{1}{2}} \quad (5)$$

where $\tau(T)$ is the mean life of the trapped electrons at temperature T, and $\tau_{\frac{1}{2}}$ is the corresponding half-life. Similarly if a 'half-dose' $R_{\frac{1}{2}}$ required to fill half the available traps N (cf. equation 1 above) in the absence of thermal drainage was defined, then:

$$p = 0.693/R_{\frac{1}{2}} \quad (6)$$

The general solution of the differential equation 3 is given by:

$$n = \frac{N \cdot rp}{\lambda + rp} \cdot (1 - e^{-(\lambda + rp)t}) + n_o \cdot e^{-(\lambda + rp)t} \quad (7)$$

where n_o is the number of filled traps at time $t = 0$.

Now consider two specific cases. First, suppose all traps are initially empty (e.g. when trap-filling first commences in the sunlight), so that $n_o = 0$. Then, equation 7 is reduced to:

$$n = \frac{N \cdot rp}{\lambda + rp} (1 - e^{-(\lambda + rp)t}) \quad (8)$$

Secondly, consider that the radio-thermal environment changes at time t_o (e.g. the time at which the boulder arrives) such that the number of filled traps at time $t = t_o$ is n_o. In this case equation 7 continues to hold, except that the values of the relevant parameters are changed to r', p' and λ', and t may be replaced by t_1 such that $t_1 = t - t_o$. The value of n_o to be used in the modified form equation 7 is obtained by substituting t_o for t in equation 8:

$$n_o = \frac{N \cdot rp}{\lambda + rp} \cdot (1 - e^{-(\lambda + rp)t_o}) \quad (9)$$

If the case where the time prior to the arrival of the boulder is very large, so that $t_o \longrightarrow \infty$ (i.e. $t_o \gg \tau$ (sunlit) or in other words, $\lambda t_o \gg 1$), then equation 9 is reduced to:

$$n_o = N \cdot rp/(\lambda + rp) = \frac{N}{1 + \lambda/rp} \tag{10}$$

The modified form of equation 7, after the arrival of the boulder, thus becomes:

$$n = \frac{N \cdot r'p'}{\lambda' + r'p'} \cdot (1 - e^{-(\lambda' + r'p')t_1}) + \frac{N \cdot rp}{\lambda + rp} e^{-(\lambda' + r'p')t_1} \tag{11}$$

It will be shown later that, in the case of the shadowed sample, the decay constant λ (sunlit) prior to the arrival of the boulder is so large for traps of interest in comparison with the corresponding values of λ' (i.e. τ (sunlit) $\longrightarrow 0$), that $n_o \longrightarrow 0$ in equation 10, so that equation 11 is reduced to:

$$n = \frac{N \cdot r'p'}{\lambda' + r'p'} \cdot (1 - e^{-(\lambda' + r'p')t_1}) \tag{12}$$

which is essentially equivalent to equation 8. Equation 8 thus effectively holds both for the sunlit sample and for the shaded sample as long as the appropriate values of the dynamic parameters are used.

Equation 8 may be re-expressed in the two equivalent forms:

$$n = \frac{N}{1 + (\lambda/rp)} \cdot (1 - \exp[-rtp(1 + \lambda/rp)]) \tag{13}$$

or

$$n = \frac{N}{1 + (R_{\frac{1}{2}}/r\tau_{\frac{1}{2}})} \cdot (1 - e^{-0.693rt/R_{\frac{1}{2}}} \cdot e^{-0.693t/\tau_{\frac{1}{2}}}) \tag{14}$$

Equations 13 and 14 are modified forms of the Randall-Wilkins relation (with all traps initially empty) and give the ratio n/N (i.e. the TL output as a result of a dose rt, expressed as a fraction of the saturation TL) in terms of the observables $R_{\frac{1}{2}}$ and $\tau_{\frac{1}{2}}$. There are a number of limiting cases of equations 13 and 14 which are of special interest here. Thus:

(i) for either $rt \gg R_{\frac{1}{2}}$ or $t \gg \tau_{\frac{1}{2}}$:

$$n_{eq} \longrightarrow \frac{N}{1 + (R_{\frac{1}{2}}/r\tau_{\frac{1}{2}})} \equiv \frac{N}{1 + (\lambda/rp)} \qquad (15)$$

and if, in addition, $r\tau_{\frac{1}{2}} \gg R_{\frac{1}{2}}$:

$$n_{eq} \longrightarrow N \qquad (16)$$

where, in equations 15 and 16, n_{eq} represents the dynamic-equilibrium, or steady-state, value of n reached either as a result of giving a massive dose ($rt = R \gg R_{\frac{1}{2}}$) to a sample, or by filling the traps for a very long time, t, compared with $\tau_{\frac{1}{2}}$. If $rt \gg R_{\frac{1}{2}}$, equation 15 is true whatever the value of $t/\tau_{\frac{1}{2}}$, i.e. whether the filling time is much larger or much smaller than, or comparable with, the half-life of the traps at the temperature concerned; similarly, if $t \gg \tau_{\frac{1}{2}}$, equation 15 is again true for all values of $rt/R_{\frac{1}{2}}$.

(ii) for $\tau_{\frac{1}{2}} \gg t$:

$$n \longrightarrow \frac{N}{1 + (R_{\frac{1}{2}}/r\tau_{\frac{1}{2}})} \cdot (1 - e^{-0.693rt/R_{\frac{1}{2}}})$$

$$\equiv \frac{N}{1 + (\lambda/rp)} \cdot (1 - e^{-rt \cdot p}) \qquad (17)$$

which represents the case when the half-life at temperature T is much larger than the filling time t (i.e. effectively no decay (or drainage) occurs during trap-filling, either because the sample is held at a very low temperature or the dose rate is very high.

(iii) for $R_{\frac{1}{2}} \gg rt$:

$$n \longrightarrow \frac{N}{1 + (R_{\frac{1}{2}}/r\tau_{\frac{1}{2}})} \cdot (1 - e^{-0.693t/\tau_{\frac{1}{2}}}) \equiv \frac{N}{1 + (\lambda/rp)} \cdot (1 - e^{-\lambda t}) \qquad (18)$$

(iv) for $\lambda \gg rp$, i.e. $R_{\frac{1}{2}} \gg r\tau_{\frac{1}{2}}$:

$$n \longrightarrow 0 \qquad (19)$$

so that effectively no trap-filling takes place and no useful information can be gained from the sample; and finally,

(v) for $\lambda \ll rp$, i.e. $r\tau_{\frac{1}{2}} \gg R_{\frac{1}{2}}$:

$$n \longrightarrow N\,(1 - e^{-rt \cdot p}) \equiv N(1 - e^{-0.693rt/R_{\frac{1}{2}}}) \qquad (20)$$

Equation 20 is a very useful relation and can be used to calculate the natural dose R = rt received by a sample over a time t, so long as saturation ($n \longrightarrow N$) has not been reached in nature and provided that the condition governing the equation is fulfilled. This is achieved by measuring the natural TL expressed as a function of the saturation TL (i.e. the ratio n/N). The values of N and $R_{\frac{1}{2}}$ in equation 20 are usually obtained by employing such a massive dose rate r in the laboratory that there is effectively no thermal drainage during the irradiation. Ideally, these values should be obtained by inducing TL in the sample at the same temperature as the one operating on it in nature.

6.9.3 Calculations and results.

The effective temperature of storage of the 'permanently shadowed' sample (76240 or 76241, termed sample A) as well as the length of its storage in the boulder shadow can be determined by comparing the thermoluminescence characteristics of that sample with those of the sunlit sample (76261, sample B) and making use of the foregoing theoretical framework.

From equation 15, which applies to the case when dynamic equilibrium has been reached in nature as a result of competition between radiative filling for a very long time (so that $rt \gg R_{\frac{1}{2}}$) and thermal drainage of traps held at temperature T, one can obtain the value of the storage temperature as:

$$T = \frac{E/k}{\ln\left[\frac{s\,R_{\frac{1}{2}}}{0.693r\left(\frac{N}{n_{eq}} - 1\right)}\right]} \qquad (21)$$

where N/n_{eq} is the ratio of the saturation TL (obtained from a separate experiment) to that found in the natural sample. If the natural dose rate r is known, T can be calculated by determining the values of E, s and $R_{\frac{1}{2}}$ for the relevant trapping level. For the purpose of the calculations, a value of r = 10rad yr^{-1} (Haffner, 1967) for unshaded lunar samples was assumed. The value of T is only weakly dependent on the values of r and N/n_{eq} used since they occur in the logarithmic term. Thus, changing the product $r \cdot ((N/n_{eq}) - 1)$ by a factor of 2 makes a change of only $\sim$ 1%. (Durrani et al, 1972a) in the value of T calculated from equation 21 in cases of interest. This means that even if the dose rate goes down by a factor of 2 after the arrival of the boulder (because of the partial shielding from, say, the solar-flare particles), the effect on the calculated storage temperature will be only slight: it will fall by a few degrees Kelvin. The same remarks apply to the effects of fading corrections on N/n_{eq} (see Section 6.10).

In Table 6.1 the experimental values of all the parameters that are needed in the calculation are recorded. The procedure which was adopted in making the calculations involved the following steps:

1) It was assumed in the case of the sunlit sample B that dynamic equilibrium had been reached in filling the traps corresponding to the TL readout area III (378 - 486°C, with E = 1.72eV) i.e. $t \gg \tau_{\frac{1}{2}}$ in sunlight. When, as a first approximation, the fading correction obtained for area III in the shaded sample A during the $\sim$ 3 yr. storage at room temperature (namely 43%, see Table 6.2) was applied to area III in the sunlit sample B, a

corrected value of $\frac{N}{n_{eq}} = 2.2$ for the latter sample (cf. the observed value 3.85, Table 6.1) was obtained. On using this corrected value of N/n_{eq}, together with the other parametric values given in Table 6.1, the lunar storage temperature T = 371°K for the sunlit sample was obtained using equation 21.

2) The storage temperature T_1 in the shade was calculated by assuming that equilibrium has been reached in TL area I of the shaded sample (216 - 306°C; E = 1.046eV). In other words, it was assumed that the trap-filling time in the shade $t_1 \gg \tau_{\frac{1}{2}}$ of the trap at temperature T_1. In this calculation a 47% fading correction to n_{eq} (cf. Table 6.2) was applied, which converted the observed value of N/n_{eq} from 7.41 to 3.93, and yields a value of $T_1 = 256°K$ in the shade. The value of $\tau_{\frac{1}{2}}$ (256°K) for area I traps is $\sim 1.7 \times 10^4$ yr, whereas t_1 calculated below from TL areas II and III ranges from $\sim 4 \times 10^4$ yr to 6.5×10^4 yr. (with r = 10 rad yr^{-1}; or a factor of 10 higher if r = 1 rad yr^{-1}); hence the assumption that $t_1 \gg \tau_{\frac{1}{2}}$ for the traps corresponding to area I is a reasonable one.

3) Using the storage temperature T_1 in the shade found from step (2) above, the value of $\tau_{\frac{1}{2}}(T_1)$ for the traps corresponding to TL area II (306 - 378°C; E = 1.134eV) as well as area III (378 - 486°C; E = 1.439eV) of the shaded sample can be calculated. It is then clear that the condition governing equation 20 is fulfilled (namely $r\tau_{\frac{1}{2}} \gg R_{\frac{1}{2}}$; cf. Table 6.1) so that the equation can be solved to obtain the length of storage t_1 in shade from either of these TL areas, using the known values of n/N. This implies that the natural TL in areas II and III is well below the corresponding saturation values.

Assuming the values for the amount of fading observed for TL areas II

and III in sample A (viz. 48% and 43% respectively; cf. Table 6.2), and using the above value for the storage temperature in the shade ($T_1 = 256^{o}K$), the following values for rt_1 from equation 20 were obtained: $rt_1 = 3.98 \times 10^5$ rad (area II); and $rt_1 = 5.65 \times 10^5$ rad (area III). If a value of r = 10 rad yr^{-1} for the dose rate in the shade was assumed, the following values for the length of storage, t_1, in the shade were obtained: from area II (sample A): 3.98×10^4 yr; from area III: 5.65×10^4 yr.

The calculations of the storage temperature in the shade ($T_1 = 256^{o}K$) and the length of the storage t_1, involved in steps 2 and 3 above are based on equations 20 and 21 which assume that the value of filled traps prior to the arrival of the boulder is negligible compared with the value subsequently attained, i.e. $n_o \longrightarrow 0$ or $n_o \ll N$ (or $n(t_1)$) for the areas I, II and III of the shaded sample 76241 (sample A); no such assumption has been made in the above derivation regarding the sunlit sample 76261 (sample B). That the above assumptions for sample A are indeed true and can be seen by substituting the relevant values of the parameters corresponding to the lunar daytime temperature ($T = 371^{o}K$) for sample A in equation 10 which gives the corrected value of the ratio $\frac{n_o}{N}$. The following values for $\frac{n_o}{N}$ are found (for r = 10 rad yr^{-1}): $\sim 1.4 \times 10^{-7}$, 5.6×10^{-6} and 1.5×10^{-2} for the TL areas I, II and II respectively, for the shaded sample, which are all clearly negligible.

The only use in steps 1-3 in the above calculations that it has been made of the TL found in the sunlit sample (76261, sample B) is to derive the temperature in the sunlight employing area III (378-486°C) in it. In that part of the calculation there is no assumption regarding the number n_o of the filled traps prior to the arrival of the boulder. No use has been made of areas I

or II in the sunlit sample.

It may be worth pointing out that in Figure 6.1, curve B refers to the sunlit sample, whereas curve A is for the shaded sample. The fact that area III in the sunlit sample (curve B) is a not negligible fraction of area III in the shaded sample (curve A) may at first sight be misleading, in that it might suggest that prior to the arrival of the boulder area III in the shaded sample also ought to be substantially populated (and n_o thus ought not to be ~ 0). It must, however be noted that, for some reason (see discussion below), the E values for areas III in samples A and B are substantially different, being 1.439 and 1.72eV respectively (Table 6.1). Thus whereas the equilibrium value of area III in sunlight ($371^{o}K$) is quite sizable in sample B, that of area III in sample A at that temperature (prior to the arrival of the boulder) is quite negligible (the ratio $\frac{n_o}{N}$ being $\sim 1.5 \times 10^{-2}$, as stated above).

One may enquire why the TL parameters for the two samples are different. The answer is not clear-cut. The difference in trap-depth values might be explained by assuming that either:

i) The arrival of the boulder, regardless of the mechanism that put it in motion (see Section 6.11), removed or disturbed the original top surface soil and also mixed it with the soil beneath it because of the movement of the boulder. If the soil underneath differed in its mineral composition from that of the surface soil, this would have led to a mixed soil of different E values from those of the undisturbed sunlit sample. Or:

ii) The top centimetre or so of the shaded soil could be of external origin, say as a result of migration of electrically charged micron-sized grains from the surrounding sunlit areas towards the shaded area

(Criswell, 1972: Section 6.11), or it could be derived from the boulder material itself, which might have fallen on top of the shaded material as a result, say, of mechanical shaking of the boulder during or after its arrival as a result of meteoritic impace, or as a result of the boulder erosion (though the time scale involved [6.5×10^4 yr] is not in favour of the erosion hypothesis). Any of these factors could give rise to a mixed soil for the shaded sample which is slightly different from that of the sunlit sample hence leading to differences in E values.

It is important to stress that the calculation of the value of the storage temperature $T_1 = 256^{\circ}K$ and the time of the storage t_1 are based entirely on the shaded sample only, using E and s values obtained from direct measurements of the shaded sample material. The sunlit sample was merely used for the comparison of the natural glow curves of the shaded, partially shaded, and sunlit sample. The E and s values for area III of the sunlit sample were, again, measured independently of the shaded sample, and used for deriving the sunlit temperature. The value of the daylight temperature $T = 371^{\circ}K$ which was calculated from the sunlit sample data (see step 1), and used only to demonstrate that such a temperature would result in the complete drainage of traps in areas I, II and III in sample A prior to the arrival of the boulder-shadow, could be taken from previous determinations by Durrani et al (1972b, 1973), e.g. $363 \pm 10^{\circ}K$ for certain Apollo 15 and $372 \pm 5^{\circ}K$ for Apollo 14 samples, which agree well with the value obtained from the sunlit sample 76261 in the present investigation. If one uses a mean value of $367.5^{\circ}K$ from the above determinations, the ratio $\frac{n_o}{N}$ for area III in the sunlit sample is found to be ~ 0.53 which is in close agreement with out value of $\frac{n_o}{N} = \frac{1}{2.27} = 0.44$ (see Table 6.3) after correction for anomalous fading.

It is also important to stress here that the duration of the boulder t_1 can be calculated independently from either area II or area III of the shaded sample, as is clear in step 3. Hence, even if one had reservations about the population of area III of the shaded sample prior to the arrival of the boulder, one could still get a value of t_1 (viz. $\sim 4 \times 10^4$ yr) from area II alone in that sample.

6.10 Correction Factor for 'Anomalous' Fading.

As will be shown below in the discussion of errors, the calculations based on the foregoing framework are found to be remarkably sensitive to the values of the parameters for the various samples and TL areas that are substituted into the equations. This has encouraged the author to try to reconcile the two values of the duration of the boulder shadow obtained above (viz. 3.98×10^4 and 5.65×10^4 yr.) by considering the only observable in Table 6.1 which is subject to a fair amount of doubt, namely the value of n_{eq}/N (or n/N) uncorrected for the fading factor.

It is clear from Table 6.2 that the fading of TL in the shaded counterpart sample (76241) during its room-temperature storage for ~ 3 years is quite large when it is compared with the TL values from the 'freezer sample' (76240). To this one must add the fading undergone by both samples during the first ~ 3 weeks after their collection from the shade. An approximate value for this was obtained by performing a separate experiment in which the amount of room-temperature fading in the freshly-induced TL was observed in the counterpart sample over a period of 2 weeks (see Section 6.7). On making this further correction, the total amount of fading, from the time of sample collection until that of the author's investigation, would appear to

vary from ~65% to ~ 50% for the TL areas I to III respectively. There is a clear relationship between the magnitudes of the fading and the readout temperature interval in the case of the partially shaded pair of samples, 72321 and 72320 (cf. Table 6.2). It is to be noted that all these fading values are in violation of the Randall-Wilkins equations, which give large mean lives τ for the relevant traps held at 20°C (namely ~ 1.5×10^8 yr, 5.9×10^3 yr., and 62 yr. respectively for TL areas III, II and I in sample A, using equations 4 and 5 above). The fading is thus anomalous (Garlick and Robinson 1972).

An empirical relation was applied to obtain 'theoretical' values for the fading factor using the value of fading (43%) adopted in step (1) above as the base-line and then reiterating the equations. The relation assumed that 'anomalous' fading at any given time t and at a given storage temperature T is inversely proportional to the trap depth E in a given phosphor. In other words:

$$1 - \frac{n}{n_o} = \frac{a(t, T)}{E} \qquad (22)$$

where n_o is the initial number of filled traps and n is the number surviving after 'anomalous' fading.

The value of a (for ~ 3 yr. storage at 20°C), which gives identical values for the storage time t_1 in the boulder shadow for areas II and III in sample A by using equation 20 (as in step 3 above), is $a = 0.7065$(eV). The number of digits after the decimal point in a is a measure of the great sensitivity of the reiterative solution to the a value. This leads to the values for the inferred fading in the various TL areas in samples A and B shown in Table 6.3 (ranging from 41% to 68%) which appear to be reasonable

TABLE 6.3

Values of TL-fading inferred from the '$\frac{1}{E}$ Law' (with $\alpha = 0.7065$) for the shaded (A) and sunlit (B) samples

	Sample A (76241,23; "freezer counterpart")			Sample B (76261,25)
Parameter	Area I (216-306°C)	Area II (306-378°C)	Area III (378-486°C)	Area III (378-486°C)
Trap depth E(eV)	1.046	1.134	1.439	1.72
Calculated fading	68%	62%	49%	41%
Measured value of N/n_{eq}	7.41	4.58	3.31	3.85
Corrected value of N/n_{eq}	2.37	1.74	1.69	2.27

in the light of the foregoing discussion.

The duration of the boulder shadow at station 6, calculated from either TL area in sample A (area II or III) after applying the fading corrections based on equation 22, is found to be $t_1 = 6.50 \times 10^4$ yr. (for r = 10 rad yr^{-1}).

6.11 Uncertainties and Implications of Results.

The four sets of parameter values recorded in Table 6.1 (namely those for TL areas I, II and III in the shaded sample A, and for area III in the sunlit sample B) give highly consistent answers for storage temperature T_1, natural dose R = rt, fading $1 - n/n_o$ and the trap depth E, involved in the calculations. For example, it is very difficult to get a value for the storage temperature in the shade differing by more than a few degrees from the one obtained (i.e. 256°K) without upsetting the values of all the other parameters. However, an attempt was made here to estimate the propagation of error in the calculations resulting from experimental uncertainties. These estimates are described below.

The maximum uncertainty in the sunlit storage temperature (371°K) calculated from equation 21, resulting from $\pm$ 3.5% error in E and a factor of 4 uncertainty in the argument of the ln (Durrani et al, 1972; see Section 6.9.3) (based on a factor of 2 uncertainty in each of r and $(\frac{N}{n_{eq}} - 1)$ values), is $\pm$ 16°K. This is in good accord with previous determinations by Durrani et al (1972b, 1973) for lunar samples (e.g. 363 $\pm$ 10°K for certain Apollo 15 and 372 $\pm$ 5°K for Apollo 14 samples), although it is believed that the value - which represents the effective storage temperature adjusted for the Boltzmann factor (Durrani et al, 1972a) - is unlikely to be as high as 387°K. A similar uncertainty ($\pm$ 15°K) applies to the storage temperature calculated for the shaded sample (namely 256°K). This uncertainty does not invalidate

the condition governing equation 20; in other words, $r\tau_{\frac{1}{2}} \gg R_{\frac{1}{2}}$ still holds for both TL areas II and III in sample A.

The value of the natural dose $R = rt_1$ in the shaded sample A, calculated from equation 20, is independent of the value of the temperature in the shade so long as the condition $r\tau_{\frac{1}{2}} \gg R_{\frac{1}{2}}$ is fulfilled. The value of the length of storage t_1 in the shade, however, obviously depends upon the dose rate r assumed to operate inside the shadow (as t_1 is deduced from the calculated value of rt_1). If one assumes the dose rate within the shadow to fall by a factor of 2 (or of 10, which is unlikely), because of the shielding from the solar-wind and solar-flare particles, the estimated length of storage will rise by the same factor.

Other uncertainties in the calculated value of rt_1 arise from errors and uncertainties in $R_{\frac{1}{2}}$ and the pre-fading value of n/N (cf. equation 20). A 10% error in the measurement of $R_{\frac{1}{2}}$ would produce the same fractional error in rt_1. An error of $\pm$ 10% in the corrected value of n/N would lead to errors of $\pm$ 13% and 15% respectively in the values of rt_1 calculated from the TL areas II and III in sample A.

The fact that it was possible to calculate (to within a factor of $\sim$2) the value of the duration of the shadow cast over the sample A (76240) and hence the time of the arrival of the boulder at its present location, has important implications for soil mechanics of the surface of the moon. Mitchell et al (1973) refer to over 300 tracks 'made by boulders rolling, bouncing and skidding down lunar slopes'. The Apollo 17 mission provided the first opportunity for a close study of these interesting features which were especially evident on the Taurus-Littrow hills. It has already referred to the apparently fresh tracks observed by the Apollo 17 astronauts on the

slopes of the North and South Massifs. For example, in connection with sample 76240 (the shaded sample A which came from station 6 in the region of the North Massif), Astrogeology 72 makes the following statement: "It probably has not been shadowed for a great length of time, because the freshness of the boulder track indicates that the boulder has not been in its present position very long". The calculations presented in this chapter indicate that the time scale involved is of the order of 6×10^4 yr. The mechanisms that set the boulders in motion are generally not well understood. Material build-up or erosion uphill or downhill respectively, cyclic thermal expansion and contraction, impact cratering and seismic events are amongst the possibilities considered by Mitchell et al (1973).

In considering the duration of boulder shadow as calculated from the preserved natural TL in the shaded soil, it may be instructive to consider the role of dust movement on the lunar surface. Griswell (1972) has postulated the migration of electrically charged micron-sized grains from the sunlit areas towards dark or partially illuminated areas. From 'horizon glow' observations made at the time of lunar sunset, Criswell calculates a value of mass-flow rate of $\sim 10^{-3}$ gm/cm^2 yr. for the surface dust, corresponding to a layer turnover rate of 6μm/yr. Such a rate of inflow would deposit a layer $\sim$ 30cm thick in 50,000 years under the boulder. That this is not the case is clear when one considers the top $\sim$ 5cm of the shadowed soil (this being the maximum depth of the scooped sample A). A thickness of 5cm would, at the above rate, be deposited in $\sim$ 8,000 years, yielding an average age of only $\sim$ 4,000 years inside the shadow, whereas the calculated length of storage in the shade for sample A is $\sim$ 40,000 years to 65,000 years. If one assumes the top 1cm in the shade to be of external

origin, the Criswell rate of inflow must be reduced by a factor of $\sim$ 40. This results in the duration of the boulder shadow being revised upwards from 6.0×10^4 yr. to 6.67×10^4 yr. to yield the observed amount of glow, assuming a homogeneous mixing of the top 5cm of soil during and since its retrieval.

The value of the storage temperature in the boulder obtained here (256°K) appears to be rather high when one considers the conductive processes on the moon. On using the latest values of the heat flow experiment on the moon (Langseth et al, 1976, who report a value of $\sim 2.0 \mu w\ cm^{-2}$ for heat flow), one obtains a value of only $\sim 25^{\circ}$K from this source. If one considers the heat dynamics of the boulder shadow in the context of the surrounding lunar mass (assumed to be at a mean equilibrium temperature of $\sim 240^{\circ}$K) then, using the conductivity values obtained from the heat flow experiment as well as that calculated by Durrani and Hwang (1974), one obtains a value of $\sim 100^{\circ}$K inside the shade; but such calculations are strongly model-dependent. The calculated value of the temperature in the shade (256°K) is quite close to the mean equilibrium temperature on the lunar surface ($\sim 240^{\circ}$K). Causes such as imperfect shadowing of the sample (which came from only $\sim$ 0.5 to 1 metre inside the boundary of the shadow) and soil mixing may explain the rather high value of the effective storage temperature in the shadow of the boulder estimated in this chapter. The calculation depends critically on the value n_{eq}/N (the fraction of total traps filled at equilibrium) in the TL glow area I of sample A. If, as a result of possible exposure to sunlight during the retrieval procedure and/or the high-temperature ($\sim 100^{\circ}$C) handling of the sample during EVA on the lunar surface, or because of a high degree of anomalous fading than has

been allowed for, the initial value n_{eq}/N will be higher than that used in this calculation and the temperature in the shade would have to be revised downward. Similarly, if dynamic equilibrium had not as yet been reached in trap-filling for area I of sample A (owing, say, to a relatively short storage time in the shade), then equation 21 would not hold and the value of storage temperature obtained here would be an over-estimate.

6.12 The Effect of the Temperature of Irradiation upon the TL Sensitivity of Lunar Samples.

Following the finding of the effect of irradiation temperature upon the TL sensitivity of quartz (Khazal, 1975; Durrani et al, 1977; see also Chapter IV), the phenomenon has been further investigated in some lunar samples. The sample principally used in this study was the shaded sample 76241,23 (freezer counterpart sample). According to the results presented in this chapter, the sample was irradiated in its natural environment, in the shade of the boulder, at a temperature as low as 256°K for a period of $\sim 6.0 \times 10^4$ yr. This feature made this sample ideal for the study of the effect of the irradiation temperature. Irradiations were carried out at three temperatures, namely, 195°K, 293°K and 393°K (the last temperature chosen to simulate the sunlit conditions). Three γ-ray doses (Co-60) were used at each temperature, namely, 200krad, 600krad and 2000krad. The TL output was integrated over the glow-curve temperature interval 378-486°C (area III) chosen to minimise any thermal fading which might occur at room temperature and particularly during irradiation at 393°K temperature. The results of this study are shown in Figure 6.9.

It can be seen from Figure 6.9 that in all cases the TL output increased steadily with the increasing temperature of irradiation; but the greatest increase was for the largest γ-ray dose used (2000krad). The percentage

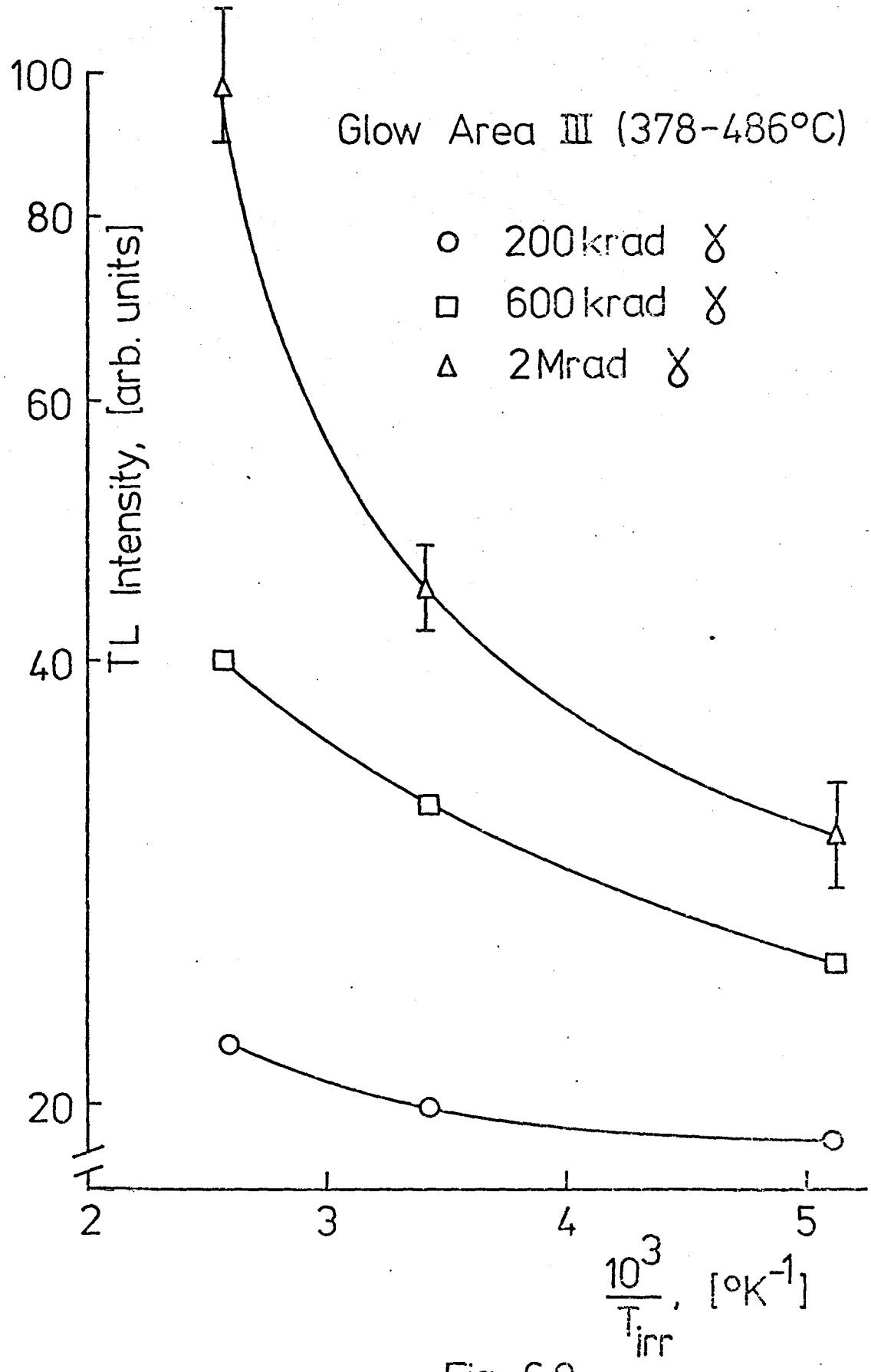
Sample 76241,23 (shaded)
Glow Area III (378-486°C)
200 krad
600 krad
2 Mrad
TL Intensity, [arb. units]
100
80
60
40
20
2
3
4
5
$\frac{10^3}{T_{irr}}$, [°K^{-1}]

Fig 6.9

increase in the integrated TL output as the temperature of irradiation was raised from 195°K to 393°K was found to be as follows: 22% (for 200krad), 60% (600krad) and 220% (2000krad). Thus the increase in TL output is proportional to dose, at these doses, between the two extremes of temperature employed. If the temperature of the boulder shadow reported previously, namely 256°K, is used as a reference, then the percentage increase in the integrated TL output as the temperature of irradiation is raised from 256°K to 393°K (sunlit) is found to be as follows: 15.8% (for 200krad), 38% (600krad) and 158% (2000krad). These results might explain the higher sensitivity and saturation level of the sunlit sample 76261 for the three glow areas compared with the corresponding areas of the shaded sample 76241 (see Figures 6.3a and 6.3b) in spite of the similarity of these samples which is supported by their identical glow-curves and TL emission spectra (Figures 6.4 and 6.5). Thus the main difference between the two samples is in their thermal environments, namely, the sample 76241 was collected from the shadow of the boulder, and the other, 76261, collected from the sunlit area just outside the shadow. Considering the glow area III (378-486°C) it was found that the percentage increase in the laboratory determined TL sensitivity from the sunlit sample over that from the shaded is 32.2%. This result was obtained by performing the irradiation for both samples at room temperature. The implication here is that a different method is required of finding the natural dose that is independent of temperature. If the true natural dose is determinable, then the irradiation temperature may be accurately found from the results presented in this section.

Regarding the values of the temperature of the boulder shadow (T_1 = 256°K) and the duration of the boulder ($t_1 = 6.50 \times 10^4$ yr.) calculated from

equations 21 and 20 respectively, these values need to be reconsidered in view of the temperature effect. In both equations 20 and 21 the ratio $(\frac{N}{n_{eq}})$ i.e. the ratio of the saturation TL (obtained at room temperature - see Figures 6.3a and 6.3b) to the natural TL (accumulated at the shadow temperature) must be corrected to allow for the temperature effect; but the occurrence of this ratio in the logarithmic term in both equations makes the temperature T_1 and the duration t_1 weakly dependent on it as was discussed in Section 6.11.

6.13 Future Work.

The work described in this thesis is by no means complete. Future work is needed to study in detail the effect of temperature of irradiation upon the TL sensitivity in quartz, which is reported in this thesis, and especially in other materials of terrestrial and extraterrestrial origin.

Regarding the quartz mineral, a detailed study of the temperature effect for each of the TL peaks is required. In the work reported in this thesis the whole area between 513°K and 753°K was studied for both X-ray and gamma-ray radiations. Single peak analysis, using X-ray radiation with the low temperature TL apparatus described in Chapter IV, was not possible. Further improvements are required to make the apparatus capable of performing thermal cleaning procedures similar to that followed in Chapter III, to decompose the TL glow curve into single peaks. For gamma-irradiation, the single peak analysis is possible using the normal (high temperature) TL apparatus described in Section 2.1 and following the procedure described in Chapter III.

A complete investigation is suggested for minerals related to TL dating, similar to that made in the study of anomalous fading (Wintle, 1974), to

establish the degree to which the effect of the temperature of irradiation exists in those various minerals. A single-peak analysis of the glow curve of each of the minerals together with the use of different types of ionizing agents such as U.V., X-rays, gamma-rays, beta-rays, neutrons and protons is required, along with different ranges of absorbed dose of ionizing radiation.

With regard to materials of extraterrestrial origin (meteorites in particular), which are irradiated for a long period of time at very low temperatures in space a detailed study of the effect of the temperature of irradiation upon the TL sensitivity of the material of these outer space bodies is suggested. A finding of such an effect in one or more of the high temperature peaks of the glow curve of these materials might enable the determination to be made of their environmental temperature and a re-assessment of their ages.

For the understanding of the relation between the impurities existing in natural quartz (e.g. Na, Al, etc.) and the effect of the temperature of irradiation upon its TL sensitivity and sensitization, a detailed study of the role of impurities on the TL characteristics of quartz and their relation to the temperature effect is required. This role can be studied by doping an artifically produced crystalline quartz with different amounts of an impurity and comparing the TL characteristics of the doped sample with those of pure and natural materials. Regarding the analysis and the results presented in Chapters III and IV, the effect of impurities such as Al and Na either added together or separately should be given priority.

Finally, in the light of the results presented in this work, an investigation into the behaviour of the sensitivity of the commonly used

dosimeters such as LiF and CaF_2:Mn with the temperature of irradiation and with dose rate and total dose is needed, particularly if these dosimeters are to be used at high exposures.

LIST OF PUBLICATIONS

Khazal K.A.R., Hwang F.S.W. and Durrani S.A. (1975). The effect of the temperature of irradiation on the TL sensitivity of quartz (abstract). In: Symp. Archaeometry Archaeological Prospection Abstracts, p.8, Research Laboratory for Archaeology, University of Oxford.

Durrani S.A., Khazal K.A.R., Malik S.R., Fremlin J.H. and Hendry G.L. (1975). Thermoluminescence and Fission-Track Studies of the Oklo Fossil Reactor Materials. I.A.E.A.-SM-204/6.

Durrani S.A. and Khazal K.A.R. (1976). Thermoluminescence studies of Apollo 17 boulder shadows (abstract). In: Lunar Science VII, pp.221-223. The Lunar Science Institute, Houston.

Durrani S.A., Khazal K.A.R. and Ali A. (1976). Temperature and duration of some Apollo 17 boulder shadows. Proc. Lunar Sci. Conf. 7th, pp.1157-1177.

Durrani S.A., Khazal K.A.R. and Ali A. (1977). "Temperature and duration of the shadow of a recently-arrived lunar boulder". Nature, 266, p.441.

Durrani S.A., Groom P.J., Khazal K.A.R. and McKeever S.W.S. (1977). "Dependence of the thermoluminiscence sensitivity upon the temperature of irradiation in quartz". J. Phys. D: Applied Phys., 10, p.1351.

Durrani S.A., Khazal K.A.R. and McKeever S.W.S. (1977). "Studies of changes in the TL sensitivity in quartz induced by proton and gamma irradiations". Radiation Phys. In press.

Khazal K.A.R. and Durrani S.A. (1977). "The effect of the temperature of irradiation upon the TL sensitivity of lunar samples" (abstract). In: The 40th Annual Meeting of the Meteoritical Society, Cambridge, England.

Khazal K.A.R. and Durrani S.A. (1977). "Determination of the temperature and duration of shadow of a recently-arrived Apollo 17 boulder using thermoluminescence methods" (abstract). In: The 40th Annual Meeting of the Meteoritical Society, Cambridge, England.

REFERENCES

Aitken M.J. (1968). Thermoluminescent dating in Archaeology: Introductory review. In: McDougall D.J. (ed.), "Thermoluminescence of Geological Materials", page 369. Academic Press.

Aitken M.J. (1974). Physics and archaeology (2nd edition). Clarendon Press, Oxford.

Aitken M.J., Tite M.S. and Fleming S.J. (1967). "Quenching of spurious thermoluminescence by nitrogen". Luminescence Dosimetry, Proc. Int. Conf., Stanford, 490-501.

Algit (Apollo Lunar Geology Investigating Team) U.S. Geological Survey (1975) Apollot 17 landing site. Interagency Report: Astrogeology 73, pp. 80, 82-83, 148-150.

Algit (Apollo Lunar Geology Investigating Team) U.S. Geological Survey (1973) Preliminary geological analysis of the Apollo 17 sits. Interagency Report: Astrogeology 72, p.75.

Arnold G.W. and Compton W.D. (1959). Phys. Rev., 116, 4, 802.

Bambauer H.V. (1961). Schweiz. Mineral Petrogr. Mitt., 41, p.335.

Batrak E.N. (1958). Kristallografica 3,102,633, 635.

Braünlich P. (1968). "Thermoluminescence and Thermally Stimulated current-tools for the determination of trapping parameters". In: McDougall D.J. (ed.), p.61. Academic Press.

Cameron J.R., Suntharalingam N. and Kenney G.N. (1968). "Thermoluminescent Dosimetry", University of Wisconsin.

Cameron J.R. and Zimmerman D.W. (1965). "TL vs. R in LiF: A proposed mathematical model". Rept. COO-1105-102, USAEC.

Chentsova L.G. (1956). Sov. Phys. Crystall., 1, 4, p.384.

Christodoulides C. (1972). Thermoluminescence Dating of Materials of Extraterrestrial or Biological Origin. Ph.D. Thesis, University of Birmingham.

Christodoulides C., Durrani S.A. and Ettinger K.V. (1970). Mod. Geol., 1, p.247-259.

Criswell D.R. (1972). In Proc. 3rd. Lunar Sci. Conf., pp.2671-2680 (Pergamon Press).

Curie D. (1963). "Luminescence in Crystals". Methuen, London.

Dalrymple G.B. and Doell R.R. (1970). Thermoluminescence of lunar samples from Apollo 11. Proc. Apollo 11 Lunar Sci. Conf., Geochim. Cosmochim. Acta, Suppl. 1, Vol. 3, pp. 2081-2092. (Pergamon Press).

Dran J.C. et al., (1972). "Track metamorphism in extraterrestrial breccias", Proc. 3rd. Lunar Sci. Conf., 3, p.2883. M.I.T. Press, Cambridge, Mass.,

Durrani S.A. (1972). Refrigeration of Lunar Samples destined for thermoluminescence studies. Nature, 240, 96-97.

Durrani S.A. Prachyabrued W., Christodoulides C., Fremlin J.H., Edgington J.A., Chen R. and Blair I.M. (1972a). Thermoluminescence of Apollo 12 samples: Implications for lunar temperature and radiation histories. Proc. Lunar Sci. Conf. 3rd, pp.2955-2970.

Durrani S.A., Prachyabrued W., Edgington J.A. and Blair I.M. (1972b). Thermoluminescence of Apollo 15 lunar samples: (II) 20 to 550°C. In The Apollo 15 Lunar Samples, pp.457-461. The Lunar Science Institute, Houston.

Durrani S.A., Prachyabrued W., Hwang F.S.W., Edgington J.A. and Blair I.M. (1973). Thermoluminescence of some Apollo 14 and 16 fines and rock samples. Proc. Lunar Sci. Conf. 4th, pp.2465-2479.

Durrani S.A. and Hwang F.S.W. (1974). Thermoluminescence and thermal environment of some Apollo 17 fines. Proc. Lunar Sci. Conf. 5th, pp. 2689-2702.

Durrani S.A. and Khazal K.A.R. (1976). Thermoluminescence Studies of Apollo 17 boulder shadows (abstract). In Lunar Science VII, pp. 221-223. The Lunar Science Institute, Houston.

Durrani S.A. and Christodoulides C. (1969). Nature, 223, pp.1219-1221.

Durrani S.A., Khazal K.A.R., Malik S.R., Fremlin J.H. and Hendry G.L. (1975). I.A.E.A.-SM-204/6.

Durrani S.A. and Khan H.A. (1970). Annealing of fission tracks in tektites: corrected ages of bediasites. Earth Planet Sci. Lett., 9, p.431.

Evans J.C. (1964). "Crystal Chemistry". Cambridge University Press, p.157.

Fowles, P. (1976). "Users manual for the X-ray set". Radiation Centre.

Garlick G.F.J. and Gibson A.F. (1948). The electron trap mechanism of luminescence in sulphide and silicate phosphors. Proc. Phys. Soc. Lond., 60, 574-590.

Garlick G.F.J. and Robinson I. (1972). The thermoluminescence of lunar samples. In The Moon (editors H.C. Urey and S.K. Runcorn), pp. 324-329. International Astonomical Union.

Garlick G.F.J. (1949). "Liminescent materials". Clarendon Press, Oxford.

Göksu H.Y. and Fremlin J.H. (1972). Thermoluminescence from unirradiated flints: regeneration thermoluminescence. Archaeometry, 14, 127-132.

Groom P.J. (1977). M.Sc. Thesis, University of Birmingham.

Haffner J.W. (1967). Radiation and Shielding in Space, p.279. Academic Press.

Halperin A. and Ralph J.E. (1963). J. Chem. Phys., 39, 1, 63-73.

Hoogenstraaten W. (1958). "Electron traps in zinc-sulphide phosphors", Philips Res. Rep., 13, p.515.

Hoyt H.P., Kardos J.I., Miyajima M., Seitz M.G., Sun S.S., Walker R.M., and Wittels M.C. (1970). Thermoluminescence, X-ray and stored energy measurements of Apollo 11 samples. Proc. Apollo 11 Lunar Sci. Conf., Geochim. Cosmochim, Acta, Suppl. 1, Vol.3, pp.2269 - 2287. Pergamon Press.

Hoyt H.P., Miyajima M., Walker R.M., Zimmerman D.W. and Zimmerman J. (1971). Radiation dose rates and thermal gradients in lunar regolith: Thermoluminescence and DTA of Apollo 12 samples. Proc. Second Lunar Sci. Conf., Geochim. Cosmochim. Acta, Suppl. 2, Vol. 3, pp. 2245-2263. M.I.T. Press.

Hwang F.S.W. and Durrani S.A. (1975). Temperature and length of storage of surface soil in the shadow of Apollo 17 boulders (abstract). In Lunar Science VI, pp. 423-425. The Lunar Science Institute, Houston.

Hwang F.S.W. (1972). Thermoluminescence Dating: The long range aspects and its application to volcanic lava. Ph.D. Thesis, University of Birmingham.

Ichikawa Y. (1968). Jap. J. Appl. Phys., 7, pp. 220-227.

Jahn R.A. (1971). The luminescent and thermoluminescent properties of Lunar material (Report). A.E.R.E., Harwell.

Johns H.E. (1961). "The Physics of Radiology" (2nd edition). Charles C. Thomas, Springfield, Illinois.

Khazal K.A.R., Hwang F.S.W. and Durrani S.A. (1975). The effect of the temperature of irradiation on the TL sensitivity of quartz (abstract). In Symp. Archaeometry Archaeological Prospection Abstracts, p. 8. Research Laboratory for Archaeology, University of Oxford.

Khan H.A. and Durrani S.A. (1972). Prolonged etching factor in solid state track detection and its applications. Radiation Effects, 13, p. 257.

Klug H.P. and Alexander L.E. (1972). "X-ray Diffraction Procedures for Polycrystalline and Amorphous Materials", 2nd edition. Wiley.

Krishnaswami S., Lal D., Prabhu N. and Tamhane A.S. (1971). Science, 174, 287.

Lal D., Murali A.V., Rajan R.S. and Tamhane A.S. (1968). Earth Planet Sci. Lett., 5, 111.

Lancelot J.R., Vitrac A. and Allegre C.J. (1975). The Oklo natural reactor: age and evolution studies by U-Pb and Rb-Sr systematics. Earth Planet Sci. Lett., 25, p. 189.

Langseth M.G., Keihm S.J. and Peters K. (1976). The revised lunar heat flow values. In Lunar Science VII, pp.474-475. The Lunar Science Institute, Houston.

Lell E., Kreidl N.J. and Hemsler J.R. (1966). Progr. Ceram. Sci., 4, 1.

Levy P.W. (1968). In: McDougall D.J. (ed.), Thermoluminescence of Geological Materials, p.25.

Mackey J.H. (1963). J. Chem. Phys., 39, 1, p.74.

Malik S.R. (1973). Studies of solid state track detectors and their applications to materials of terrestrial, extraterrestrial and biological origin. Ph.D. Thesis, University of Birmingham.

McDougall D.J. (1968). Ed. Thermoluminescence of Geological Materials. Academic Press.

McKeever S.W.S. (1976). Private communication.

McMorris D.W. (1969). Nature, 222, p.870.
McMorris D.W. (1971). J. Geophys. Res., 76, 32, pp.7875-7887.
Medlin W.L. (1963). J. Chem. Phys., 38, 5, p.1132.
Mehtha P.P. and Rama (1969). Earth Planet Sci. Lett., 7, p.82.
Michell J.K., Carrier W.D., Costes N.C., Houston W.N., Scott R.F. and Hovland H.J. (1973). Soil mechanics. In Apollo 17 Preliminary Science Report, pp. 8.1 - 8.22. National Aeronautics and Space Administration, Washington, D.C.

Naudet R. (1974). Summary Report on the Oklo Phenomenon. French C.E.A. Rep. BIST No.193. English translation.

Naudet R. (1975). Letters No.75/112 RN/DS and 75/222 RN/DS Project Franceville.

Nicholas K.H. and Woods J. (1964). Brit. J. Appl. Phys., 15, p.783.

Nuffield E.W. (1966). X-ray diffraction methods. John Wiley and Sons Inc., New York.

O'Brien M.C.M. (1955). Proc. Roy. Soc. A231, p.404.

Prachyabrued W. (1972). Thermoluminescence of Tektites, Meteorites and Lunar Materials. Ph.D. Thesis, University of Birmingham.

Price P.B. and Walker R.M. (1962). Phys. Rev. Letters, 8, p.217.

Randall J.T. and Wilkins M.H.F. (1945). Phosphorescence and electron traps. Proc. Roy. Soc. London A184, pp.366-407.

Riehl N. and Schön M. (1939). Z. Physik., 114, p.682.

Schlesinger M. (1964). Phys. Lett., 10, 1, p.49.

Shekhmametev R.I. (1973). Opt. Spectrosc., 34, 3, p.288.

Silk E.C.H. and Barnes R.S. (1959). Phil. Mag., 4, p.970.

Somogyi G., (1966). Nucl. Instr. and Methods., 42, p.312.

Somogyi G., Varnagy M. and Peto G. (1968). Nucl. Instr. and Methods, 59, p.299.

Somogyi G. and Schlenk B. (1970). Radiation Effects, 5, p.61.

Stevels J.M. and Volger J. (1962). Philips Res. Rept. 17, p.283.

Storzer D. and Wagner G.A. (1969). Earth Planet Sci. Lett., 5, p.463.

Tite M.S. (1968). Some complicating factors in thermoluminescent dating and their implications. In: McDougall D.J. (ed.), Thermoluminescence of Geological Materials, p.389. Academic Press.

Urbach F. (1930). Akad. Wiss. Wein. Ber., 20, p.354.

West N.G., Hendry G.L. and Bailey N.T. (1974). The analysis of slags from primary and secondary copper smelting processes by X-ray fluorescence. X-ray Spectrometry, 3, p.78.

Williams F.E. and Eyring H. (1947). "Mechanism of the luminescence of solids". J. Chem. Phys., 15, 289.

Wintle A.G. (1973). Anomalous fading of thermoluminescence in mineral samples. Nature, 244, 143-4.

Wintle A.G. (1974). Ph.D. Thesis, University of Oxford.

Wright P.M., Weil J.A., Buch T. and Anderson J.H. (1963). Nature, 197, p.246.

Yokato R. (1953). Phys. Rev., 91, p.1013.